THE UNIVERSITY *of* EDINBURGH

Investigating the Chemistry of Binuclear Chromium and Uranium Pacman Complexes

Charlotte J. Stevens

University of Edinburgh

Submitted for the degree of Doctor of Philosophy

2014

Declaration

The work described in this thesis is entirely my own, except where I have either acknowledged help from a named person or given reference to a published source. Text taken from another source will be enclosed in quotation marks and a reference given. This thesis has not been submitted, in whole or in part, for any other degree.

Signature:

Date:

Abstract

Drawing inspiration from nature where enzymes containing multi-metallic active sites are ubiquitous, chemists have designed various ligands to bind more than one metal in precise structural arrangements. In Chapter One, a class of binucleating Schiff base pyrrole (Pacman) macrocycles which are both straightforward to synthesise and can be varied systematically to alter the metal environment and intermetallic separation are introduced, along with the state-of-the-art in this area. Previously reported complexes of these ligands with late transition metals, lanthanides and actinides are also reviewed. The results and discussion chapters of the thesis focus on the isolation and investigation of previously unexplored early transition-metal Pacman complexes and present new advances in low oxidation state uranium Pacman chemistry.

In Chapter Two, binuclear chromium(II) complexes of two Schiff base macrocycles, H_4L^{Me} and H_4L^{A} are described. $[Cr_2(L^{Me})]$ features an *ortho*-phenyl spacer between the macrocycle donor compartments whereas the Cr(II) ions are separated by a larger anthracenyl spacer in $[Cr_2(L^{A})]$. Both compounds have been characterised in solution and the solid state. Reactivity studies were carried out for $[Cr_2(L^{Me})]$. Reactions of $[Cr_2(L^{Me})]$ with isocyanides and triphenylphosphine oxide were investigated leading to the isolation of the contrasting co-ordination compounds $[Cr_2(OPPh_3)_2(L^{Me})]$ and $[Cr_2(\mu\text{-}CNR)(L^{Me})]$ (R = xylyl, ^{t}Bu). Oxidation of $[Cr_2(L^{Me})]$ with I_2 yields the Cr(III)/Cr(III) Pacman products $[Cr_2(\mu\text{-}I)(I)(THF)(L^{Me})]$ and $[Cr_2(\mu\text{-}I)(py)_2(L^{Me})][I]$ when carried out in THF or pyridine, respectively. Cr(III) alkyl compounds are obtained by reaction of $[Cr_2(\mu\text{-}I)(I)(THF)(L^{Me})]$ with the non-reducing alkyl transfer reagents MgBrEt and $ZnEt_2$. When $ZnEt_2$ in toluene is employed, one zinc cation is incorporated in the molecular cleft, whereas use of MgBrEt in THF yields the simple chromium alkyl complex $[\{Cr(Et)\}_2(\textit{endo}\text{-}THF)(L^{Me})]$. One ethyl group may be abstracted from $[\{Cr(Et)\}_2(\textit{endo}\text{-}THF)(L^{Me})]$ by $[CPh_3][B(C_6F_5)_4]$ to form a cationic alkyl complex. The activity of both the neutral and cationic alkyl species towards ethylene was investigated. Conclusions are discussed at the end of the chapter.

Previously, investigation of low oxidation state uranium Pacman chemistry has been confined to the smaller macrocycle, H_4L^{Me}, and frequently resulted in the formation of insoluble polymeric materials that were intractable and challenging to analyse. In Chapter Three, metallation of the larger macrocycle, H_4L^{A}, with UI_3 to generate a single soluble species is described, although this product could not be isolated or characterised in the solid state. A new synthesis of $[U(BH_4)_3(THF)_2]$ from UI_3 and $NaBH_4$ affords an alternative U(III)

precursor to UI_3. Metallation of H_4L^A using a sodium base and $U(BH_4)_3(THF)_2$ yields the ionic product $[Na(THF)_4][\{U(BH_4)\}_2(\mu\text{-}BH_4)(THF)_2(L^A)]$ which was characterised in solution and the solid state. Reaction of this compound with $KO(C_6H_2(^tBu)_3)$ forms the ligand substitution product $[\{U(OAr)\}_2(\textit{endo}\text{-}BH_4K)(THF)_2(L^A)]$ which undergoes selective reaction with excess S_8 or CS_2 to form $[\{U(OAr)\}_2(\mu\text{-}S_2)(L^A)]$ and $[\{U(OAr)\}_2(\mu\text{-}S)(L^A)]$ respectively. It was discovered that the $[U(BH_4)_3(THF)_2]$ metallation strategy could be successfully extended to H_4L^{Me} to form $[Li(THF)_4][\{U(BH_4)\}_2(\mu\text{-}BH_4)(L^{Me})]$. Protonolysis of the borohydride ligands of the complexes of the two different macrocycles was investigated using the weak acid $[HNEt_3][BPh_4]$. NMR spectroscopy indicated that both *exo* BH_4^- groups in both complexes can be successively removed to generate neutral and cationic complexes but these were not isolated. Metallation of H_4L^A with UCl_4 forms the ionic product $[Li(THF)_4][\{U(Cl)\}_2(\mu\text{-}Cl)_3(L^A)]$. Various ligand substitution reactions were attempted but the only structurally characterised product was $[\{U(O^tBu)(Cl)\}\{U(O^tBu)(py)\}(\mu\text{-}Cl)(L^A)]$, formed by reaction with KO^tBu. Conclusions are discussed at the end of the chapter.

Experimental and characterising data are provided in Chapter Four.

Acknowledgements

I would like to thank my supervisors Jason and Polly for their constant help, guidance and enthusiasm during my PhD. I am grateful also to the EaStCHEM School of Chemistry for funding my project.

I am indebted to Dr Alex Presciomone and Dr Carole Morrison for carrying out high pressure X-ray crystallography and computational studies, and also to Prof. Eric McInnes and Dr Floriana Tuna at the University of Manchester for their expertise in SQUID and EPR spectroscopy.

I am very grateful for all the good humoured help I have received from Dr Lorna Murray and Mr Juraj Bella with NMR spectroscopy, Dr Gary Nichol with X-ray crystallography and Mr Donald Robertson with IR spectroscopy.

Thank you to all the brilliant postdocs in the Love/Arnold group who have given me so much of their time, especially Stephen, Joy and Nicola. Thank you to Guy, Isobel, Rebecca, Markus, Jamie and all my other Lab 34 friends for helping me enjoy my time in Edinburgh.

Finally, thank you to my family and to Andy for their love and support.

"As the circle of light expands, so does the circumference of darkness."

- *Albert Einstein*

Abbreviations

General

acac	acetylacetonate, $\{CH_3(CO)\}_2CH$
Ad	adamantyl
Ar	aryl
B	magnetic field strength
Cp	C_5H_5
Cp*	C_5Me_5
DABCO	1,4-diazabicyclo[2.2.2]octane
DCM	dichloromethane
Dipp	2,6-diisopropylphenyl
DMAP	*N*,*N*-dimethylaminopyridine
DME	dimethoxyethane
DMF	dimethylformamide
dmpe	dimethylphosphinoethane
G	Gauss, unit of magnetic field strength
GPa	Giga Pascals, unit of pressure
H_2L'	*trans*-calix[2]benzene[2]pyrrole macrocycle
H_4L	generic *ortho*-phenyl hinged Pacman macrocycle
H_4L^A	anthracenyl hinged macrocycle
H_4L^{Me}	*ortho*-phenyl hinged octamethyl macrocycle
H_4L^X	any Pacman macrocycle
M	metal
Mes	mesityl, 2,4,6-$C_6H_2(Me)_3$
N″	$N(SiMe_3)_2$
[O]	oxidant
OTf	CF_3SO_3
py	pyridine
pyr	pyrrole/pyrrolide
RT	room temperature
s	spin of individual metal ion
S	total spin of complex
sol	solvent
SQUID	Superconducting Quantum Interference Device
T	temperature
t	time
tacn	triazacyclononane
THF	tetrahydrofuran
Tpa	terephthalic acid
xs	excess
Xyl	xylyl, 2,6-$C_6H_3(Me)_2$
Δ	heat
λ	wavelength
ν	frequency
χ	magnetic susceptibility

NMR

δ	chemical shift
s	singlet
d	doublet
t	triplet
q	quartet
(v) br	(very) broad
J	coupling constant
$W_{½}$	width at half-height

Contents

Chapter One

Introduction to Binucleating Ligands

1.1 Inspiration

In nature, enzymes catalyse an enormous array of chemical reactions. From the reduction of N_2 to ammonia in leguminous plants, to the oxidation of water to O_2 during photosynthesis, biology achieves numerous selective redox transformations of small molecules under ambient conditions. This far surpasses the achievements of laboratory chemists; the Haber Bosch process for industrial ammonia production consumes roughly 1 % of annual global energy output.[1] Advances in biochemistry and protein crystallography have revealed that metalloproteins are responsible for catalysing many of these biological transformations. Though metalloproteins typically have complex extended structures, substrate activation often occurs at a relatively small, precisely ordered multi-metallic active site. One such metalloprotein is cytochrome *c* oxidase which mediates the 4 e^- reduction of O_2 to water during respiration. The X-ray crystal structure reveals that the active site is bimetallic and consists of a porphyrin-supported iron centre at a separation of 4.5 Å from a histidine-bound copper ion (Figure 1.1).[2] O_2 reduction is achieved co-operatively between the metal centres.

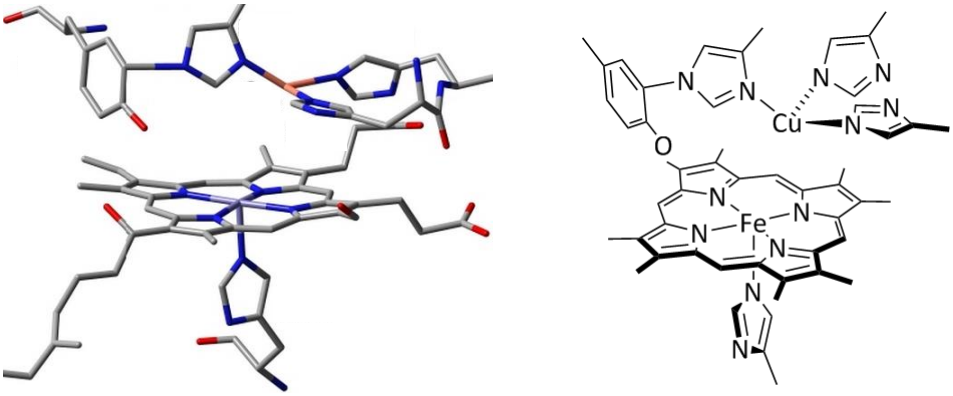

Figure 1.1 Crystal structure of the O_2 reduction site in cytochrome *c* oxidase (bovine heart) reproduced from Tsukihara *et al*.[2] (left) and ChemDraw representation (right).

The development of efficient redox transformations of small molecules such as N_2, CO, CO_2 and CH_4 will become increasingly important if we are to meet growing global demands for energy and materials. Drawing inspiration from nature's metalloenzymes, chemists are developing novel multi-metallic systems which they hope will mimic the remarkable activity of biological systems,[3] though this introduction will focus solely on the synthesis and reactivity of bimetallic complexes. A wide range of different ligand classes can promote the aggregation of two metal ions and these have been reviewed extensively.[4] The majority of binucleating ligands consist of a bridging group which spans the metal centres

and auxiliary chelate groups that stabilise the complex. Figure 1.2 shows examples of binuclear complexes of ligands with formamidinate, triazole and carboxylate bridging groups and auxiliary phosphine, pyridine and cyclic ammine chelators.

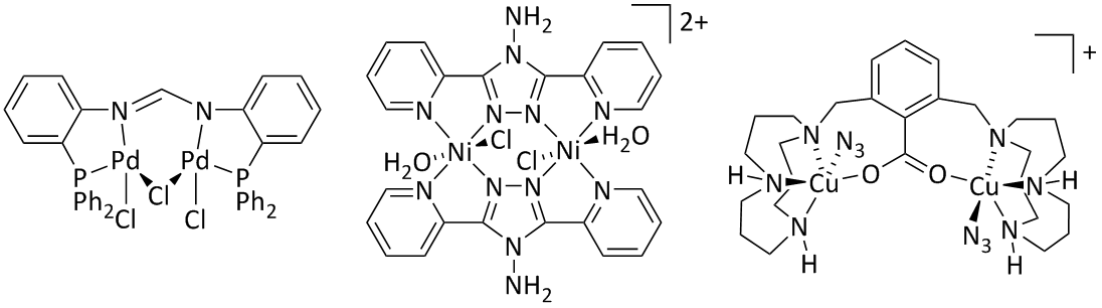

Figure 1.2 Examples of bimetallic complexes supported by different ligand sets.[5-7]

This class of binucleating ligands has certain disadvantages. The presence of a direct metal bridging group can result in steric congestion of the metal centres, reducing their potential to effect co-operative substrate activation. Furthermore, the intermetallic separation in such complexes is in large part determined by the identity of the bridging ligand. Changing the bridging group to achieve systematic variation of the intermetallic separation without significantly altering the rest of the complex is not straightforward. Diporphyrins belong to a separate and much smaller class of binucleating ligands which do not feature a direct metal bridging group but combine well-defined metal binding sites with good control of the intermetallic separation.

1.2 Diporphyrin ligands

Diporphyrin ligands were developed in the 1970s.[8-11] The first generation diporphyrins consisted of two porphyrin macrocycles strapped together by two to four linking chains in either the *meso*- or β-positions of the porphyrins (Figure 1.3, left). Due to the flexibility of the linking groups, most of these multiply strapped diporphyrins adopt a conformation where the two rings have slipped laterally with respect to each other (typically by *ca.* 3.5 Å) in order to maximise off-set π-π interactions between the macrocycles. This means that the metals do not sit directly above one another in the pockets and increases the M···M separation. A second generation of diporphyrin ligands was developed in the 1980s in which the two macrocycles were linked by a single rigid aromatic spacer (Figure 1.3, right and bottom).[12-14] In these single-pillared ligands, hereafter designated "co-facial diporphyrins", the slipping of the macrocycles is limited and the metals are kept reasonably vertically aligned. By changing the aromatic linker of a co-facial diporphyrin, the intermetallic separation and the angle between the porphyrin rings may be altered. The single

strap also imparts a degree of bite angle flexibility meaning the macrocycles can tilt inwards or outwards with respect to each other thus incorporating various different intermediates within the molecular cleft. This ability to "bite" on substrates is termed the "Pacman effect".[15]

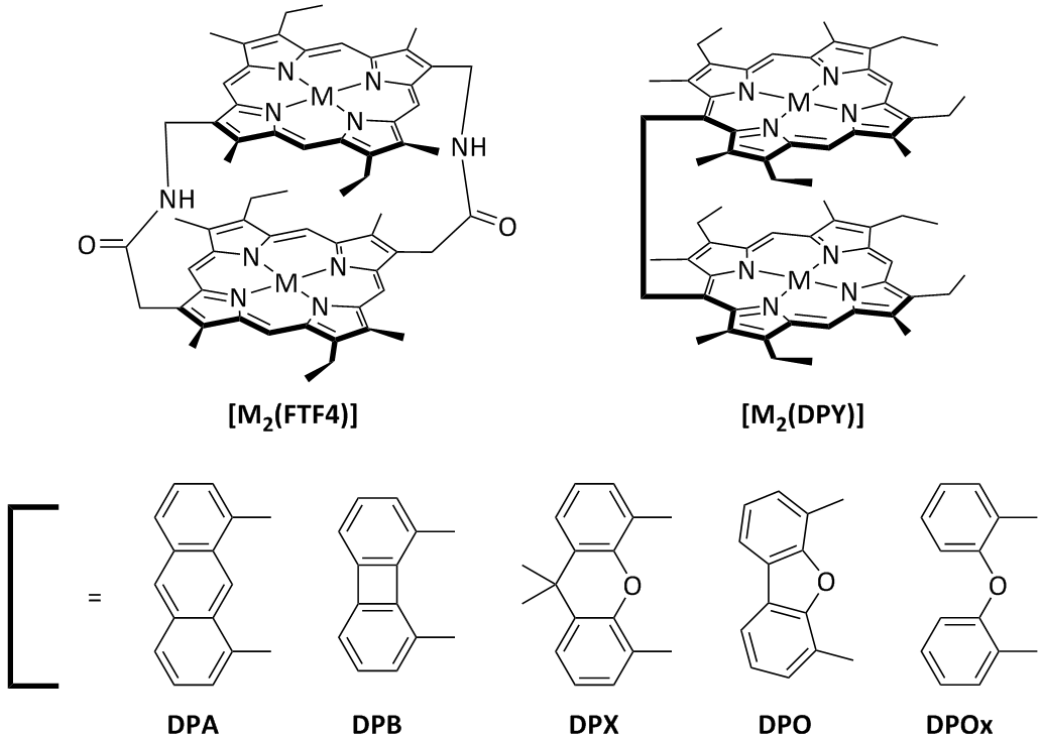

Figure 1.3 First (left) and second (right) generation diporphyrin complexes. FTF4 denotes a "face to face" diporphyrin with 4 atoms in the bridging straps. DPY refers to a generic singly strapped diporphyrin.

1.2.1 Reactivity of co-facial diporphyrin complexes

Numerous bimetallic complexes of co-facial diporphyrins have been prepared, mostly containing mid-to-late transition metals. Several of these metallated diporphyrins have been shown to be effective in a range of stoichiometric and catalytic transformations of small molecules.[16] For example, Collman and co-workers reported the successful electrocatalytic proton-coupled 4 e^- reduction of O_2 to water by a binuclear cobalt diporphyrin, [Co_2(FTF4)], absorbed on a graphite electrode.[17] No hydrogen peroxide was produced during catalysis, mirroring the activity of the enzyme cytochrome *c* oxidase. The binuclear Rh(II)/Rh(II) diporphyrin complex **1A** investigated by the Wayland group was found to co-operatively achieve the 2 e^- oxidative cleavage of alkyl C-H bonds within the intermetallic cleft to yield the Rh(III)/Rh(III) alkyl hydride complex **1B** (Scheme 1.1, left).[18] The reaction displayed remarkable selectivity for alkyl C-H bonds over aryl C-H or O-H

bonds, and the rate was significantly enhanced compared to similar reactions of mononuclear Rh(II) complexes.

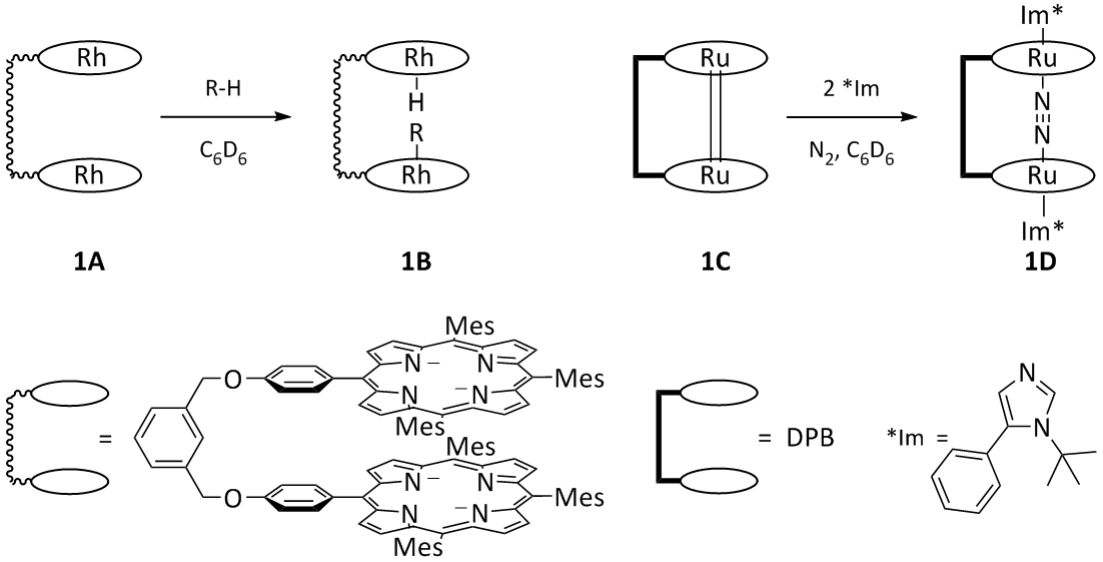

Scheme 1.1 Activation of alkyl C-H bonds (left)[18] and dinitrogen (right)[19] by binuclear co-facial diporphyrin complexes.

At each metal centre in a binuclear diporphyrin complex there are two vacant axial binding sites: *exo* and *endo* with respect to the intermetallic cleft. In certain cases it is necessary to block the *exo* axial co-ordination sites in order to direct the substrate to the *endo* intermetallic site. The presence of *exo* axial ligands can also enhance the activity of the complex by increasing the electron density at the metal centres. For example, Collman and co-workers synthesised the binuclear Ru(II) complex [Ru_2(DPB)] (**1C**) that contains a Ru=Ru bond and is unreactive towards N_2. *Exo* axial co-ordination of bulky imidazole donors resulted in cleavage of the Ru=Ru bond and in-cleft co-ordination of dinitrogen to form [(RuIm*)$_2$(μ-N_2)(DPB)] (**1D**, Scheme 1.1, right).[19,20] In contrast to similar monomeric ruthenium dinitrogen complexes, complex **1D** is robust; there was no evidence of dinitrogen dissociation after several freeze-pump-thaw degassing cycles.

Oxidation and alkylation of **1C** yielded [(RuR)$_2$(DPB)] (**1E$_{Ru}$**, Scheme 1.2), a bimetallic Ru(III) diporphyrin complex with alkyl ligands blocking the *exo* faces of the porphyrins. The osmium analogue, **1E$_{Os}$**, was prepared by an identical strategy. Both complexes were found to be moderate catalysts for the reduction of protons to H_2 at mercury pool electrodes in THF.[21] A similar transformation is carried out by hydrogenase enzymes in biological systems. The authors suggest that the relative orientation and proximity of the *endo* hydride ligands favoured the elimination of dihydrogen.

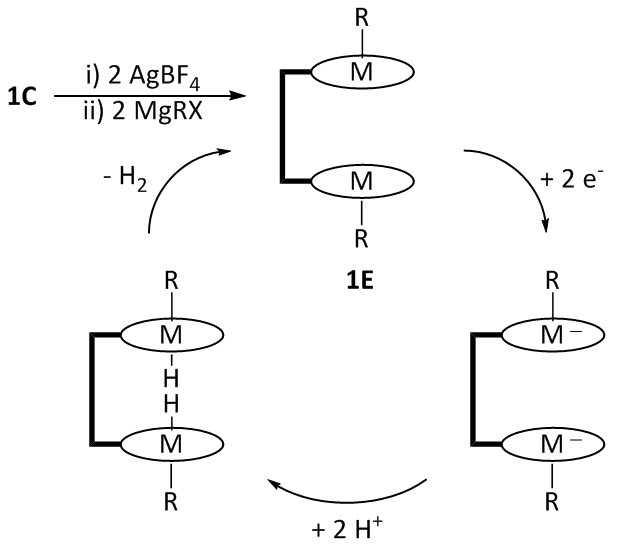

Scheme 1.2 Electrocatalytic reduction of protons to H_2.[21] The DPB ligand is shown in cartoon form. M = Ru, Os, R = Me, 4-C_6H_4Me, 3,5-$C_6H_3(CF_3)_2$.

Metallated co-facial diporphyrins have been proven to achieve a number of small molecule transformations but they have one significant disadvantage; the synthesis of the ligands is arduous and low yielding, with the original preparations of H_4DPA and H_4DPB involving 24 and 21 steps respectively.[12-14] Though subsequent optimisation has reduced the synthesis to 15 steps, the overall yield (*ca.* 3 %) remains poor.[22]

1.3 Pacman calixpyrroles

1.3.1 Synthesis

To overcome these limitations Love *et al.*[23] and Sessler *et al.*[24] independently developed and reported a new class of Pacman calixpyrroles which are far easier to synthesise and can fold into a geometry similar to a single pillared co-facial diporphyrin. The synthesis of Pacman calixpyrroles uses straightforward Schiff-base condensation methodology and is high yielding. The macrocycle is built from two basic building blocks: a ketone and a diamine. Initially the ketone undergoes an acid-catalysed condensation reaction with pyrrole to form a substituted dipyrromethane which is converted to the corresponding diformyldipyrromethane in a Vilsmeier-Haack reaction. The acid-templated condensation of two equivalents of the dialdehyde with two equivalents of a chosen diamine yields the [2+2] macrocyclic product after basic work-up (Scheme 1.3).[25]

The resultant macrocycles contain two pyrrole/imine N_4 donor pockets separated by aromatic spacers which derive from the diamine used in the cyclo-condensation. The *meso* substituents are determined by the ketone chosen. The macrocycle synthesis is tolerant of a

range of ketones and diamines, allowing preparation of ligands with different donor pocket separations and different *meso* head groups.[26] Of the various possibilities, two macrocycles are shown in Scheme 1.3: the octamethyl macrocycle, H_4L^{Me}, in which the donor pockets are separated by *ortho*-phenyl spacers, and the anthracene macrocycle, H_4L^{A}, which features longer, anthracenyl spacers. These are the two Pacman calixpyrroles used in the experimental work presented in this thesis.

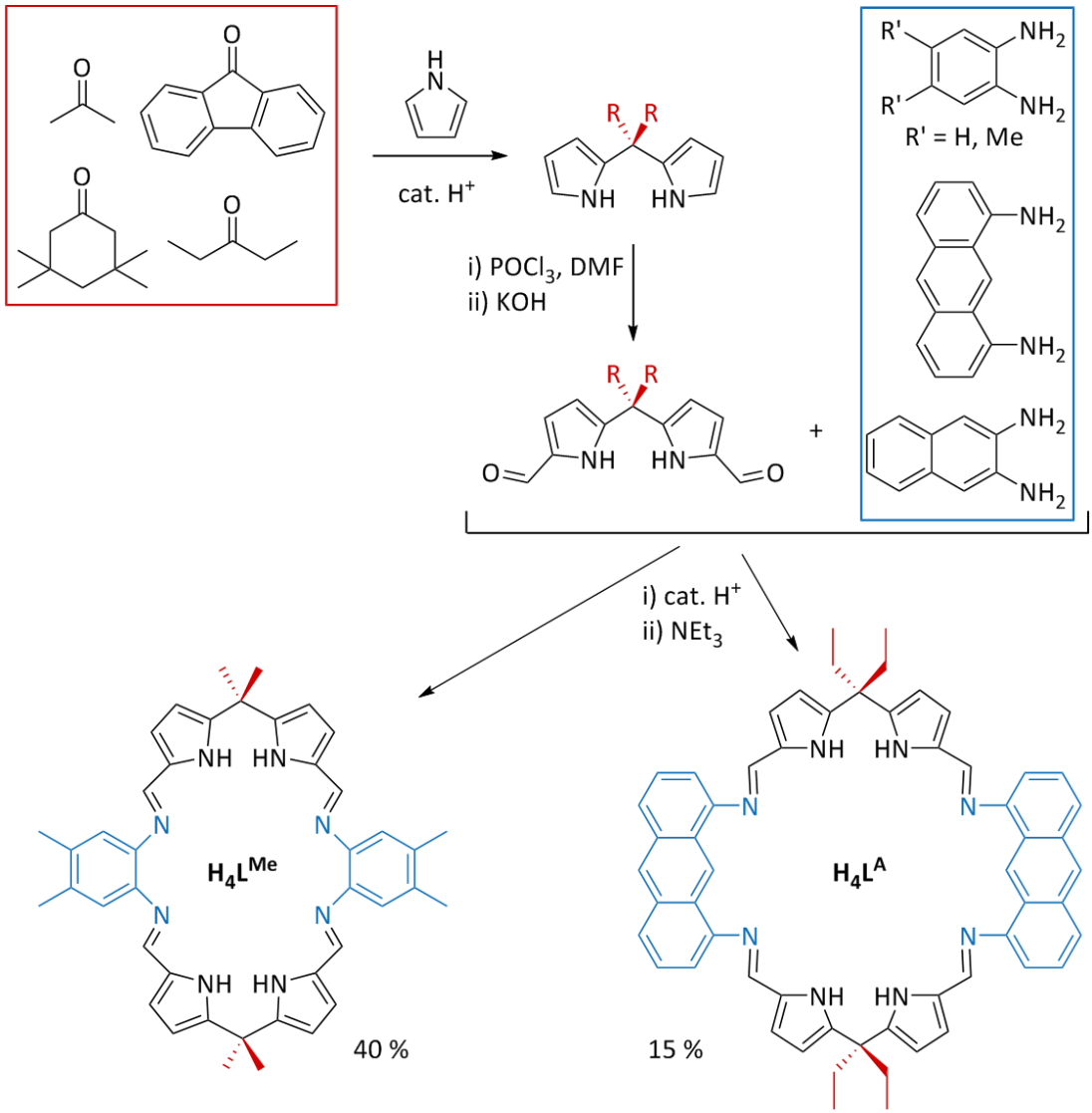

Scheme 1.3 Schiff-base synthesis of Pacman calixpyrroles. Yields are based on ketone.

The 1,2-diamino-substituted benzene required to prepare H_4L^{Me} is commercially available but 1,8-diaminoanthracene (DAAcene), required for the synthesis of H_4L^{A} is not. DAAcene is prepared in a two-step synthesis from commercially available 1,8-dinitroanthraquinone (DNAQ, Scheme 1.4). First, DNAQ is reduced to 1,8-diaminoanthraquinone (DAAQ) using excess sodium sulphide, then DAAQ is reduced to

DAAcene by excess sodium borohydride. This latter step must be carried out in the absence of light because DAAcene is photosensitive, decomposing to intractable dark solids if exposed to light. The subsequent condensation reaction to form H_4L^A must similarly be carried out in the dark but the macrocycle is light-stable once isolated and dried.[26]

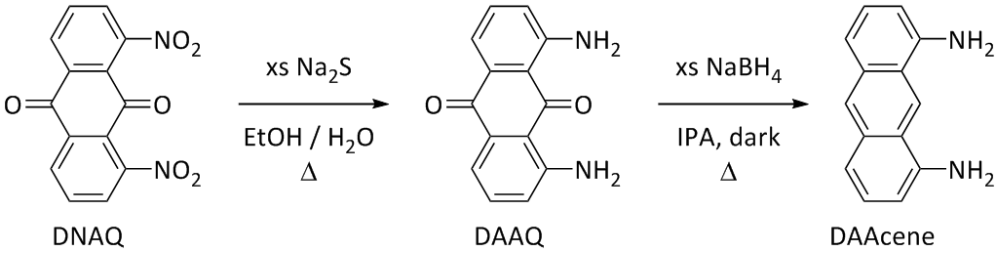

Scheme 1.4 Synthesis of 1,8-diaminoanthracene spacer.

The H_4L^A macrocycle bearing *meso* ethyl groups is the only anthracenyl hinged macrocycle that has been prepared. However, several *ortho*-phenyl hinged macrocycles have been synthesised with different *meso* groups and different substituents on the phenyl hinges. In general, the incorporation of the *ortho*-phenyl spacer in large part determines the structures of the metal complexes of these ligands, with the *meso* and phenyl substituents exerting more subtle steric and electronic effects. Therefore, unless it is necessary to specify otherwise, H_4L will be used to denote any *ortho*-phenyl hinged Pacman macrocycle in the remainder of this introduction, though the specific ligand will be shown explicitly in diagrams. H_4L^X refers to any Pacman calixpyrrole, with *ortho*-phenyl or anthracenyl spacers.

1.3.2 Metallation

Deprotonation of all four pyrrole NH groups of a H_4L^X macrocycle yields a 2− charge on each N_4 donor pocket. Therefore the macrocycles are ideally designed to incorporate M(II) ions. Three distinct metallation strategies have been employed (Scheme 1.5). If the metal starting material MX_2 is not strongly basic, such as MCl_2 or $M(OAc)_2$, then two options are available: (1) reaction of MX_2 with H_4L^X in the presence of a neutral base which co-operatively deprotonates the macrocycle or (2) initial deprotonation of H_4L^X by an alkali metal base, such as an amide or hydride, to generate the alkali metal salt of the macrocycle, which then undergoes a salt elimination reaction with MX_2. If the metal starting material is strongly basic, such as $M(NR_2)_2$, then a transamination strategy can be effective, where $M(NR_2)_2$ both deprotonates the macrocycle and provides M(II) ions in a single step (3).[25] Metal hexamethylsilylamides, $[M\{N(SiMe_3)_2\}_x]$, are commonly used in transamination reactions due to their high solubility in hydrocarbon solvents and the steric protection

provided by the bulky silylamide ligands to the metal centre. Hereafter the hexamethylsilylamide group will be abbreviated to N″.

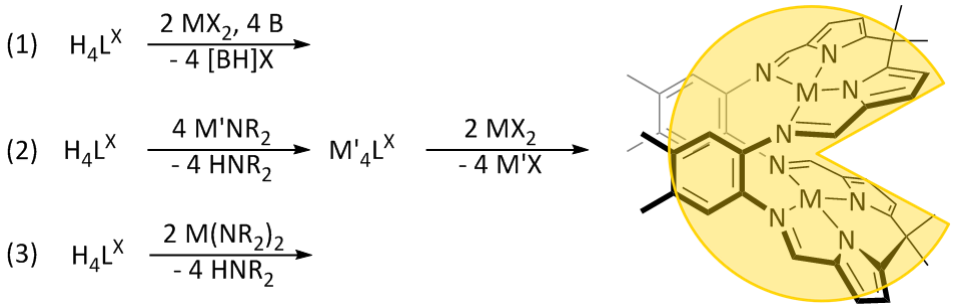

Scheme 1.5 Metallation strategies for Pacman macrocycles. For example: X = Cl, OAc, B = DABCO, NEt_3, M′ = Li, Na, K.

1.3.3 Metal binding modes

The *meso* sp^3 hybridised carbon atoms impart flexibility to the H_4L^X family of macrocycles, allowing then to accommodate a variety of metals and metallic fragments in different binding modes. In the generic $[M_2(L)]$ complex shown in Scheme 1.5 the ligand has folded upon metallation into the classic wedged-shaped Pacman geometry, reminiscent of the structures of the co-facial diporphyrins. The *ortho*-substituted aryl rings act as a pair of hinges about which the macrocycle folds, and as spacers between the two *pseudo* square planar N_4 donor compartments. When the macrocycles fold into the Pacman geometry, the *meso* substituents, which are equivalent in the free macrocycles, become desymmetrised since two groups are now *exo* with respect to the macrocyclic cleft and the other two are *endo*.

Pacman $[M_2(L^X)]$ complexes, where L^X is any Pacman calixpyrrole, have been synthesised for many transition metals, including Co(II),[27] Zn(II),[28] Mn(II), Ni(II), Cu(II) and Pd(II).[25] To facilitate structural comparison of Pacman complexes, it is useful to define two parameters: the bite angle, θ, and the torsional twist angle of the aryl hinges, Φ (Figure 1.4). The bite angle is only relevant to complexes of the *ortho*-phenyl hinged macrocycles and is defined as the angle between M1, the centroid of all twelve aryl hinge carbons, and M2. The torsional twist angle quantifies the lateral slipping of the two macrocycle pockets and is defined as the mean angle between the perpendiculars to the N_4 planes and the planes of the aryl hinges.

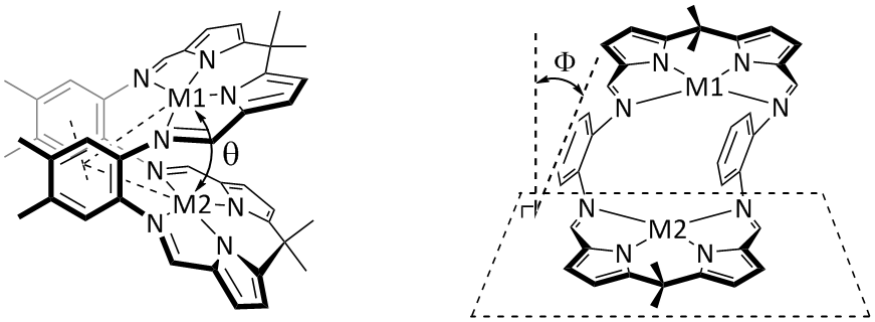

Figure 1.4 Illustration of the bite (θ) and twist (Φ) angles of Pacman complexes.

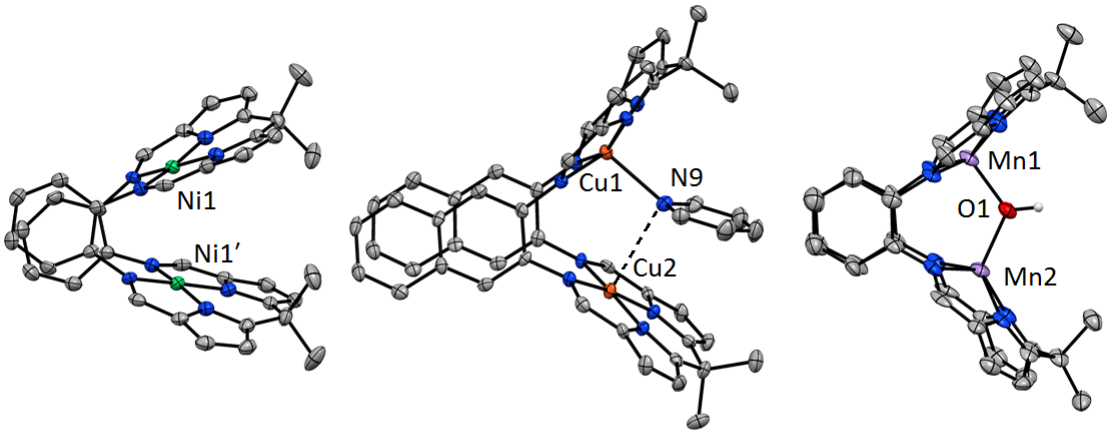

	$[Ni_2(L)]$	$[Cu_2(py)(L)]$	$[Mn_2(\mu\text{-}OH)(L)]$
θ (°)	55	60	50
Φ (°)	28	20	7

Figure 1.5 Solid state structures of three different transition metal Pacman complexes, detailing their bite (θ) and twist (Φ) angles.[25]

The simple Pacman complex $[Ni_2(L)]$ has a pronounced lateral twist of 28 ° which results in a bite angle of 55 ° that is decreased from the ideal 60° (Figure 1.5, left). This twisting maximises favourable off-set π-π stacking interactions between the aryl hinges of the macrocycle. If there is a bridging atom between the two metal centres within the macrocyclic cleft, as in the mixed-valent complex $[Mn_2(\mu\text{-}OH)(L)]$ (Figure 1.5, right), then the bridging group acts to anchor the two metals in vertical alignment and reduces the twisting of the macrocycle, in this case to 7 °. The bite angle in $[Mn_2(\mu\text{-}OH)(L)]$ is also lowered, to 50 °, because the bridging hydroxide causes the Mn ions to distort out of the N_4 planes, into the macrocyclic cleft. A solvent molecule may also be incorporated within the macrocyclic cleft, as in $[Cu_2(\textit{endo}\text{-py})(L)]$ (Figure 1.5, centre). The *pseudo* bridging binding mode of the pyridine in this complex is highly unusual and is induced by the constrained environment of the intermetallic cleft. There is considerable lateral slipping of the macrocycle pockets in $[Cu_2(\textit{endo}\text{-py})(L)]$ (twist angle = 20 °) which emphasises that there is no significant bonding interaction between N9 and Cu2.

The flexibility of the H_4L macrocycles means other metal binding modes are also accessible, unlike for the rigid co-facial diporphyrin ligands. If the macrocycles do not fold at the aryl hinge groups but instead flex about the *meso* carbon atoms then bowl-shaped complexes are produced (Figure 1.6). In Pacman complexes, the metal ions are bound to the two pyrrolides on either side of one *meso* carbon and the adjacent imines, one attached to each aryl hinge. In bowl complexes, the macrocycle co-ordination mode is switched so that the metal ion binds to both imines attached to a single arene ring and, in some cases, the two adjacent pyrrolide nitrogens. The bowl conformation has not been observed for complexes of the anthracenyl macrocycle, H_4L^A, because the separation of the two imines attached to each anthracene hinge is too great for one metal to be co-ordinated by both nitrogens.

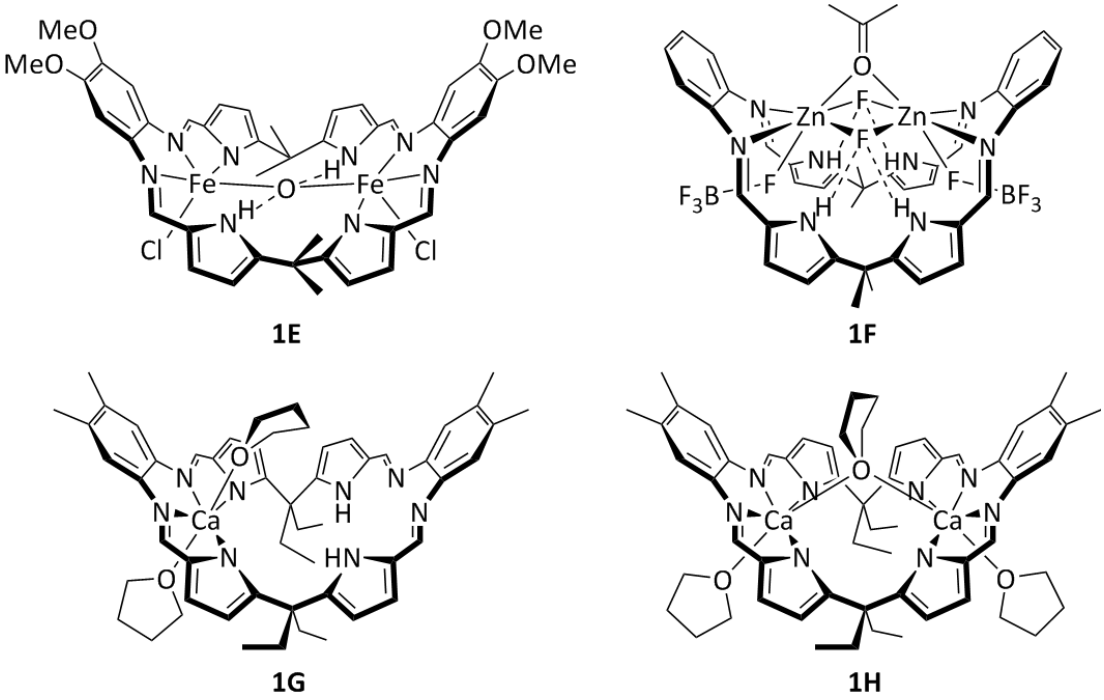

1E **1F**

1G **1H**

Figure 1.6 Bowl shaped complexes of calixpyrroles prepared by the Sessler (top)[29,30] and Love (bottom)[31,32] groups.

The bowl binding motif is most commonly observed when the pyrrole NHs are not fully deprotonated. Sessler and co-workers found that reaction of $[Fe_2Mes_4]$ with H_4L in THF followed by aerobic oxidation yielded the oxo-bridged Pacman complex $[Fe_2(\mu\text{-}O)(L)]$. However, carrying out the same reaction with the acid salt of the ligand $[H_4L(HCl)_2]$ generated $[(FeCl)_2(\mu\text{-}O)(H_2L)]$ (**1E**, Figure 1.6) in which each Fe(III) cation binds to two imine nitrogens and one pyrrolide nitrogen and the other two pyrroles remain protonated and hydrogen bond to the bridging oxo group.[29] The bowl complex $[Zn_2(\mu\text{-}F)_2(\mu\text{-}OCMe_2)(BF_4)_2(H_4L)]$ (**1F**) was prepared by reaction of $Zn(BF_4)_2$ with H_4L.[30] The Zn(II) cations co-ordinate solely to the imine nitrogens of the macrocycle which is a neutral

chelator since all four pyrrole nitrogens remaining protonated. The Zn(II) ions are *pseudo* octahedral, also binding to two bridging fluorides, a bridging acetone molecule and a BF_4^- ion. Hydrogen bonding between the pyrrole NHs and bridging fluorides stabilises the complex. Very recently it has also been demonstrated that the bowl geometry is adopted in preference to the Pacman geometry when large metal cations are introduced, even in fully deprotonated complexes. Reaction of one or two equivalents of $[Ca(N'')_2(THF)]$ with H_4L formed the monometallic or bimetallic bowl complexes, $[Ca(THF)_2(H_2L)]$ (**1G**)[31] or $[Ca_2(\mu\text{-}THF)(THF)_2(L)]$ (**1H**),[32] respectively. In both these complexes each Ca(II) ion binds to two imines and two pyrrolides with THF ligands occupying the axial sites.

1.4 Transition metal Pacman complexes

1.4.1 Oxygen reduction catalysis

Pacman calixpyrrole complexes have proven to be functional, as well as structural, models for co-facial diporphyrin complexes, with cobalt Pacman complexes also able to catalyse the 4 e^- reduction of O_2 to water. Love and co-workers reported that a THF solution of the binuclear cobalt complex of an *ortho*-phenyl hinged macrocycle, $[Co_2(L^0)]$, reacted immediately with O_2 upon exposure to air. NMR spectroscopy revealed that two different products were formed in a 9:1 ratio. Addition of pyridine to the reaction mixture facilitated structural characterisation of the major product, the Co(III)/Co(III) peroxide bridged complex **1J** (Scheme 1.6). The minor product was assigned as the Co(III)/Co(III) superoxide-bridged radical cation **1K**, on the basis of EPR spectroscopy. This mixture of compounds was able to slowly catalyse the reduction of oxygen to water. Its poor activity was attributed to the low concentration of the superoxide species, which is believed to be the route into the catalytic cycle, and the formation of unreactive peroxide and hydroxide bridged products.[33]

Love and co-workers made modifications to the ligand framework to try to improve catalytic activity. An *ortho*-phenyl hinged complex carrying bulky fluorenyl substituents at the *meso* positions, $[Co_2(L^F)]$, was prepared. It was hoped that the increased steric bulk at the *meso* positions would induce a greater lateral twist of the macrocycle pockets preventing formation of unreactive mono-atom bridged species. Reaction of $[Co_2(L^F)]$ with air formed a mixture of the superoxide-bridged complex $[Co_2(\mu\text{-}O_2)(L^F)(py)_2][OH]$ (**1L**) and the mixed valence Co(II)/Co(III) hydroxide-bridged complex $[Co_2(\mu\text{-}OH)(L^F)(py)]$ (**1M**), both of which were structurally characterised (Scheme 1.6). No peroxide species were observed. This

mixture of products proved to be a better oxygen reduction catalyst but evidently formation of unreactive bridged species was still inhibiting catalysis.[34]

Next $[Co_2(L^A)]$ was synthesised, in which the macrocycle hinges were extended from *ortho*-phenyl to anthracenyl. $[Co_2(L^A)]$ was unreactive towards O_2 in either THF or pyridine solution but formation of a new species was observed by ^1H NMR spectroscopy upon exposure of a PhCN solution of $[Co_2(L^A)]$ to O_2. The reaction was found to be reversible; applying vacuum regenerated the starting material $[Co_2(L^A)]$. The authors suggested that an adduct such as $[Co^{II}_2(O_2)(L^A)]$ (**1N**) was formed in the presence of O_2, facilitated by *exo* axial co-ordination of PhCN to the Co(II) centres. $[Co_2(L^A)]$ was found to be an efficient and selective catalyst for the reduction of oxygen to water in the presence of PhCN and could operate under less acidic conditions than the previously studied [Co_2(diporphyrin)] catalysts.[27] Formation of hydroxide or peroxide bridged decomposition products was successfully inhibited in the $[Co_2(L^A)]$ system by the increased intermetallic separation. This series of cobalt Pacman complexes illustrates the importance of being able to make straightforward and systematic variations to a ligand system.

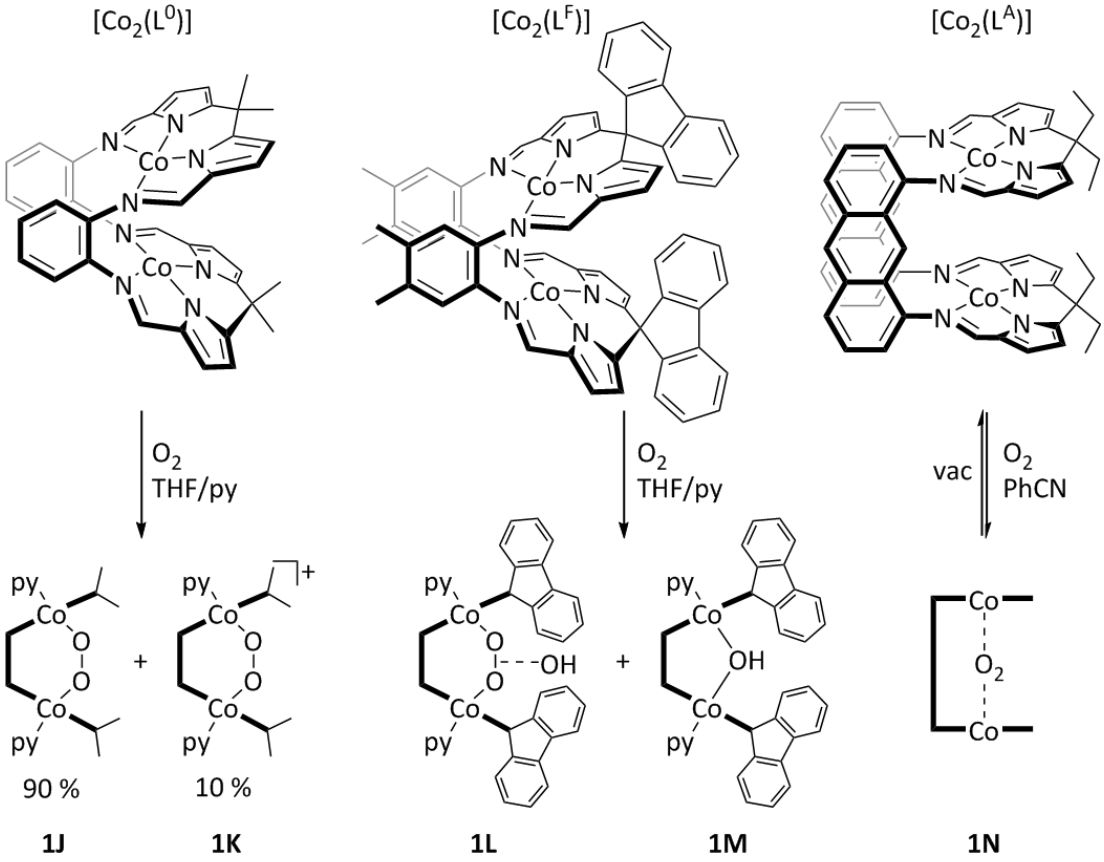

Scheme 1.6 Reactivity of binuclear cobalt Pacman complexes of different calixpyrroles towards O_2.[27,33,34] All $[Co_2(L)]$ complexes were synthesised by reaction of two equivalents of $[Co(N'')_2]$ with H_4L. The ligand frameworks are shown in cartoon form in complexes **1J** – **1N**.

1.4.2 Anion recognition

The intermetallic cleft established in Pacman complexes of the anthracenyl macrocycle was also found to be of ideal geometry for anion binding. Love and co-workers synthesised the binuclear zinc Pacman complex $[Zn_2(L^A)]$ by heating a mixture of $ZnEt_2$ and H_4L^A (Scheme 1.7).[28] $[Zn_2(L^A)]$ existed as $[Zn_2(L^A)]_n$ aggregates in solution, giving rise to a very complicated ^1H NMR spectrum. De-aggregation could be induced by dilution or addition of a very strongly co-ordinating solvent such as DMF. Salt elimination was also investigated as an alternative method of preparing $[Zn_2(L^A)]$. However, deprotonation of the macrocycle with excess KH followed by addition of $ZnCl_2$ resulted in isolation of the "-ate" salt $[K(THF)_6][Zn_2(\mu\text{-}Cl)(L^A)]$, in which one chloride ion is trapped in the macrocyclic cavity, bridging the Lewis acidic zinc ions.

This observation encouraged the authors to investigate the affinity of $[Zn_2(L^A)]$ towards the different halide ions. Addition of $[NBu_4][X]$, where X= Cl, Br, I and OH, to a THF solution of $[Zn_2(L^A)]_n$ promoted de-aggregation of the starting material. However in-cleft anion binding was only observed for the chloride and hydroxide anions. In these cases, two sharp sets of resonances were observed in the resultant ^1H NMR spectra corresponding to monomeric $[Zn_2(L^A)]$ and the anion incorporated complex $[NBu_4][Zn_2(\mu\text{-}X)(L^A)]$. Over time $[NBu_4][Zn_2(\mu\text{-}X)(L^A)]$ was formed exclusively (Scheme 1.7). The observed selectivity for Cl^- over Br^- or I^- was supported by theoretical calculations which showed that the Br^- and I^- anions would be poorly accommodated within the macrocyclic cleft, resulting in much less stable complexes. The calculations also revealed that hydroxide bound far more strongly than chloride, limiting the potential halide sensing applications of $[Zn_2(L^A)]$ to rigorously anhydrous systems.

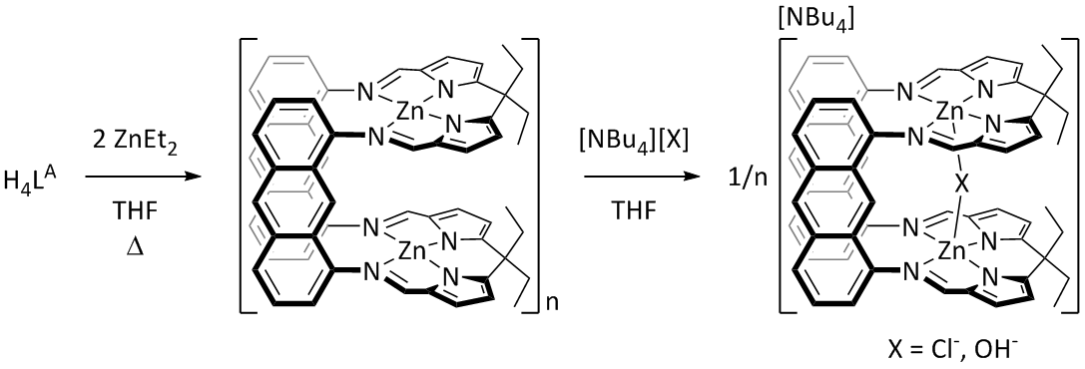

Scheme 1.7 Synthesis of a zinc Pacman complex and in-cleft anion incorporation in its reaction with ammonium salts.[28]

1.4.3 Early transition metal Pacman complexes

All the co-facial diporphyrin and Pacman calixpyrrole complexes discussed above have contained mid-to-late transition metals. Indeed, very little exploration of the early transition metal chemistry of these systems has been undertaken. Love and co-workers have synthesised materials of empirical formula $[(MCl)_2(L)]$, where M = Ti and V, by deprotonating H_4L with excess KH and then performing a salt elimination reaction with two equivalents of $MCl_3(THF)_3$ (Scheme 1.8).[35] Neither complex was characterised in the solid state so it is not known whether their structures are monomeric or oligomeric with chloride ions bridging between different macrocycles. However, serendipitous partial oxidation/hydrolysis of the vanandium compound $[(VCl)_2(L)]$ resulted in crystallisation of the mixed-valent V(III)/V(IV) complex [(V=O)(THF)(VCl)(L)] (**1P**).

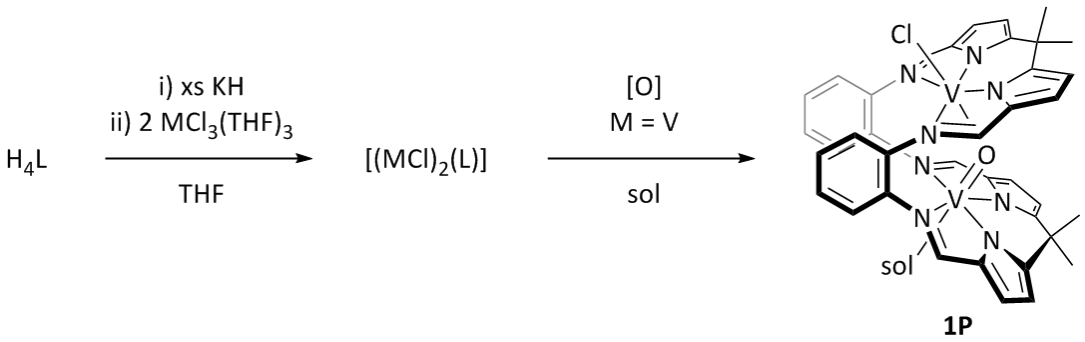

Scheme 1.8 Sythesis of Ti(III) and V(III) Pacman complexes and partial hydrolysis to form a mixed-valent V(III)/V(IV) complex.[35] M = Ti, V, sol = THF, py.

In complex **1P** one V ion has been oxidised to the vanadyl cation, $(V^{IV}O)^{2+}$ while the other remains in the +3 oxidation state. Both V centres are octahedral; the remaining Cl^- ligand occupies the *exo* axial site at the V(III) ion while a molecule of donor solvent (THF or pyridine) co-ordinates *exo* to the vanadyl cation and the *endo* vanadyl oxo group bridges to the V(III) ion. Compound **1P** is the first structurally characterised mixed-valent bridging vanadyl complex and this unusual vanadyl co-ordination mode is likely imposed by the constrained Pacman environment. Complex **1P** remains the only early transition metal Pacman complex that has been characterised in the solid state.

1.5 Uranium Pacman complexes

The bulk of the uranium Pacman investigations undertaken in the Arnold and Love groups have focussed on high oxidation state uranium chemistry. There is much interest in the complexation and transformation of the uranyl dication, $(UO_2)^{2+}$, a soluble, highly stable, linear species where uranium is in its highest oxidation state of +6. In the environment, uranium exists predominantly in this form but cation-cation interactions with other solution metal species can lead to reduction of $(UO_2)^{2+}$ to insoluble U(IV) species *via* the unstable uranyl monocation, $(UO_2)^{+}$. Study of the reactivity of the uranyl dication in a controlled environment may provide valuable insight into the reactions and speciation occurring in nuclear waste.[36]

1.5.1 Mono-uranyl Pacman complexes

The uranyl dication cannot be incorporated into the cavity of porphyrin macrocycles due to the large ionic radius of uranium. However, the flexibility of the Pacman calixpyrroles facilitated uranyl complexation. The room temperature transamination reaction between H_4L and the uranyl silylamide $[UO_2(N'')_2(THF)_2]$ formed exclusively the mono-uranyl Pacman complex $[(UO_2)(sol)(H_2L)]$ (**1Q**, Scheme 1.9, sol = THF, py), even if excess $[UO_2(N'')_2(THF)_2]$ was added.[37] The U centre in **1Q** is pentagonal bipyramidal, binding to the four N donors of the macrocycle and a molecule of THF which sits between the aryl hinges and the two axial oxo groups, one of which is *exo* and one *endo* with respect to the macrocyclic cleft. The complex is stabilised by hydrogen bonding between the remaining pyrrole NHs in the bottom macrocycle pocket and the *endo* oxo group. Significantly, the uranyl dication is desymmetrised in **1Q** due to the differing *endo* and *exo* environments of the two O atoms. This asymmetry has been exploited in further reactivity.

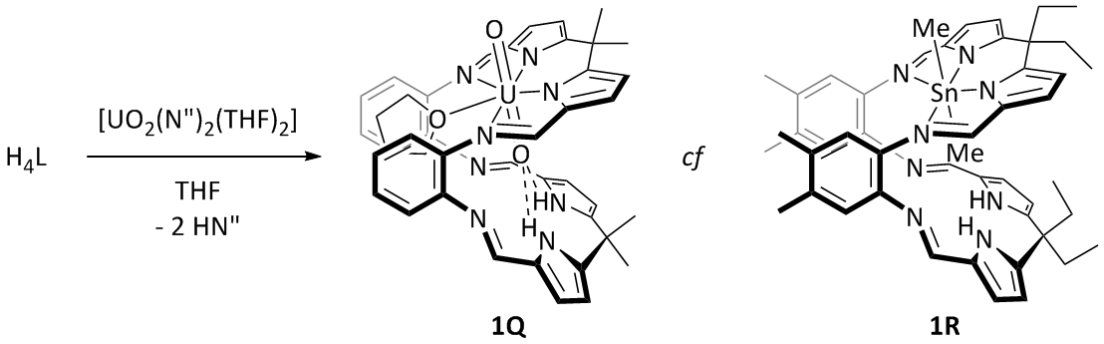

Scheme 1.9 Synthesis of mono-uranyl Pacman complex **1Q** [37] and structural comparison with dimethyl tin complex **1R**.[38]

With the exception of the mono-calcium bowl complex **1G**, all the other metal complexes of Pacman ligands discussed have contained two metal ions, one occupying each macrocycle pocket. The preparation of monometallic Pacman complexes is difficult because the binding of one metal cation causes the macrocycle to fold, simultaneously establishing the second metal binding pocket so insertion of a second metal ion into the same macrocycle is favoured over metallation of another, unfolded macrocycle. In the case of **1Q** mono-metallation occurs because of the steric demands of the strictly linear uranyl unit; if one $(UO_2)^{2+}$ unit were incorporated in each macrocycle pocket the two *endo* oxo groups would clash. Similar steric selectivity has been observed in the formation of a monometallic tin Pacman complex. Reaction of $SnMe_2Cl_2$ with H_4L in the presence of DABCO formed $[(SnMe_2)(H_2L)]$ (**1R**, Scheme 1.9) in which linearly disposed *exo* and *endo* methyl groups are bound to the tin centre.[38]

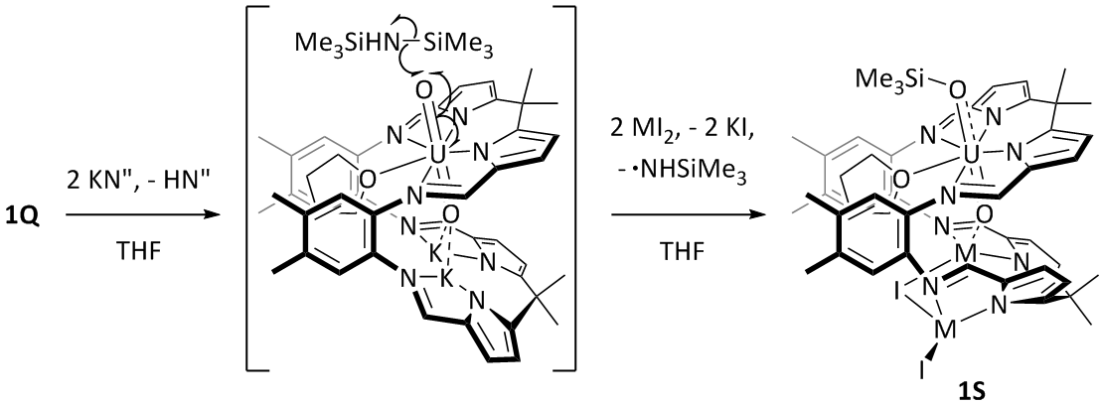

Scheme 1.10 Reductive silylation of the uranyl dication. M = Fe, Zn.[39]

The vacant lower binding pocket in complex **1Q** has allowed the preparation of a variety of hetero bi- and multi-metallic uranyl Pacman complexes,[40] some of which feature reduced uranyl(V) units. The one pot reaction between **1Q**, KN″, and MI_2, where M = Fe, Zn, resulted in formation of complex **1S** (Scheme 1.10) in which the uranyl dication has been reduced to the uranyl(V) monocation with a silylated *exo* oxo group, and two (MI) units are bound within the lower macrocycle pocket.[39] Following mechanistic investigation, it was suggested that initial deprotonation of the remaining pyrrole NHs formed an intermediate species in which two K^+ ions co-ordinate to the *endo* oxo, thereby activating the uranyl moiety towards homolytic cleavage of an N-Si bond in the silylamine by-product (Scheme 1.10). A salt elimination reaction with MX_2 then yields the observed product **1S**.

Complex **1S** contains a reduced uranyl(V) unit bound to a d-block metal but similar complexes featuring s- and f- metals have also been synthesised. It was found that reaction of **1Q** with two equivalents of lithium diisopropylamide (LDA) in pyridine solution formed the uranyl(V) complex **1T** (Figure 1.7, left) where lithium cations are co-ordinated to both the *exo* and *endo* uranyl oxo groups.[41] Uranyl reduction takes place upon addition of the second equivalent of LDA. Homolytic cleavage of the Li-N bond yields **1T** and releases an aminyl radical which is quenched by the solvent. Similarly, reaction of **1Q** with lanthanide reagents LnA_3 (A = N″, OAr) resulted in insertion of the Ln(III) cation into the bottom pocket of the macrocycle where it co-ordinates to the *endo* uranyl oxo group and reduces the U(VI) centre to U(V) by homolysis of the remaining Ln-A bond. The uranyl(V) complexes dimerise with the *exo* oxo groups bridging between the U(V) centres (**1U**, Figure 1.7, right).[42,43] These reductions of the uranyl dication are highly unusual. Classic reducing agents were not employed in any of the reactions. Instead, the observed products illustrate the propensity of uranyl(VI) to undergo 1 e^- reduction in the presence of substrates containing bonds that are susceptible to homolytic cleavage.

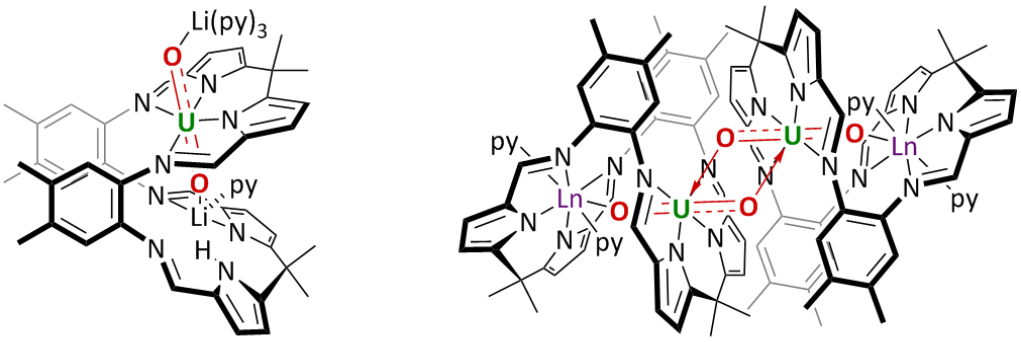

1T **1U**

Figure 1.7 Uranyl(V) complexes formed by reaction of **1Q** with s- [41] and f-block [42,43] metal reagents. Ln = Sc, Y, Ce, Sm, Eu, Gd, Dy, Er, Yb, Lu.

1.5.2 Bis-uranyl Pacman complexes

Expansion of the Pacman macrocycle hinges from *ortho*-phenyl to anthracenyl allowed two linear $(UO_2)^{2+}$ units to be incorporated. Reaction of H_4L^A with two equivalents of $[UO_2(N'')_2(py)_2]$ in pyridine solution formed the bis-uranyl Pacman complex $[(UO_2)_2(L^A)(py)_2]$ (**1V**, Scheme 1.11).[44] The U(VI) centres in **1V** are once again pentagonal bipyramidal, this time with a molecule of pyridine co-ordinated in the fifth equatorial site between the ligand hinges. The pockets of the macrocycle are laterally twisted (Φ = 23 °) in order to maximise the separation of the *endo* oxo groups, but even so the *endo* O···O separation is short at 2.709(6) Å.

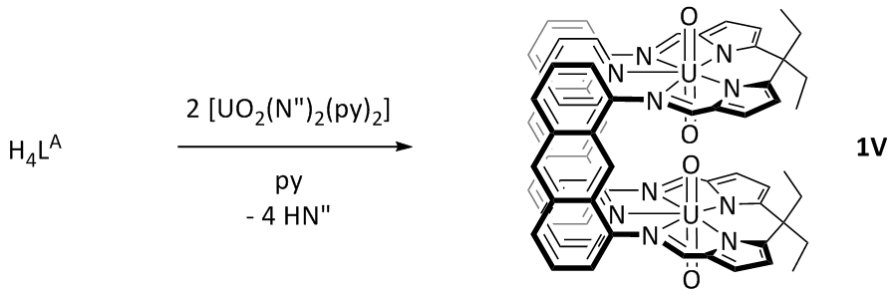

Scheme 1.11 Synthesis of the bis-uranyl Pacman complex **1V**.[44]

Recently it was discovered that under forcing conditions it is in fact possible to insert two uranyl groups into the *ortho*-phenyl hinged macrocycle H_4L^{Me}. Thus, reaction of mono-uranyl complex **1Q** with a further 1.5 equivalents of $[UO_2(N'')_2(py)_2]$ in pyridine at 120 °C or reaction of the free macrocycle with 2.5 equivalents of $[UO_2(N'')_2(py)_2]$ under the same conditions resulted in formation of the reduced, silylated bis-uranyl(V) complex **1W** along with an oligomeric by-product (Scheme 1.12).[45]

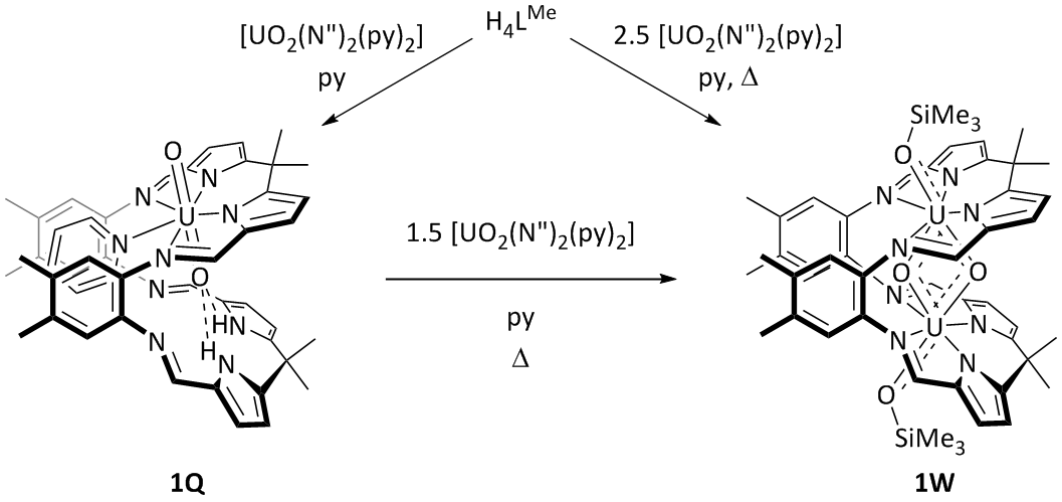

Scheme 1.12 Synthetic routes to the silylated bis-uranyl(V) Pacman complex **1W**.[45]

Complex **1W** features U(V) ions bounds in each N_4 donor pocket of the macrocycle, each with an *exo* axial siloxide ligand, and bridged by two *endo* oxo groups, forming a diamond shaped U_2O_2 core. The resultant U···U separation of 3.3557(5) Å is extremely short and there is strong electronic coupling between the U(V) centres. The complex is highly unusual because the normal mutually *trans* arrangement of the uranyl oxo ligands has been disrupted; one of the *endo* oxo groups remains *trans* to both *exo* siloxide ligands but the other *endo* oxo is *cis* to both *exo* axial siloxides. The uranyl(VI) starting materials were reduced to uranyl(V) during the formation of **1W** and the *exo* oxo groups were silylated. These silyl groups originated from the uranyl silylamide starting material and their incorporation accounts for the need for super-stoichiometric quantities of $[UO_2(N'')_2(py)_2]$ in

the reaction. Presumably, the reductive silylation occurs through homolytic cleavage of N-Si bonds in the excess $[UO_2(N'')_2(py)_2]$.

Complex **1W** proved to be remarkably inert towards disproportionation, oxidation or hydrolysis. An elegant study of the redox reactivity of **1W** reported by Arnold, Love and co-workers demonstrated that the source of this stability was the *exo* silyl groups, which effectively act as protecting groups.[46] Reaction of **1W** with two equivalents of potassium yielded the potassium salt of the doubly reduced U(IV)/U(IV) Pacman complex **1X** (Scheme 1.13, step i). Addition of iodine to **1X** quantitively regenerated the U(V)/U(V) starting material **1W** with the elimination of KI. However re-oxidation of **1X** with pyridine-N-oxide formed the new U(V)/U(V) material $K_2[(UO_2)_2(L^{Me})]$ (**1Y**, step ii) with the elimination of $(SiMe_3)_2O$, presumably driven by the formation of strong Si-O bonds. Complex **1Y** contains two uranyl(V) centres bridged by two *endo* oxo groups and is therefore analogous to complex **1W** but without the protecting $SiMe_3$ groups. In contrast to **1W**, **1Y** reacted rapidly with dry O_2 to yield the oxidised bis-uranyl(VI) "-ate" complex **1Z** where the U(VI) centres are bridged by an η^2 bound peroxide anion (step iii).

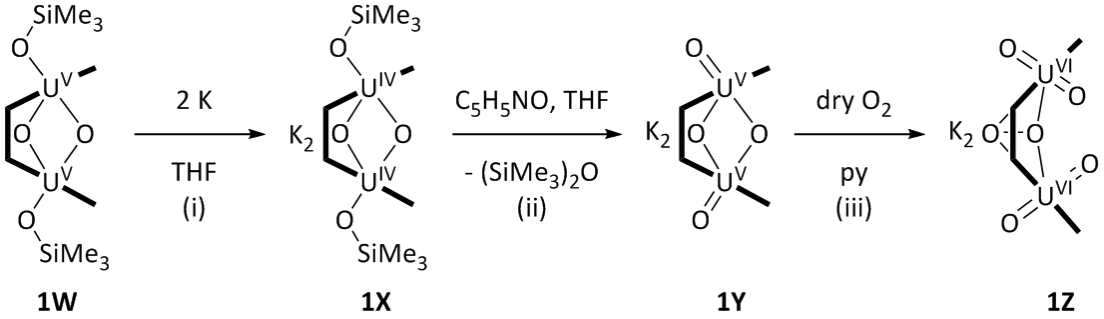

Scheme 1.13 Successive reactions of the bis-uranyl(V) Pacman complex with oxidising and reducing agents.[46] The ligand is shown in cartoon form and solvent molecules bound to the K^+ ions and the resulting complex nuclearities are not shown.

Therefore, by forming the reduced bis-uranyl(V) complex **1W**, deprotecting it and then oxidising it, it was in fact possible to form a bis-uranyl(VI) complex of an *ortho*-phenyl hinged Pacman macrocycle. However, the macrocycle has to distort considerably to incorporate the two linear $(UO_2)^{2+}$units. The bite angle of complex **1Z** has expanded to 90 ° compared to 61 ° in **1W** in order to maximise the *endo* oxo separation (O···O = 2.679(9) Å), which is only slightly shorter than that seen in the bis-uranyl anthracene Pacman complex **1V**. The U···U separation of 3.9824(4) Å is significantly increased from that found in the strongly coupled complex **1W**. This series of uranyl complexes emphasises the considerable flexibility of the Pacman calixpyrroles.

1.5.3 Low oxidation state uranium Pacman chemistry

The reactivity of low oxidation state, non-uranyl, uranium precursors with Pacman macrocycles has been much less extensively researched and the investigations that have been undertaken have focussed on the lowest readily accessible oxidation state of uranium, U(III).

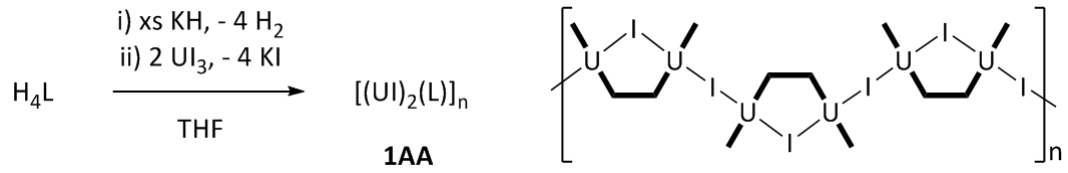

Scheme 1.14 Synthesis of binuclear uranium Pacman complex **1AA** and its suggested solid state structure (right).[47] The ligand is shown in cartoon form.

The reaction between the *ortho*-phenyl hinged Pacman macrocycle, H_4L, bearing methyl or ethyl *meso* substitutents, with excess potassium base followed by two equivalents of UI_3 was investigated and brown solids of composition $[(UI)_2(L)]$ (**1AA**) were obtained from the reaction mixture (Scheme 1.14).[47] Further characterisation of the product was challenging due to the poor solubility of the isolated material in common laboratory solvents and single crystals were not obtained. Solid state magnetic measurements suggested that **1AA** has an oligomeric structure with neighbouring macrocycles linked by iodide bridges (Scheme 1.14, right) and this model is consistent with its low solubility. The only further reactivity attempted with **1AA** was its reaction with KBH_4. The new material obtained, of composition $[\{U(BH_4)\}_2(L)]$, was similarly intractable and is also believed to have an oligomeric structure in the solid state.

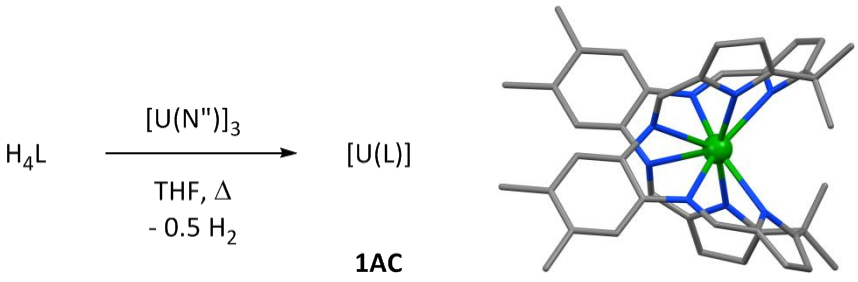

Scheme 1.15 Synthesis of encapsulated U(IV) Pacman complex **1AC** and its solid state structure.[48]

The transamination reaction between H_4L and $U(N'')_3$ was also investigated.[48] In THF solution at room temperature the reaction formed a mixture of two products, **1AB**, assigned as $[U(N'')(H_2L)]$ and **1AC**. Repeating the reaction in boiling THF yielded solely the thermodynamic product **1AC**. Structural characterisation of **1AC** revealed it to be the monometallic, macrocycle-encapsulated U(IV) complex [U(L)] (Scheme 1.15). Complex **1AC** is assumed to be formed from **1AB** by transamination of one remaining pyrrole N-H

bond followed swiftly by homolytic cleavage of the other, resulting in 1 e^- oxidation of U(III) to U(IV) and release of H_2. The U(IV) ion in **1AC** is eight co-ordinate with distorted square anti prismatic geometry. As is evident from the solid state structure, the macrocycle distorts considerably, with the aryl hinges rotating away from each other to enable the jaws to clamp down on the single U(IV) ion, encapsulating it fully.

1.6 Aims

Pacman calixpyrroles have proven to be versatile ligands, promoting the formation of well-defined binuclear complexes of a range of metals from different areas of the periodic table. Binuclear Pacman complexes have effected catalytic transformations of small molecules and revealed hitherto unknown actinide bonding motifs. However, there is much Pacman chemistry still to be explored. There is a notable lack of binuclear early transition metal Pacman or co-facial diporphyrin complexes and consequently, virtually no study of the reactivity of such systems has been undertaken. In the Arnold and Love groups there is a particular interest in uranium chemistry. Though the uranyl Pacman complexes have revealed much about the reactivity of the uranyl dication, previously considered an inert unit, well-characterised binuclear U(III)/U(III) Pacman complexes have not been prepared. Low oxidation state uranium complexes have much greater potential application in small molecule activation (see 3.1).

Therefore the aims of the experimental work presented in this thesis were two-fold. The first aim was to synthesise and fully characterise a binuclear early transition metal Pacman complex and explore its reactivity. For this purpose, chromium was selected due to the wealth of redox chemistry it exhibits and its significant role in industrial polymerisation (see 2.1). The second aim was to synthesise and fully characterise a binuclear U(III)/U(III) Pacman complex and investigate its interactions with small molecules. There has been very limited exploitation of the uranium chemistry of the anthracene Pacman ligand so this was identified as a starting point for investigations.

1.7 References

(1) B. E. Smith, *Science*, **2002**, *297*, 1654.

(2) T. Tsukihara, H. Aoyama, E. Yamashita, T. Tomizaki, H. Yamaguchi, K. Shinzawa-Itoh, R. Nakashima, R. Yaono, S. Yoshikawa, *Science*, **1995**, *269*, 1069.

(3) T. M. Powers, T. A. Betley, *J. Am. Chem. Soc.*, **2013**, *135*, 12289.

(4) A. L. Gavrilova, B. Bosnich, *Chem. Rev.*, **2004**, *104*, 349.

(5) N. Tsukada, O. Tamura, Y. Inoue, *Organometallics*, **2002**, *21*, 2521.

(6) F. S. Keij, R. A. G. de Graaff, J. G. Haasnoot, J. Reedijk, *J. Chem. Soc., Dalton Trans.*, **1984**, 2093.

(7) X.-H. Bu, S.-L. Lu, R.-H. Zhang, D.-Z. Liao, S. Aoki, T. Clifford, E. Kimura, *Inorg. Chim. Acta*, **2000**, *298*, 50.

(8) H. Ogoshi, H. Sugimoto, Z.-i. Yoshida, *Tetrahedron Lett.*, **1977**, *18*, 169.

(9) C. K. Chang, M.-S. Kuo, C.-B. Wang, *J. Heterocycl. Chem.*, **1977**, *14*, 943.

(10) N. E. Kagan, D. Mauzerall, R. B. Merrifield, *J. Am. Chem. Soc.*, **1977**, *99*, 5484.

(11) J. P. Collman, C. M. Elliott, T. R. Halbert, B. S. Tovrog, *Proc Natl Acad Sci U S A*, **1977**, *74*, 18.

(12) C. K. Chang, I. Abdalmuhdi, *J. Org. Chem.*, **1983**, *48*, 5388.

(13) C. K. Chang, I. Abdalmuhdi, *Angew. Chem., Int. Ed. Engl.*, **1984**, *23*, 164.

(14) S. S. Eaton, G. R. Eaton, C. K. Chang, *J. Am. Chem. Soc.*, **1985**, *107*, 3177.

(15) Y. Deng, C. J. Chang, D. G. Nocera, *J. Am. Chem. Soc.*, **1999**, *122*, 410.

(16) J. P. Collman, P. S. Wagenknecht, J. E. Hutchison, *Angew. Chem., Int. Ed. Engl.*, **1994**, *33*, 1537.

(17) J. P. Collman, M. Marrocco, P. Denisevich, C. Koval, F. C. Anson, *Journal of Electroanalytical Chemistry and Interfacial Electrochemistry*, **1979**, *101*, 117.

(18) W. Cui, B. B. Wayland, *J. Am. Chem. Soc.*, **2004**, *126*, 8266.

(19) J. P. Collman, J. E. Hutchison, M. A. Lopez, R. Guilard, R. A. Reed, *J. Am. Chem. Soc.*, **1991**, *113*, 2794.

(20) J. P. Collman, J. E. Hutchison, M. A. Lopez, R. Guilard, *J. Am. Chem. Soc.*, **1992**, *114*, 8066.

(21) J. P. Collman, Y. Ha, P. S. Wagenknecht, M. A. Lopez, R. Guilard, *J. Am. Chem. Soc.*, **1993**, *115*, 9080.

(22) J. Rosenthal, D. G. Nocera, *Acc. Chem. Res.*, **2007**, *40*, 543.

(23) G. Givaja, A. J. Blake, C. Wilson, M. Schröder, J. B. Love, *Chem. Commun.*, **2003**, 2508.

(24) J. L. Sessler, W.-S. Cho, S. D. Dudek, L. Hicks, V. M. Lynch, M. T. Huggins, *J. Porph. Phthalocy.*, **2003**, *7*, 97.

(25) G. Givaja, M. Volpe, J. W. Leeland, M. A. Edwards, T. K. Young, S. B. Darby, S. D. Reid, A. J. Blake, C. Wilson, J. Wolowska, E. J. L. McInnes, M. Schröder, J. B. Love, *Chem. Eur. J.*, **2007**, *13*, 3707.

(26) E. Askarizadeh, A. M. J. Devoille, D. M. Boghaei, A. M. Z. Slawin, J. B. Love, *Inorg. Chem.*, **2009**, *48*, 7491.

(27) A. M. J. Devoille, J. B. Love, *Dalton Trans.*, **2012**, *41*, 65.

(28) A. M. J. Devoille, P. Richardson, N. L. Bill, J. L. Sessler, J. B. Love, *Inorg. Chem.*, **2011**, *50*, 3116.

(29) J. M. Veauthier, W.-S. Cho, V. M. Lynch, J. L. Sessler, *Inorg. Chem.*, **2004**, *43*, 1220.

(30) E. Tomat, L. Cuesta, V. M. Lynch, J. L. Sessler, *Inorg. Chem.*, **2007**, *46*, 6224.

(31) J. W. Leeland, PhD Thesis, University of Edinburgh, 2011, *"Macrocyclic pacman complexes for secondary coordination sphere control"*.

(32) E. A. Connolly, J. B. Love, *unpublished work*

(33) G. Givaja, M. Volpe, M. A. Edwards, A. J. Blake, C. Wilson, M. Schröder, J. B. Love, *Angew. Chem., Int. Ed. Engl.*, **2007**, *46*, 584.

(34) E. Askarizadeh, S. B. Yaghoob, D. M. Boghaei, A. M. Z. Slawin, J. B. Love, *Chem. Commun.*, **2010**, *46*, 710.

(35) M. Volpe, S. D. Reid, A. J. Blake, C. Wilson, J. B. Love, *Inorg. Chim. Acta*, **2007**, *360*, 273.

(36) P. L. Arnold, J. B. Love, D. Patel, *Coord. Chem. Rev.*, **2009**, *253*, 1973.

(37) P. L. Arnold, A. J. Blake, C. Wilson, J. B. Love, *Inorg. Chem.*, **2004**, *43*, 8206.

(38) J. W. Leeland, A. M. Z. Slawin, J. B. Love, *Organometallics*, **2010**, *29*, 714.

(39) P. L. Arnold, D. Patel, C. Wilson, J. B. Love, *Nature*, **2008**, *451*, 315.

(40) P. L. Arnold, D. Patel, A. J. Blake, C. Wilson, J. B. Love, *J. Am. Chem. Soc.*, **2006**, *128*, 9610.

(41) P. L. Arnold, A. F. Pecharman, E. Hollis, A. Yahia, L. Maron, S. Parsons, J. B. Love, *Nat. Chem.*, **2010**, *2*, 1056.

(42) P. L. Arnold, E. Hollis, F. J. White, N. Magnani, R. Caciuffo, J. B. Love, *Angew. Chem., Int. Ed.*, **2011**, *50*, 887.

(43) P. L. Arnold, E. Hollis, G. S. Nichol, J. B. Love, J.-C. Griveau, R. Caciuffo, N. Magnani, L. Maron, L. Castro, A. Yahia, S. O. Odoh, G. Schreckenbach, *J. Am. Chem. Soc.*, **2013**, *135*, 3841.

(44) P. L. Arnold, G. M. Jones, Q.-J. Pan, G. Schreckenbach, J. B. Love, *Dalton Trans.*, **2012**, *41*, 6595.

(45) P. L. Arnold, G. M. Jones, S. O. Odoh, G. Schreckenbach, N. Magnani, J. B. Love, *Nat. Chem.*, **2012**, *4*, 221.

(46) G. M. Jones, P. L. Arnold, J. B. Love, *Angew. Chem., Int. Ed. Engl.*, **2012**, *51*, 12584.

(47) P. L. Arnold, N. A. Potter, N. Magnani, C. Apostolidis, J.-C. Griveau, E. Colineau, A. Morgenstern, R. Caciuffo, J. B. Love, *Inorg. Chem.*, **2010**, *49*, 5341.

(48) P. L. Arnold, N. A. Potter, C. D. Carmichael, A. M. Z. Slawin, P. Roussel, J. B. Love, *Chem. Commun.*, **2010**, *46*, 1833.

Chapter Two

Chromium Pacman Complexes

2.1 Introduction to chromium chemistry

Metallic chromium was first isolated in 1798. Its name derives from the Greek word *chroma*, meaning colour, due to the variety of colours found in its compounds. Chromium is the 24th element of the periodic table and the lightest element of Group VI. The Group VI metals, chromium, molybdenum and tungsten, exhibit particularly rich redox chemistry; compounds in every oxidation state from +6 down to -2 are known for all three metals.[1] The +3 oxidation state is by far the most stable for chromium while Cr(VI) compounds such as CrO_3 tend to be highly oxidising and find wide application in organic chemistry. The co-ordination and organometallic chemistry of chromium is varied and well developed. Therefore this short introduction will seek to highlight some recent exciting advances in the field of low oxidation state chromium chemistry, and review important industrial chromium-catalysed processes.

2.1.1 Quintuple Cr-Cr bond formation

The chemistry of binuclear, low oxidation state chromium complexes is dominated by a tendency to form M-M multiple bonds.[2] Until recently it was commonly accepted that quadruple M-M bonds, as featured in the classic paddle wheel structures $[M_2(OAc)_4]$ (M = Cr, Mo), were the highest order bond that could be stabilised under normal conditions. However, in 2005 Power reported the synthesis of a dimeric Cr(I)/Cr(I) complex containing the first quintuple M-M bond.[3] Reduction of the chloride bridged Cr(II)/Cr(II) dimer $[Ar'Cr(\mu\text{-}Cl)]_2$ with KC_8 resulted in the formation of the terphenyl-supported, quintuply bonded species [(Ar′)CrCr(Ar′)] (**2A**) (Scheme 2.1). Each Cr(I) centre in **2A** is stabilised by a bonding interaction with the *ipso* carbon of one of the Dipp rings of the terphenyl ligand bound to the other Cr(I) ion (dashed bonds). The Cr-Cr bond length in **2A** is 1.8351(4) Å.

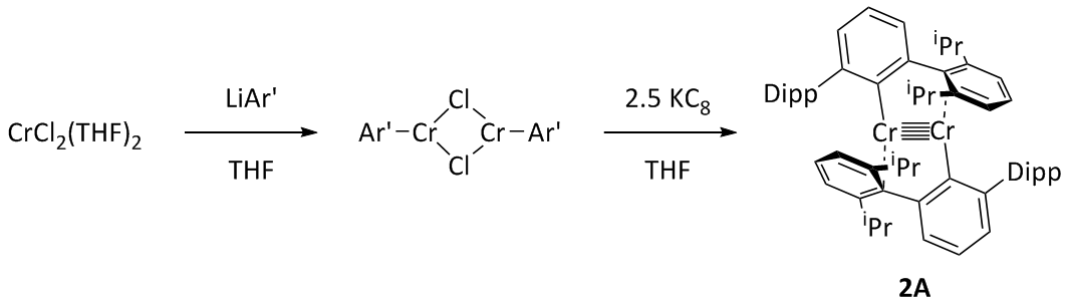

2A

Scheme 2.1 Synthesis of the first quintuply bonded Cr/Cr dimer **2A**.[3]

This seminal discovery prompted a rush to identify other ligands capable of supporting Cr-Cr quintuple bonds. Using the same methodology as Power, several other groups reported the successful reductive coupling of the corresponding chloride precursors to

form a range of Cr-Cr quintuply bonded complexes. In contrast to **2A**, all subsequently isolated Cr-Cr quintuply bonded complexes reported by other researchers have been supported by bidentate N-donor ligands (Figure 2.1). The Tsai and Kempe groups employed amidinate ligands to form neutral and anionic complexes of the type **2B** and **2E**.[4-6] Systematic variation of the substituent groups R and R′ in **2B** has allowed identification of the ligand system which results in the shortest Cr-Cr interaction; with R = 2,6 dimethylpiperidinide and R′ = Dipp an extremely short Cr-Cr separation of 1.7056(12) Å was observed, which is the same length as an alkane C-C bond.[7] The Theopold group published complex **2D** which contains singly reduced radical anion diimine ligands,[8] and substituted pyridine ligands have also been employed (**2C**).[9] The features common to all the different ligands used are bidenticity to promote dimerisation and bulky aryl substituents to discourage the formation of higher oligomers.

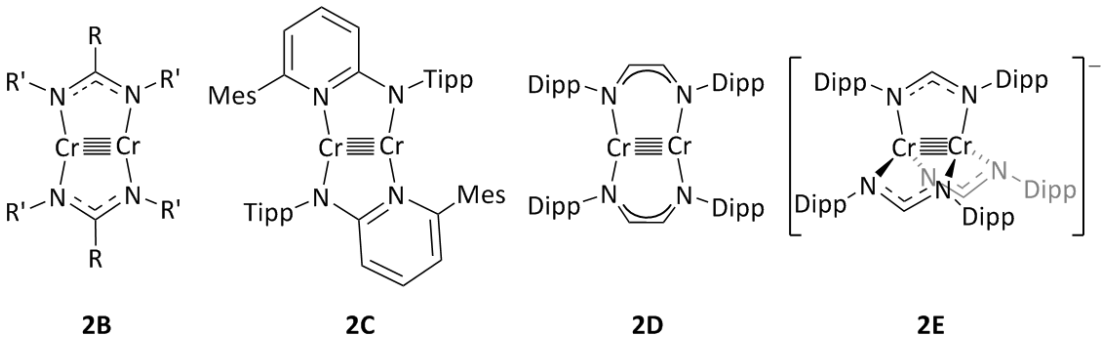

2B **2C** **2D** **2E**

Figure 2.1 N-donor supported Cr-Cr quintuply bonded complexes.[4-9]

One exception to these general rules was reported in 2012 by Tsai and co-workers who used tridentate substituted pyridine ligands to support the stepwise reduction of a halide-free Cr(II)/Cr(II) dimer (**2F**) to the mixed valence Cr(I)/Cr(II) species (**2G**) and then to the quintuply bonded Cr(I)/Cr(I) complex (**2H**) (Scheme 2.2).[10] This example is a somewhat special case: incorporation of the two K^+ counterions bound by the amido nitrogens in the structure of **2H** is vital for the stabilisation of the Cr-Cr quintuple bond. If 18-crown-6 is added to **2H** to abstract a K^+ ion, the newly freed amido nitrogen bites into the nearest Cr(I) ion axial to the Cr-Cr bond resulting in its complete destruction and disproportionation to Cr(II) and Cr(0) species.

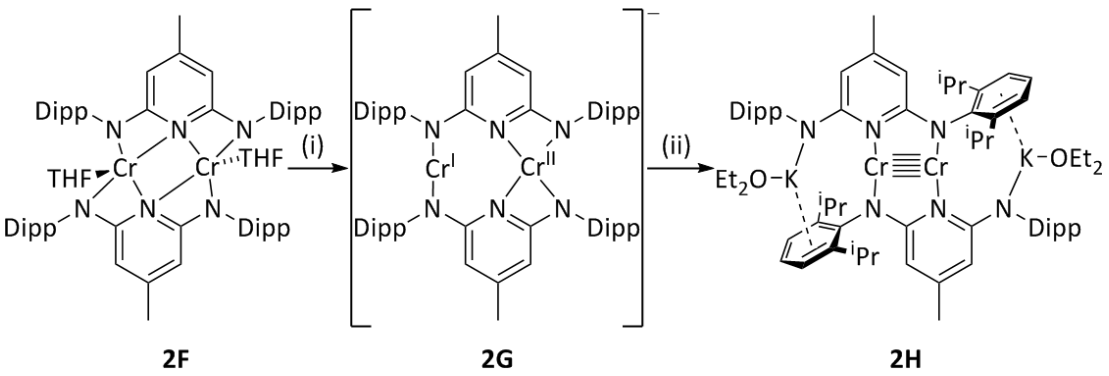

2F **2G** **2H**

Scheme 2.2 Formation of a Cr-Cr quintuple bond by stepwise reduction of a Cr(II)/Cr(II) precursor.[10] Reagents: (i) KC_8, 18-crown-6, THF, (ii) 3 KC_8, 5 KI, THF, recrystallised from Et_2O. The $[K(18\text{-crown-6})]^+$ counterion is omitted from **2G**.

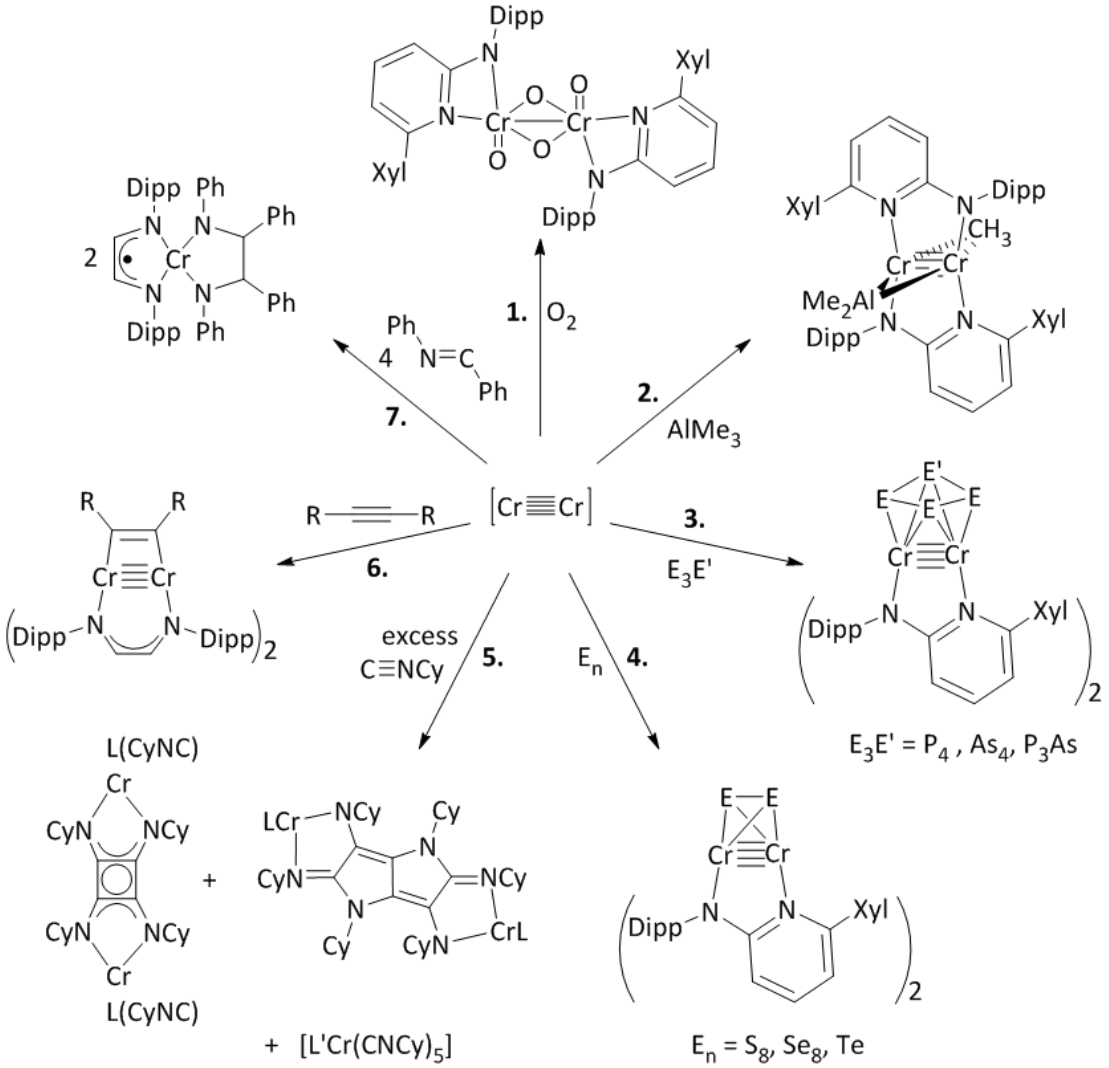

Scheme 2.3 Selected reactions of quintuply bonded complexes **2C** and derivatised **2D**.[11-14] L = $[(Dipp)NCHCHN(Dipp)]^-$, L' = [(Dipp)N=CHCH=N(Dipp)], R = Me, Et.

Following the successful isolation of a range of stable complexes containing quintuple Cr-Cr bonds, the first studies of the reactivity of these unique systems have been

published. Selected examples are shown in Scheme 2.3. Kempe has reported a remarkably selective oxidation of the Cr-Cr quintuple bond by O_2 to form a diamagnetic Cr(V)/Cr(V) dimer which maintains a single Cr-Cr bond and features terminal and bridging oxo groups (path **1.**). The group also reported the reaction of derivatised **2D** with $AlMe_3$ to form the unprecendented carboalumination product in which one of the Cr-Cr bonds has inserted into one Al-Me bond (path **2.**).[11] Derivatised **2D** also reacts selectively with white phosphorous, AsP_3, yellow arsenic and the elemental chalcogenides (paths **3.** and **4.**) to generate the co-ordinated polyanions E_2^{2-} (E = S, Se, Te) and E_4^{2-} (E_4 = P_4, AsP_3, As_4).[12,13] *Cyclo*- AsP_3^{2-} and As_4^{2-} ligands have not been previously observed.

The Theopold group have demonstrated the capability of **2C** to effect interesting transformations of organic molecules. They have reported that one of the Cr-Cr bonds in **2C** undergoes a [2+2] cycloaddition with alkynes to form the Cr(II)/Cr(II) metallacyclo alkene product (path **6.**).[12] C-C coupling has also been achieved. Reaction of **2C** with 4 equivalents of *trans* benzylideneaniline resulted in reductive coupling of the C=N bonds to form a Cr(III) 1,2 di-amido complex (path **7.**).[13] Addition of excess cyclohexyl isocyanide to **2C** formed a mixture of products path (**5.**). The major product was the octahedral Cr(0) complex [Cr{(Dipp)N=CHCH=N(Dipp)}$(CNCy)_5$] but two minor coupled products were also formed. In the first, four isocyanides underwent reductive C-C coupling to form $\{C_4(NCy)_4\}^{2-}$, the (NCy) substituted analogue of the squarate dianion $(C_4O_4)^{2-}$, which bridges between two Cr(II) centres. The second minor product was the result of reductive coupling of six isocyanides to form two fused heterocycles featuring new C-C and C-N bonds. Amido and immine functionalities at each end of the heterocycles ligate the Cr(II) centres. The organic bicyclic fragment could be liberated by protonolysis. After optimization, this reaction might be a useful method for the production of unusual fused heterocycles.[14] Doubtless the continuing exploration of the reactivity of Cr-Cr quintuple bonds will prove a fruitful research area for years to come.

2.1.2 Dinitrogen binding and activation by chromium

The chemistry of dinitrogen binding and fixation has been dominated by chromium's heavier neighbours, molybdenum and tungsten.[15,16] Only three homogeneous systems have achieved the catalytic reduction of N_2 to ammonia under mild conditions; two are Mo-based and one is an iron catalyst.[17-19] However chromium dinitrogen complexes have been known since 1972, though the number of examples remains small.[20] Interest in the topic has reignited in recent years. In 2007, the Theopold group reported the synthesis of an unusual side-on bridging dinitrogen chromium complex (**2J**) by reduction of the chloro-bridged

Cr(II) "nacnac" supported dimer with magnesium under an N_2 atmosphere (Scheme 2.4).[21] A modest degree of reduction of the dinitrogen ligand was indicated by the observed lengthening of the N≡N bond from 1.0976 Å to 1.249(5) Å. However dinitrogen was readily displaced from **2J** by competitive ligands suggesting that **2J** should best be considered as a veiled Cr(I)/Cr(I) complex. Thus, although **2J** did not activate dinitrogen towards hydrogenation, it did allow study of the chemistry of a unique Cr(I) fragment.[22] Two of the reactions explored are included in Scheme 2.4. Reaction of **2J** with azobenzene resulted in displacement of N_2, co-ordination of PhN=NPh and complete cleavage of the N=N double bond to form the Cr(III)/Cr(III) imido bridged complex **2K**, demonstrating the reductive power of the Cr(I) centres. Addition of the π-acid CO to **2J** also caused displacement of N_2 to form the remarkable asymmetric complex **2L** in which disproportionation of the Cr(I)/Cr(I) starting material has occurred to form a Cr(II)/Cr(0) dimer bridged by isocarbonyls. The Cr(II) ion in **2L** is square planar and bound by the O atoms of the two isocarbonyls whilst the Cr(0) centre is square pyramidal and binds to the C atoms of the isocarbonyls and an additional terminal CO molecule.

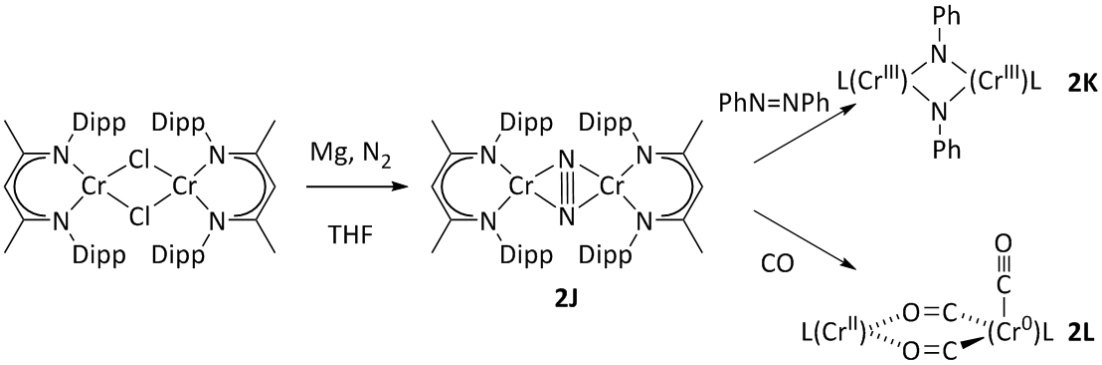

Scheme 2.4 Synthesis of a side-on bound chromium dinitrogen complex and its reactivity with CO and azobenzene.[21,22] The ligand is abbreviated to L in **2K** and **2L**.

Also in 2007, Gambarotta reported the first example of complete cleavage of the N≡N triple bond in a chromium dinitrogen complex.[23] The Gambarotta group favour the diimine pyridine ligand to support formally low oxidation state chromium complexes [24] because the ligand is able to accommodate electrons in its π system. These electrons are still available for reduction chemistry but the metal centre is able to rest in a higher oxidation state. Gambarotta reported that reduction of $[Cr^{II}Cl_2(L)]$ (**2P**) with two equivalents of NaH or Na metal produced the rare, end-on bridging dinitrogen chromium complex **2Q** (Scheme 2.5). The nitrogen ligand is reduced to $[N_2]^{2-}$ (N-N bond length = 1.241(6) Å) and each pyridine ligand is also reduced to its dianion so the oxidation states of the Cr centres are +3. Addition of a further two equivalents of NaH to **2Q** resulted in the formal two e^- reduction of the N_2 fragment, which is bridged by two Na^+ cations in the product **2R**, coupled with

hydrogen atom transfer from the ligand to one N atom, confirmed by IR spectroscopy. The N-N separation in **2R** is lengthened to 1.288(5) Å and the authors suggest that the +3 oxidation state of the Cr centres is maintained. Complete cleavage of the N-N bond was achieved by addition of a final equivalent of NaH to **2R** to form the imido complex [Cr(L)NHNa(THF)] (**2S**) in which the Na^+ cation binds to the imido N and in an η^6 fashion to one aryl ring of the ligand. In **2S** the pyridine ligand is formulated as a radical anion and the Cr centre is in the +2 oxidation state. In Scheme 2.5, the reducing electrons required to break the N≡N triple bond were provided by NaH rather than the Cr ion and the pyridine ligand acted as an electron reservoir preventing the oxidation state of Cr dropping below +2.

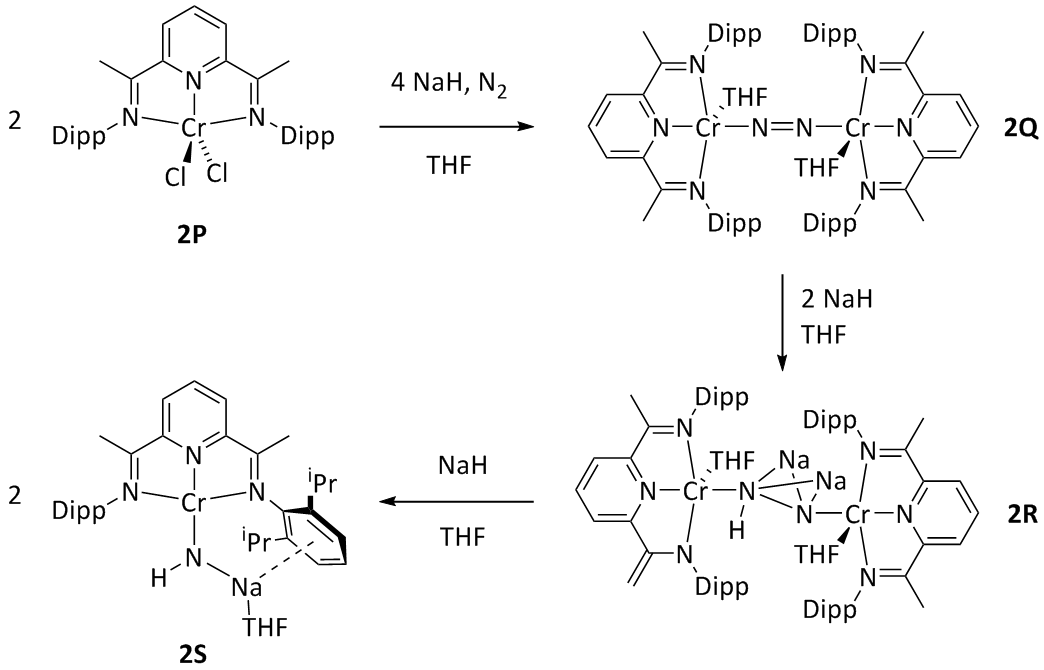

Scheme 2.5 Successive reductions of a Cr(II) precursor to form a bridging dinitrogen complex and ultimately a chromium imido complex as a result of N≡N cleavage.[23]

Mock and co-workers reported a further advance in 2013 in which they demonstrated the reduction of dinitrogen to hydrazinium and ammonium salts by a Cr(0) complex where the reducing electrons originated from the chromium.[25] $CrCl_2$ was added to two equivalents of a neutral eight membered P_2N_2 macrocycle (Scheme 2.6). Rather than formation of the expected product, $[CrCl_2(P_2N_2)_2]$, a small amount (5 %) of an expanded 16 membered P_4N_4 macrocycle ligated material $[CrCl_2(P_4N_4)]$ (**2M**) was isolated. The authors suggest that the presence of the Cr(II) precursor is key in enabling the macrocyclic expansion. Reduction of **2M** with magnesium under a nitrogen atmosphere resulted in formation of the rare, terminal *trans* bis(dinitrogen) chromium (0) complex **2N** in good yield. Treatment of **2N**, formed using labelled $^{15}N_2$, with 8 equivalents of triflic acid in d_8-THF at

−50 °C resulted in the slow formation of free hydrazinium triflate and trace amounts of ammonium triflate, identified in the ^{1}H and ^{15}N NMR spectra of the mixture. Experimental observations and computational analysis suggest that protonation of two of the pendant amine groups of the macrocycle occurs initially. One of the co-ordinated N_2 molecules then dissociates which increases the basicity of the remaining N_2 ligand and facilitates proton transfer from the macrocycle to the co-ordinated N_2. The eventual oxidised Cr species formed have not been characterised. These two examples from the Gambarotta and Mock groups indicate that judicious choice (or fortuitous formation) of an appropriate ligand set for chromium can enable unique chemistry.

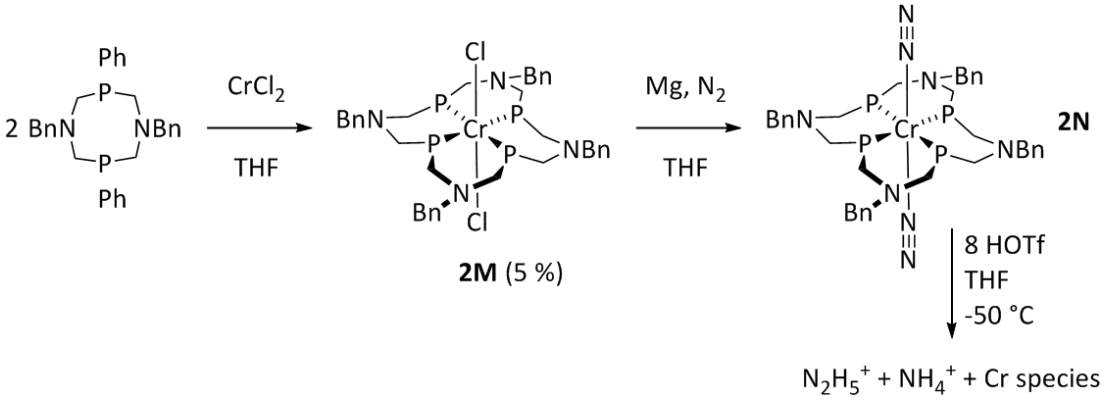

Scheme 2.6 Synthesis of a rare terminal dinitrogen complex of chromium and its reaction with triflic acid.[25] Ph groups attached to P atoms have been omitted in **2M** and **2N**.

2.1.3 Ethylene polymerisation and oligomerisation chemistry

2.1.3.1 Polymerisation

The major industrial use of chromium is in the heterogeneous catalysis of ethylene polymerisation. Roughly one third of global high density polyethylene (HDPE) is produced using the Phillips catalyst system, first patented in 1958.[26] The Phillips catalyst is prepared by impregnation of a silica support with any of a range chromium starting materials followed by calcination in oxygen.[27] This process oxidises the chromium to the +6 state but upon contact with ethylene gas it is reduced to the active catalyst (Scheme 2.7, top).[28] An alternative catalyst was developed by Union Carbide which is formed by impregnating dehydroxylated silica with chromocene, Cp_2Cr.[29,30] The chromium catalyst is adsorbed onto the support by reaction with remaining hydroxyl groups to eliminate CpH and form Cr-O surface bonds (Scheme 2.7, bottom). Both of these heterogeneous catalyst systems polymerise ethylene with high activity and do not require the addition of any co-catalyst.

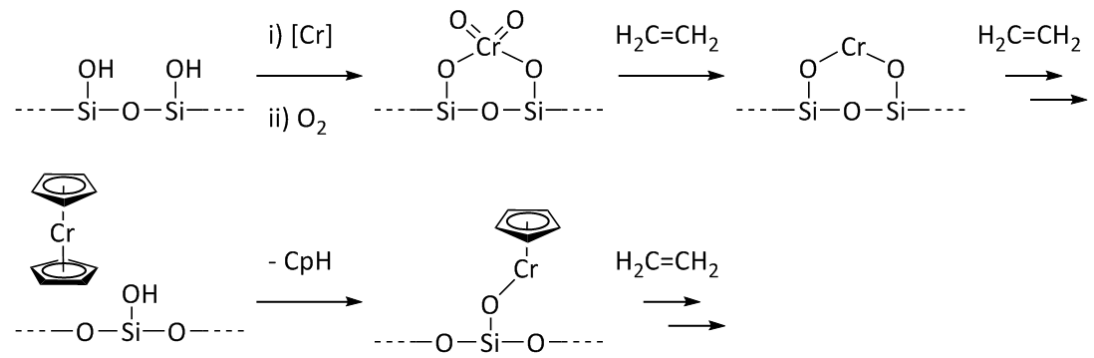

Scheme 2.7 Suggested generation of the surface-bound Phillips (top) and Union Carbide (bottom) catalysts.[28]

While it is accepted that the polymer chain grows by a migratory insertion mechanism, the nature of the industrial active catalytic species is still not well understood. There has been much academic interest in the area and a huge range of chromium co-ordination compounds have been reported to polymerise ethylene in the presence of a large molar excess of an aluminium activator, typically AlR_3 or methylaluminoxane (MAO). It is thought that the activator can fulfil several functions: reduction and/or alkylation of chromium, ionisation of the chromium complex by halide/alkyl abstraction and scrubbing of trace oxygen and water from the ethylene feed. It is difficult to deduce the nature of the active catalytic species formed since changes in the co-ordination sphere and oxidation state of the Cr centre in the precatalyst are expected. Noting that neither the Phillips nor the Union Carbide catalysts require the addition of an activator, the Theopold group set out to develop and study well-defined homogeneous model systems for ethylene polymerisation based on the suggested surface-bound structures of the two industrial catalysts.

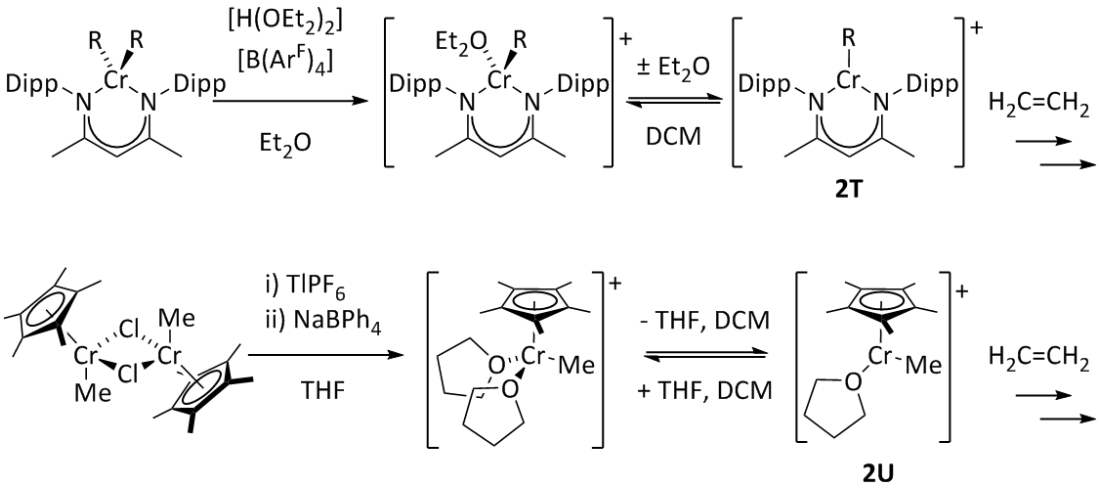

Scheme 2.8 Synthesis of functional structural models of the Phillips catalyst (**2T**)[31] and Union Carbide catalyst (**2U**).[32] R = CH_2SiMe_3. Ar^F = $C_6H_3(CF_3)_2$. The $[B(Ar^F)_4]^-$ and $[BPh_4]^-$ anions are omitted from the cationic complexes.

The structural model for the Phillips catalyst is a Cr(III) alkyl cation of a bidentate "nacnac" ligand with bulky aryl substituents. The active catalyst, **2T**, is revealed by dissociation of a bound ether molecule in DCM solution (Scheme 2.8, top) to form the co-ordinatively unsaturated alkyl complex which is moderately active in ethylene polymerisation.[31] Compared to the suggested structure of the Phillips catalyst the co-ordination geometry of **2T** is similar but N donors have replaced the O donors and the "nacnac" ligand contributes a 1− charge rather than the combined 2− charge of 2 siloxide groups. The Union Carbide model complex (**2U**) synthesised by the Theopold group is also a Cr(III) alkyl cation, this time bound to a Cp* ligand and one neutral THF donor (in the active form of the catalyst).[32] The major difference between **2U** and the Union Carbide catalyst is that the O donor is neutral rather than anionic. Solutions of **2U** in DCM catalysed the polymerisation of ethylene without any added co-catalyst. The rate was severely inhibited by addition of THF due to driving of the equilibrium towards the co-ordinatively saturated bis(THF) adduct, in which there is no available site for ethylene to co-ordinate. These observations led Theopold to conclude that the minimum requirement for ethylene polymerisation is a co-ordinatively unsaturated chromium complex bearing at least one alkyl (or hydride) ligand, though the group do not speculate upon the origin of the alkyl/hydride in the industrial catalyst systems.

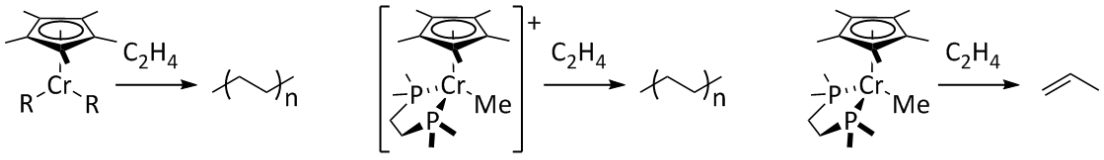

2W **2X** **2Y**

Scheme 2.9 Reactivity of different Union Carbide model complexes towards ethylene.[28] The PF_6^- anion is omitted from **2X**. R = CH_2SiMe_3.

Further studies were undertaken to probe whether a co-ordinatively unsaturated Cr alkyl complex must necessarily be cationic and in the +3 oxidation state for successful polymerisation (Scheme 2.9). The neutral dialkyl Cr(III) complex, **2W**, was found to be a good polymerisation catalyst.[28] However the structurally analogous cationic Cr(III) and neutral Cr(II) compounds **2X** and **2Y** exhibited different activities towards ethylene. While **2X** was effective in ethylene polymerisation, the product of the reaction of ethylene with **2Y** was propene. This indicates that for the Cr(II) complex β-hydride elimination is favoured over chain growth after ethylene binding and insertion into the Cr-Me bond. Therefore in these model systems Cr(III) was found to be the catalytically relevant oxidation state, though the charge on the complex did not matter. In practice however, it is often easier to prepare a

co-ordinatively unsaturated cationic complex since dimerisation of like-charged fragments is disfavoured.

2.1.3.2 Selective oligomerisation

An expanding area of both commercial and academic interest is the use of chromium catalysts for the selective oligomerisation of ethylene to 1-hexene and 1-octene. Linear α-olefins (LAOs) of chain length C_4 to C_{20} are valuable commodity petrochemicals. C_4 to C_8 materials are particularly sought after for use as co-monomers in the production of linear low density polyethylene (LLDPE). Formation of 1-hexene was first noted by Manyik and co-workers when experimenting with some modifications to the Phillips catalyst.[33] The generally accepted mechanism for catalytic ethylene trimerisation was proposed by Briggs and involves the formation of a metallacyclopentane by coupling of two ethylene molecules at the Cr centre, insertion of another monomer and then β-hydride elimination followed by reductive elimination of 1-hexene (Scheme 2.10). Successful, selective, 1-hexene formation relies upon the greater stability of the metallacyclopentane *vs*. the metallacycloheptane such that the former undergoes a further insertion reaction and the latter undergoes rapid elimination.[34] In 2004, researchers at Sasol demonstrated that selective tetramerisation of ethylene to 1-octene may also be achieved by modifying the supporting ligand set.[35] A similar catalytic cycle operates but in this case the metallacycloheptane is stable with respect to elimination allowing a further ethylene insertion to occur, forming a 9-membered metallacycle from which 1-octene is eliminated.[36]

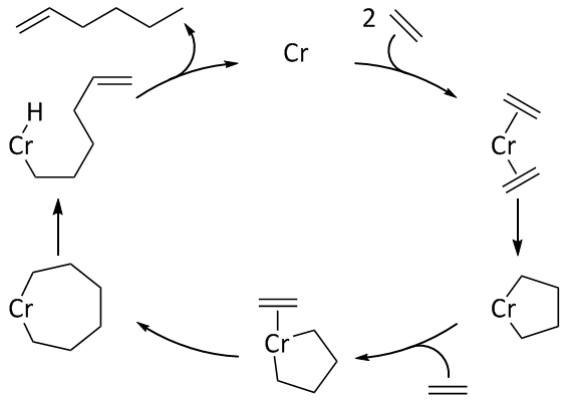

Scheme 2.10 Mechanism of chromium catalysed metallacyclic trimerisation.[36]

From the oligomerisation mechanism it is apparent that three co-ordination sites are required at the Cr centre. Therefore many of the catalytic systems developed employ a tridentate ligand combined with a Cr(III) precursor such as $CrCl_3$. Once again a large quantity of activator, typically AlR_3 or MAO, is usually added to generate the active catalyst by alkylation and/or halide abstraction.[37] As in the case of the polymerisation systems, the

structure of the active catalyst is difficult to deduce. However, Bercaw and co-workers have published an elegant study on stoichiometrically activated ethylene trimerisation catalysts.[38,39] The ligand studied was a neutral "PNP" ligand bearing four *ortho*-methoxy substituted aryl rings. In addition to the two phosphorus atoms, up to two of the methoxy groups can bind to the metal to provide extra stabilisation. The Bercaw group prepared a "PNP" ligand in which all the methoxy groups had been deuterated and synthesised the Cr(III) complex [(PNP)$CrPh_3$], (**2Z**). A ^2H NMR study revealed the fluxional co-ordination of one methoxy arm to the Cr(III) centre. Treatment of **2Z** with one equivalent of $[H(OEt_2)_2][B(Ar^F)_4]$ yields the cationic Cr(III) complex **2AA** which catalyses ethylene trimerisation (Scheme 2.11). Bercaw suggested that **2AA** is likely stabilised by co-ordination of a second methoxy group to Cr(III).

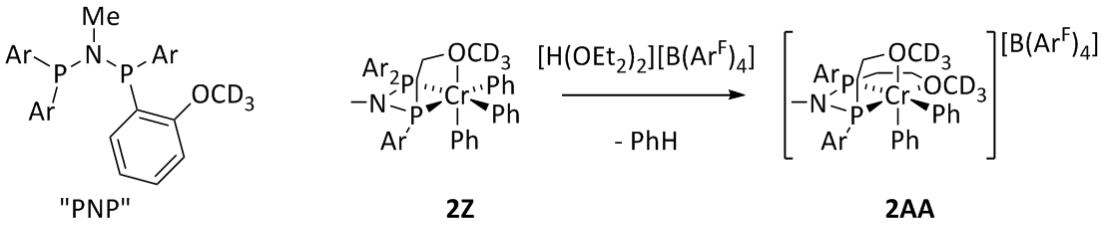

Scheme 2.11 Stoichiometric activation of the catalyst precursor **2Z**.[39] $Ar^F = C_6H_3(CF_3)_2$.

The group also probed the route from complex **2AA** into the catalytic cycle. Reductive elimination of biphenyl from **2AA** would immediately yield a Cr(I) complex capable of co-ordinating two ethylene molecules, but only trace amounts of biphenyl were detected in the reaction mixture. Instead, styrene and other phenyl containing hydrocarbons were observed implying that the Cr-Ph bonds are cleaved by ethylene insertion and β-hydride eliminations to yield the active catalyst (Scheme 2.12). The cationic Cr centre is then expected to cycle between the +1 and +3 oxidation states during catalysis.

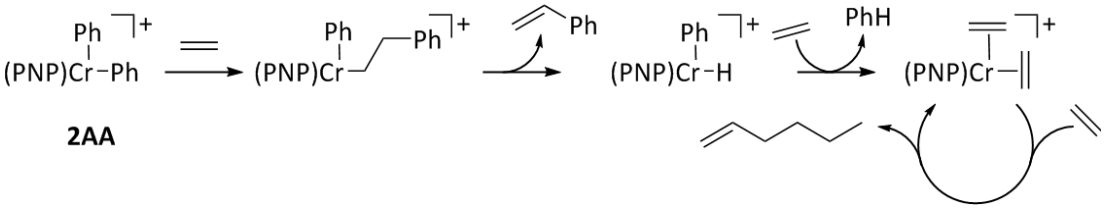

Scheme 2.12 Suggested mechanism of initiation of ethylene trimerisation.[39] $[B(Ar^F)_4]^-$ anions are omitted.

In summary, chromium is an industrially relevant metal capable of catalysing uniquely selective transformations of small molecules. Our understanding of these organometallic systems is continually improving through the study of well-defined homogeneous analogues.

2.2 Preparation of chromium Pacman complexes

Both transamination and salt elimination strategies proved effective in the insertion of two Cr(II) ions into the *ortho*-phenyl hinged macrocycle H_4L^{Me}. Thus addition of two equivalents of $[Cr(N'')_2(THF)_2]$ to H_4L^{Me} or reaction of K_4L^{Me} (formed *in situ*) with two equivalents of $CrCl_2$ (Scheme 2.13) form the binuclear chromium Pacman complex $[Cr_2(L^{Me})]$ (**1**). Both reactions have comparable yields (≈ 70 %) but salt elimination is preferred since the literature synthesis of $[Cr(N'')_2(THF)_2]$ from $CrCl_2$ is low yielding.[40] The ^{1}H NMR spectrum of **1** in d_5-pyridine at 298 K shows paramagnetically broadened and contact-shifted resonances at δ 16.9, 14.0, 6.7, −29.2, and −97.7 ppm, which are not assignable to specific ligand protons. Two, broad, residual *protio*-pyridine resonances are visible at δ 8.7 and 7.2 ppm, rather than the expected three resonances. At 393 K, the resonance at 7.2 ppm separates into two sharper resonances at δ 7.3 and 7.2 ppm, which indicates that pyridine binds transiently to the paramagnetic chromium complex in solution.

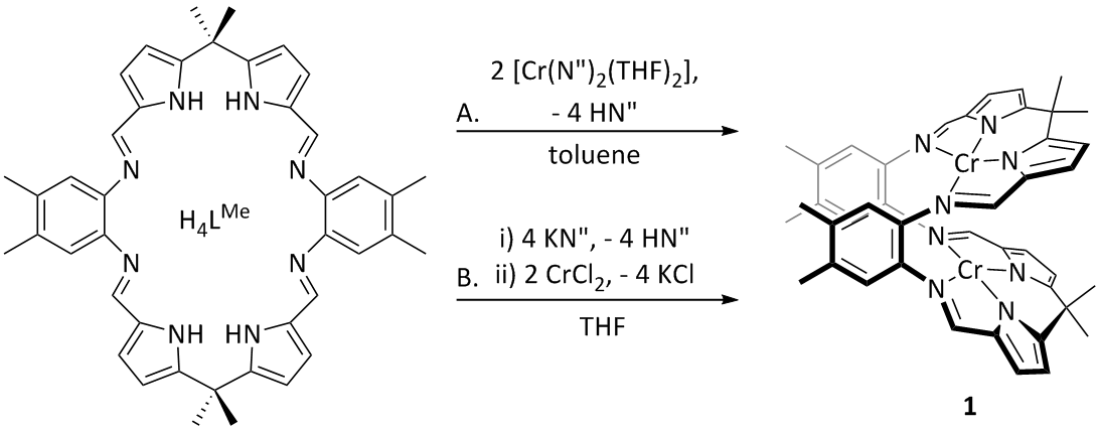

Scheme 2.13 Synthesis of **1** by transamination (A) and salt elimination (B) strategies.

2.2.1 Electronic characterisation of $[Cr_2(L^{Me})]$

The electronic configuration of the Cr(II) ion is $3d^4$. The solution magnetic moment of **1** determined by the Evans' method [41] was measured in THF/C_6D_6 solution as 6.34 μ_B. This value is approaching the spin only value of 6.93 μ_B for two non-interacting S = 2 ions, calculated according to the equation below.

$$\mu_{S.O.} = \mu_B\sqrt{4S_1(S_1+1)+4S_2(S_2+1)}$$

The electronic structure of **1** was probed in greater depth by variable temperature magnetic susceptibility and EPR measurements which were carried out by Dr Floriana Tuna and Prof. Eric McInnes at the National Facility for EPR Spectroscopy at the University of

Manchester. The SQUID magnetometry data (Figure 2.2) are consistent with strong antiferromagnetic coupling between the Cr(II) ions leading to a diamagnetic ground state for the complex below 2 K. The χ *vs.* T curve does not reach zero at 0 K; χ increases below 25 K and the magnetisation saturates at roughly 0.05 μ_B below 2 K. This is thought to be due to a minor (5 %) paramagnetic impurity, most likely a partially oxidized Cr(II)/Cr(III) Pacman complex with overall spin S = ½. The data were adequately simulated (red curves) using the Hamiltonian for two magnetically interacting ions, $H = -2JS_1S_2$, which has eigenvalues $E(S) = -J[S(S+1) - S_1(S_1+1) - S_2(S_2+1)]$ where the values of the total spin are $S = S_1 + S_2,\ S_1 + S_2 - 1, \ldots |S_1 - S_2|$, and $S_1 = S_2 = 2$, confirming a high spin electron configuration for both Cr(II) ions. The energy separation between consecutive spin states is given by $\Delta E_S = E(S) - E(S-1) = -2JS$, with the isotropic exchange parameter J = −53.5 cm^{-1}. The ground state of the complex is S = 0 due to the antiferromagnetic coupling between the two Cr(II) ions with the excited S = 1, 2, 3, 4 states, at energies of 2J, 6J, 12J, 20J above the ground state, being thermally populated according to the Boltzman distribution.

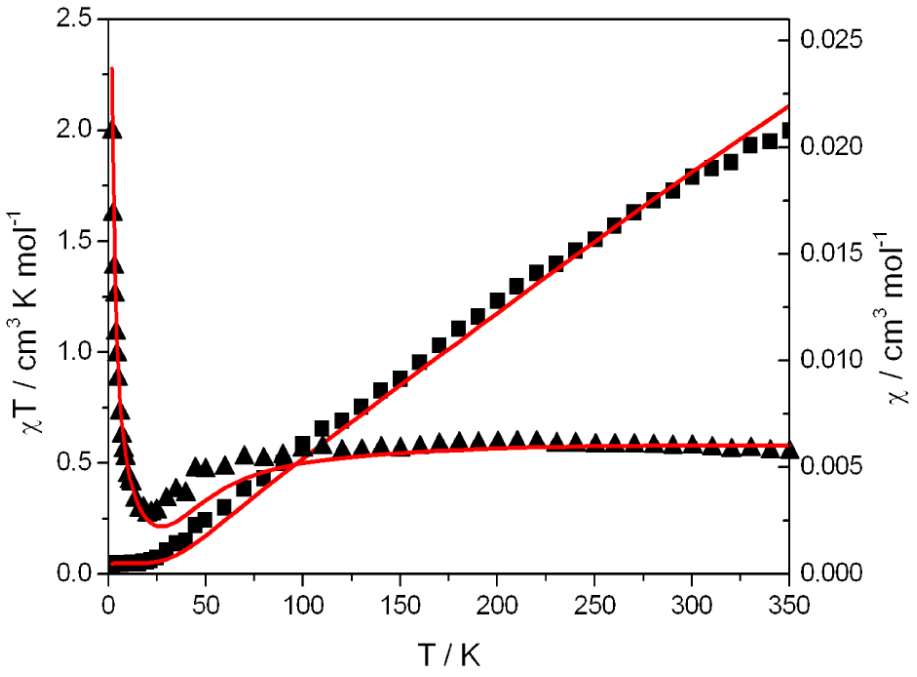

Figure 2.2 Plots of the measured (black) and simulated (red) variable temperature magnetic susceptibility data for **1**. χ = triangles, χT = squares.

1 displays a rich EPR spectrum at 200 K which collapses to a single, sharp feature at 12.2 kG upon cooling (Figure 2.3, top); the sharp singlet seen at 5 K is associated with the 5 % Cr(II)/Cr(III) impurity. The disappearance of the other features is in agreement with **1** having a diamagnetic ground state, as determined from the SQUID measurements. The features observed in the 0 - 10,000 G region arise from thermally populated total spin S = 2

and $S = 3$ states of **1**. At 200 K, the populations of the $S = 2$ and $S = 3$ spin states are 17 % and 2 % respectively. Most of the features in the EPR spectrum and the variable temperature behaviour can be satisfactorily modelled with the axial zero field splitting parameter $D = -1.8$ cm^{-1} (Figure 2.3, bottom) which is comparable to the value determined for the square planar N_4-ligated Cr(II) complex $[Cr(MeCN)_4]^{2+}$ of $D = -2.2$ cm^{-1}.[42]

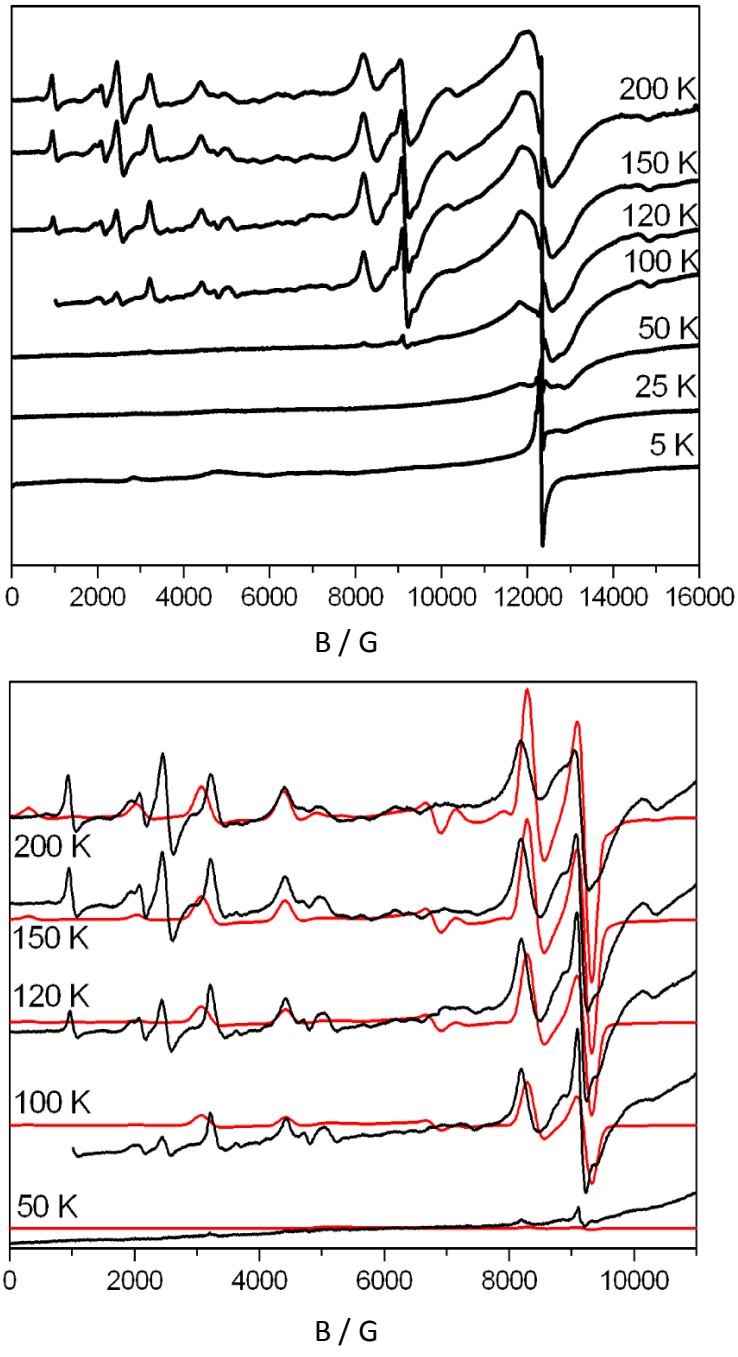

Figure 2.3 Variable temperature Q-band EPR spectra of **1** measured at 34 GHz (top) and enlargement of 0 – 10000 G field region (bottom, black) overlaid with simulated spectra (red).

2.2.2 Solid state structure of $[Cr_2(L^{Me})]$

Single crystals suitable for X-ray diffraction analysis were grown by slow cooling a saturated benzene solution of **1** from 80 °C to room temperature. The X-ray crystal structure reveals that the macrocycle adopts a C_2 symmetric Pacman geometry (Figure 2.4) with the two pockets of the macrocycle twisted with respect to each other in order to maximise favourable, offset π-π stacking interactions between the aryl hinges of the ligand. Both Cr(II) ions are bound in equivalent *pseudo*-square-planar environments comprising N_4 pyrrolide and imine donor sets. The mean Cr-N(pyrrolide) distance of 1.97 Å is significantly shorter than the mean Cr-N(imine) distance of 2.10 Å, though both lie within the usual range. This difference is likely imposed by the ligand architecture rather than by increased electrostatic attraction since in the related bis-imine bis-pyrrolide Cr(II) complex [Cr{(2,6-*i*-$Pr_2C_6H_3$)N=CH(C_4H_3N)}$_2$] (**2AB**, Figure 2.6, left) the mean Cr-N(imine) and Cr-N(pyrrolide) distances are both 2.08 Å.[43] The adoption of square planar geometry is by no means unusual for a Cr(II) ion; reported four coordinate complexes are a mixture of square planar, *pseudo*-square-planar and distorted tetrahedral depending on the steric demands of the ligand set. This can be rationalised by considering the Jahn Teller effect.[44] In tetrahedral (or octahedral) symmetry a high spin d^4 electronic configuration is orbitally degenerate so the complex must necessarily distort toward square planar symmetry to break the degeneracy. In the lattice, molecules of **1** are arranged in alternating chains with benzene molecules which cap the *exo* faces of the macrocycles at a Cr···C short contact distance of 3.608(2) Å (Figure 2.5).

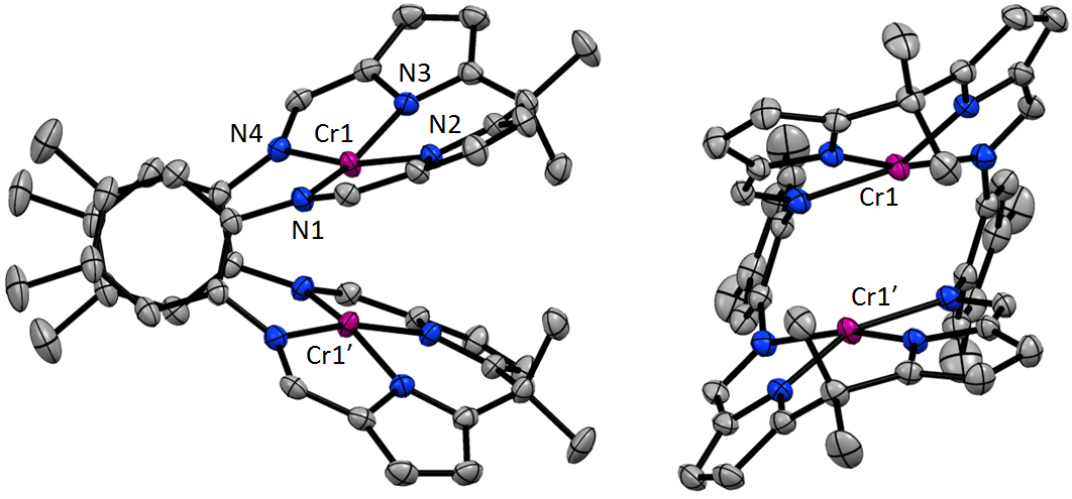

Figure 2.4 Solid state structure of **1** showing side view (left) and view into the jaws of the macrocycle (right). Thermal ellipsoids are drawn at 50 % probability. For clarity, lattice solvent and H atoms are omitted.

Table 2.1 Selected distances (Å) and angles (°) for **1**.

Cr1···Cr1′	3.1221(1)	N4-Cr1-N1	114.02(6)
Cr1-N1	2.114(2)	N1-Cr1-N2	80.06(6)
Cr1-N2	1.970(2)	N2-Cr1-N3	85.52(6)
Cr1-N3	1.976(2)	N3-Cr1-N4	78.64(6)
Cr1-N4	2.078(2)	bite angle	48
Cr1-N_4 plane	−0.19	twist angle	34

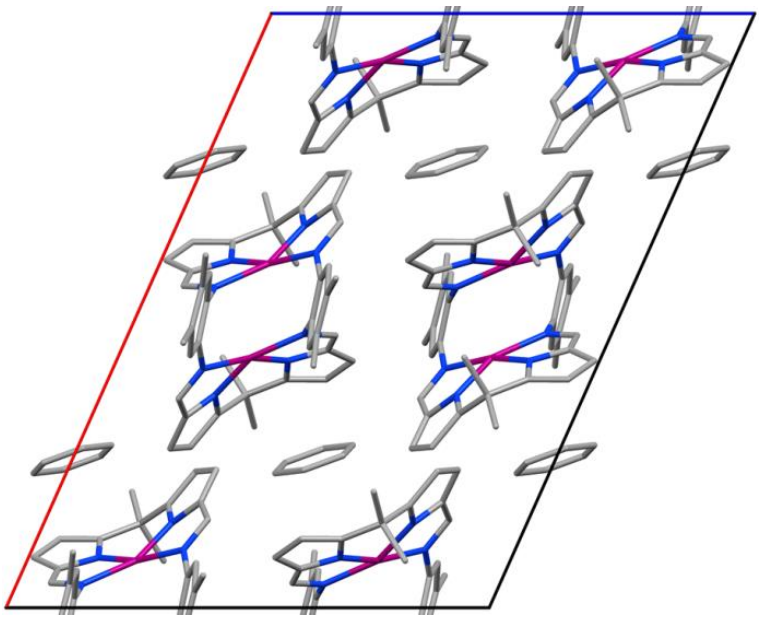

Figure 2.5 Packing within the unit cell of **1**, viewed along the *b* axis.

The sum of the four N-Cr-N angles is 358° because the Cr(II) ions are displaced −0.19 Å out of the N_4 plane. In this formalism the negative sign signifies the direction of displacement as in-to-cleft as opposed to a positive, out-of-cleft displacement. This reduces the bite angle of the macrocycle to 48 ° (from the ideal 60 °) and results in a Cr···Cr separation of 3.1221(1) Å, the shortest M-M distance observed in any $[M_2(L)]$ complex of this type.[45] A binuclear chromium complex, **2AC**, reported by the Wolczanski group provides an interesting structural comparison (Figure 2.6, right).[46] The two halves of complex **2AC** self-assemble with concomitant C-C bond formation (grey bonds) and reduction of two imine moieties to form a triply bonded Cr(II)/Cr(II) compound with a Cr-Cr bond length of 2.5515(3)Å. In all published structures where two metal-metal bonded Cr centres are supported by an N_4 donor set, Cr-Cr bond lengths range from 1.86 to 3.00 Å, with the median value being 2.40 Å.[47] The Cr···Cr separation in **1** lies beyond this range and is also considerably greater than double the covalent radius of chromium (1.39(5) Å).[48] Furthermore the SQUID and EPR data do not indicate the presence of Cr-Cr bonding.

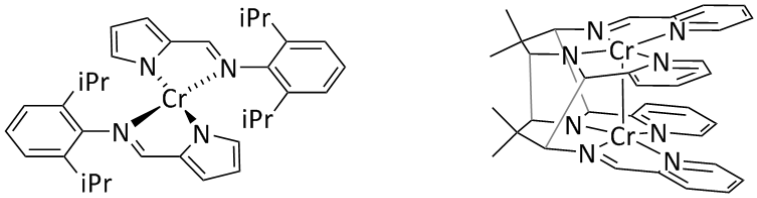

2AB **2AC**

Figure 2.6 Mono- [43] and binuclear [46] N_4 supported Cr(II) complexes.

2.2.3 High pressure X-ray crystallography studies of $[Cr_2(L^{Me})]$

The effect of pressure on single crystals of **1** was investigated to determine if increasing the pressure would cause the jaws of the Pacman macrocycle to close, bringing the Cr(II) centres close enough to allow a M-M bonding interaction to develop. High pressure X-ray diffraction data were collected for **1** by Dr Alessandro Prescimone of the University of Edinburgh at the Diamond Light Source over the pressure range 0.14 – 3.00 GPa at 300 K. A single crystal of **1** was inserted into a diamond-anvil cell containing a hydrostatic medium and a ruby chip, from the luminescence of which the cell pressure was determined.[49] Dr Alessandro Prescimone carried out the structure solution and refinement for all high pressure data sets. Unfortunately, in the following analysis no rigorous comparisons can be made to the ambient pressure structure because the ambient pressure data was collected at 170 K rather than 300 K.

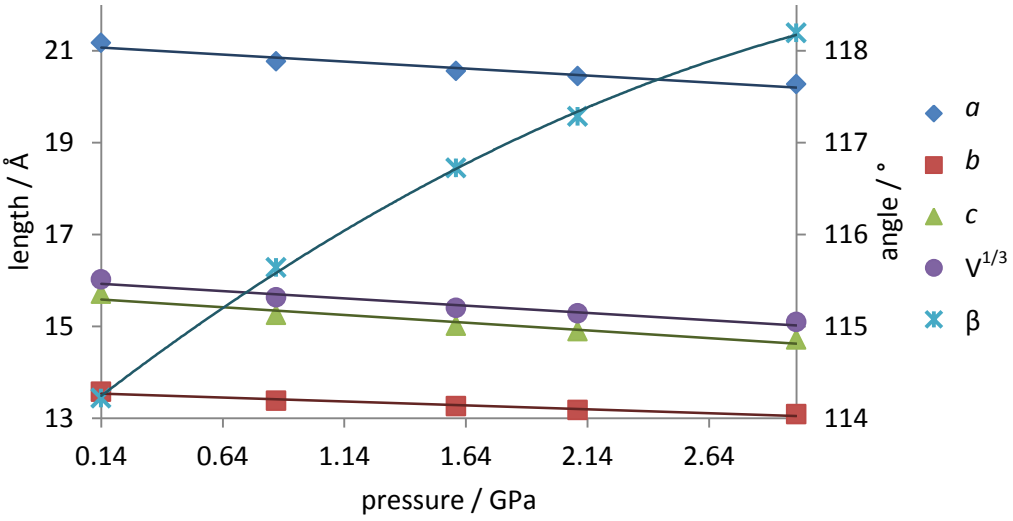

Graph 2.1 Plot of the unit cell parameters of **1** against pressure.

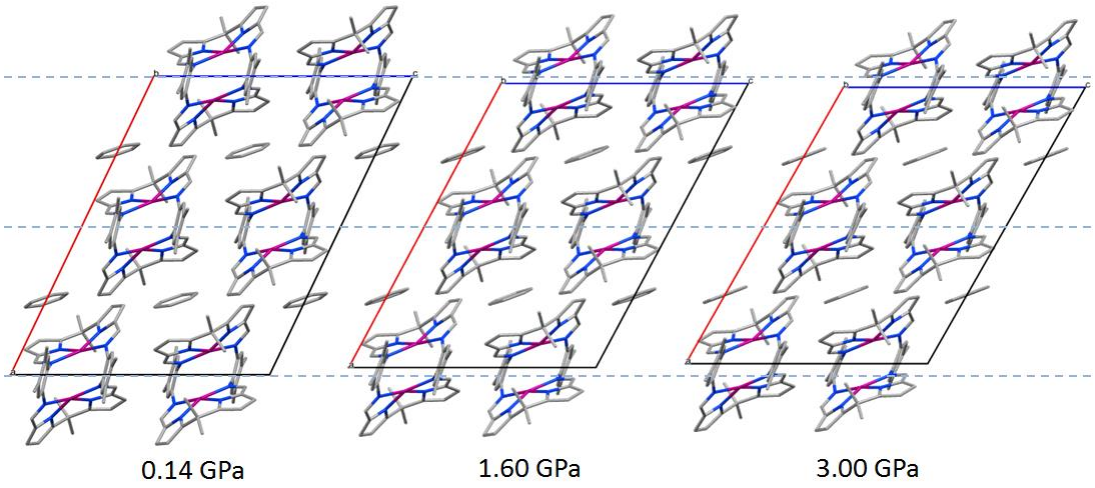

Figure 2.7 Variation in the unit cell of **1** (viewed along the *b* axis) with increasing pressure.

At ambient pressure **1** crystallises in the monoclinic space group *C2/c*. The crystal does not undergo a phase change as the pressure is increased to 3.0 GPa and the crystal symmetry is maintained. Linear compression of all three unit cell axes is observed with increasing pressure whilst the β angle increases from 114.216(6) ° at 0.14 GPa to 118.194(6) ° at 3.0 GPa (Graph 2.1, Figure 2.7). The result is a decrease in unit cell volume, *V*, from 4116.5(5) $Å^3$ at 0.14 GPa to 3438.1(4) $Å^3$ at 3.0 GPa.

As the pressure is increased the jaws of the Pacman macrocycle do not close. Instead, the two pockets of the macrocycle slip past each other resulting in a linear increase in the torsional twist angle of the aryl hinges (Φ) with increasing pressure (Graph 2.2). There is an associated small decrease in the angle between the planes of the two aryl rings (ω) increasing the aryl coplanarity (Figure 2.8). The increased torsional twist results in a very slight increase in the Cr···Cr separation and the macrocycle bite angle (θ). Evidently, subjecting **1** to high pressure does not induce Cr-Cr bond formation. However, as the unit cell is compressed, the lattice chains of Pacman complexes and benzene molecules are also compressed resulting in the formation of long range η^6 bonding interactions between the Cr(II) ions and the benzene lattice solvent molecules. The Cr···ring(centroid) separation decreases from 4.07 Å at 0.14 GPa to 3.55 Å at 3.0 GPa. This is combined with a tilting of the benzene rings so that they become more coplanar with the N_4 donor planes of the macrocycle (Graph 2.2, Figure 2.8).

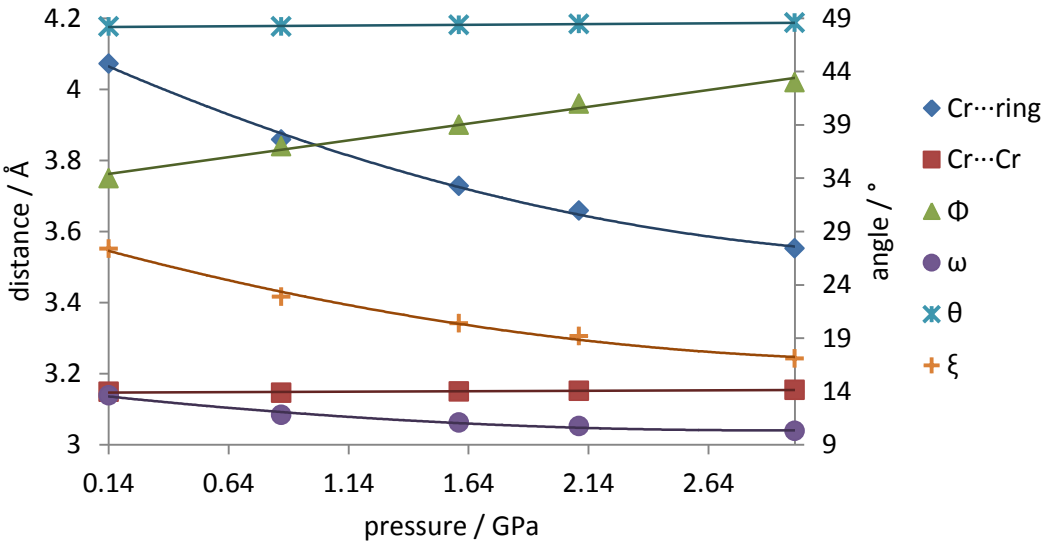

Graph 2.2 Variation of structural parameters of **1** with pressure. Φ = twist angle, ω = arene interplanar angle, θ = bite angle, ξ = N_4-benzene interplanar angle.

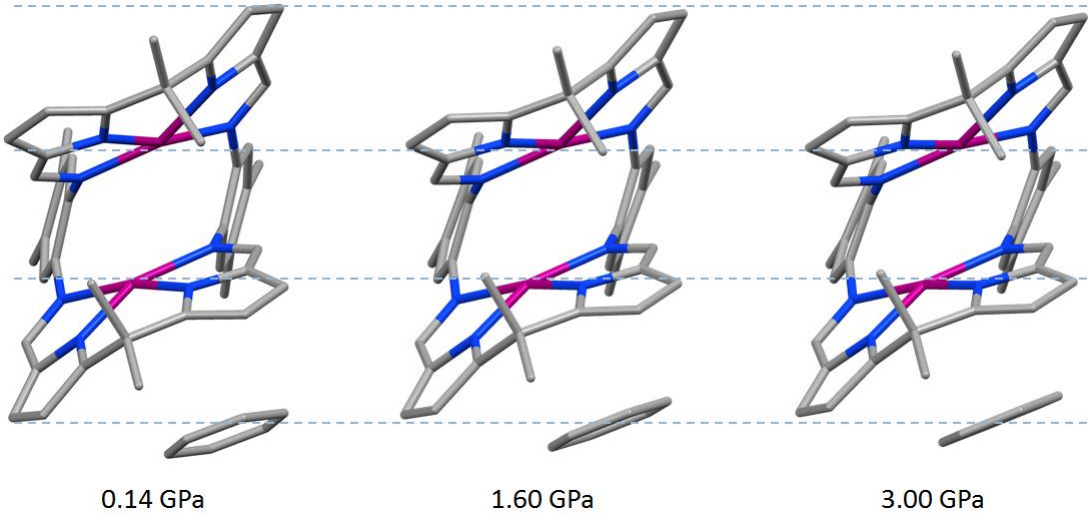

Figure 2.8 Solid state structures of **1** at different pressures, viewed along the *b* axis.

The Cr(II)–ring(centroid) distance of 3.55 Å in the 3.0 GPa structure of **1** is long compared to reported distances for η^6-arene complexes of chromium. The Cr-ring(centroid) distance in bis(benzene)chromium (**2AD**) is 1.61 Å [50] and the longest reported Cr-ring(centroid) distance is 1.70 Å in the half sandwich Cr(0) complex **2AE** (Figure 2.9, centre).[51] While η^6-arene complexes of Cr(0) are ubiquitous and many examples have also been reported for Cr(I), Cr(II) arene complexes are rare. One example of the latter is the mixed sandwich complex [CrCp*{η^6-(C_6H_5)BPh_3}] (**2AF**, Figure 2.9, right) which features a similar Cr-ring(centroid) separation of 1.67 Å.[32] Therefore it must be concluded that even at high pressures, the Cr-benzene interaction in **1** remains weak.

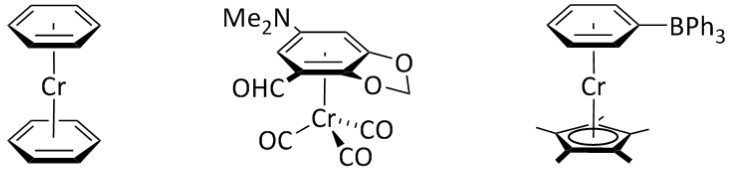

	3AD	**3AE**	**3AF**
Cr-ring$_{cent.}$	1.61 Å	1.67, 1.70 Å	1.67 Å

Figure 2.9 Examples of Cr(0) (left and centre)[50,51] and Cr(II) (right)[32] arene complexes.

2.2.4 Preparation of $[Cr_2(L^A)]$

Metallation of the anthracenyl hinged macrocycle H_4L^A was investigated in order to synthesise an analogue of **1** in which the separation of the Cr(II) ions is increased. Transamination was found to be an effective strategy for forming a binuclear chromium complex of $(L^A)^{4-}$. Reaction of two equivalents of $[Cr(N'')_2(THF)_2]$ with H_4L^A in THF resulted in precipitation of the *exo*-THF adduct $[Cr_2(L^A)(THF)_2]$ ($\mathbf{2_{THF}}$) confirmed by single crystal X-ray diffraction. The coordinating THF molecules dissociate upon exposure of $\mathbf{2_{THF}}$ to high vacuum to yield the product $[Cr_2(L^A)]$ (**2**) as a red powder in good yield (60 %, Scheme 2.14). Isolated **2** has some solubility in arene solvents but is insoluble in THF and pyridine. This implies that the solvated complexes $\mathbf{2_{THF}}$ and $\mathbf{2_{py}}$ which form in the presence of the coordinating solvents are less soluble than the base-free complex **2**. The ^{1}H NMR spectrum of **2** in C_6D_6 shows paramagnetically broadened and contact-shifted resonances at δ 26, 14, 11, 9, 6, −50, and −56 ppm, which are not assignable to specific ligand protons. Unlike **1**, complex **2** cannot be conveniently synthesized by a salt elimination methodology in THF solution because the poor solubility of $\mathbf{2_{THF}}$ leads to problems in separating the desired complex from the salt by-product.

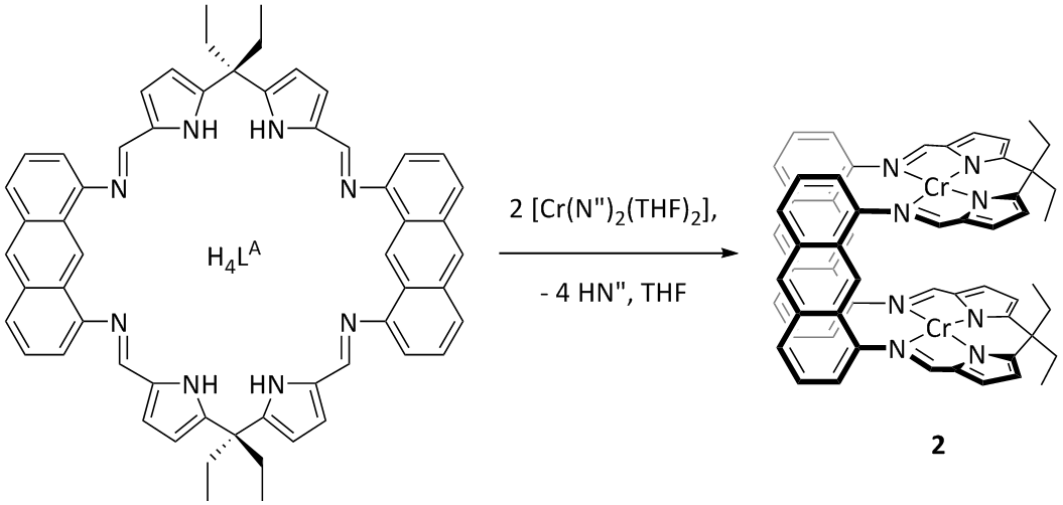

Scheme 2.14 Synthesis of $[Cr_2(L^A)]$, **2**.

Single crystals of $\mathbf{2_{THF}}$ formed in an NMR-tube reaction between $[CrN''_2(THF)_2]$ and H_4L^A in THF. The X-ray structure (Figure 2.10) reveals that the Pacman geometry is adopted. The Cr(II) ions occupy square pyramidal coordination sites with the macrocycle providing two imine and two pyrrolide donors to form the base of the pyramid and a single molecule of coordinated THF occupying the *exo* apical position. The Cr···Cr separation in **2** is lengthened to 5.6353(1) Å, compared to 3.1221(1) Å in **1**, due to the elongation of the aryl hinges of the macrocycle from phenyl to anthracenyl. This prevents any possible M-M bonding interaction. The jaws of the macrocycle are now closer to coplanarity (the angle between the N_4 donor planes is measured at 20 ° *cf*. 35 ° in **1**) as dictated by the 1,8 substitution pattern of the anthracene hinges. The mean Cr-N(imine) and Cr-N(pyrrolide) distances of 2.15 and 1.99 Å respectively are slightly lengthened compared to those observed in **1** (2.10 and 1.97 Å). This may be due to the presence of the THF donor. The displacement of the Cr(II) ions from the N_4 plane is reduced to an average of 0.10 Å and, in contrast to **1**, the direction of displacement is out of the intermetallic cleft towards the apical THF ligands.

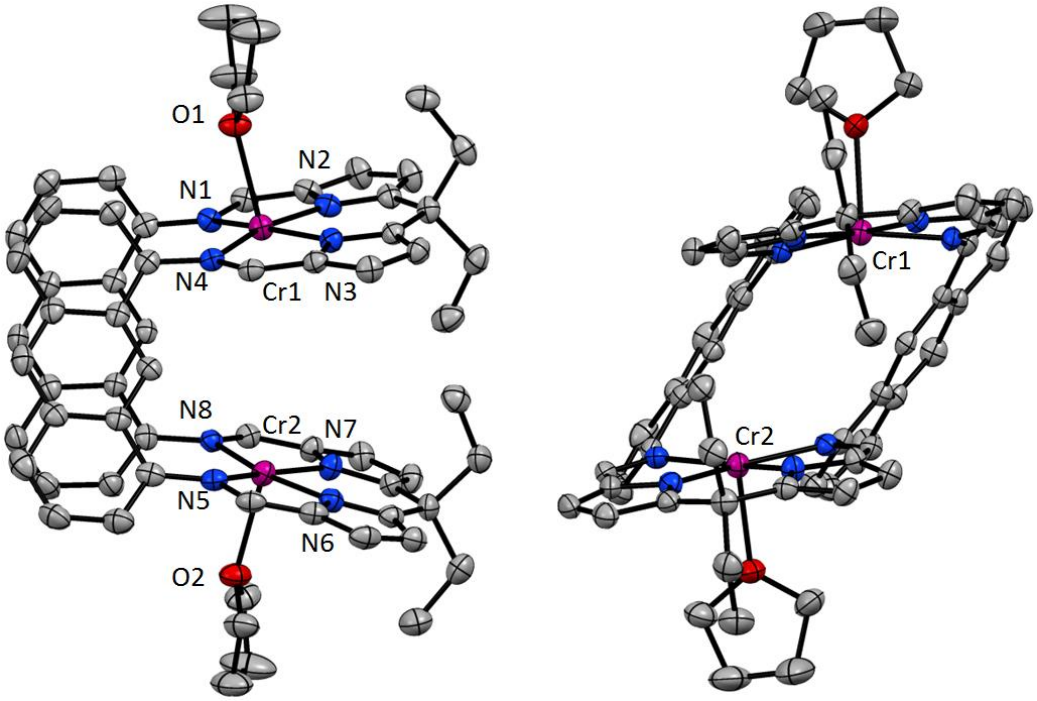

Figure 2.10 Solid state structure of $\mathbf{2_{THF}}$ showing side view (left) and view into the jaws of the macrocycle (right). Two molecules are present in the asymmetric unit; only one is shown here. Thermal ellipsoids are drawn at 50 % probability. For clarity, lattice solvent and H atoms are omitted.

Table 2.2 Selected distances (Å) for $\mathbf{2_{THF}}$.

Cr1···Cr2	5.6353(1)	mean Cr-N_{pyr}	1.99
Cr1-O1	2.349(3)	mean Cr-N_4 plane	+0.10
Cr2-O2	2.356(3)	twist angle	36
mean Cr-N_{im}	2.15		

The Cr-O_{THF} bond lengths in five co-ordinate Cr(II) complexes bearing a coordinated THF molecule fall into two distinct ranges: 2.01 - 2.23 Å and 2.28 – 2.47 Å.[47] The former range consists of pentagonal bipyramidal structures and square pyramidal structures in which the THF occupies an equatorial or basal position (eg. **2AG**, **2AH**, Figure 2.11) whilst the latter group is made up of square pyramidal structures in which the THF binds in the apical position (eg. **2AJ**, Figure 2.11). The Cr-O distances observed in $\mathbf{2_{THF}}$ of 2.349(3) and 2.356(3) Å are consistent with the latter range. The lengthening of the apical Cr-O bond is due to the occupation of the σ* 3d(z^2) orbital.

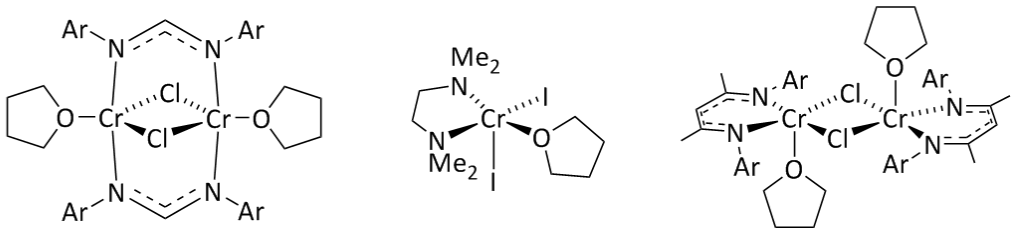

	2AG	**2AH**	**2AJ**
Cr-O_{THF} (Å)	2.124(2)	2.074(2)	2.394(1)

Figure 2.11 Examples of 5 co-ordinate Cr(II) complexes bearing THF ligands in different sites. Ar = 2,6-$C_6H_3(Me)_2$.[52-54]

2.3 Coordination chemistry of $[Cr_2(L^{Me})]$

The coordination of Lewis bases to Pacman and cofacial diporphyrin complexes can influence their reactivity towards small molecule substrates. The Love group reported that successful electrocatalytic reduction of O_2 to H_2O by the cobalt Pacman complex $[Co_2(L^A)]$ only occurs in the presence of benzonitrile (PhC≡N),[55] whilst Collman and co-workers showed that a bis-ruthenium cofacial diporphyrin complex binds dinitrogen irreversibly once activated by the addition of a bulky imidazole.[56] These donors bind to the metals in the *exo* axial coordination sites thereby fulfilling the dual role of directing the substrate to the *endo* intermetallic site and boosting the reactivity of the complex by increasing the electron density available at the metal centres. The coordination chemistry of **1** was investigated to gain an understanding of which Lewis bases form the most stable adducts with Cr(II) in the macrocyclic microenvironment.[57] All initial reactivity studies have been carried out on **1**

since it is more straightforward to prepare than **2** and benefits from enhanced solubility and crystallinity.

2.3.1 Reaction with triphenylphosphine oxide

Triphenylphosphine oxide has long been recognised as an excellent donor for "hard" first row transition metals.[58] Reaction of **1** with an excess of $OPPh_3$ in toluene resulted in precipitation of the 2:1 *exo* adduct $[Cr_2(OPPh_3)_2(L^{Me})]$ (**3**) as a microcrystalline solid in 63 % yield (Scheme 2.15). The ^1H NMR spectrum of **3** in C_6D_6 (in which **3** is sparingly soluble) shows paramagnetically broadened and contact-shifted resonances at δ 17.6, 7.7, 6.9, 4.6, −26, and −42 ppm, which are not assignable to specific ligand protons. While **3** dissolves readily in THF, the ^1H NMR spectrum in THF/C_6D_6 solution shows resonances consistent with **1** and broad features in the aromatic region corresponding to the phenyl protons of free $OPPh_3$. No resonances were present in the room temperature $^{31}P\{H\}$ NMR spectrum but upon cooling to -70°C a broad resonance was observed at 24 ppm corresponding to free $OPPh_3$. Therefore, in coordinating solvent the phosphine oxide ligands are labile and an equilibrium is likely established between the THF and phosphine oxide adducts of **1**.

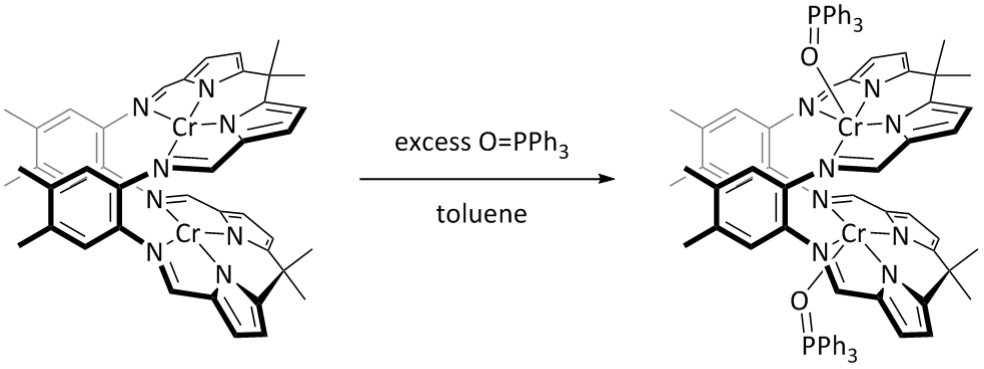

1 **3**

Scheme 2.15 Preparation of the phosphine oxide adduct **3**.

Single crystals of **3** were obtained from an NMR scale reaction in toluene. X-ray analysis confirmed the formation of the desired 2:1 *exo* adduct in which one phosphine oxide coordinates to each Cr(II) ion in the *exo* axial coordination site (Figure 2.12). The Cr centres adopt square pyramidal geometries with a Cr-O distance of 2.327(2) Å. Although a wide range of first row transition metal phosphine oxide complexes have been crystallised, to our knowledge this is the first structurally characterised Cr(II) phosphine oxide complex. With the exception of one manganese cluster compound, all other reported *3d* metal $OPPh_3$ structures feature considerably shorter M-O interactions than **3**, ranging from 1.91 to 2.26 Å.[47] Examples of Cr(III)[59] (**2AK**) and Mn(II)[60] (**2AL**) porphyrin-supported $OPPh_3$

complexes are shown in Figure 2.13. These complexes feature M-O distances of 2.034(4) and 2.05(1) Å respectively. The elongation of the Cr-O bond in **3** is expected on the basis of the increased ionic radius of Cr(II) *vs*. Mn(II), the decreased electrostatic attraction of Cr(II) *vs*. Cr(III) and the occupation of the σ* d(z^2) orbital in Cr(II) complexes but not Cr(III) complexes. The structural parameters of **3** are very similar to those of **2** as might be expected for two square pyramidal Cr(II) complexes with apical O-donors. The Cr1-O1-P1 bend angle of 137.6(1) orients the two propeller shaped PPh_3 units in opposite directions (Figure 2.12, right) giving the structure overall C_2 symmetry.

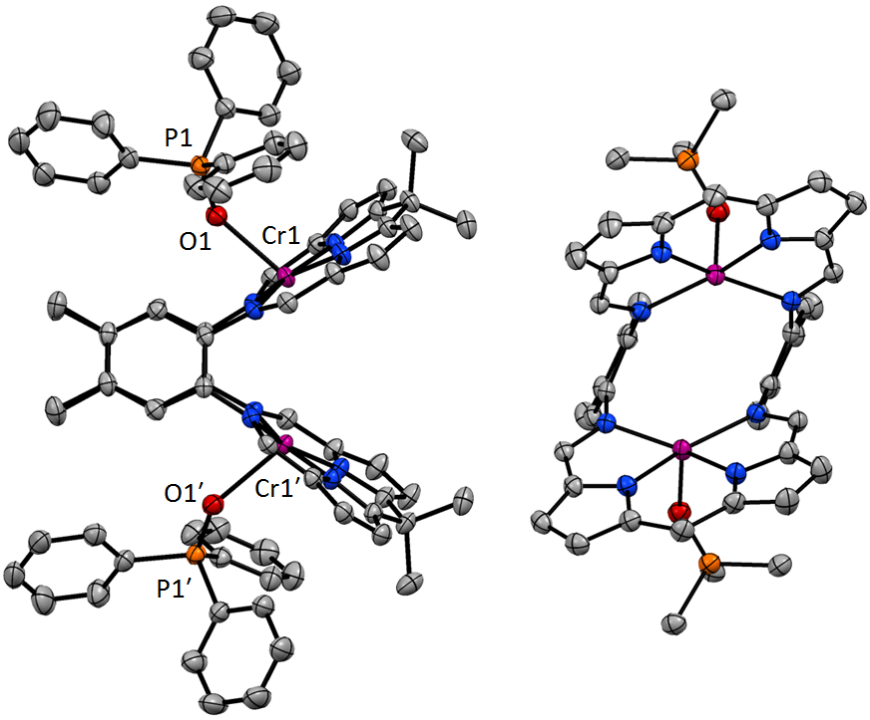

Figure 2.12 Solid state structure of **3** showing side view (left) and view into the jaws of the macrocycle (right). Thermal ellipsoids are drawn at 50 % probability. Lattice solvent and H atoms are omitted. For clarity, the *meso* Me groups and all but the *ipso* carbons of the $OPPh_3$ rings have been removed from the right hand structure.

Table 2.3 Selected distances (Å) and angles (°) for **3**.

Cr1···Cr1′	4.3210(5)	mean Cr-N_{pyr}	1.99
Cr1-O1	2.327(2)	Cr-N_4 plane	+0.16
O1-P1	1.497(2)	bite angle	67
Cr1-O1-P1	137.6(1)	twist angle	24
mean Cr-N_{im}	2.13		

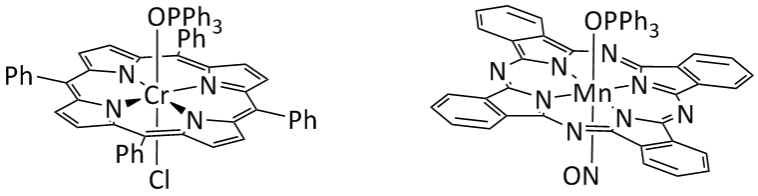

2AK **2AL**

Figure 2.13 Porphyrin-supported transition metal $OPPh_3$ complexes.[59,60]

The reactions of other Lewis bases with **1** were also investigated by NMR spectroscopy and a similar reactivity pattern was observed. When excess phosphine PR_3 (R = Me, Ph) was added to **1** in C_6D_6 a suspension formed, which is assumed to be the 2:1 adduct $[Cr_2(PR_3)_2(L^{Me})]$ (Scheme 2.16, right), and resonances corresponding to **1** were absent from the ^1H NMR spectrum. A new ^1H NMR spectrum acquired following addition of a couple of drops of THF to re-dissolve the suspension displayed resonances corresponding to **1** and broadened phosphine signals indicating fluxional co-ordination. By contrast, the adduct formed between **1** and 1,2-dimethylimidazole (im), presumably $[Cr_2(im)_2(L^{Me})]$ (Scheme 2.16, left), is robust in the presence of THF though unfortunately insoluble. However when this adduct was dissolved in d_5-pyridine, again resonances corresponding to **1** and broadened imidazole signals were observed. These observations suggest that stronger Lewis bases need to be employed to form a robust and soluble adduct.

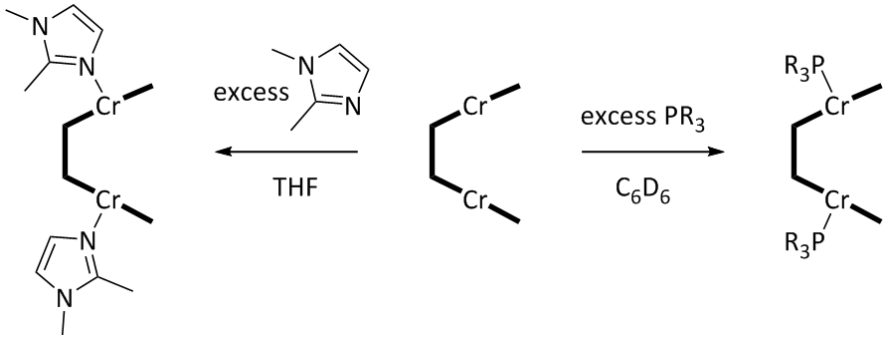

Scheme 2.16 Reactions of **1** with imidazole and phosphine bases. R = Me, Ph. The macrocycle is shown in cartoon form.

2.3.2 Reaction with isocyanides

Isocyanide ligands C≡NR are isolobal and isoelectronic to carbon monoxide and engage in analogous synergic bonding with transition metals (Figure 2.14). They are generally better σ-donors and poorer π-acceptors than CO, though their electronic and steric properties are tunable by modification of the organic substituent R.[61] Furthermore, transition metal isocyanide complexes have been employed to achieve C-F bond activation, selective hydrogenation of alkynes, nitriles and isocyanides, and alkene polymerisation.[62] Recently, a

co-ordinatively unsaturated cobalt(−I) complex supported by bulky *m*-terphenyl isocyanide ligands was isolated and was shown to bind dinitrogen, as well as undergoing reactions with a range of organic substrates.[63]

Figure 2.14 Illustration of the isolobal nature of CO and isocyanides in both the neutral and charge-separated canonical forms. The principle σ (blue) and π*(red) orbitals employed in metal binding are shown.

The reactions of **1** with two isocyanides, 2,6-xylyl and *tert*-butyl, were evaluated. The steric and electronic properties of these two isocyanides are considerably different: the xylyl isocyanide is flat whilst the *tert*-butyl isocyanide has appreciable three dimensional steric bulk, and the xylyl isocyanide is a poorer σ-donor but better π-acceptor than the *tert*-butyl isocyanide due to conjugation with the phenyl ring. An excess of the isocyanides C≡NR (R = Xyl, ^{t}Bu) were added to solutions of **1**. Single crystals were obtained from the reaction carried out in fluorobenzene (R = Xyl) and a THF/C_6D_6 mixture (R = ^{t}Bu). Determination of the structures revealed the formation of the 1:1 *endo* adducts [Cr_2(μ-CNXyl)(L^{Me})] (**4**) and [Cr_2(μ-CN^{t}Bu)(L^{Me})] (**5**) in which the isocyanide adopts a bridging position within the macrocyclic cleft, rather than the anticipated 2:1 *exo* adducts (Scheme 2.17).

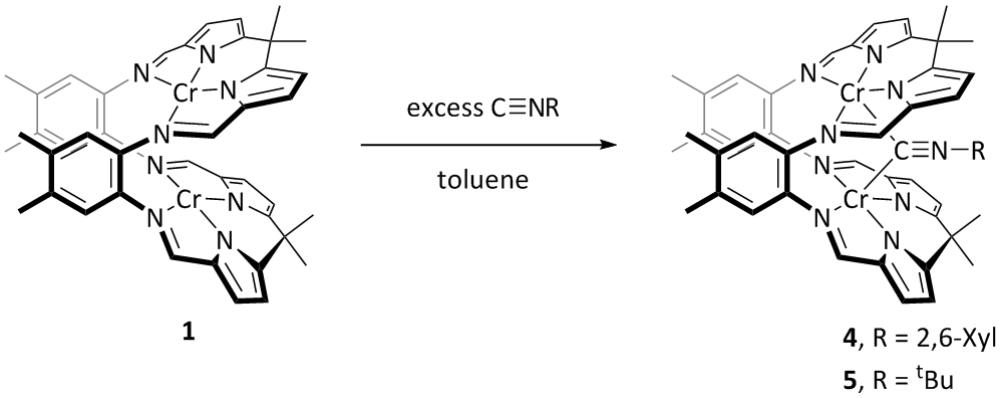

1

4, R = 2,6-Xyl
5, R = ^{t}Bu

Scheme 2.17 Synthesis of the bridging isocyanide complexes **4** and **5**.

On a preparative scale **4** and **5** may be synthesized in toluene, benzene or THF in good yields. The reaction between **1** and CNXyl is instantaneous and accompanied by a solution color change from dark red-brown to dark green. Dark red crystals of **4** precipitate rapidly from the reaction mixture regardless of which solvent is employed. Isolated **4** is only sparingly soluble in THF with no resonances observed in the ^{1}H NMR spectrum acquired in THF/C_6D_6 and **4** is stable under vacuum and as a suspension in THF. However, the ^{1}H NMR

spectrum recorded in d_5-pyridine shows resonances corresponding to **1** and a broad resonance at 1.8 ppm attributed to the *ortho*-Me groups of the free isocyanide. This implies that co-ordination of pyridine to the Cr centres is competitive with isocyanide co-ordination.

In contrast, **1** reacts slowly with CN^{t}Bu at room temperature in toluene, benzene or THF, though the reaction is complete within 48 h at 80 °C. Complex **5** is highly soluble in benzene and exhibits paramagnetically broadened and contact shifted resonances in the ^{1}H NMR spectrum (C_6D_6) at δ 20, 2.3 and −50 ppm. Complex **5** is stable under vacuum, in THF or pyridine solution, and even upon addition of the highly Lewis basic 4-dimethylaminopyridine. These observations suggest that an activation barrier must be overcome to co-ordinate the sterically hindered *tert*-butyl isocyanide within the intermetallic cleft but that once co-ordination has occurred the isocyanide is kinetically trapped and not vulnerable to competitive displacement. The magnetic moment of **5** in C_6D_6 solution was measured as 4.75 μ_B, which is significantly less than the magnetic moment of **1** (6.34μ_B). Therefore the presence of the isocyanide bridge increases the electronic communication between the two Cr(II) centres and facilitates antiferromagnetic coupling.

The solid state structures (Figure 2.15) reveal that the isocyanides bridge symmetrically between the square pyramidal Cr(II) centres, which are displaced considerably out of the N_4 donor pockets into the macrocyclic cleft (Table 2.4, 7.). In **4** the planar xylyl ring is perpendicular to the aryl hinges of the macrocycle, minimising steric interactions with the *endo meso* Me groups, C7 and C28. One of the protons bound to C7 is oriented towards the electron rich π-system of the isocyanide ligand (C7···C44 3.349(3) Å, C7···N9 3.568(3) Å) indicating that intramolecular hydrogen bonding occurs, similar to that seen in [Cu_2(μ-py)(L)].[45] In contrast, the three-dimensional steric bulk of the ^{t}Bu group in **5** forces the isocyanide to protrude sideways out of the macrocycle jaws to avoid clashing with the *meso* Me groups (Figure 2.15, bottom right). We reason that these steric constraints prevent the ^{t}Bu isocyanide from approaching closer to the Cr centers, resulting in the longer Cr-C separation observed in **5** of 2.490(2) Å compared to 2.259(2) Å and 2.261(2) Å in **4** and the more acute Cr-C-Cr bridging angle of the *tert*-butyl isocyanide (96.35(7) ° in **5** *vs*. 105.080(9) in **4)**.

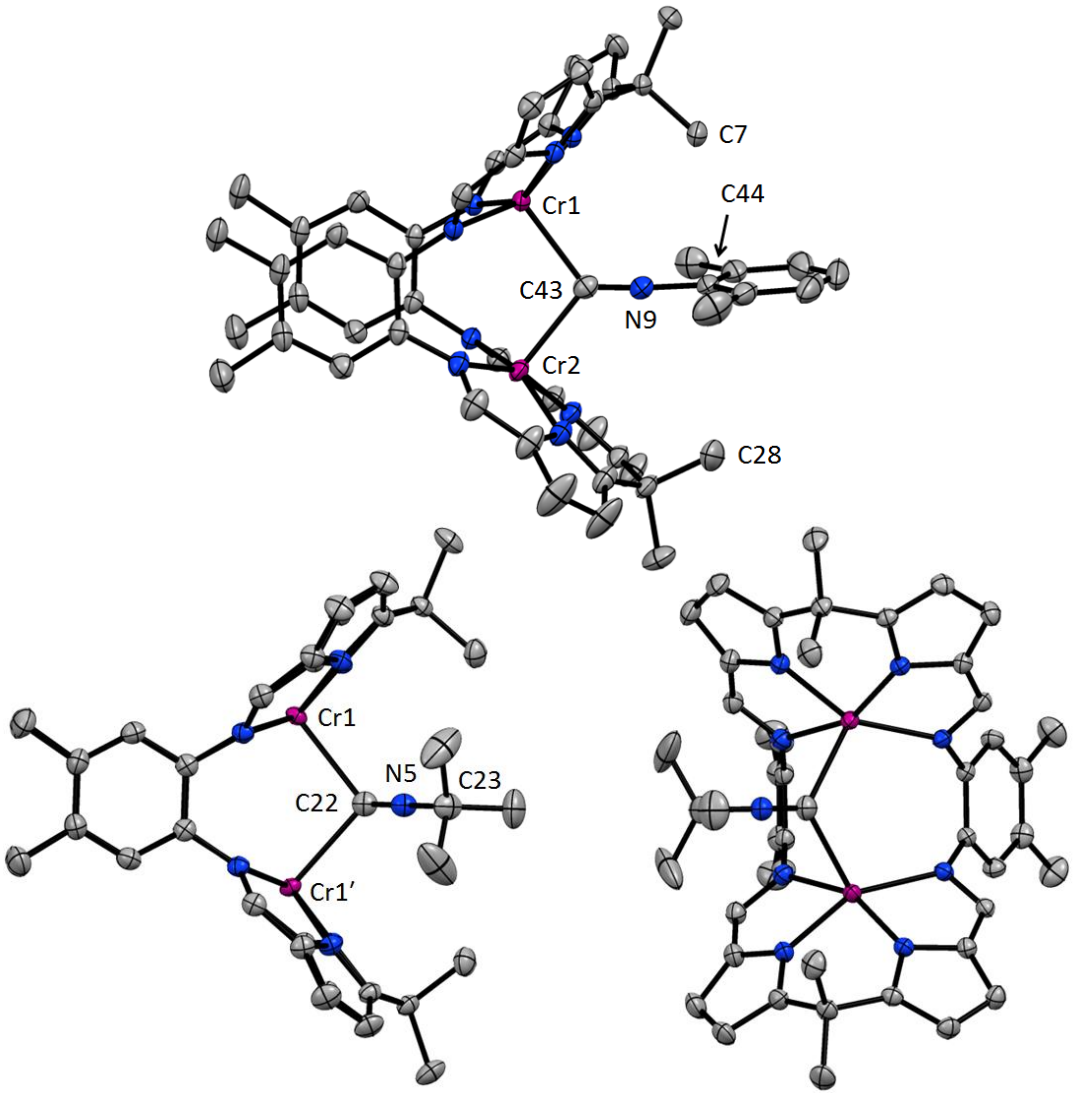

Figure 2.15 Solid state structures of **4** (top) and **5** (bottom). Thermal ellipsoids are drawn at 50 % probability. Lattice solvent and H atoms are omitted. Both a side view and the view into the jaws of the macrocycle are shown for **5**. The *tert*-butyl group of the isocyanide ligand in **5** was found to be rotationally disordered, the major conformer is shown.

Table 2.4 Comparison of selected structural parameters of **4** and **5**. Distances (Å), angles (°).

		4	**5**
1.	Cr···Cr	3.5877(5)	3.7101(3)
2.	Cr-C_{CNR}	2.259(2), 2.261(2)	2.490(2)
3.	C_{CNR}-N_{CNR}	1.169(3)	1.151(3)
4.	Cr-C_{CNR}-Cr	105.08(9)	96.35(7)
5.	Cr-C_{CNR}-N_{CNR}	127.9(2), 126.7(2)	128.50(2)
6.	C_{CNR}-N_{CNR}-C_{CNR}	175.9(2)	172.8(2)
7.	mean Cr-N_4 plane	−0.39	−0.37
8.	bite angle	53	56
9.	twist angle	2	10

In both **4** (C43-N9-C44 175.9(2) °) and **5** (C22-N5-C23 172.8(2) °) the bridging isocyanide retains the linear geometry of the free ligand. This is not uncommon for a bridging isocyanide (see for example **2AN**, Figure 2.16).[64,65] The frequency of the C≡N stretching band in the IR spectrum is more indicative of the degree of back donation than the isocyanide geometry. In the IR spectrum (nujol mull) of **5**, $\nu_{C\equiv N}$ is 2150 cm^{-1}. This is shifted to slightly higher energy than in free CN^{t}Bu (2132 cm^{-1}) and indicates that little π back donation occurs from the Cr(II) centres to the isocyanide. The metal-ligand interaction is dominated by σ-donation which occurs from a carbon-based orbital that is anti-bonding with respect to the (C≡N)π system of the isocyanide, explaining the increase in $\nu_{C\equiv N}$.[66] In contrast, two C≡N stretching bands are observed in the IR spectrum of **4** at 1990 cm^{-1} and 1970 cm^{-1}, a phenomenon which has been observed before in complexes containing a single bridging isocyanide and is attributed to solid state effects.[67] These bands are shifted to considerably lower energy than in free CNXyl (2114 cm^{-1}) indicating that significant π back donation occurs. The observed increase in back donation is likely due to the greater π-acceptor ability of the conjugated aryl isocyanide compared to CN^{t}Bu and the shorter Cr-C_{CNR} separation in **4** compared to **5** resulting in increased M-L orbital overlap.

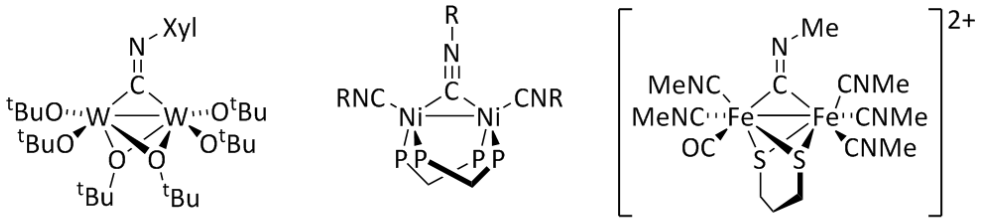

bend angle	**2AM**	**2AN**	**2AP**
C-N-C	130(2) °	159.0(2) ° (R=^{t}Bu), 180 ° (R=Xyl)	163.9(4) °

Figure 2.16 Examples of homobimetallic W(III),[68] Ni(0) [65] and Fe(II) [69] isocyanide bridged complexes. Eight phenyl groups bound to the P atoms of **2AN** have been omitted.

Although bimetallic complexes with bridging isocyanide ligands are common in late transition metal chemistry, those of early transition metals are rare. The only homo-bimetallic examples reported are two molybdenum and three tungsten complexes, one of which, **2AM**, is shown in Figure 2.16.[68,70-72] Since these are the first binuclear chromium μ-CNR complexes, comparison with other first row transition metal complexes is instructive. A number of mid to late first row transition metal complexes containing the motifs {M_2(μ-CNR)} or {M_3(μ^3-CNR)} have been reported, including for R = ^{t}Bu, Xyl. For the binuclear complexes, the mean M-C_{CNR} distance is 1.98 Å.[47] The longest M-C_{CNR} bond previously reported is 2.381(4) Å in a binuclear Fe(II) compound bridged by CNMe (**2AP**, Figure

2.16),[69] meaning that the M-C_{CNR} distance observed in **5** (2.490(2) Å) is by far the longest for a *3d* metal isocyanide bridged complex.

To summarize, the isocyanide ligands display exclusive preference for the *endo* intermetallic bridging site where they are held between the two Cr(II) ions as if in a pincer. The *tert*-butyl isocyanide complex **5** is a soluble and kinetically stable adduct of **1**. However **5** is expected to be of limited use in further reactivity studies since the intermetallic site designed for the cooperative binding of substrates is blocked by the isocyanide ligand.

2.3.3 Attempted reactions with gases

Since **1** readily binds isocyanides in the *endo* intermetallic site, its reactivity towards CO was also evaluated. To our surprise, ^{1}H NMR spectroscopy indicated that no reaction occurred between a THF solution of **1** and an atmosphere of CO gas at 1.0 bar. As mentioned above, CO is generally a poorer σ-donor but a better π-acceptor than isocyanides and less sterically demanding. We conclude that σ-donor strength must determine whether or not adduct formation with **1** is favoured. In this instance, CO, unlike the isocyanides, cannot out-compete the THF solvent.

THF solutions of **1** were also found to be unreactive towards CO_2 and H_2. Introduction of an atmosphere of O_2 to a pyridine solution of **1** did not result in any obvious colour change or formation of a precipitate but the resonances corresponding to **1** were absent from the subsequent ^{1}H NMR spectrum. This indicates that a reaction occurred but the products were not successfully isolated or characterised.

2.4 Redox chemistry of [$Cr_2(L^{Me})$]

There have been very few reports on the synthesis or reactivity of early transition metal complexes of binucleating ligands. Therefore, it seemed pertinent to explore the redox chemistry of **1** to investigate the effect of the steric restrictions imposed by the ligand environment and determine whether the metal ions act as two independent redox centres.

2.4.1 Attempted reduction of [$Cr_2(L^{Me})$]

Since the metal centres in **1** are not sufficiently reducing to react with CO_2, H_2 or CO, attempts were made to reduce the Cr(II)/Cr(II) Pacman complex to either a Cr(I)/Cr(II) or Cr(I)/Cr(I) Pacman complex. Binuclear Cr(I) species have been shown to be sufficiently reducing to bind, and in some cases activate N_2, CO, alkynes and alkenes.[13,21] Trial reactions of **1** with potassium reducing agents were carried out with a view to forming a reduced salt

of general formula $K_x[Cr_2(L^{Me})]$ (x = 1 or 2). Conceivably such a salt could be stabilised, and solubilised, by η^6 or η^5 interactions between the ligand arene groups or ligand pyrrolides and the K^+ cation(s).

Slightly more than two equivalents of potassium metal, potassium graphite or potassium naphthalenide were added to a THF solution of **1** (Scheme 2.18). Reaction occurred in all cases, accompanied by a colour change from red-brown to dark brown. THF soluble products were formed in the reactions with potassium graphite and potassium naphthalenide but these products or mixtures of products are NMR silent. In contrast, copious quantities of dark brown precipitate formed in the potassium metal reaction after overnight heating at 80 °C. The elevated temperature was necessary to melt the potassium and facilitate reaction, however, it is possible that the products underwent thermal decomposition after formation. Attempts to obtain single crystals for X-ray analysis from the potassium graphite and potassium naphthalenide reaction mixtures were unsuccessful. The addition of 18-crown-6, which often increases the crystallinity of potassium salts, did not result in the formation of single crystals. Since we were unable to establish whether a single product or mixture of products is formed in these reactions, or identify any component of the reaction mixture, reactivity studies of the reduction products were not pursued.

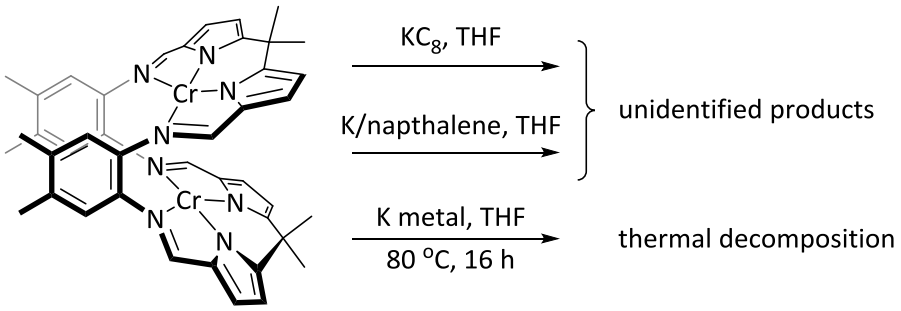

Scheme 2.18 Attempted potassium reductions of **1**.

2.4.2 Oxidation of $[Cr_2(L^{Me})]$

The Pacman macrocycles, with their two $(N_4)^{2-}$ donor pockets, are designed to form simple binary complexes with metals in the +2 oxidation state, without the need for any auxiliary anionic ligands. Indeed, the majority of the Pacman complexes reported by the Love group to date are of the form $[M^{II}_2(L)]$.[45] If the study of early transition metal Pacman complexes is to be extended beyond chromium, an understanding of Pacman complexes of metals in the +3 oxidation state and higher will be necessary since monomeric M(II) precursors of group III, IV, V and the heavier group VI metals are not generally available.[1]

2.4.2.1 Synthesis of $[Cr_2(\mu\text{-}I)(I)(THF)(L^{Me})]$

Iodine was investigated as an alternative oxidant to O_2, the advantages being that iodine is straightforward to purify by sublimation and enables good stoichiometric control. Stoichiometric O-based oxidants such as pyridine-N-oxide were avoided since the synthetic versatility of halides in salt elimination reactions made $[(CrI)_2(L^{Me})]$ a more attractive target for future reactivity studies than $[Cr_2(O)(L^{Me})]$.

Compound **1** was combined with one equivalent of I_2 in THF and the mixture stirred overnight at ambient temperature. During this time the colour of the solution changed from red-brown to deep crimson. Removal of the volatiles followed by hexane washing allowed the isolation of $[Cr_2(\mu\text{-}I)(I)(THF)(L^{Me})]$ (**6**) as a red microcrystalline solid in 84 % yield (Scheme 2.19). The ^{1}H NMR spectrum of **6** displays several very broad resonances between δ 24 and −67 ppm which cannot be assigned to individual ligand proton environments. The solution phase magnetic moment of **6** measured in THF/C_6D_6 by the Evans' method was determined as 5.43 μ_B, which is very similar to the spin only value of 5.48 μ_B calculated for two non-interacting s = 3/2 ions. This indicates that the bridging iodide anion does not facilitate magnetic exchange between the two Cr(III) ions. The reduction in the magnetic moment of **6** compared to that of **1** (6.34 μ_B) is consistent with the oxidation of the chromium centres from Cr(II) to Cr(III). Addition of half an equivalent of I_2 to **1** also resulted in the formation of **6** (confirmed by unit cell check) and, presumably, unreacted starting material. In this case it is not possible to selectively oxidise just one chromium centre to form a mixed valence Cr(III)/Cr(II) compound.

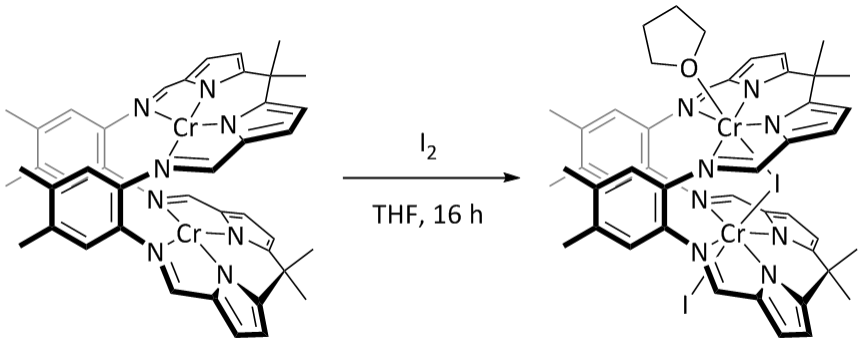

Scheme 2.19 Oxidation of $[Cr_2(L^{Me})]$ with iodine in THF to form **6**.

Single crystals suitable for diffraction analysis were grown by vapour diffusion of hexane into a THF solution of **6** at ambient temperature over 3 days. The solid state structure (Figure 2.17) reveals that the Pacman geometry is maintained with one iodide ligand *endo* to the cleft, bridging the two Cr(III) centres and the other iodide *exo* to the cleft in a terminal binding site. The two Cr(III) ions occupy inequivalent *pseudo* octahedral coordination sites.

In contrast to Cr(II), Cr(III) ($3d^3$) displays a strong preference for octahedral co-ordination due to the favourable ligand field stabilisation energy generated by this electronic configuration in an octahedral environment. Four equatorial N-donors are provided by each pocket of the macrocycle and both Cr(III) ions bind to the *endo* iodide I1. The *exo* axial site at Cr1 is occupied by a coordinated THF molecule whilst Cr2 is bound to the *exo* iodide I2. The Cr(III) ions are barely displaced out of the N_4 donor pockets of the macrocycle, the bite angle of 67 ° is close to the theoretical free macrocycle bite angle of 60 °, and the O1-Cr1-I1 and I2-Cr-I1 angles of 179.96(9) ° and 179.05(3) ° are near linear, all of which indicate that the bridging iodide is incorporated with very little strain imposed on the macrocyclic framework. The Cr(III)-N(imine/pyrrolide) distances in **6** have contracted slightly compared to those in the Cr(II) compounds **1** to **5**, as is consistent with the increase in oxidation state of the Cr centres. The mean Cr-N(imine) and Cr-N(pyrrolide) distances in **6** are 2.09 Å and 1.96 Å respectively compared to mean Cr-N(imine) and Cr-N(pyrrolide) distances of 2.13Å and 1.99Å respectively in **1** to **5**.

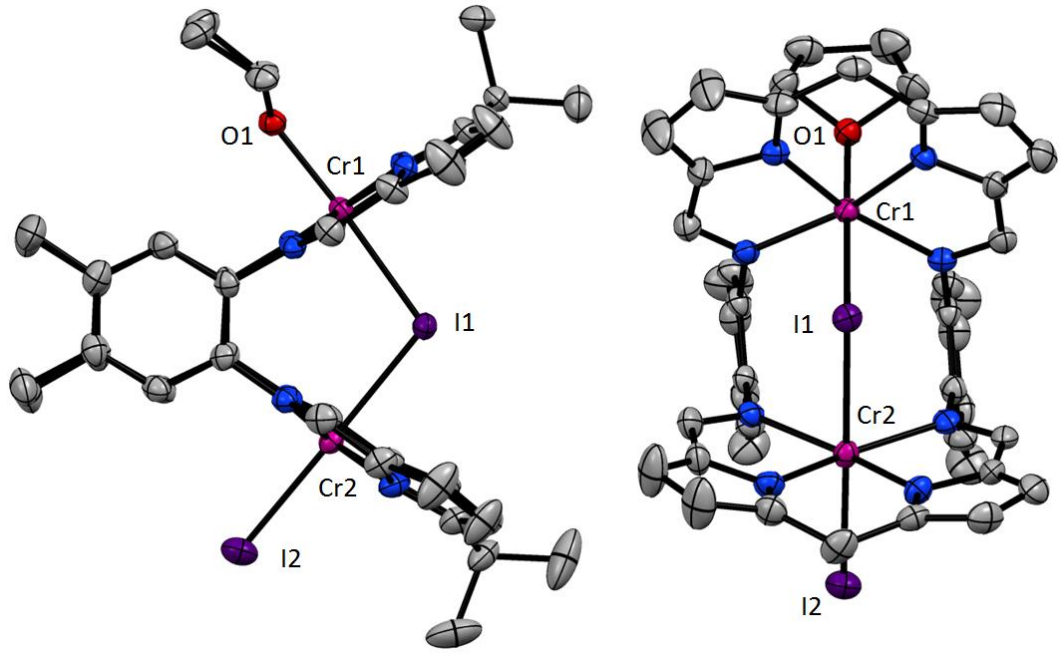

Figure 2.17 Solid state structure of **6** showing side view (left) and view into the jaws of the macrocycle (right). Thermal ellipsoids are drawn at 50 % probability. For clarity, lattice solvent and H atoms are omitted and the *meso* Me groups have been removed from the right hand structure.

Table 2.5 Selected distances (Å) and angles (°) for **6**.

Cr1···Cr2	4.3811(9)	mean Cr-N_4 plane	+0.07
Cr1-I1	2.7131(7)	Cr1-I1-Cr2	105.56(2)
Cr2-I1	2.7883(7)	O1-Cr1-I1	179.96(9)
Cr1-O1	2.076(3)	I2-Cr2-I1	179.05(3)
Cr2-I2	2.7018(8)	bite angle	67
mean Cr-N_{im}	2.09	twist angle	5
mean Cr-N_{pyr}	1.96		

The terminal I2-Cr2 bond length of 2.7018(8) Å is typical for a Cr(III) iodide complex; reported Cr(III)-I distances range from 2.5768(7) Å to 2.7816(7) Å, with a mean value of 2.69 Å.[47] The Cr1-I1 bond length of 2.7131(7) Å is significantly shorter than the Cr2-I1 bond of 2.7883(7) Å, presumably due to the differing *exo* ligands attached to Cr1 and Cr2. The {Cr^{III}-(μ-I)-Cr^{III}} motif exhibited in **6** is an unusual one. Though a large number of chloride-bridged chromium complexes have been crystallographically characterised, examples containing bromide or iodide bridges are rare. Indeed, there are no reports of Cr(III) centres bridged by a single iodide.

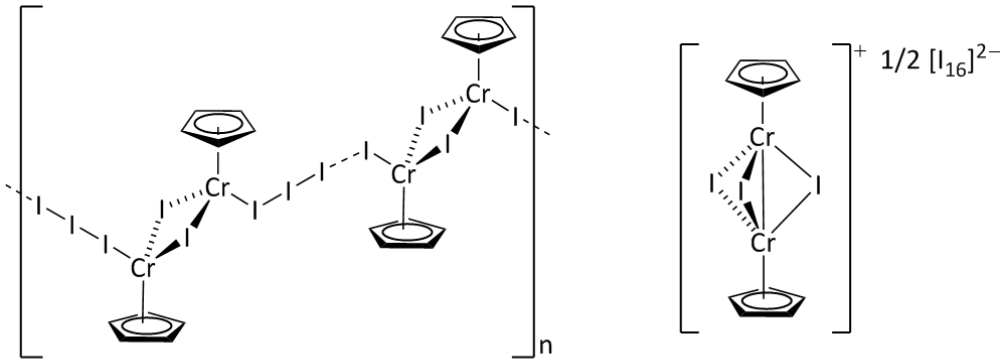

2AQ **2AR**

Figure 2.18 Molecular structures of the iodide bridged chromium (III) complexes with empirical formulae [Cp*CrI_3] (**2AQ**) and [Cp*$CrI_{5.5}$] (**2AR**).[73] The Me groups are omitted from the Cp* rings.

Rauchfuss reported an interesting series of complexes with the empirical formulae [Cp*$Cr^{III}I_x$] (x = 2, 3, 5.5) which feature polyiodide bridges.[73] The structures of the x = 3 (**2AQ**) and x = 5.5 (**2AR**) members are shown in Figure 2.18. In the solid state **2AQ** is an alternating copolymer of [Cp*Cr(μ-I)I]$_2$ and [Cp*Cr(μ-I)(I_3)]$_2$ dimers whilst **2AR** is formulated as [Cp*$_2$$Cr_2$(μ-I)$_3$]$_2$[$I_{16}$], containing the polyiodide cluster anion $[I_{16}]^{2-}$. The authors suggest that the short Cr-Cr distance observed in **2AR** (Table 2.6) and the sharpening of the Cp*signal in the ^{1}H NMR spectrum relative to that of **2AQ** indicate that there is some degree of *d*-electron pairing and M-M bonding. Comparing selected structural parameters of **6**, **2AQ** and **2AR** (Table 2.6) clearly illustrates the effect of increasing number of bridging

iodides: Cr···Cr separation decreases, Cr-I bond length decreases and the Cr-I-Cr bridging angle becomes more acute.

Table 2.6 Comparison of selected structural parameters for different iodide-bridged chromium complexes.

	6	**2AQ**	**2AR**
number of (μ-I)	1	2	3
Cr···Cr (Å)	4.38	3.71	3.01
Cr-(μ-I) (Å)	2.75	2.71	2.69
Cr-(μ-I)-Cr (°)	106	86	68

2.4.2.2 Synthesis of [Cr_2(μ-I)(py)$_2$(L^{Me})][I]

The reaction of **1** with iodine in pyridine solvent was also investigated. In contrast to the reaction in THF which proceeds over several hours with a subtle colour change, when **1** and iodine were combined in pyridine immediate precipitation of a red-bronze solid was observed. Repeating the experiment, this time slow-diffusing a pyridine solution of **1** into a pyridine solution of iodine allowed the isolation of poor quality single crystals. X-ray diffraction analysis revealed the product to be the salt [Cr_2(μ-I)(py)$_2$(L^{Me})][I] (**7**) (Scheme 2.20, Figure 2.19). Once again the Pacman geometry is maintained and a bridging iodide occupies the intermetallic cleft. However, both *exo* axial Cr binding sites are occupied by pyridine and the remaining iodide sits within the crystal lattice as an isolated anion. The Cr(III) ions therefore occupy equivalent *pseudo* octahedral binding sites and the macrocycle is symmetric. The structural resolution of **7** is poor and a number of restraints were necessarily imposed during refinement (see 4.6.7) meaning that numerical analysis of the structure should be treated with caution. The structure of the cation of **7** is similar to that of **6**. Once again the N-Cr-(μ-I) angles (179.0(4) °, 179.3(5) °) are essentially linear and the Cr1-I1-Cr2 angle in **7** of 106.59(7) ° is very close to that seen in **6** (105.56(2) °). The Cr···Cr separations observed in **6** and **7** are 4.3811(9) Å and 4.417(4) Å respectively and the macrocycles in both complexes display very similar bite and twist angles. One minor difference between **6** and **7** is that the *endo* iodide bridges more symmetrically between the two Cr(III) ions in **7** due to the increased symmetry of the macrocyclic environment with all pyridine *exo* donors; Cr1-I1 = 2.756(3) Å and Cr2-I1 = 2.754(2) Å in **7** whereas in **6** there is a difference in the Cr-(μ-I) bond lengths of *ca.* 0.08 Å. No spectroscopic data were obtained for **7** due to its extremely poor solubility.

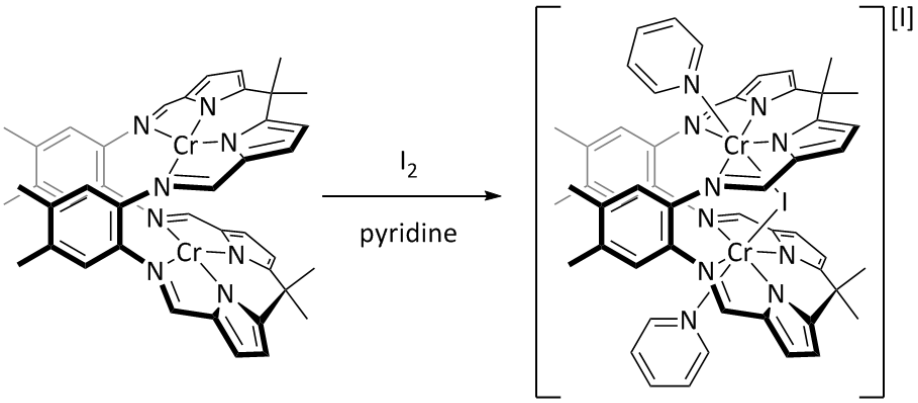

1 **7**

Scheme 2.20 Oxidation of $[Cr_2(L^{Me})]$ with iodine in pyridine to form **7**.

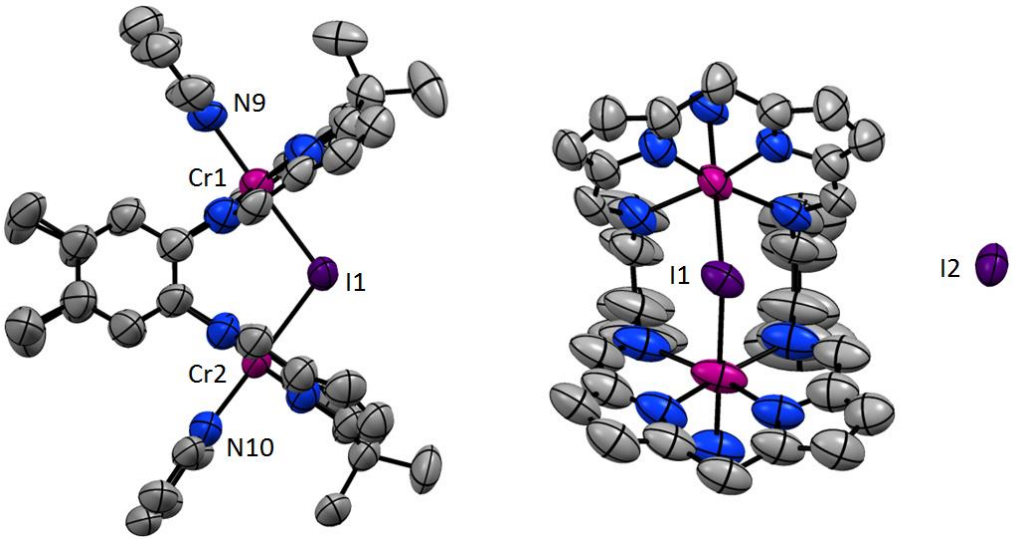

Figure 2.19 Solid state structure of **7** showing side view of the cation (left) and view into the jaws of the macrocycle (right). Thermal ellipsoids are drawn at 50 % probability. Lattice solvent and H atoms are omitted. For clarity, the *meso* Me groups and the carbon atoms of the pyridine rings have been removed from the right hand structure.

Table 2.7 Selected distances (Å) and angles (°) for **7**.

Cr1···Cr2	4.417(4)	mean Cr-N_4 plane	+0.09
Cr1-I1	2.756(3)	Cr1-I1-Cr2	106.59(7)
Cr2-I1	2.754(2)	N9-Cr1-I1	179.0(4)
Cr1-N9	2.10(2)	N10-Cr2-I1	179.3(5)
Cr2-N10	2.08(1)	bite angle	69
mean Cr-N_{im}	2.06	twist angle	3
mean Cr-N_{pyr}	1.96		

The formation of the ionic product **7** rather than a neutral pyridine solvated analogue of **6** is clearly caused by the change in solvent from THF to the more polar, more Lewis basic pyridine. It has long been known that a degree of ionisation occurs in binary

iodine/pyridine mixtures.[74] The relevant equilibria are shown in Scheme 2.21. Equilibria (2) and (3) may be replaced by the single process (4). Besnard and co-workers have demonstrated that attainment of equilibrium (4) is rapid (nanosecond timescale) and that the equilibrium concentration of the triiodide anion is roughly 4 % of the initial I_2 concentration.[75]

$$py + I_2 \rightleftharpoons \{pyI_2\} \quad (1)$$

$$\left[\begin{array}{rl} \{pyI_2\} & \rightleftharpoons [pyI]^+ + I^- \quad (2) \\ I^- + \{pyI_2\} & \rightleftharpoons I_3^- + py \quad (3) \end{array}\right]$$

$$2\{pyI_2\} \rightleftharpoons [py_2I]^+ + I_3^- \quad (4)$$

Scheme 2.21 Equilibria established in binary iodine/pyridine mixtures. $\{pyI_2\}$ represents an outer-sphere co-ordination complex.[75]

Upon combination of **1** with iodine in pyridine, the potential reactive species present are I_2 and $[py_2I][I_3]$. Therefore both molecular and ionic reaction pathways must be considered, as outlined in Scheme 2.22. In the ionic pathway, the two Cr(II) centres of **1** co-operatively reduce the cation in $[py_2I][I_3]$ to form $[Cr_2(\mu\text{-}I)(py)_2(L^{Me})][I_3]$ (step i). The pyridine solvent then abstracts I_2 from the I_3^- ion to form **7** (step ii) and the outer-sphere complex $\{pyI_2\}$, according to the reverse of equilibrium (3) (Scheme 2.21). In the molecular route, **1** reacts with I_2 to form the neutral pyridine solvated analogue of **6**, $[Cr_2(\mu\text{-}I)(I)(py)(L^{Me})]$ ($\mathbf{6_{py}}$) (step iv). Conceivably, $\mathbf{6_{py}}$ could be converted into **7** by ionisation driven by pyridine coordination (step v) and likewise **7** formed *via* the ionic route could be converted to $\mathbf{6_{py}}$ by displacement of a pyridine molecule by the I^- counterion (step iii).

Complex **7** precipitates from the reaction mixture in 50 % yield and the supernatant decanted retains a deep pink-red colour. Therefore it seems likely that a second more soluble product is also formed which is proposed to be the neutral complex $\mathbf{6_{py}}$, though this has not been spectroscopically observed, isolated or characterised. By analogy to the reaction of **1** with iodine in THF, formation of $\mathbf{6_{py}}$ *via* the molecular pathway is expected to be moderately slow, taking place over hours. The experimental observation that **7** precipitates within minutes indicates firstly that **7** is probably not formed by the molecular pathway and secondly that reaction of **1** with ionic $[py_2I][I_3]$ must be rapid; step (i) is faster than competing step (iv). This could account for the formation of an appreciable quantity of **7**, despite the low equilibrium concentration of $[py_2I][I_3]$ present. The insolubility of **7** will also help to drive equilibrium (ii) towards its formation.

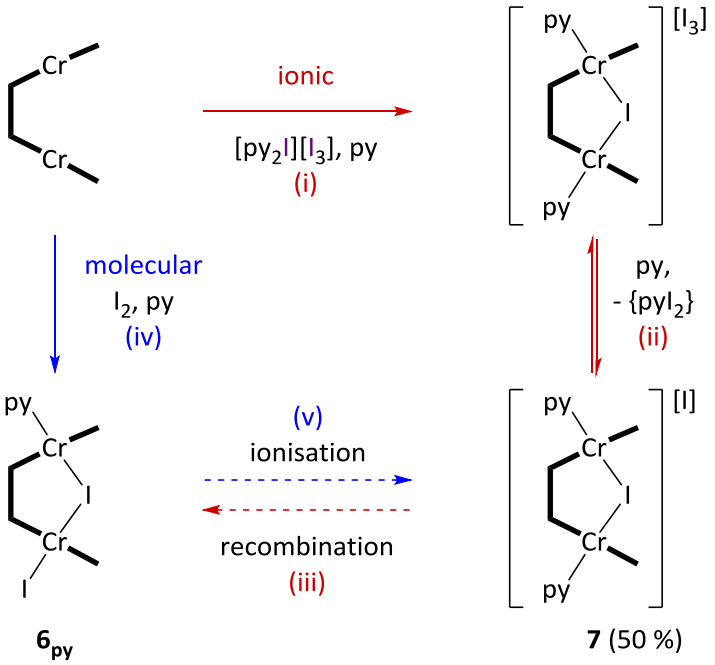

Scheme 2.22 Possible pathways to the formation of $\mathbf{6_{py}}$ and **7**.

Isolated **7** is insoluble in pyridine. However, when a suspension of **7** in pyridine was left to sit for 2 weeks the solid dissolved forming a pink-red solution. This provides some evidence that the recombination of the iodide anion to form the neutral, soluble complex $\mathbf{6_{py}}$ (step (iii)) may indeed be feasible, though the rate is slow. This is presumably due to the poor solubility of **7** coupled with the expected kinetic stability of the $3d^3$ Cr^{3+} ion. When **6** was dissolved in pyridine, presumably forming the pyridine solvate $\mathbf{6_{py}}$, no solid formation was observed over the course of 1 week indicating that solvation driven ionisation of $\mathbf{6_{py}}$ to form **7** does not occur and step (v) is not feasible.

We conclude that **7** is exclusively formed by reaction of **1** with the ionic species $[py_2I][I_3]$ which proceeds rapidly. The reaction of **1** with I_2 to form $\mathbf{6_{py}}$ is a competing process. The rate of the latter reaction is slower but the starting concentration of I_2 is much greater than that of $[py_2I][I_3]$, resulting in an approximate 50:50 product distribution. Although experimental observations indicate that **7** may be converted into $\mathbf{6_{py}}$, this process is slow compared to the timescale of the reaction.

2.4.2.3 Anion substitution of $[Cr_2(\mu\text{-}I)(py)_2(L^{Me})][I]$

In an effort to isolate a more soluble derivative of **7** which might prove more versatile in further reactivity studies, an anion exchange reaction was carried out. The anion chosen was a highly soluble, non-co-ordinating aryl borate $[B\{(OC_6H_2(^tBu)_2)_2\}_2]^-$. Addition

of the sodium salt $[Na(THF)_2][B\{OC_6H_2(^tBu)_2\}_2]$ to a mixture of **1** and I_2 in pyridine, followed by heating to 115 °C for 5 min results in complete dissolution of the suspended product **7**. Removal of the volatiles followed by toluene extraction allows isolation of the anion exchange product $[Cr_2(\mu\text{-}I)(py_2)(L^{Me})][B\{OC_6H_2(^tBu)_2\}_2]$ (**8**) as a red powder in 40 % yield (Scheme 2.23). Single crystals of **8** were obtained but the X-ray diffraction data could not be solved so the formulation of **8** is evidenced by elemental microanalysis.

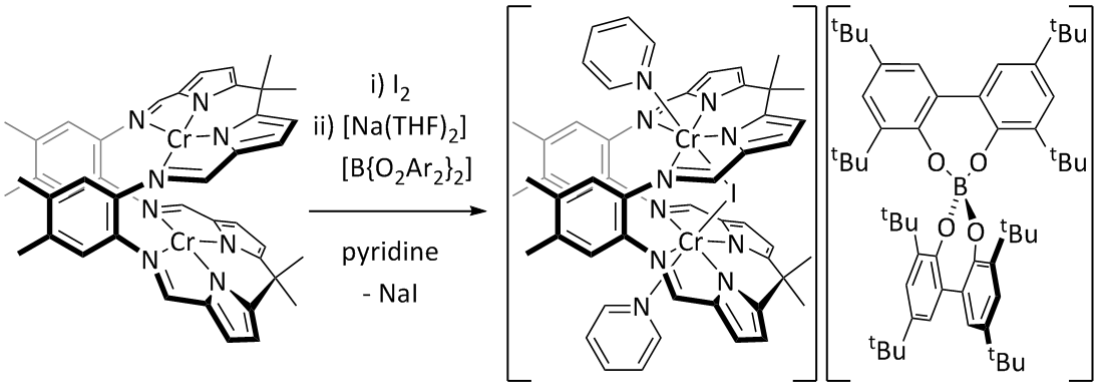

1 **8**

Scheme 2.23 Synthesis of chromium borate salt **8**.

Since the sodium borate is added to a reaction mixture containing $\mathbf{6_{py}}$ and **7**, it is conceivable that both these species could be converted into **8** by iodide abstraction and anion exchange processes respectively. If the yield of **8** were higher than that of **7**, then this would indeed seem to be a reasonable conclusion. However, the yield of **8** is slightly reduced compared to that of **7**. The ligands at the Cr(III) centres in $\mathbf{6_{py}}$ are expected to be reasonably inert due to the favourable ligand field stabilisation energy associated with their d^3 electronic configuration and the abstraction of an iodide from $\mathbf{6_{py}}$ would involve separation of charge. Therefore it is suggested that **8** is formed exclusively by from **7** since exchange of the free iodide anion in **7** will have a much lower activation barrier than substitution of an axial iodide ligand in $\mathbf{6_{py}}$.

2.5 Synthesis and reactivity of chromium alkyls

The use of organometallic catalysts to effect transformations of organic molecules is ubiquitous in industry and research. Transition metal alkyl complexes are essential intermediates in many of these processes, whether it be olefin polymerisation/oligomerisation, Pd-catalysed cross-couplings, hydroformylation or alkene metathesis, to mention but a few.[76] Successful completion of these catalytic cycles relies on the ability of transition metal alkyls to undergo a variety of insertion, migration and

elimination reactions. The synthesis of transition metal alkyl complexes is desirable in order to study their structures and reactivity and gain insight into the function of heterogeneous industrial catalysts. This is particularly relevant to chromium which is employed as an industrial catalyst for the production of 1-hexene and high density polyethylene.

2.5.1 Reactions of $[Cr_2(\mu\text{-}I)(I)(THF)(L^{Me})]$ with $ZnEt_2$

Initially reaction of the transmetallation reagent $ZnEt_2$ with **6** was investigated. **6** was used as the starting material rather than **7** or **8** because it is soluble in both co-ordinating and non-co-ordinating solvents and may be prepared in high yield. $ZnEt_2$ was chosen over the more highly reducing alkali metal alkylating reagents in order to decrease the likelihood of reduction of the Cr(III) centres to Cr(II).

2.5.1.1 Formation of $[\{Cr(Et)\}_2(\mu\text{-}I\text{-}ZnEt)(L^{Me})]$

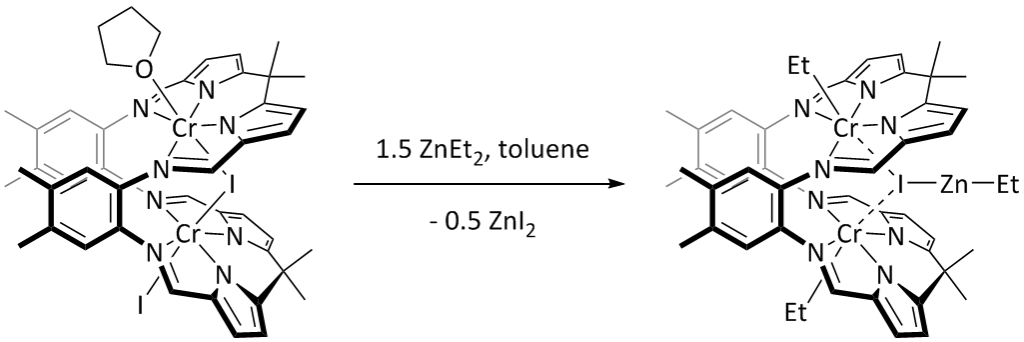

6 **9**

Scheme 2.24 Suggested balanced equation for the formation of **9.**

Addition of a slight excess (1.1 equivalents) of $ZnEt_2$ (1 M in hexanes) to a toluene solution of **6** resulted in an immediate colour change from red to dark green. Precipitation of pale solids, presumably ZnI_2, was observed. These were removed and hexane was added to the filtrate which was stored at −30°C. A small number of highly air-sensitive large green crystals formed, one of which was analysed by single crystal X-ray diffraction. The product was identified as the mixed metal complex $[\{Cr(Et)\}_2(\mu\text{-}I\text{-}ZnEt)(L^{Me})]$ (**9**) in which salt elimination has occurred to form two *exo* axial Cr-bound ethyl groups but a bridging iodide ligand is still present and is bound to a {ZnEt} moiety which has undergone partial transmetallation (Figure 2.20). In order to write a balanced equation for the formation of **9** from **6**, 1.5 equivalents of $ZnEt_2$ are required (Scheme 2.24). It is quite possible that more than 1.1 equivalents of $ZnEt_2$ were added to the reaction since there would have been uncertainty in both the volume of $ZnEt_2$ stock solution added and its concentration. Efforts were not made to isolate **9** on a preparative scale since the presence of alkyl groups bound to both chromium and zinc would necessarily complicate further reactivity studies.

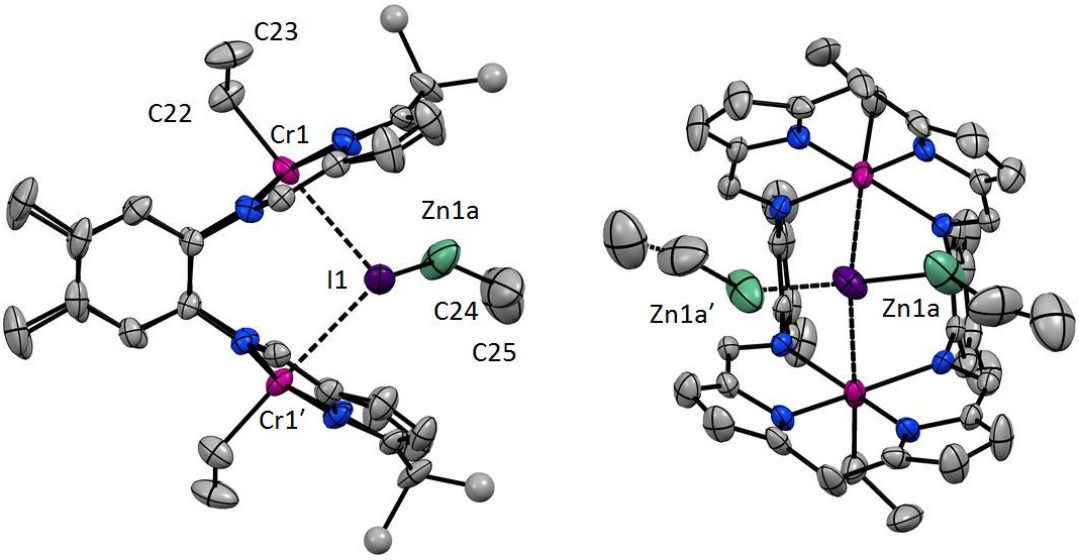

Figure 2.20 Solid state structure of **9** showing side view (left) and view into jaws of macrocycle (right). The major orientation of the *meso* methyl groups is shown. The zinc atom is disordered over two sites and about the crystallographic C_2 axis meaning that there are four separate zinc sites. Only the major-occupied zinc site is shown and its symmetry generated equivalent (with dashed bonds) is shown on the right. Thermal ellipsoids are drawn at 50 % probability. For clarity, H atoms and lattice solvent are omitted and the *meso* Me groups have been removed from the right hand structure.

Table 2.8 Selected distances (Å) and angles (°) for **9**.

Cr1···Cr1′	4.621(1)	Zn1b-I1	2.701(6)
mean Cr1-N_{im}	2.09	Zn1b-C24	1.92(2)
mean Cr1-N_{pyr}	1.97	C22-Cr1-I1	177.2(2)
Cr1-N_4 plane	+0.22	Cr1-I1-Cr1′	95.34(3)
Cr1-C22	2.063(7)	Cr1-C22-C23	118.6(5)
Cr1···I1	3.126(1)	I1-Zn1a-C24	151.6(8)
C22-C23	1.51(1)	I1-Zn1b-C24	143.4(8)
I1-Zn1a	2.497(3)	bite angle	71
Zn1a-C24	2.04(1)	twist angle	8

The structure of **9** is considerably different to the anticipated product [Cr_2(μ-Et)(Et)(THF)(L^{Me})] which would be generated from **6** by direct iodide/ethyl exchange. At first glance, one might assume that the bridging iodide, which is sandwiched between the two Cr(III) centres within the macrocyclic cleft is inert to substitution. However, analysis of the geometric parameters of the structure indicates that this is not the case. The Cr1···I1 separation of 3.126(1) Å is greatly elongated compared to the Cr-(μ-I) bond lengths of 2.7131(7) (Cr1-I1) and 2.7883(7) Å (Cr2-I1) in **6** and the Cr-I-Cr angle is consequently reduced from 105.56(2)° to 95.34(3) °. The longest Cr-I bond reported to date is 3.068(2) Å, found in the Jahn-Teller distorted complex [$Cr^{II}(I)_2$(depe)$_2$] (depe =

diethylphosphinoethane),[77] whilst the Cr2-I1 bond in **6** is in fact the longest of all reported Cr^{III}-I bonds. Therefore it is questionable whether a bond actually exists between the Cr(III) centres and the *endo* iodide in **9** or whether the compound is better considered as a host-guest complex in which, in the absence of a competitive donor, the δ− end of the [IZnEt] unit sits within the macrocyclic cleft between the δ+ Cr(III) ions.

The metrics of the [IZnEt] unit do not bear close scrutiny due to the significant disorder of the Zn atom. The ethyl carbon atoms also have severely elongated thermal ellipsoids indicating further disorder which could not be resolved satisfactorily. Despite the application of appropriate restraints to the Zn-I and Zn-C_{Et} distances the length of the Zn1a-I1 bond is improbably short at 2.497(3) Å compared to the Zn1b-I1 bond length of 2.701(6) Å and the geometries of the Zn1a and Zn1b containing components are dissimilar (Table 2.8). For comparison, IZnEt crystallises as an iodide-bridged co-ordination polymer and features a Zn-I separation of 2.640(6) Å, a Zn-C_{Et} separation of 1.95(4) Å and an I-Zn-C angle of 144.4 (2) ° within each IZnEt unit.[78] The Cr-Et metrics of **9** are discussed in 2.5.2.

2.5.1.2 Formation of [{Cr(Et)}$_2$(endo-py)(L^{Me})]

In order to investigate the hypothesis that the [IZnEt] unit in **9** is weakly bound in the macrocyclic cleft, the reaction of **6** with $ZnEt_2$ was repeated in pyridine solvent. Removal of the volatiles from the mixture followed by consecutive extraction into toluene and recrystallisation from THF/hexane afforded single crystals of the *endo*-pyridine adduct [{Cr(Et)}$_2$(*endo*-py)(L^{Me})] (**10**) (Scheme 2.25). In **10** a single molecule of pyridine occupies the macrocyclic cleft, binding to just one of the Cr(III) ions, thus confirming that in the presence of a strong competing donor [IZnEt] is not incorporated. The solid state structure of **10** is shown in Figure 2.21 and the structural parameters are discussed in 2.5.2.

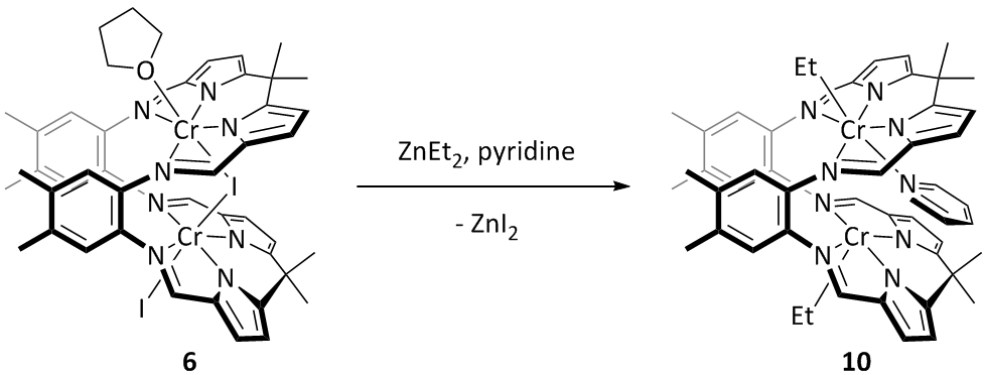

6 **10**

Scheme 2.25 Reaction of **6** with $ZnEt_2$ in pyridine to form **10**.

Unfortunately it was found that the synthesis of **10** was not repeatable and could not be scaled to provide sufficient clean material for reactivity studies due to contamination of the product with zinc salts. The known complex $[ZnI_2(py)_2]$ may well have some solubility in toluene and therefore may not be successfully excluded by extraction of the product, particularly if a small amount of residual free pyridine is present. A further complication is the likely formation of species such as $[ZnI(Et)(py)_2]$ which would be expected to have much increased solubility in toluene.

2.5.2 Synthesis of [{Cr(Et)}$_2$(*endo*-THF)(L^{Me})]

The Grignard reagent EtMgBr was identified as an alternative ethyl transfer agent to $ZnEt_2$. Magnesium halides typically have poor solubility in aromatic and ethereal solvents so separation of the salt by-product from the product should be easier to achieve. Furthermore, since a Grignard bears only one alkyl group, partial transmetallation to form a magnesium fragment analogous to [IZnEt] cannot occur.

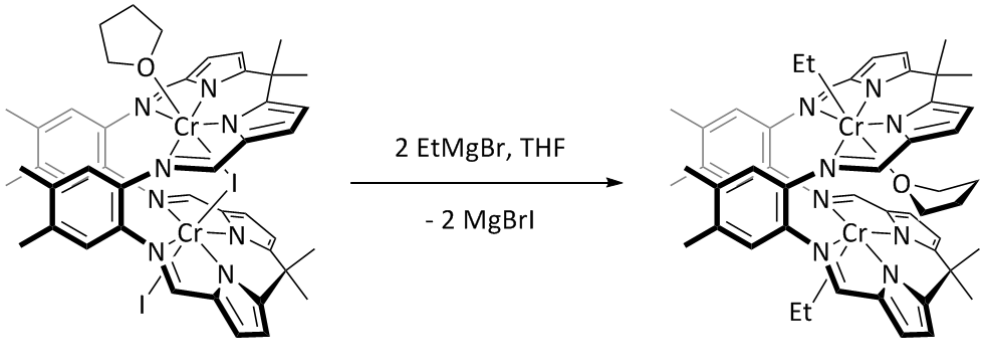

6 **11**

Scheme 2.26 Synthesis of **11.**

Addition of 2 equivalents of EtMgBr (1 M in THF) to a THF solution of **6** results in an immediate colour change from red to brown-green and precipitation of pale brown MgBrI from solution. Filtration followed by addition of hexanes and cooling to −30 °C allows the isolation of the magnesium free alkylation product [{Cr(Et)}$_2$(*endo*-THF)(L^{Me})] (**11**) as dark green crystals in moderate (38 %) yield (Scheme 2.26). Again, one molecule of THF occupies the intermetallic cleft and ligates just one of the Cr(III) ions in much the same fashion as the pyridine molecule in **10**. The ^{1}H NMR spectrum of **11** in C_6D_6 displays several very broad resonances between δ 21 and −42 ppm which cannot be assigned to individual ligand proton environments.

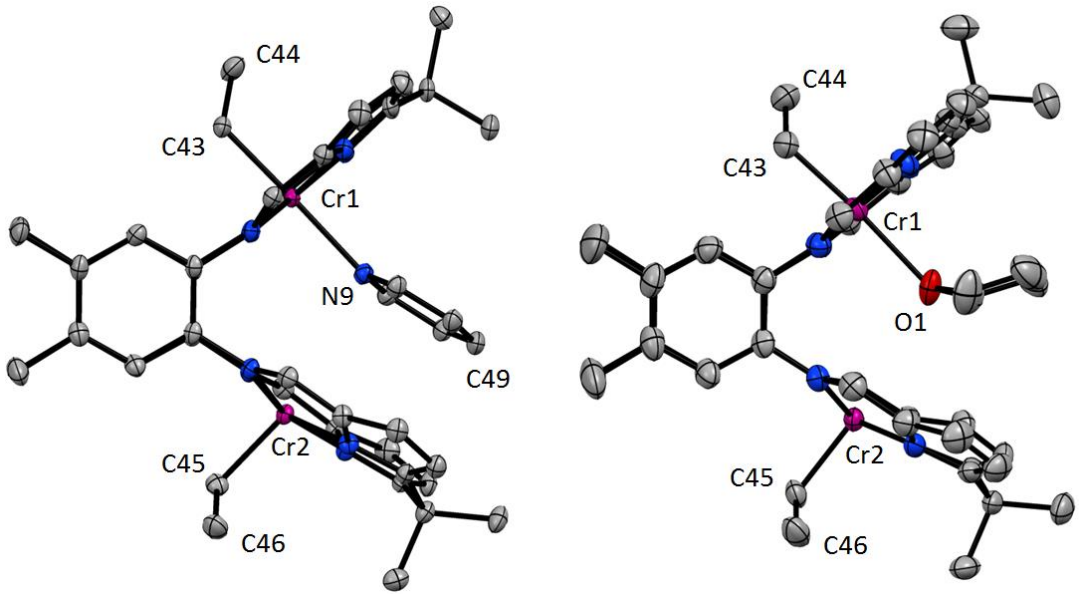

Figure 2.21 Solid state structures of **10** (left) and **11** (right). Thermal ellipsoids are drawn at 50 % probability. H atoms and lattice solvent are omitted.

Table 2.9 Comparison of selected distances (Å) and angles (°) in the structures of **10** and **11**.

	10	**11**		**10**	**11**
Cr1···Cr2	4.550(1)	4.602(9)	*Cr1-N9/O1*	2.196(3)	2.359(3)
mean Cr-N_{im}	2.11	2.10	*Cr2···N9/O1*	3.379(3)	3.345(3)
mean Cr-N_{pyr}	1.98	1.98	*C43-Cr1-N9/O1*	177.5(1)	175.6(1)
Cr1-N_4 plane	−0.02	−0.03	*Cr1-C43-C44*	118.0(3)	116.6(2)
Cr2-N_4 plane	+0.27	+0.30	*Cr2-C45-C46*	115.7(2)	115.7(3)
Cr1-C43	2.087(3)	2.087(4)	*Cr1-N9-C49*	164.8(1)	-
Cr2-C45	2.051(4)	2.064(4)	*Cr2-N9-C49*	87.5(1)	-
C43-C44	1.512(5)	1.520(6)	*bite angle*	71	71
C45-C46	1.513(5)	1.509(6)	*twist angle*	7	5

The solid state structures of **10** and **11** are very similar (Figure 2.21). In both cases one Cr(III) cation occupies each N_4 donor pocket of the macrocycle and is bound to one ethyl ligand in the *exo* axial co-ordination site. A single molecule of donor solvent (pyridine or THF) occupies the intermetallic cleft binding solely to Cr1. The resultant co-ordination geometries are octahedral about Cr1 and square based pyramidal about Cr2. This assignment is unambiguous since the Cr2···N9/O1 separations (3.379(3) / 3.345(3) Å) are much longer than the Cr1-N9/O1 bond lengths (2.196(3) / 2.359(3) Å) and the Cr2 cations are in fact displaced out of the N_4 plane away from the *endo* solvent molecule by 0.27 and 0.30 Å in **10** and **11** respectively. The Cr1-N9-C49 angle in **10** is 164.8(1) ° which is approaching the optimum pyridine-M co-ordination angle of 180 ° whilst the Cr2-N9-C49 angle of 87.5(1) Å is prohibitive to N9-Cr2 orbital overlap, assuming sp^2 hybridisation of the nitrogen orbitals.

It is interesting to note that the Cr1-O1 bond (2.359(3) Å) in **11** is longer than the Cr1-N9 bond (2.196(3) Å) in **10**, when the reverse would be expected based on the smaller atomic radius of O (0.60 Å) compared to N (0.65 Å).[79] It is likely that the planar pyridine molecule is incorporated within the macrocyclic cleft with less steric strain than the bent THF molecule allowing the N-donor to approach closer to Cr1 than the O-donor, in an analogous fashion to the xylyl and *tert*-butyl isocyanides in complexes **4** and **5**.

In **10** and **11** the Cr1-C43 bond lengths of 2.087(3) and 2.087(4) Å, respectively, are longer than the Cr2-C45 bond lengths of 2.051(4) and 2.064(4) Å, respectively, indicating that the 5-co-ordinate Cr(III) ion has a slightly stronger interaction with the ethyl ligand than the octahedral Cr(III) ion. The Cr-C_{Et} bond length observed in the {IZnEt}-incorporated complex **9** of 2.063(7) Å (Table 2.8) is similar to the Cr2-C45 distances in **10** and **11** which supports the suggestion that the Cr···(*endo*-I) interaction is weak and that the Cr(III) centres are effectively 5-co-ordinate in **9**. Reported Cr^{III}-C_{alkyl} distances range from 1.99 to 2.20 Å with a mean value of 2.10 Å [47] so the observed Cr-C_{Et} distances in compounds **9** – **11** are within the normal range. The structurally similar, square-pyramidal imine/pyrrolide Cr(III)-Et complex **2AS** reported by Gibson and co-workers (Figure 2.22, left) features a shorter Cr-C_{Et} interaction of 2.02(2) Å,[43] though due to the larger uncertainty in the literature value, the difference from the observed Cr-C_{Et} bond lengths in **9** - **11** is not statistically significant.

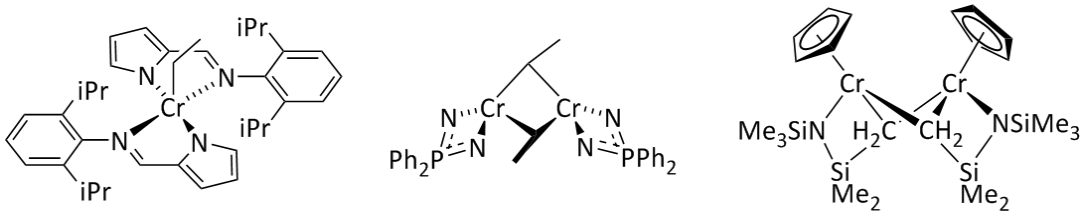

2AS **2AT** **2AU**

Figure 2.22 Examples of neutral Cr alkyl complexes synthesised by the Gibson (left),[43] Gambarotta (centre),[80] and Noels groups [81] (right).

Direct substitution of the iodide ligands in **6** for ethyl groups may have been expected to yield [Cr_2(μ-Et)(Et)(sol)(L^{Me})] (sol = py or THF). However none of the chromium alkyl complexes **9** - **11** contain bridging ethyl groups; all feature only *exo* axial alkyls. There is certainly enough space for an ethyl group to be incorporated within the macrocyclic cleft and the formation of alkyl bridged chromium complexes is by no means unusual; a bis-(μ-Et) Cr(II)/Cr(II) example from the Gambarotta group, **2AT**, is shown in Figure 2.22. There are no structurally characterised binuclear chromium complexes containing a single bridging alkyl ligand. However, as discussed above, this was also the case for iodide bridged binuclear chromium complexes but the sterically constrained

macrocyclic environment enabled the isolation of the first mono-(μ-I) Cr(III)/Cr(III) complexes **6** and **7**. Exertion of similar steric control could be reasonably expected to produce a mono-(μ-Et) Cr(III)/Cr(III) complex. The probable reason for the exclusive formation of terminal Cr-Et bonds in **9** – **11** is that in order to attain optimum orbital overlap between two Cr centres and a bridging R^- group, the separation of the Cr centres needs to be shorter than is allowed by the Pacman ligand framework. In the alkyl-bridged Cr complex **2AT**, the Cr···Cr distance is 2.3282(5) Å and the longest published Cr···Cr separation in an alkyl-bridged binuclear chromium complex is 2.662(1) Å, in the Cr(III)/Cr(III) metallated silylamide dimer **2AU** (Figure 2.22, right). The Cr···Cr separations in **9** – **11** are 4.621(1), 4.550(1) and 4.602(9) Å and the shortest Cr···Cr separation that we have observed for a chromium Pacman complex with a low twist angle (required to allow bridging of the metal centres) is 3.5877(5) Å in **4**. Therefore we suggest that the Cr(III) ions in the Pacman macrocycle are too distant to be bridged by an alkyl ligand.

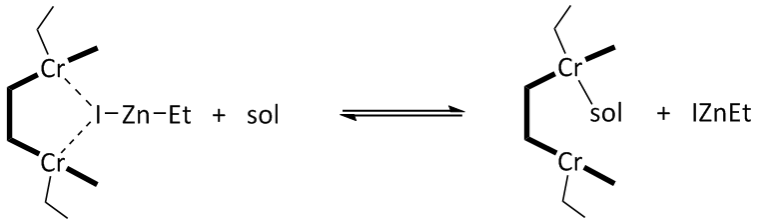

Scheme 2.27 Probable equilibrium established in solution following reaction of **6** with excess $ZnEt_2$. Sol = py, THF. The ligand is shown in cartoon form.

The similarities in the structures and solvent co-ordination modes of **10** and **11** raises the question of whether THF would be a good enough competing donor to prevent formation of the [IZnEt] incorporated product **9** if the reaction between **6** and $ZnEt_2$ were carried out in THF. In the reaction between **6** and $ZnEt_2$ in toluene, there is one molar equivalent of THF present originating from the THF-ligated starting material and this does not displace the [IZnEt] unit from the cleft, possibly because all the available THF is bound to the various zinc-containing species present. However, it is likely that the presence of a large excess of THF could perturb the position of the equilibrium presented in Scheme 2.27 sufficiently to result in displacement of the zinc fragment.

2.5.3 Reactivity of [{Cr(Et)}$_2$(*endo*-THF)(L^{Me})]

Preliminary investigations into the reactivity of **11** have been carried out. It was found that a benzene solution of **11** does not react with either CO or H_2. Commonly, transition metal alkyl complexes do react with these gases to form acyl and hydride complexes respectively (Scheme 2.28). However, both of these reactions require a vacant site at the metal centre *cis* to the alkyl group for the substrate reagent to bind. The Pacman macrocycle motif prohibits ligand rearrangement of **11** so the only vacant co-ordination site is the *endo* in-cleft site (assuming that the *endo* THF ligand dissociates), which is *trans* to both Et^- ligands. Therefore it is not surprising that **11** does not show reactivity towards CO or H_2. In fact, the lack of a vacant *cis* co-ordination site likely increases the stability of **11** by also preventing β-hydride elimination.

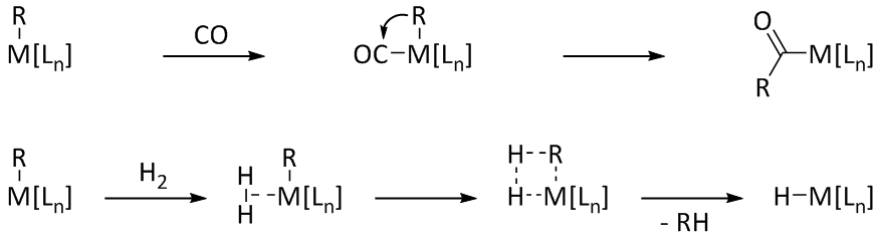

Scheme 2.28 General reactions of CO (top) and H_2 (bottom) with a transition metal alkyl complex.

The reaction of **11** with the alkyl abstraction reagent $[CPh_3][B(Ar^F)_4]$ ($Ar^F = C_6F_5$) was also investigated in the hope of synthesising a cationic alkyl chromium Pacman complex that may have enhanced reactivity with respect to neutral **11**. One equivalent of $[CPh_3][B(Ar^F)_4]$ was added to a dark green solution of **11** in C_6D_6. The mixture immediately turned brown and formation of oily brown solid was observed. The ^{1}H NMR spectrum of the mixture revealed that $HCPh_3$ and ethene were present in solution, implying that $[CPh_3]^+$ abstracts a hydride rather than an ethyl group from **11** to form a chromium ethene complex, from which the ethene then dissociates (Scheme 2.29). The reaction was repeated in d_8-THF in the hope that all the products would be soluble. Initially a brown-red solution was formed but this was converted into a gel overnight, presumably by polymerisation of the THF solvent. This result indicates that the chromium species formed is indeed more reactive than the parent alkyl complex **11**, which is prepared in THF.

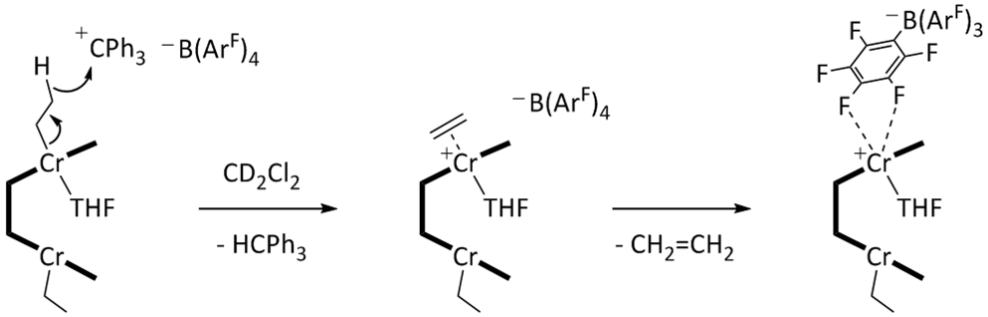

Scheme 2.29 Suggested reaction of $[CPh_3][B(Ar^F)_4]$ with **11**. The ligand in shown in cartoon form.

The polar non co-ordinating solvent dichloromethane was identified as an alternative solvent since it has been used successfully by the Theopold group for the isolation and catalytic testing of Cr(III) alkyl cations.[31,32] Addition of one equivalent of $[CPh_3][B(Ar^F)_4]$ to a green solution of **11** in CD_2Cl_2 resulted in the formation of a red-brown solution. Once again $HCPh_3$ and ethene were observed in the ^1H NMR spectrum along with a set of broad, paramagnetically shifted resonances appearing between 18 and −50 ppm assigned to the chromium containing product. The ^{11}B NMR spectrum displays a singlet at −16.63 ppm corresponding to the $[B(Ar^F)_4]^-$ anion which is not shifted from the expected value. However the ^{19}F NMR spectrum of the mixture contains three broadened resonances with no visible multiplicity at −133, −163 and −167 ppm. The relative intensities of these three resonances have been observed to vary between 12:2:2 and 5:2:3 for different repeats of the reaction but do not appear to change over time for a single reaction mixture. However, they are affected by changes in temperature. It is not clear whether all three resonances correspond to a single product, with the discrepancies in resonance intensity between different samples being a product of temperature differences and changes in the concentration of paramagnetic species present, or whether multiple products are formed.

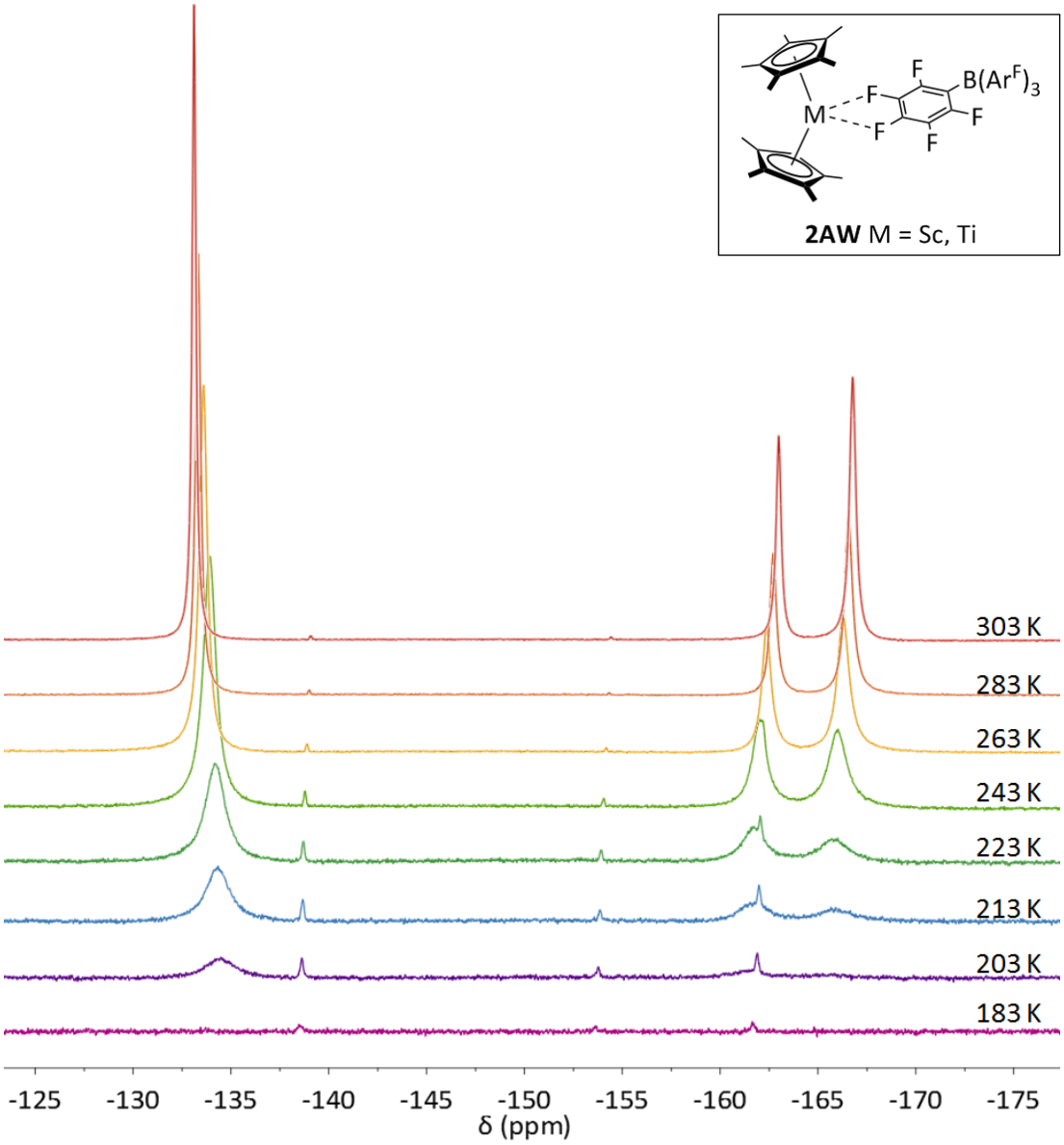

Figure 2.23 Variable temperature ^{19}F NMR spectra of the **11** + $[CPh_3][B(Ar^F)_4]$ reaction mixture in CD_2Cl_2. Inset: example of a transition metal complex featuring the $\{\kappa^2\text{-}F(C_6F_5)B(C_6F_5)_3\}$ binding mode of $[B(Ar^F)_4]^-$.[82]

From the ^{19}F NMR data we can deduce that the $[B(Ar^F)_4]^-$ anion cannot be truly non-co-ordinating in this reaction mixture otherwise only the NMR signals corresponding to free $[B(Ar^F)_4]^-$ would be observed. In fact, due to the addition of a slight excess of $[CPh_3][B(Ar^F)_4]$ to the reaction, minor ^{19}F resonances for free $[B(Ar^F)_4]^-$ are observed at –137, −154 and −162 ppm, which are distinct from the three major signals. Therefore it is likely that $[B(Ar^F)_4]^-$ interacts with a chromium species in solution. In recent years a handful of structures have been published in which a fluorinated borate anion co-ordinates to an early transition metal *via* one or two F atoms of a C_6F_5 ring (eg. **2AW**, Figure 2.23, inset).[82-85] In

solution the anion co-ordination is reported to be fluxional for all these complexes and the ^{19}F NMR spectra display only one set of resonances. Fluxional chromium co-ordination by $[B(Ar^F)_4]^-$ would account for the observed loss of multiplicity and broadening of the ^{19}F signals. A variable temperature NMR study was carried out on the reaction mixture in an attempt to probe the fluxional processes occurring (Figure 2.23). The ^{19}F signals broaden as the temperature is lowered, being absorbed into the base line at 183 K but the low temperature limiting spectrum could not be resolved within the liquid range of the solvent. In light of these observations a plausible structure for the product of the reaction of **11** with $[CPh_3][B(Ar^F)_4]$ is the contact ion pair $[\{Cr(Et)\}\{Cr(\kappa^2\text{-}F(C_6F_5)B(C_6F_5)_3)(THF)(L^{Me})]$ depicted in Scheme 2.29, but we have not been able to verify this by X-ray crystallography or elemental analysis.

Cationic Cr(III) alkyl complexes have been shown to be proficient in the activator-less polymerisation and oligomerisation of ethylene.[32] With this in mind, an atmosphere of ethylene (1.0 bar) was introduced to the NMR tube containing the reaction mixture of **11** and $[CPh_3][B(Ar^F)_4]$ in CD_2Cl_2. No solid polyethylene was formed and no new organic oligomeric species were observed by ^1H NMR spectroscopy, and the ^{19}F spectrum of the mixture was unchanged. However the solution changed colour from red-brown to crimson red over 16 h and a new set of broad, paramagnetically shifted resonances were observed between 36 and −70 ppm. This could indicate that the mixture of **11** and $[CPh_3][B(Ar^F)_4]$ reacts stoichiometrically, rather than catalytically, with ethylene to produce a new chromium species but it is equally possible that a slow reaction with the CD_2Cl_2 solvent occurs leading to degradation.

The reaction between **11** in CD_2Cl_2 with ethylene in the absence of $[CPh_3][B(Ar^F)_4]$ was also evaluated. In this case NMR spectroscopy indicated that no reaction occurred over 48 h and no physical changes to the solution were noted. However the reaction mixture gradually turned crimson red over 2 weeks after which time new paramagnetically shifted resonances were observed in the ^1H NMR spectrum between 16 and 0 ppm. Again, it cannot be determined whether **11** reacts very slowly with ethylene or whether it simply degrades in CD_2Cl_2 solution over long periods. Due to time restraints no further investigations into the reactivity of **11** have been undertaken.

2.6 Conclusions

Binuclear chromium(II) complexes of two different macrocyclic ligands, H_4L^{Me} and H_4L^{A}, have been synthesised. These represent the first structurally characterised early transition metal Pacman complexes that may be routinely and reproducibly prepared. The structure and reactivity of $[Cr_2(L^{Me})]$ (**1**) has been extensively studied.

The electronic structure of **1** has been probed by variable temperature magnetic susceptibility measurements and EPR spectroscopy to reveal that the ligand framework facilitates strong antiferromagnetic coupling between the high spin Cr(II) ions, though there is no direct Cr-Cr bond formation. Subjecting a single crystal of **1** to increasing pressure resulted in contraction of the crystal lattice but did not induce Cr-Cr bond formation; an increase in the torsional twist of the complex was observed and a long range η^6 interaction developed with the benzene lattice solvent but no reduction in macrocycle bite angle occurred. It appears that the macrocycle pockets cannot be forced close enough together to allow M-M bond formation.

The co-ordination chemistry of **1** may be rationalised by considering the steric demands of the different Lewis bases in concert with the restrictive environment of the Pacman macrocycle, and the co-ordination preferences of the d^4 Cr(II) ion. Thus, formation of octahedral complexes is not observed and the $OPPh_3$ ligands in $[Cr_2(OPPh_3)_2(L^{Me})]$ (**3**), which necessarily occupy the *exo* axial sites due to their bulk, are labile in co-ordinating solvents. The less sterically demanding isocyanide ligands form the complexes $[Cr_2(\mu\text{-}CNR)(L^{Me})]$ (R = Xyl **4**, ^{t}Bu **5**) where the isocyanide occupies the intermetallic cleft. These are substantially less labile; the xylyl isocyanide dissociates from **4** only in pyridine solution whilst **5** is stable in the presence of pyridine or DMAP. The reduced lability of **5** is likely due to the stronger σ-donation from the alkyl isocyanide to the Cr(II) ions. The increased stability or **4** and **5** relative to **3** can be attributed to the "pincer" effect of two Cr(II) ions biting down on the isocyanide ligands and steric shielding of the *endo* isocyanides by the macrocycle. Bridging two chromium centres is an unprecedented binding mode for an isocyanide; it must be facilitated in this case by the pre-organisation of the two Cr(II) centres within the Pacman framework.

The oxidation of **1** with iodine yields $[Cr_2(\mu\text{-}I)(I)(THF)(L^{Me})]$ (**6**) or $[Cr_2(\mu\text{-}I)(py)_2(L^{Me})][I]$ (**7**) when carried out in THF or pyridine respectively. These complexes provide two different possible structural models for the complexes $[(MCl)_2(L^{Me})]$ (M = Ti, V) which have been previously synthesised but not characterised in the solid state.[86] Again,

the $\{Cr_2(\mu\text{-}I)\}$ binding motif has not been previously observed, emphasising the unique co-ordination environment established by the Pacman ligand. Iodides are desirable auxiliary ligands because they may be substituted for different groups by employing a salt elimination strategy, allowing several derivatives to be prepared. Furthermore the iodides in both **6** and **7** occupy two distinct environments: *endo* and *exo* in **6**, *endo* and counterion in **7**. This non-equivalence was exploited in the synthesis of the anion exchange product $[Cr_2(\mu\text{-}I)(py_2)(L^{Me})][B\{OC_6H_2(^tBu)_2\}_2]$ (**8**) from **7**. An interesting extension to the work presented here would be the synthesis of a series of mixed-ligand chromium Pacman complexes from **6** by the selective substitution of just one of the I^- ligands.

Formation of alkyl chromium Pacman complexes from **6** has been demonstrated employing either $ZnEt_2$ of EtMgBr as alkyl transfer reagents. Though use of $ZnEt_2$ facilitated the structural characterisation of $[\{Cr(Et)\}_2(\mu\text{-I-ZnEt})(L^{Me})]$ (**9**) an unusual mixed-metal alkyl species, and $[\{Cr(Et)\}_2(\textit{endo}\text{-py})(L^{Me})]$ (**10**), the Grignard was found to be the most synthetically useful alkyl source, allowing the isolation of pure $[\{Cr(Et)\}_2(\textit{endo}\text{-THF})(L^{Me})]$ (**11**). The ethyl ligands in these complexes bind exclusively in the *exo* axial positions with either a solvent molecule or the organometallic fragment {IZnEt} trapped in the intermetallic cleft. The dialkyl complex **11** is unreactive towards CO, H_2 and CH_2CH_2 but does react rapidly with $[CPh_3][B(Ar^F)_4]$, possibly generating an ion pair of the form $[\{Cr(Et)\}\{Cr(\kappa^2\text{-}F(C_6F_5)B(C_6F_5)_3)(THF)(L^{Me})]$. Further work is required to fully characterise the product of this reaction and it would also be interesting to investigate the use of different Grignard reagents to synthesise a series of alkyl chromium Pacman complexes. The potential of **11** to undergo useful organic transformations is hampered by the lack of an available co-ordination site *cis* to the alkyl groups.

Between the different structurally characterised chromium complexes of H_4L^{Me} the Cr···Cr separation varies from 3.1221(1) Å to 4.621(1) Å and the bite angle of the complexes from 48 ° to 71 °. The term "Pacman" was coined to describe the ability of a flexible bimetallic complex to "chew" upon substrates of different sizes; it is clearly an appropriate descriptor for complexes of the H_4L^{Me} macrocycle. The work described in this chapter represents the first study of the structure and reactivity of a series of early transition metal Pacman complexes and will hopefully serve as a blueprint for extending such investigations to other metals.

2.7 References

(1) N. N. Greenwood, A. Earnshaw, *Chemistry of the Elements*; 2nd ed.; Butterworth-Heinemann, 1997.

(2) F. A. Cotton, C. A. Murillo, R. A. Walton, *Multiple Bonds Between Metal Atoms*; 3rd ed.; Springer Science and Business Media, Inc., 2005.

(3) T. Nguyen, A. D. Sutton, M. Brynda, J. C. Fettinger, G. J. Long, P. P. Power, *Science*, **2005**, *310*, 844.

(4) C.-W. Hsu, J.-S. K. Yu, C.-H. Yen, G.-H. Lee, Y. Wang, Y.-C. Tsai, *Angew. Chem., Int. Ed. Engl.*, **2008**, *47*, 9933.

(5) Y.-C. Tsai, C.-W. Hsu, J.-S. K. Yu, G.-H. Lee, Y. Wang, T.-S. Kuo, *Angew. Chem., Int. Ed. Engl.*, **2008**, *47*, 7250.

(6) A. Noor, G. Glatz, R. Müller, M. Kaupp, S. Demeshko, R. Kempe, *Z. Anorg. Allg. Chem.*, **2009**, *635*, 1149.

(7) A. Noor, T. Bauer, T. K. Todorova, B. Weber, L. Gagliardi, R. Kempe, *Chem. Eur. J.*, **2013**, *19*, 9825.

(8) K. A. Kreisel, G. P. A. Yap, O. Dmitrenko, C. R. Landis, K. H. Theopold, *J. Am. Chem. Soc.*, **2007**, *129*, 14162.

(9) A. Noor, F. R. Wagner, R. Kempe, *Angew. Chem., Int. Ed. Engl.*, **2008**, *47*, 7246.

(10) Y.-L. Huang, D.-Y. Lu, H.-C. Yu, J.-S. K. Yu, C.-W. Hsu, T.-S. Kuo, G.-H. Lee, Y. Wang, Y.-C. Tsai, *Angew. Chem.*, **2012**, *124*, 7901.

(11) A. Noor, G. Glatz, R. Müller, M. Kaupp, S. Demeshko, R. Kempe, *Nat. Chem.*, **2009**, *1*, 322.

(12) J. Shen, G. P. A. Yap, J.-P. Werner, K. H. Theopold, *Chem. Commun.*, **2011**, *47*, 12191.

(13) J. Shen, G. P. A. Yap, K. H. Theopold, *Chem. Commun.*, **2014**, *50*, 2579.

(14) J. Shen, G. P. A. Yap, K. H. Theopold, *J. Am. Chem. Soc.*, **2014**, *136*, 3382.

(15) M. D. Fryzuk, S. A. Johnson, *Coord. Chem. Rev.*, **2000**, *200–202*, 379.

(16) Y. Tanabe, Y. Nishibayashi, *Coord. Chem. Rev.*, **2013**, *257*, 2551.

(17) D. V. Yandulov, R. R. Schrock, *Science*, **2003**, *301*, 76.

(18) K. Arashiba, Y. Miyake, Y. Nishibayashi, *Nat. Chem.*, **2011**, *3*, 120.

(19) J. S. Anderson, J. Rittle, J. C. Peters, *Nature*, **2013**, *501*, 84.

(20) D. Sellmann, G. Maisel, *Z. Naturforsch.*, **1972**, *27B*, 465 and 718.

(21) W. H. Monillas, G. P. A. Yap, L. A. MacAdams, K. H. Theopold, *J. Am. Chem. Soc.*, **2007**, *129*, 8090.

(22) W. H. Monillas, G. P. A. Yap, K. H. Theopold, *Inorg. Chim. Acta*, **2011**, *369*, 103.

(23) I. Vidyaratne, J. Scott, S. Gambarotta, P. H. M. Budzelaar, *Inorg. Chem.*, **2007**, *46*, 7040.

(24) I. Vidyaratne, J. Scott, S. Gambarotta, R. Duchateau, *Organometallics*, **2007**, *26*, 3201.

(25) M. T. Mock, S. Chen, M. O'Hagan, R. Rousseau, W. G. Dougherty, W. S. Kassel, R. M. Bullock, *J. Am. Chem. Soc.*, **2013**, *135*, 11493.

(26) J. P. Hogan, R. L. Banks, US Patent, 1958.

(27) M. P. McDaniel In *Adv. Catal.*; D.D. Eley, H. P., Paul, B. W., Eds.; Academic Press: 1985; Vol. Volume 33, p 47.

(28) K. H. Theopold, *Eur. J. Inorg. Chem.*, **1998**, *1998*, 15.

(29) G. L. Karapinka, US Patent, 1973.

(30) F. J. Karol, G. L. Karapinka, C. Wu, A. W. Dow, R. N. Johnson, W. L. Carrick, *J. Polym. Sci., Part A: Polym. Chem.*, **1972**, *10*, 2621.

(31) L. A. MacAdams, G. P. Buffone, C. D. Incarvito, A. L. Rheingold, K. H. Theopold, *J. Am. Chem. Soc.*, **2005**, *127*, 1082.

(32) B. J. Thomas, S. K. Noh, G. K. Schulte, S. C. Sendlinger, K. H. Theopold, *J. Am. Chem. Soc.*, **1991**, *113*, 893.

(33) R. M. Manyik, W. E. Walker, T. P. Wilson, *J. Catal.*, **1977**, *47*, 197.

(34) J. R. Briggs, *J. Chem. Soc., Chem. Commun.*, **1989**, 674.

(35) A. Bollmann, K. Blann, J. T. Dixon, F. M. Hess, E. Killian, H. Maumela, D. S. McGuinness, D. H. Morgan, A. Neveling, S. Otto, M. Overett, A. M. Z. Slawin, P. Wasserscheid, S. Kuhlmann, *J. Am. Chem. Soc.*, **2004**, *126*, 14712.

(36) D. F. Wass, *Dalton Trans.*, **2007**, 816.

(37) J. T. Dixon, M. J. Green, F. M. Hess, D. H. Morgan, *J. Organomet. Chem.*, **2004**, *689*, 3641.

(38) T. Agapie, S. J. Schofer, J. A. Labinger, J. E. Bercaw, *J. Am. Chem. Soc.*, **2004**, *126*, 1304.

(39) S. J. Schofer, M. W. Day, L. M. Henling, J. A. Labinger, J. E. Bercaw, *Organometallics*, **2006**, *25*, 2743.

(40) B. Horvath, J. Strutz, E. G. Horvath, *Z. Anorg. Allg. Chem.*, **1979**, *457*, 38.

(41) D. F. Evans, *J. Chem. Soc.*, **1959**, 2003.

(42) A.-L. Barra, A. Døssing, T. Morsing, J. Vibenholt, *Inorg. Chim. Acta*, **2011**, *373*, 266.

(43) V. C. Gibson, C. Newton, C. Redshaw, G. A. Solan, A. J. P. White, D. J. Williams, *J. Chem. Soc., Dalton Trans.*, **2002**, 4017.

(44) H. A. Jahn, E. Teller, *Proc. R. Soc. Lond. A*, **1937**, *161*, 220.

(45) G. Givaja, M. Volpe, J. W. Leeland, M. A. Edwards, T. K. Young, S. B. Darby, S. D. Reid, A. J. Blake, C. Wilson, J. Wolowska, E. J. L. McInnes, M. Schröder, J. B. Love, *Chem. Eur. J.*, **2007**, *13*, 3707.

(46) E. B. Hulley, P. T. Wolczanski, E. B. Lobkovsky, *J. Am. Chem. Soc.*, **2011**, *133*, 18058.

(47) F. H. Allen, *Acta Crystallogr., Sect. B: Struct. Sci.*, **2002**, *58*, 380.

(48) B. Cordero, V. Gomez, A. E. Platero-Prats, M. Reves, J. Echeverria, E. Cremades, F. Barragan, S. Alvarez, *Dalton Trans.*, **2008**, 2832.

(49) R. A. Forman, G. J. Piermarini, J. D. Barnett, S. Block, *Science*, **1972**, *176*, 284.

(50) E. Keulen, F. Jellinek, *J. Organomet. Chem.*, **1966**, *5*, 490.

(51) M. Filomena Costa, M. R. G. da Costa, M. J. Marcelo Curto, M. Magrinho, A. M. Damas, L. Gales, *J. Organomet. Chem.*, **2001**, *632*, 27.

(52) F. A. Cotton, L. M. Daniels, C. A. Murillo, P. Schooler, *J. Chem. Soc., Dalton Trans.*, **2000**, 2001.

(53) W. Monillas, G. A. Yap, K. Theopold, *J. Chem. Crystallogr.*, **2009**, *39*, 842.

(54) F. Charbonneau, P. O. Oguadinma, F. Schaper, *Inorg. Chim. Acta*, **2010**, *363*, 1779.

(55) A. M. J. Devoille, J. B. Love, *Dalton Trans.*, **2012**, *41*, 65.

(56) J. P. Collman, J. E. Hutchison, M. A. Lopez, R. Guilard, *J. Am. Chem. Soc.*, **1992**, *114*, 8066.

(57) C. J. Stevens, G. S. Nichol, P. L. Arnold, J. B. Love, *Organometallics*, **2013**, *32*, 6879.

(58) F. A. Cotton, E. Bannister, *J. Chem. Soc.*, **1960**, 1873.

(59) M. Inamo, N. Matsubara, K. Nakajima, T. S. Iwayama, H. Okimi, M. Hoshino, *Inorg. Chem.*, **2005**, *44*, 6445.

(60) M. Göldner, B. Geniffke, A. Franken, K. S. Murray, H. Homborg, *Z. Anorg. Allg. Chem.*, **2001**, *627*, 935.

(61) F. A. Cotton, G. Wilkinson *Advanced Inorganic Chemistry* 3ed.; Interscience, 1972.

(62) Y. Yamamoto, *Coord. Chem. Rev.*, **1980**, *32*, 193.

(63) A. E. Carpenter, G. W. Margulieux, M. D. Millard, C. E. Moore, N. Weidemann, A. L. Rheingold, J. S. Figueroa, *Angew. Chem., Int. Ed. Engl.*, **2012**, *51*, 9412.

(64) J. D. Lawrence, T. B. Rauchfuss, S. R. Wilson, *Inorg. Chem.*, **2002**, *41*, 6193.

(65) G. M. Ferrence, E. Simon-Manso, B. K. Breedlove, L. Meeuwenberg, C. P. Kubiak, *Inorg. Chem.*, **2004**, *43*, 1071.

(66) A. C. Sarapu, R. F. Fenske, *Inorg. Chem.*, **1975**, *14*, 247.

(67) J. Díez, M. P. Gamasa, J. Gimeno, A. Aguirre, S. García-Granda, *Organometallics*, **1997**, *16*, 3684.

(68) M. H. Chisholm, D. L. Clark, D. Ho, J. C. Huffman, *Organometallics*, **1987**, *6*, 1532.

(69) C. A. Boyke, T. B. Rauchfuss, S. R. Wilson, M. M. Rohmer, M. Benard, *J. Am. Chem. Soc.*, **2004**, *126*, 15151.

(70) D. Lentz, I. Brüdgam, H. Hartl, *J. Organomet. Chem.*, **1986**, *299*, C38.

(71) D. Lentz, S. Willemsen, *J. Organomet. Chem.*, **2000**, *612*, 96.

(72) F. A. Cotton, J. P. Donahue, M. B. Hall, C. A. Murillo, D. Villagrán, *Inorg. Chem.*, **2004**, *43*, 6954.

(73) D. B. Morse, T. B. Rauchfuss, S. R. Wilson, *J. Am. Chem. Soc.*, **1990**, *112*, 1860.

(74) L. F. Audrieth, E. J. Birr, *J. Am. Chem. Soc.*, **1933**, *55*, 668.

(75) T. Tassaing, M. Besnard, *J. Phys. Chem. A*, **1997**, *101*, 2803.

(76) C. Elschenbroich *Organometallics*; 3rd ed.; WILEY-VCH, 2006.

(77) D. M. Halepoto, D. G. L. Holt, L. F. Larkworthy, G. J. Leigh, D. C. Povey, G. W. Smith, *J. Chem. Soc., Chem. Commun.*, **1989**, 1322.

(78) P. T. Moseley, H. M. M. Shearer, *J. Chem. Soc., Dalton Trans.*, **1973**, 64.

(79) J. C. Slater, *J. Chem. Phys.*, **1964**, *41*, 3199.

(80) K. Albahily, V. Fomitcheva, Y. Shaikh, E. Sebastiao, S. I. Gorelsky, S. Gambarotta, I. Korobkov, R. Duchateau, *Organometallics*, **2011**, *30*, 4201.

(81) R. Messere, M.-R. Spirlet, D. Jan, A. Demonceau, A. F. Noels, *Eur. J. Inorg. Chem.*, **2000**, 1151.

(82) M. W. Bouwkamp, P. H. M. Budzelaar, J. Gercama, I. Del Hierro Morales, J. de Wolf, A. Meetsma, S. I. Troyanov, J. H. Teuben, B. Hessen, *J. Am. Chem. Soc.*, **2005**, *127*, 14310.

(83) A. Berkefeld, W. E. Piers, M. Parvez, L. Castro, L. Maron, O. Eisenstein, *J. Am. Chem. Soc.*, **2012**, *134*, 10843.

(84) X. Li, M. Nishiura, K. Mori, T. Mashiko, Z. Hou, *Chem. Commun.*, **2007**, 4137.

(85) X. Li, J. Baldamus, M. Nishiura, O. Tardif, Z. Hou, *Angew. Chem., Int. Ed. Engl.*, **2006**, *45*, 8184.

(86) M. Volpe, S. D. Reid, A. J. Blake, C. Wilson, J. B. Love, *Inorg. Chim. Acta*, **2007**, *360*, 273.

Chapter Three

Uranium Pacman Complexes

3.1 Introduction to uranium chemistry

Uranium is the heaviest naturally occurring element with an atomic number of 92. It was first identified in 1789 and named after the planet Uranus, also discovered in that year. However, it was not until the discovery of nuclear fission in the 1930s that the importance of uranium for nuclear energy generation was realised.[1] Depleted uranium, the by-product of uranium enrichment for the nuclear industry, is utilised in academic laboratories to study the chemical reactivity of the element. The major isotope present in depleted uranium is ^{238}U (> 99.7 %) which is a long half-life α-emitter and may be handled safely without the need for special precautions.

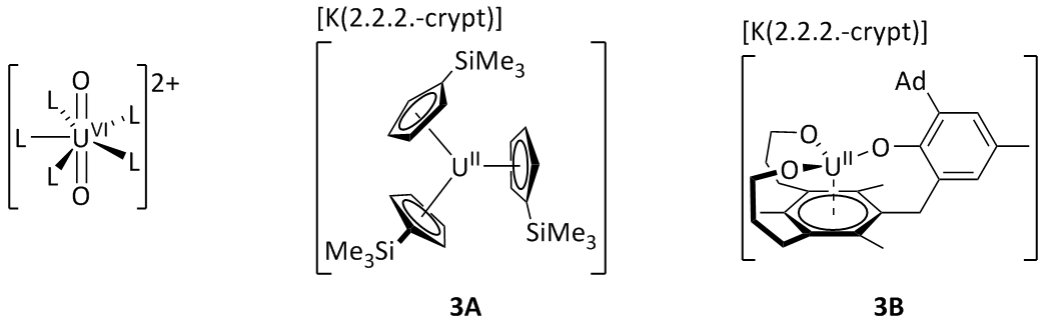

Figure 3.1 Illustration of the geometry of the uranyl dication (left) and the two U(II) complexes, **3A** [2] and **3B**,[3] isolated to date. Only one arm of the aryloxide ligand in **3B** is represented in full, the others are identical.

Uranium is an early actinide and the heaviest element in Group VI. It exhibits oxidation states from +6 to +2 in its compounds. This is in contrast to the lanthanides and late-actinides which exist almost exclusively in the +3 oxidation state. The 5f valence orbitals of uranium can participate more readily in bonding because of their high energy and large radial extent, which are attributed partly to the presence of a radial node and partly to the relativistic contraction of the shielding s and p outer core orbitals.[4] In aerobic conditions the +6 oxidation state of uranium dominates, typified by the soluble, stable, linear, *trans*-dioxo uranyl dication, $[UO_2]^{2+}$ (Figure 3.1, left). One electron reduction of the uranyl dication in the environment [5] affords the unstable uranyl monocation $[UO_2]^{+}$ which disproportionates back to $[UO_2]^{2+}$ and U(IV) species, which tend to be insoluble and can be problematic contaminants.[6] U(III) can only be isolated in strictly anaerobic and anhydrous conditions. The +3 oxidation state was long thought to be the lowest accessible in uranium compounds, but in 2013 Evans reported the synthesis of the first U(II) complex (**3A**, Figure 3.1) by reduction of $[U(C_5H_4SiMe_3)_3]$ with K metal in the presence of 2.2.2.-cryptand, at low temperature.[2] Following an identical methodology, the Meyer group prepared a second U(II) complex (**3B**, Figure 3.1) in 2014.[3]

In its complexes, uranium typically adopts high co-ordination numbers due to its large size, and exhibits a range of different co-ordination geometries. The formation of "-ate" salts, where more anionic ligands than are required for charge neutrality are co-ordinated to the metal centre as in complexes **3A** and **3B**, is commonly observed. The propensity of uranium cations to form "-ate" salts is attributed to their large size and high Lewis acidity.[4] The remainder of this introduction will focus on selected chemistry of U(III) compounds since the +3 oxidation state of uranium is most relevant in small molecule activation.

3.1.1 Uranium(III) precursors

The number of binary U(III) precursors available is very limited. Before 1989, U(III) chemistry was generally accessed *via* $UCl_3(THF)_x$, UH_3 or polymeric UI_3. $UCl_3(THF)_x$ must be generated *in situ* and is an unstable and poorly understood material,[7,8] whilst the preparation of UH_3 and polymeric UI_3 require harsh conditions and specialist equipment.[9,10] However, the field of uranium(III) chemistry has exploded since 1989 when Sattelberger and co-workers published the first, straightforward, solution synthesis of a soluble U(III) precursor, $UI_3(THF)_4$, by the reaction of uranium turnings with 1.5 equivalents of iodine in THF solution at 0 °C (Equation 3.1).[11,12] Though the isolation of $UI_3(THF)_4$ represented a significant advance, THF is not an ideal reaction solvent since the U(III) ions tend to ring open the cyclic ether, hence the requirement for low reaction temperatures to control side-product formation. Further improvements were reported by the Arnold [13] and Kiplinger [14] groups who repeated the reaction at room temperature in diethylether and 1,4-dioxane solvents to produce base free UI_3 and $UI_3(dioxane)_{1.5}$, respectively (Equation 3.1).

Equation 3.1

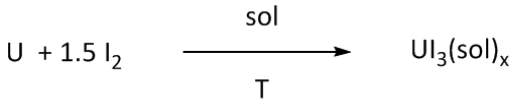

sol	x	T
THF	4	0 °C
Et_2O	0	RT
1,4-dioxane	1.5	RT

The synthesis of $UI_3(sol)_x$ has enabled the subsequent preparation of a wide range of U(III) complexes by salt elimination strategies. Uranium(III) aryloxides, silylamides and cyclopentadienyls have been prepared, as well as complexes of larger macrocyclic and chelating ligands.[15] The utility of UI_3 is underpinned by its stability. Not only is UI_3 the only stable trivalent halide of uranium, it is also stable with respect to the U(IV) iodide, UI_4. At room temperature UI_4 decomposes to UI_3 with the release of iodine.[16]

3.1.1.1 Uranium(III) borohydrides

Another class of uranium compounds which display thermal instability of the U(IV) state with respect to the U(III) state is the uranium borohydrides. Ephritikhine and co-workers reported the thermal decomposition of $U(BH_4)_4$ in mesitylene solution at 150 °C to yield the U(III) arene complex $[U(BH_4)_3(C_6H_3Me_3)]$ (**3C**, Scheme 3.1, left).[17] The solid state structure of the hexamethylbenzene derivative $[U(BH_4)_3(C_6Me_6)]$ (**3D**) features U···B separations of 2.49(4), 2.54(3) and 2.69(3) Å which are characteristic of three hydrides from each BH_4^- ligand bridging to the U(III) centre: a $\{(\mu\text{-}H)_3BH\}$ binding mode. In a related demonstration of the stability of U(III) borohydrides, Daly and Girolami reported that the reaction of UCl_4 with $Na(H_3BNMe_2BH_3)$ exclusively formed the U(III) product $[U(H_3BNMe_2BH_3)_3]$ (**3E**, Scheme 3.1, right).[18] In complex **3E** the U···B separations range from 2.842(6) to 2.935(6) Å and are consistent with $\{(\mu\text{-}H)_2BHR\}$ binding modes.

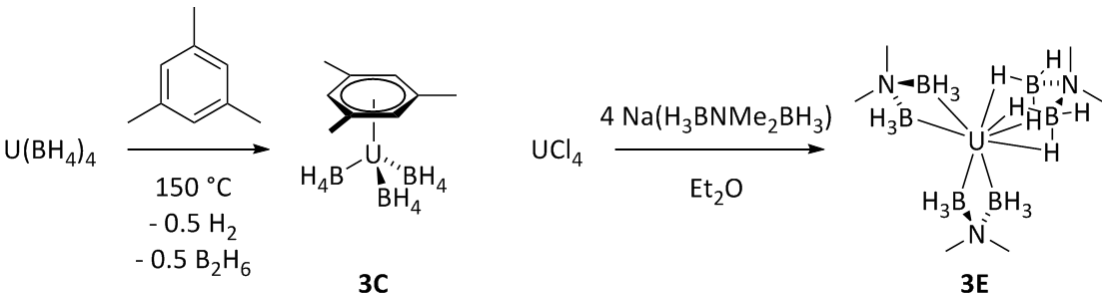

Scheme 3.1 Formation of U(III) borohydride complexes from U(IV) starting materials.[17,18] The borohydride binding mode is only shown explicitly for one $[H_3BNMe_2BH_3]^-$ ligand in **3E**.

$U(BH_4)_4$ was originally targeted during the Manhattan project because of its volatility but its synthesis is non-trivial, prepared either by reaction of UF_4 with neat $Al(BH_4)_3$ [19] or by vacuum milling of a solid mix of UCl_4 and $LiBH_4$.[20] Therefore synthesis of $U(BH_4)_4$ followed by its thermal decomposition is not a convenient method of preparing U(III) borohydrides in most synthetic laboratories. The reaction of UH_3 with diborane in THF solution was reported to form $[U(BH_4)_3(THF)_3]$ (**3F**, Figure 3.2), which was structurally characterised, but the reaction was slow and the yield (4 %) was poor.[21] Reaction of $NaBH_4$ with *in situ* prepared $UCl_3(THF)_x$ yielded red solids which were not fully characterised,[7] though addition of the chelating phosphine dmpe allowed the isolation and structural analysis of $[U(BH_4)_3(dmpe)_2]$ (**3G**, Figure 3.2).[22]

The structures of the adducts **3F** and **3G** are dissimilar. The co-ordination geometry about U(III) is octahedral in **3F** with the three BH_4^- ligands and three THF molecules in facial arrangements. The U···B distances range from 2.63 to 2.70 Å indicating that all three BH_4^- ligands bind through three bridging hydrides making **3F** structurally analogous to the

arene complex **3C**. The U(III) ion in **3G** exhibits pentagonal bipyramidal co-ordination with the two bidentate phosphines and one BH_4^- in the equatorial plane and the other two borohydrides in the axial positions. The axial U···B distances are 2.68(4) Å, corresponding to {(μ-H)$_3$BH} co-ordination but the equatorial U···B separation is longer at 2.84(3) Å and indicates a {(μ-H)$_2$BH$_2$} binding mode. Limited further reactivity of these U(III) borohydride complexes has been reported. In summary, BH_4^- is an attractive alternative supporting ligand to I^- for U(III) chemistry and has not been extensively explored.

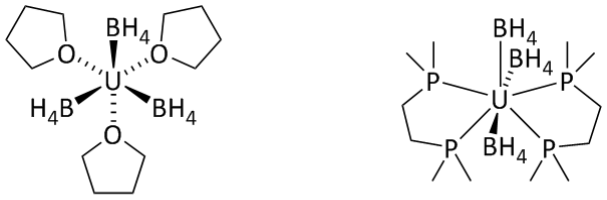

3F **3G**

Figure 3.2 Different Lewis base adducts of U(BH$_4$)$_3$.[21,22]

3.1.2 Small molecule activation by uranium(III)

Uranium in the +3 oxidation state is highly reducing. U(III) complexes have been shown to activate diverse small molecules.[23] On-going research efforts are focussed on developing more selective and useful transformations with the ultimate aim of achieving novel catalysis.[24] An overview of the reactions of U(III) complexes with selected small molecules is given below, focussing on those of particular relevance to the experimental work presented in this thesis.

3.1.2.1 N_2

Early Haber-Bosch catalysts contained uranium, reflecting the significant reducing power of the element, but relatively few organometallic dinitrogen complexes of uranium have been reported. The first example was synthesised by Scott and co-workers who formed the side-on bound dinitrogen complex [{U(NN′$_3$)}$_2$(μ-η^2:η^2-N$_2$)] (**3H**) by exposure of the U(III) precursor to an atmosphere of N_2.[25] The N-N bond length in **3H** of 1.109(7) Å is essentially unchanged from that of free N_2 (1.0976 Å) indicating a minimal degree of reduction and the N_2 ligand was found to dissociate under vacuum. Significant reduction of the N_2 ligand has been observed in other complexes. The N-N bond length is 1.232(10) Å in the pentalene-supported uranium dinitrogen complex **3J** (Figure 3.3) which is considered to be a U(IV)/U(IV) complex bridged by $(N_2)^{2-}$.[26] Despite this formal reduction, **3J** also readily loses N_2 to reform the monomeric U(III) parent complex, presumably driven by relief of steric crowding. Reduction of dinitrogen to $(N_2)^{2-}$ with concomitant oxidation of the U(III) centres to U(IV) was similarly observed in the formation of the dinitrogen complex **3K** with

aryloxide ligands (Figure 3.3) which features N-N bond lengths of 1.190(18) and 1.236(5) Å, depending on the solvent of crystallisation.[27] Complex **3K** is stable under vacuum, though the N_2 unit may be displaced by addition of competing ligands.

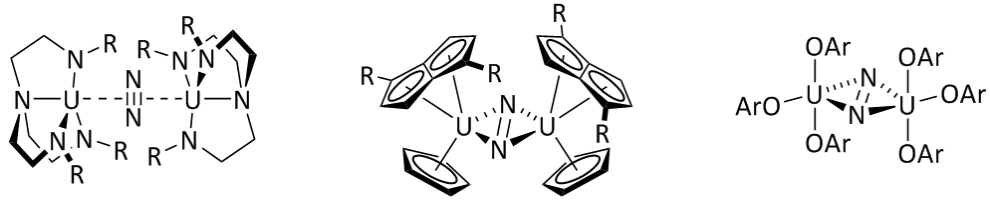

3H R = Si^tBuMe_2 **3J** R = Si^iPr_3 **3K** Ar = 2,4,6-$C_6H_2(^tBu)_3$

Figure 3.3 Side-on bridging dinitrogen complexes of uranium.[25-27]

A greater degree of N_2 activation was observed in the hetero-binuclear end-on bound dinitrogen complex **3L** (Figure 3.4) which was formed by exposure of an equimolar toluene solution of [U{N(^{t}Bu)Ar}$_3$(THF)] and [Mo{N(^{t}Bu)Ph}$_3$] to an atmosphere of N_2.[28] The bond lengths of the {U-N-N-Mo} unit indicate a degree of multiple bonding in both the U-N and Mo-N bonds. Complex **3L** is an unusual example of end-on co-ordination of dinitrogen at uranium. The Gambarotta group reported the remarkable complete cleavage of N_2 between two calix[4]tetrapyrrole supported U(III) centres upon addition of reducing equivalents of potassium naphthalenide.[29] The product was the mixed-valence U(V)/U(IV) bis(nitride) bridged anion **3M** (Figure 3.4).

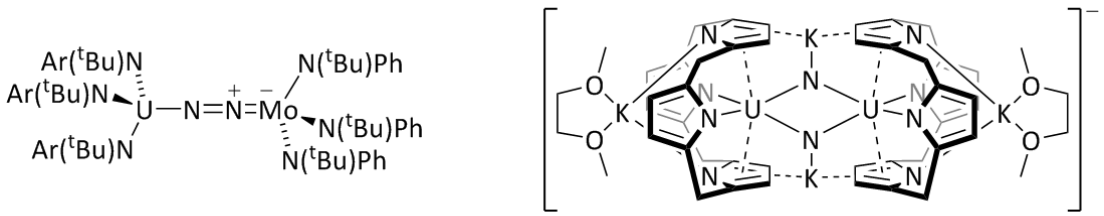

3L **3M**

Figure 3.4 Uranium complexes containing strongly activated N_2 units.[28,29] Ar = 3,5-$C_6H_3Me_2$.

3.1.2.2 CO

CO is isoelectronic with N_2 but unlike N_2, CO is a polar molecule. The C≡O bond is the strongest chemical bond known with a dissociation energy of 1072 kJmol^{-1} compared to 942 kJmol^{-1} for the N≡N bond. The polarity of CO enhances both its σ donor and π acceptor characteristics compared to N_2 and accounts for the rich co-ordination chemistry of CO in combination with transition metals.[30] By contrast, stable actinide carbonyl complexes are rare due to the reduced π back-donation ability of f orbitals compared to d orbitals. Only three uranium carbonyl complexes are stable enough to have been isolated and structurally

characterised (Scheme 3.2). The U(III) cyclopentadienyl carbonyl complexes **3N** and **3P** were formed by exposure of solutions of the corresponding U(III) metallocenes to CO gas. The CO co-ordination mode is approximately linear in both complexes and ν_{CO} is 1880 cm^{-1} in **3N** [31] and 1922 cm^{-1} in **3P**.[32] Both these values are considerably reduced compared to that of free CO (ν_{CO} = 2143 cm^{-1}) and therefore indicate that a degree of π back-donation occurs from U to C. Despite this, neither complex is stable under vacuum; CO dissociation occurs to regenerate the starting complexes. In 2005, the Meyer group reported that exposure of $[U^{III}\{tacn(OAr^{tBu})_3\}]$ to CO gas resulted in formation of the unprecedented end-on CO bridged binuclear product **3Q** (Scheme 3.2, right).[33] Complex **3Q** is the only uranium carbonyl complex which is stable under vacuum. It is assigned as a mixed-valence U(IV)/U(III) species containing a reduced CO unit and exhibits ν_{CO} at 2092 cm^{-1}.

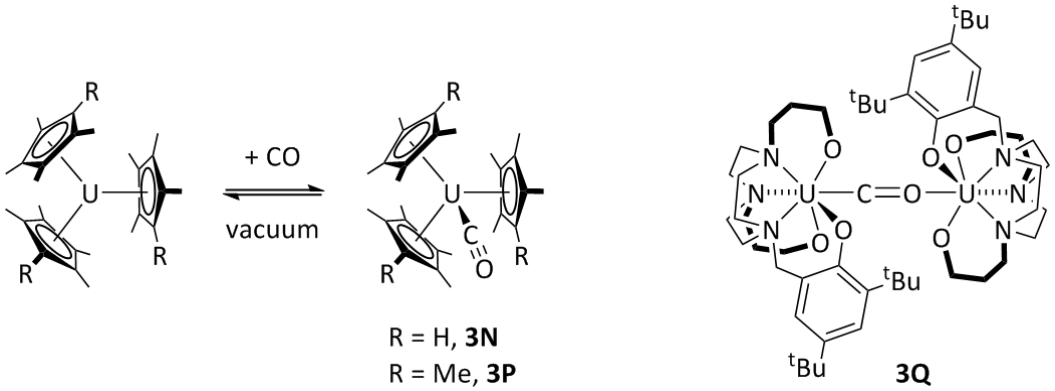

Scheme 3.2 Structurally characterised uranium carbonyl complexes.[32,33] Only one ligand arm is shown explicitly in **3Q**; all three are identical.

Reductive coupling of CO with concurrent C-C bond formation has been demonstrated between U(III) centres. In 2008, Cloke and co-workers reported the reaction of a pentane solution of the mixed sandwich compound $[U\{C_8H_6(Si^iPr_3)_2\}(C_5Me_5)(THF)]$ with 1 bar of CO gas to form complex **3R** which contains the newly formed deltate dianion $(C_3O_3)^{2-}$ bridging between two U(IV) centres (Scheme 3.3).[34] The triangular C_3 core of the deltate anion features two short C-C bonds and one longer C-C bond that forms an agostic interaction to one U(IV) centre. In solution, **3R** appears symmetric by ^1H NMR spectroscopy indicating that the deltate co-ordination mode is fluxional. It was discovered that modifying the reaction stoichiometry so that just 0.9 equivalents of CO were added to a toluene solution of $[U\{C_8H_6(Si^iPr_3)_2\}(C_5Me_5)(THF)]$ allowed the isolation of a different product: the ynediolate $(C_2O_2)^{2-}$ bridged complex **3S**.[35] The Arnold [27] and Liddle [36] groups have also reported coupling of CO between U(III) centres to selectively form ynediolate complexes even in the presence of excess CO. The ynediolate core in **3S** is essentially linear and the C-C distance is short (1.177(12) Å) which is consistent with a C≡C triple bond. Interestingly,

3S cannot be converted into **3R** by the addition of further equivalents of CO. Fine tuning of the sterics of the starting sandwich complex was also observed to control the product distribution. Thus addition of CO gas (1 bar) to a toluene solution of $[U\{C_8H_6(Si^iPr_3)_2\}(C_5HMe_4)(THF)]$ at −30 °C resulted in formation of the squarate $(C_4O_4)^{2-}$ bridged binuclear U(IV)/U(IV) complex **3T**.[37] These reductive coupling reactions represent the selective transformation of CO, a C_1 feedstock, to higher order C_n homologues, which is a vitally important industrial process. Liberation of the $(C_nO_n)^{2-}$ cores from the U(IV) centres has been demonstrated for some of the above and related complexes, indicating that once optimised these reactions could be of synthetic use.[36,38]

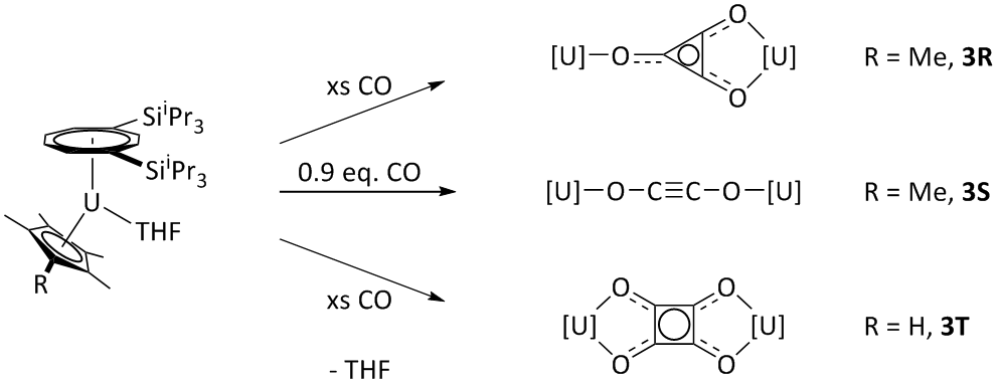

Scheme 3.3 Reductive coupling of CO by U(III) to form various $(C_nO_n)^{2-}$ anions.[34,35,37]

3.1.2.3 CO_2

Another cheap and plentiful C_1 source is carbon dioxide. CO_2 is more susceptible to reduction than CO. Oxide abstraction and reduction of CO_2 to CO was first demonstrated for a U(III) complex in 1991. Ephritikhine and co-workers reported that exposure of the U(III) metallocene complex $[U(C_5H_4SiMe_3)_3]$ to CO_2 resulted in formation of the oxo-bridged U(IV)/U(IV) dimer $[\{U(C_5H_4SiMe_3)_3\}_2(\mu\text{-O})]$.[39] More recently, the Meyer group has illustrated the importance of sterics in determining the reaction outcome. Addition of CO_2 to the *ortho*-^{t}Bu substituted U(III) aryloxide tacn complex $[U\{tacn(OAr^{tBu})_3\}]$ yields the oxo-bridged product **3U** with elimination of CO gas (Scheme 3.4, left).[33] By contrast, if the more sterically congested *ortho* adamantyl substituted U(III) tacn complex $[U\{tacn(OAr^{Ad})_3\}]$ is employed, the highly unusual monomeric CO_2 complex $[U\{tacn(OAr^{Ad})_3\}(\eta^1\text{-OCO})]$ (**3V**) is isolated (Scheme 3.4, right).[40] The CO_2 molecule in **3V** co-ordinates to the uranium centre in a linear end-on fashion and has been singly reduced to a radical anion so the oxidation state of the U ion in the product is +4. Complex **3V** is the only known example of a linear O-bound CO_2 ligand. The authors suggest that oxo complex **3U** is formed *via* a transient CO_2-bridged binuclear species from which CO is then eliminated. Monomeric CO_2 complex **3V**

can be isolated because the increased bulk of the adamantyl substituted ligand disfavours the approach of a second molecule of [U{tacn(OAr^{Ad})$_3$}], preventing formation of a CO_2-bridged binuclear species followed by collapse to the oxo-bridged dimer.

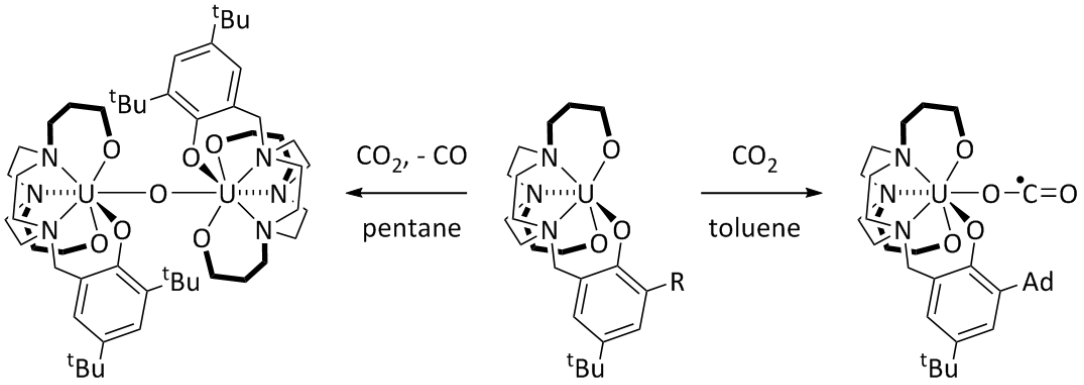

3U **3V**

Scheme 3.4 Contrasting reactivity of different U(III) tacn complexes with CO_2.[33,40]

The Arnold group reported simultaneous oxo abstraction and CO_2 insertion into uranium-ligand bonds in the reaction of CO_2 with the aryloxide-supported dinitrogen-bridged dimer **3K** (Scheme 3.5).[27] Initial elevated temperatures were required to displace the dinitrogen unit. Following this, the two U(III) centres co-operatively reduced one molecule of CO_2 to form a bridging oxide between two U(IV) ions and CO gas. Two further equivalents of CO_2 inserted into two of the U-OAr bonds to form two bridging arylcarbonate groups in the product **3W**.

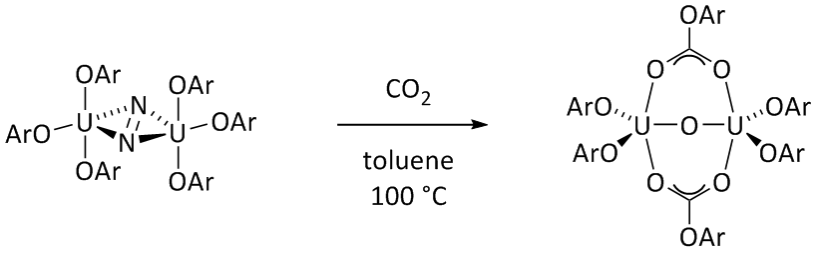

3K **3W**

Scheme 3.5 Reaction of the veiled U(III) aryloxide complex **3K** with CO_2.[27] Ar = 2,4,6-$C_6H_2(^tBu)_3$.

Reductive disproportionation of CO_2 to CO_3^{2-} and CO by uranium is also known. The Cloke,[41] Meyer [42,43] and Mazzanti [44] groups have all reported the activation of CO_2 between two U(III) centres to form bridging carbonate complexes. Three examples of these are shown in Figure 3.5. Two distinct carbonate bridging modes are observed in these complexes: μ-κ^1(O):κ^2(O′,O″) in **3X** and **3Y**, and μ-κ^2(O,O′):κ^2(O,O″) in **3Z**. Although the carbonate bridging mode is asymmetric in the solid state for **3X** and **3Y**, only one set of ligand resonances is observed for both complexes in solution by ^{1}H NMR spectroscopy

indicating that carbonate co-ordination is fluxional, which is similar to the binding of the deltate dianion discussed above. It is suggested that carbonate formation proceeds *via* oxo abstraction to form a U(IV)/U(IV) bridging-oxo complex into which another molecule of CO_2 inserts to form the carbonate anion. This reaction pathway has been verified for the formation of **3Z**. The *ortho* neopentyl substituted U(III) tacn complex [U{tacn(OAr^{neop})$_3$}] was exposed to an atmosphere of N_2O gas allowing the isolation of the oxo-bridged binuclear complex [(U{tacn(OAr^{neop})$_3$})$_2$(μ-O)]. Upon CO_2 addition the oxo-bridged complex was transformed cleanly into the carbonate complex **3Z**.[43]

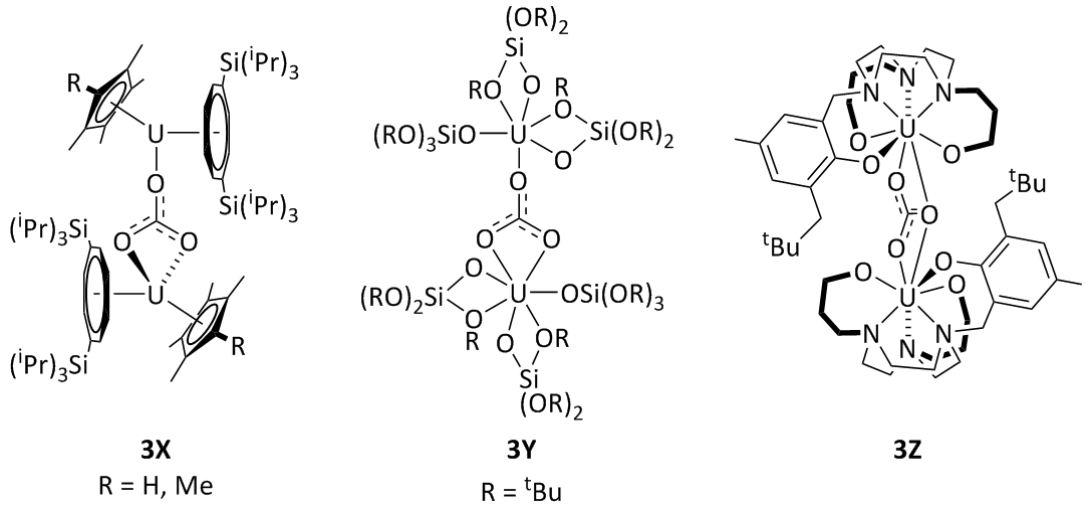

3X
R = H, Me

3Y
R = ^{t}Bu

3Z

Figure 3.5 Examples of carbonate bridged uranium complexes reported by the Cloke (left),[41] Mazzanti (centre)[44] and Meyer (right)[43] groups. Only one ligand arm is shown explicitly in **3Z**; all three are identical.

3.1.2.4 S_8

Elemental sulphur is an oxidising small molecule so its activation is much less challenging than that of N_2, CO or CO_2. Nevertheless, sulphur co-ordination compounds are of interest because they can display unique binding modes and are useful comparative models for oxygen-containing compounds. In recent years, some novel uranium sulphur chemistry has been reported. In 2013, the Hayton group reported the stoichiometric oxidation of U(N″)$_3$ with S_8 to yield the sulphide-bridged binuclear U(IV)/U(IV) complex **3AA** (Scheme 3.6).[45] Sulphide bridged uranium complexes are not uncommon but trace amounts of a second product, the novel persulphide-bridged binuclear U(IV)/U(IV) complex **3AB** were also formed in the reaction. The S-S distance in the $(S_2)^{2-}$ unit of **3AB** is 2.105(2) Å. The authors could not selectively prepare the persulphide complex but noted that the amount of **3AB** formed appeared to be increased by the presence of the metallated U(IV) impurity [U($CH_2SiMe_2NSiMe_3$)(N″)$_2$] in the U(N″)$_3$ starting material. However, reaction of

pure $[U(CH_2SiMe_2NSiMe_3)(N'')_2]$ with S_8 did not produce **3AB** and therefore they do not speculate on the possible role played by the metallated impurity in the formation of **3AB**. Furthermore **3AA** could not be converted into **3AB** by addition of S_8 or $S{=}PPh_3$ under any conditions.

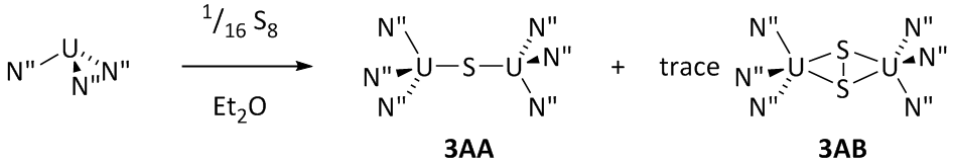

Scheme 3.6 Oxidation of $U(N'')_3$ with elemental sulphur.[45]

In 2014, Mazzanti and co-workers synthesised the first terminal uranium persulphide complex $[U\{(SiMe_2NPh)_3tacn\}(\eta^2\text{-}S_2)]$ (**3AC**) by reaction of 0.25 equivalents of S_8 with the U(III) tacn complex $[U\{(SiMe_2NPh)_3tacn\}]$ (Scheme 3.7).[46] The S-S bond length in **3AC** (2.050(8) Å) is consistent with a persulphide ion and spectral data also support the assignment of the uranium oxidation state as U(V). Addition of triphenylphosphine to a solution of **3AC** resulted in abstraction of a sulphide ion as $S{=}PPh_3$. A mixture of reduced uranium products was observed including the sulphide bridged U(IV)/U(IV) complex $[\{U((SiMe_2NPh)_3tacn)\}_2(\mu\text{-}S)]$ and a second example of a bridging uranium persulphide complex, $[\{U((SiMe_2NPh)_3tacn)\}_2(\mu\text{-}S_2)]$ (**3AD**), which could not be isolated but was characterised crystallographically. The observed S-S distance in **3AD** is identical to that in **3AB**.

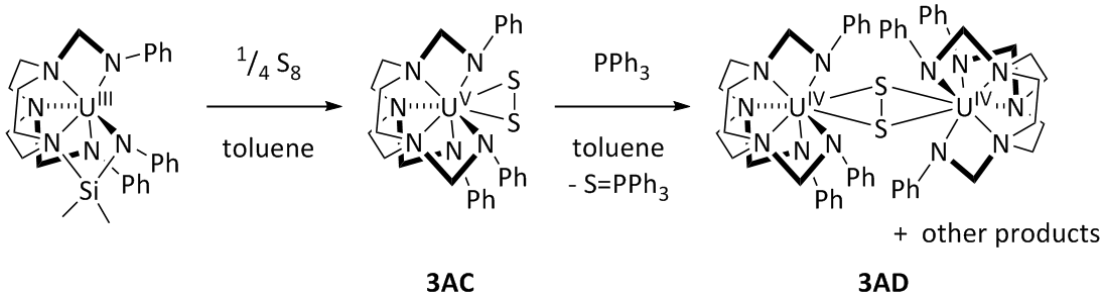

Scheme 3.7 Formation of terminal and bridging uranium persulphide complexes. One ligand arm is shown explicitly in the starting complex; all others are identical.[46]

The ability of uranium to co-ordinate multiple sulphur atoms has been further illustrated by Meyer and co-workers in that the binuclear U(IV)/U(IV) bridged sulphide complex **3AE**, prepared by stoichiometric reaction of S_8 with the U(III) complex $[U\{(^{Ad}ArO)_3N\}(DME)]$, readily incoporates three more sulphur atoms to form $[\{U((^{Ad}ArO)_3N)\}_2(\mu\text{-}S_2)_2]$ (**3AF**, Scheme 3.8).[47] The S-S bond lengths in **3AF** range from 2.044(2) to 2.053(2) Å. It is not possible to confidently assign the oxidation state of the U

centres in **3AF**. The structural and spectral data are not inconsistent with an assignment of either a U(IV)/U(IV) complex with supersulphide ligands or a U(V)/U(V) complex with persulphides, though the authors note that no f-block supersulphide complexes have been reported. Selenium compounds analogous to **3AE** and **3AF** were also prepared by the same method. However, an extra intermediate member of the selenium series was isolated, the perselenide-bridged complex [{U((^{Ad}ArO)$_3$N)}$_2$(μ-Se$_2$)]. It was suggested that formation of **3AF** from **3AE** proceeds *via* the analogous persulphide complex [{U((^{Ad}ArO)$_3$N)}$_2$(μ-S$_2$)] but this was not observed.

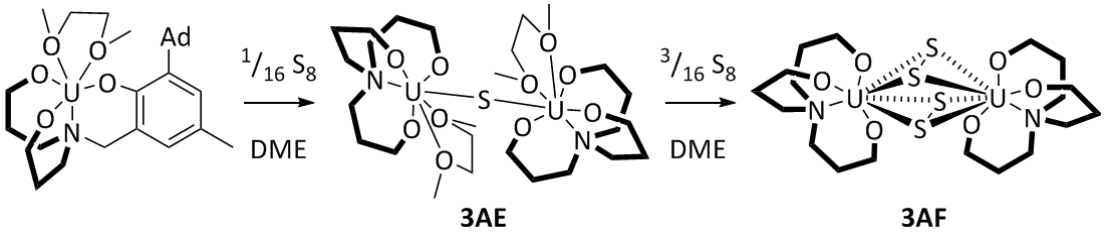

Scheme 3.8 Synthesis of a bridging uranium sulphide complex and its reaction with further equivalents of S_8.[47,48] One ligand arm is shown explicitly in the starting complex; all others are identical.

3.1.3 Binuclear uranium(III) complexes

A common aspect of the majority of the small molecule activations by U(III) detailed above is their co-operativity. Typically, one substrate molecule is bound and activated between two U(III) ions, which each contribute 1 e^- to effect an overall 2 e^- reduction. If the U(III) starting material is mononuclear this process necessitates a three-body collision. The synthesis of binuclear uranium(III) complexes is attractive and preorganisation of two U(III) centres within an organic framework at an appropriate separation should lead to enhanced rates of small molecule activation, since substrate activation becomes a two-body problem. In spite of these incentives, progress in this area has been limited.

The first structurally characterised binuclear U(III)/U(III) complex of a single ligand was reported earlier this year by Arnold and co-workers. The small cavity *trans*-calix[2]benzene[2]pyrrole macrocycle, H_2L', was deprotonated using two equivalents of lithium amide and then two equivalents of UI_3 were added to generate the binuclear complex [U_2I_4(L′)] (**3AG**) (Scheme 3.9).[49] One U(III) ion is bound in an η^5: η^5 fashion between the pyrrolide rings and the other is bound κ^1: κ^1 to each pyrrolide nitrogen and η^6: η^6 between the two aryl rings of the macrocycle. A short U···U separation of 3.8639(5) Å is observed in **3AG**. The synthesis of **3AG** must be carried out with the rigorous exclusion of co-ordinating

solvents because exposure of **3AG** to, for example, THF resulted in its partial dissociation to the mononuclear complex [UI(L′)(THF)] (**3AH**) and UI_3 (Scheme 3.9, right). Unfortunately however, the binuclear complex **3AG** is poorly soluble in arene and hydrocarbon solvents, which hampered further investigation into its reactivity.

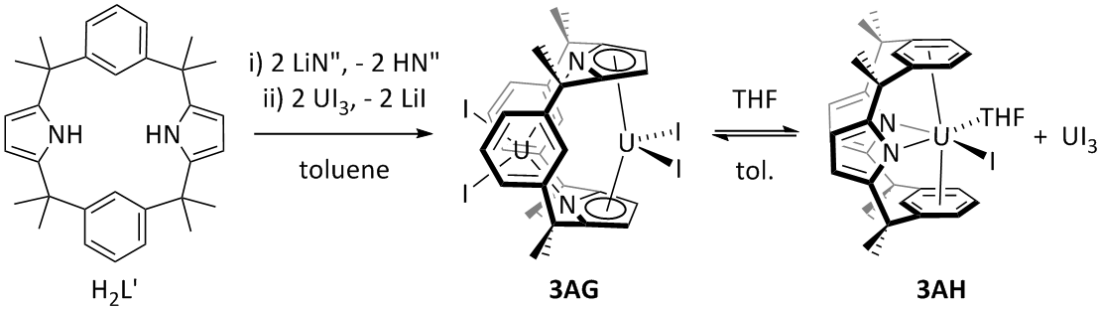

Scheme 3.9 Synthesis of the binuclear U(III)/U(III) complex **3AG** and its dissociation in co-ordinating solvent.[49]

The only other reported binuclear U(III)/U(III) complexes of a single ligand are the oligomeric uranium iodide Pacman compound [$(UI)_2$(L)] (**1AA**) and its borohydride derivative [{$U(BH_4)$}$_2$(L)], discussed in 1.5.3.[50] Although **1AA** was magnetically interesting, it was also of little further synthetic use due to its poor solubility. Therefore the chemistry of binuclear U(III)/U(III) complexes of preorganised ligands remains essentially unexplored. The aim of this project was to synthesise a well-defined U(III)/U(III) Pacman complex and to investigate its reactivity towards small molecules.

3.2 Metallation reactions using UI_3

Previous efforts to synthesise a binuclear uranium(III) Pacman complex were focussed exclusively on the *ortho*-phenyl hinged Pacman macrocycles. The proposed product structure contains bridging iodide ligands in both the *exo* site linking separate macrocycles and the *endo* site within the macrocyclic cleft. It was reasoned that the size of the macrocyclic cavity, as controlled by the aryl hinge groups, would impose geometric restraints on the *endo* bridging iodide and hence have a significant effect upon the stability and properties of the complex formed. Therefore the reaction of UI_3 with the deprotonated anthracenyl macrocycle was evaluated as a comparison.

3.2.1 Reaction of K_4L^A with UI_3

The reaction was initially investigated on a small scale using NMR spectroscopy. H_4L^A was combined with four equivalents of KN″ in a THF/C_6D_6 mixture to form a bright orange suspension of K_4L^A. The mixture was left to stand for ten minutes and then added to solid UI_3, forming a dark green solution containing a pale yellow precipitate, presumably KI. The ^{1}H NMR spectrum of the solution displays twelve paramagnetically contact-shifted resonances attributable to a single product (**12**) which has a symmetric ligand environment (Figure 3.6). The four *meso* ethyl groups, which are equivalent in the free macrocycle, are desymmetrised in the product appearing as two sets of resonances, as highlighted in Figure 3.6, which is consistent with the separate *exo* and *endo* environments established when the macrocycle folds into the Pacman geometry.

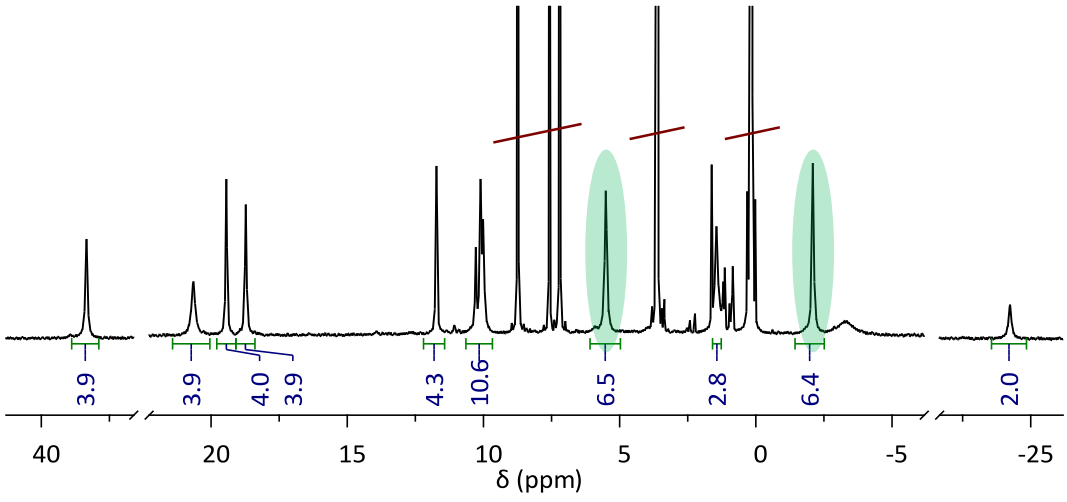

Figure 3.6 ^{1}H NMR spectrum of **12** formed by reaction between H_4L^A, 4 KN″ and 2 $UI_3(dioxane)_{1.5}$ in d_5-pyridine. Resonances corresponding to *protio* pyridine, dioxane and HN″ are scored through. Highlighted resonances correspond to the *exo* and *endo meso* $CH_2C\underline{H}_3$ environments of the macrocycle.

Formation of **12** is observed using either UI_3, $UI_3(THF)_4$ or $UI_3(dioxane)_{1.5}$ as the uranium starting material and either THF/C_6D_6 or d_5-pyridine as the reaction solvent. It is expected that the co-ordinating reaction solvent employed will bind to the product. Henceforth, the THF and pyridine solvates of **12** will be designated $\mathbf{12_{THF}}$ and $\mathbf{12_{py}}$ respectively. If the initial deprotonation of the macrocycle is carried out using LiN″ instead of KN″ then the ^{1}H NMR spectrum acquired after addition of UI_3 displays only a small number of very low intensity resonances which cannot be assigned to a single product. Since the macrocycle can be effectively deprotonated by either base, the fact that the reaction employing LiN″ does not proceed to yield the same product as that with KN″ indicates either that the salt elimination of LiI does not proceed successfully or that a potassium cation is necessarily incorporated into the product. **12** could not be successfully isolated on a preparative scale. It was discovered that removal of the solvent from a solution of $\mathbf{12_{THF}}$ resulted in decomposition to form insoluble yellow solids. Attempts to crystallise $\mathbf{12_{THF}}$ at low temperature or by slow diffusion of hexane anti-solvent similarly yielded only intractable orange/yellow material. The pyridine solvate $\mathbf{12_{py}}$ appeared to be more stable; removal of the solvent yielded sticky green solids which when analysed by NMR spectroscopy were still found to contain $\mathbf{12_{py}}$, in addition to unidentified by-products. Attempts to crystallise $\mathbf{12_{py}}$ were also unsuccessful.

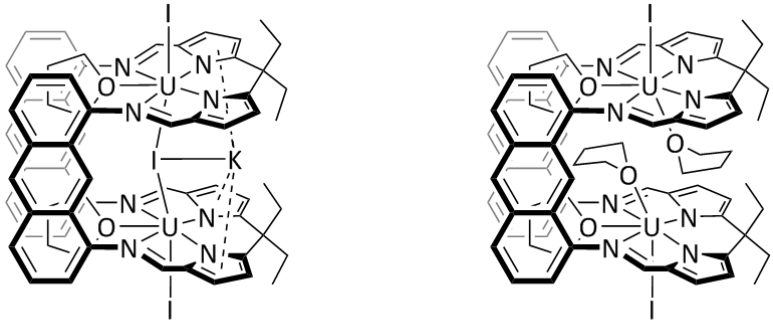

I **II**

Figure 3.7 Proposed structures for $\mathbf{12_{THF}}$ formed by the reaction of K_4L^A with UI_3 in THF. The analogous pyridine solvates, $\mathbf{12_{py}}$, would be expected for the reaction in pyridine.

Two different structures for **12**, are proposed (Figure 3.7), one in which KI is incorporated (**I**) and one with no alkali metal cation incorporation (**II**). The co-ordination number of uranium in both structures is 7 which is common for U(III), and in this case facilitated by solvent ligation. The binding of THF and pyridine to uranyl complexes of both the *ortho*-phenyl and anthracenyl macrocycles in the equatorial site between the macrocycle hinges has been observed previuosly. As yet no complexes of H_4L^A containing two metal-bound solvent molecules within the cleft, as proposed in **II**, have been isolated but a

binuclear magnesium complex $[Mg_2(py_{exo})_2(py_{endo})(L^A)]$ which features one bound pyridine molecule within the cleft has been structurally characterised.[51] The *endo* binding mode of the alkali metal cation proposed in **I** has been observed for the anthracenyl macrocycle with K^+ and Na^+ cations but not Li^+ (see 3.4.1 below). There are no reports of binuclear uranium complexes containing a single bridging iodide ligand so it is difficult to predict whether the dimensions of the ligand could support the proposed bridging iodide in **I**. Instead, the $\{U_2(\mu\text{-}I)_2\}$ motif is the most common [52-54] but the sterically restricted macrocyclic cleft is not expected to be able to incorporate two bulky iodide anions hence $[\{U(THF)\}_2(\mu\text{-}I)_2(L^A)]$ is not suggested as a structure for **12**.

THF is a weaker Lewis base than pyridine. Therefore it may be feasible to remove bound THF from $\mathbf{12_{THF}}$ under reduced pressure but not bound pyridine from $\mathbf{12_{py}}$. The reduction in co-ordination number at U(III) may then destabilise the complex and induce decomposition. Since both **I** and **II** contain bound solvent molecules, the observation that $\mathbf{12_{THF}}$ is less stable under vacuum than $\mathbf{12_{py}}$ is consistent with both proposed structures, though the extent of destabilisation might be expected to be greater for the neutral structure **II** which features THF molecules bound within the macrocyclic cleft, insulating the two U(III) centres from each other. However, the observation that **12** cannot be synthesised from Li_4L^A supports the proposal of the "-ate" complex **I**. The bridging iodide is expected to be stabilised by the incorporation in the cleft of the K^+ counterion which is large enough to be bound symmetrically between the four pyrrolides of the macrocycle. It is anticipated that Li^+ would be too small to occupy this binding pocket.

3.2.2 Structure of U(IV)/U(IV) decomposition product

On one occasion slow diffusion of hexane into a pyridine solution of $\mathbf{12_{py}}$ inside the glovebox resulted in the formation of single crystals of the decomposition product $[\{UI(py)\}\{U(OH)(py)\}(\mu\text{-}O)(L^A)]$ (**13**) (Scheme 3.10), presumably through reaction with trace quantities of water and/or oxygen present in the glovebox atmosphere. The identification of this decomposition product allows us to infer that complex **12** is indeed a binuclear uranium complex containing at least one iodide ligand. Furthermore, the feasibility of co-ordinating a solvent molecule in the equatorial site between the ligand hinges is confirmed in this low oxidation state uranium Pacman complex.

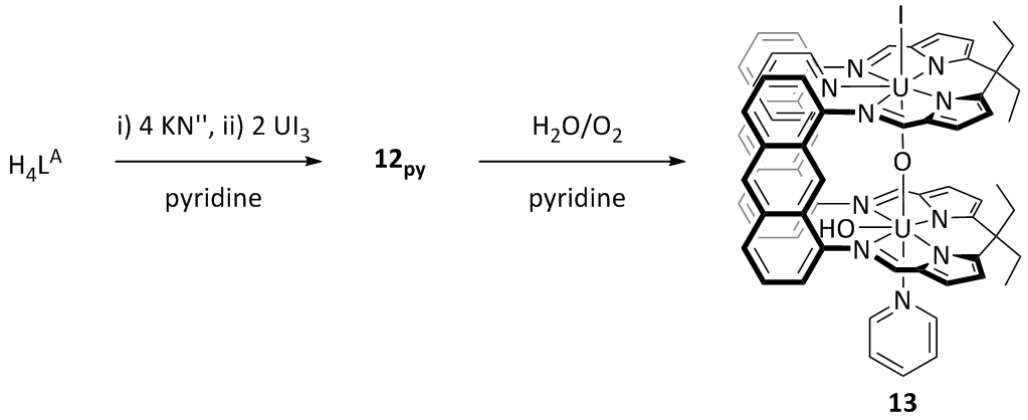

Scheme 3.10 Formation of the decomposition product [{UI(py)}{U(OH)(py)}(μ-O)(L^A)] **13**.

The solid state structure of **13** reveals that the two uranium ions occupy inequivalent pentagonal bipyramidal co-ordination sites (Figure 3.8). In addition to the four N donors of the macrocycle, U1 is bound to an axial iodide, a molecule of pyridine solvent in the equatorial site between the ligand hinges and the bridging oxo, O1. In addition to the macrocycle, U2 binds to the bridging oxo, a hydroxide ligand and a molecule of pyridine. However in this case, the hydroxide occupies the equatorial site and the pyridine the axial site, presumably due to the much reduced steric bulk of OH^- *vs* pyridine and I^-. The {U-(μ-O)-U} unit is essentially linear with a U1-O1-U2 angle of 177.0(4) °.

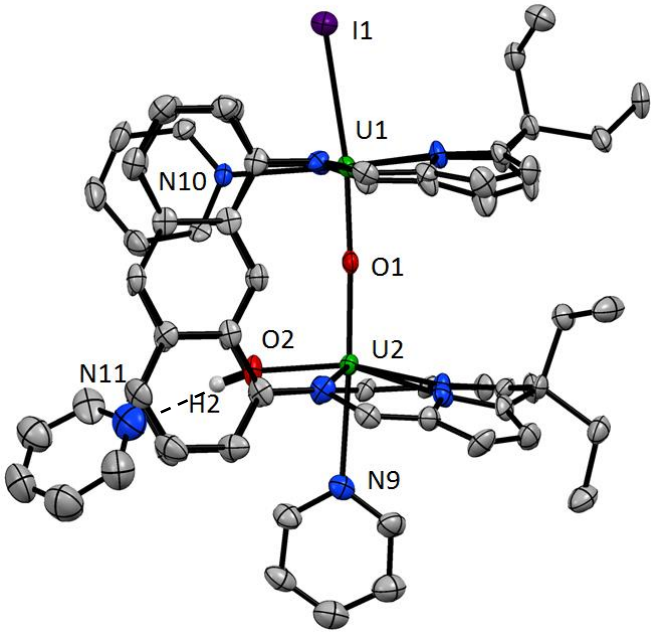

Figure 3.8 Solid state structure of **13**. Thermal ellipsoids are drawn at 50 % probability. Lattice solvent and H atoms are omitted except for the hydroxide proton and the molecule of pyridine lattice solvent which hydrogen bonds to it.

Table 3.1 Selected bond distances (Å) and angles (°) for **13**.

U1···U2	4.2472(5)	mean U2-N_{im}	2.58
U1-I1	3.1032(8)	mean U2-N_{pyr}	2.52
U1-N10	2.655(8)	U1-$N_{4\ plane}$	0.13
U1-O1	2.047(7)	U2-$N_{4\ plane}$	0.54
U2-O1	2.201(7)	H2-N11	2.05(4)
U2-O2	2.065(8)	U1-O1-U2	177.0(4)
U2-N9	2.629(7)	I1-U1-O1	171.5(2)
mean U1-N_{im}	2.55	O1-U2-N9	176.4(2)
mean U1-N_{pyr}	2.43	O2-H2-N11	177(10)

The proton of the hydroxide ligand, was located in the residual electron density map during structure refinement and its inclusion is strongly supported by the orientation of one molecule of pyridine lattice solvent directly towards the proton with a N11-H2 separation of 2.05(4) Å, thus facilitating hydrogen bonding. With the identity of O2 confirmed as a hydroxide rather than oxide, charge balancing necessitates assignment of either a U(IV)/U(IV) complex or a mixed-valent U(III)/U(V) complex. The U1-I1 separation of 3.1032(8) Å is within the normal range for U(IV)-I bonds [55] and, though there are few structurally characterised U(IV) hydroxide complexes to facilitate comparison, the observed U2-O2 distance of 2.065(8) Å lies within the reported range of 2.040(2) Å in $[U(OH)(OTf)_3(py)_4]$ [56] to 2.147(1) Å in $[U(OH)_2(Tpa)_3]^{2+}$.[57] Furthermore the U-N_{py} distances at the two U centres are similar with values of 2.655(8) Å (U1-N10) and 2.629(7) Å (U2-N9). Therefore **13** is assigned as a U(IV)/U(IV) complex.

However one unusual feature of the structure of **13** is that the bridging oxo is not bound symmetrically between the two U centres: the U1-O1 separation of 2.047(7) Å is markedly shorter than the U2-O1 separation of 2.201 Å. Typically, the oxo group is symmetrically bound in oxo-bridged U(IV)/U(IV) complexes. For example, the U-O bond lengths in $[\{UCp_3\}_2O]$ are identical at 2.0881(4) Å [58] and $[\{U(N'')_3\}_2O]$ features U-O distances of 2.142(6) and 2.147(6) Å which are statistically indistinguishable.[59] However, both these complexes are symmetric upon inversion whereas the two U centres in **13** are in different chemical environments: U1 is bound to an axial iodide ligand and an equatorial pyridine ligand whilst U2 is bound to an axial pyridine ligand and an equatorial hydroxide. In contrast to the *trans* influence in transition metal complexes where a metal-ligand bond *trans* to a strong metal-ligand bond is weakened, an inverse *trans* influence is observed in actinide compounds with mutually *trans* metal-ligand bonds experiencing synergic thermodynamic stabilisation. The extent of this stabilisation has been linked to ligand σ-donor ability.[60] On this basis it is suggested that the presence of the axial iodide ligand at U1

strengthens and shortens the U1-O1 bond compared to the U2-O2 bond. It has also been shown that uranyl U-O bonds are weakened by increasing the number of equatorial anionic hydroxide ligands at the expense of neutral water donors.[61] Therefore the presence of the equatorial hydroxide ligand O2 at U2, compared to the neutral equatorial pyridine donor N10 at U1, likely also contributes to the relative lengthening of the U2-O2 bond.

3.2.3 Attempted *in situ* reactions with 12

Although **12** was not successfully isolated, the formation in solution of a single, discreet compound, as indicated by NMR spectroscopy, was still a more promising result than the previously observed, poorly soluble, oligomeric compounds resulting from reactions of the *ortho*-phenyl macrocycle with UI_3. Therefore a number of reactions were carried out with **12** formed *in situ* with the aim of preparing a more stable derivative. The reagents investigated and the results of the reactions as monitored by ^{1}H NMR spectroscopy are summarised in Table 3.2.

Table 3.2 *In situ* reactions carried out with **12**.

Reagent	*Solvent*	*Outcome*
DMAP (2 eq.)	THF/C_6D_6	Decomposition.
CO (1 bar)	d_5-pyridine	No reaction.
LiCl (xs)	THF/C_6D_6	Decomposition, formation of diamagnetic species.
KO^{t}Bu (2 eq.)	d_5-pyridine	Multiple paramagnetic products formed.
$NaBH_4$ (xs)	THF/C_6D_6	New paramagnetic resonances observed that could not be assigned to a Pacman product.
S_8 (xs)	d_5-pyridine	Oxidation to multiple paramagnetic products.
KC_8 (2 eq.)	d_5-pyridine	Slow formation of multiple paramagnetic products.

Despite investigation of a range of different reagents, including Lewis bases, ligand substitution reagents, oxidants and reductants, clean conversion of **12** to a single product was not observed in any of the reactions trialled. It would appear that the elusive solution species **12** does not provide a viable route into U(III) Pacman chemistry.

3.3 Metallation reactions using $U(BH_4)_3$

UI_3 was not found to be a convenient starting material for the synthesis of stable, isolable U(III)/U(III) Pacman complexes. An investigation into the reactivity of the other commonly available U(III) starting materials $U(N'')_3$ and $U(OAr)_3$ (where Ar = 2,6-$C_6H_3(^tBu)_2$, 2,4,6-$C_6H_2(^tBu)_3$) with H_4L^A swiftly revealed that neither of these complexes were suitable precursors: no reaction occurred between $U(N'')_3$ and H_4L^A or $U(OAr)_3$ and Li_4L^A. Therefore $[U(BH_4)_3(sol)_x]$ was identified as a little-exploited, alternative U(III) starting material.

3.3.1 Synthesis of $[U(BH_4)_3(THF)_2]$

As discussed in section 3.1.1.1, no convenient synthesis of $[U(BH_4)_3(sol)_x]$ from a U(III) starting material has been published. Therefore the feasibility of preparing $[U(BH_4)_3(sol)_x]$ from UI_3 was investigated. UI_3 was chosen as the starting material since it may be synthesised in a single step from uranium metal and allows for the implementation of salt elimination methodologies. Dr Joy Farnaby carried out initial NMR scale reactions between UI_3 and 3.3 equivalents of the different alkali metal borohydrides, MBH_4 (M = Li, Na, K), in d_8-THF. Upon combination of UI_3 with either $LiBH_4$ or $NaBH_4$ in d_8-THF an immediate colour change occurred from deep blue to red. New, paramagnetically broadened and contact-shifted resonances were observed in the ^1H and ^{11}B NMR spectra of the $NaBH_4$ reaction mixture at 95 and 230 ppm respectively. By contrast no new resonances were observed in the NMR spectra of the $LiBH_4$ mixture. No immediate colour change was observed following addition of KBH_4 to UI_3 in THF, though the reaction mixture did gradually turn maroon over two weeks. The ^1H NMR spectrum acquired after two weeks displayed broad contact shifted resonances at 70 and 20 ppm and two signals were also present in the ^{11}B NMR spectrum at 270 and 250 ppm. On a larger scale, addition of THF to solid UI_3 with 3.3 equivalents of $NaBH_4$ or $LiBH_4$ immediately produced deep red mixtures. The $UI_3/NaBH_4$ mixture was a red solution containing a small amount of white precipitate, the excess $NaBH_4$. However microcrystalline red solid formed rapidly in the $UI_3/LiBH_4$ mixture. This may indicate that one of the products of the reaction between UI_3 and $LiBH_4$ is an "-ate" salt with reduced solubility, such as $[Li(THF)_x][U(BH_4)_4(THF)_y]$.

Equation 3.2

$$UI_3 + 3\,NaBH_4 \xrightarrow{THF} U(BH_4)_3(THF)_x + 3\,NaI$$

On the basis of these observations, $NaBH_4$ was selected since it reacts rapidly with UI_3 to generate a single, soluble species, presumably $[U(BH_4)_3(THF)_x]$ (Equation 3.2). A

trial NMR scale reaction in d_8-THF was carried out between 2 equivalents of $[U(BH_4)_3(THF)_x]$, generated *in situ* from UI_3 and $NaBH_4$, and K_4L^A formed *in situ* from H_4L^A and KN″. The ^1H NMR spectrum of the resultant mixture displayed contact-shifted resonances assignable to a single symmetric macrocyclic product. Following this promising result it seemed worthwhile to isolate and fully characterise $[U(BH_4)_3(THF)_x]$ before embarking on further reactivity studies or preparative scale reactions.

In order to isolate $[U(BH_4)_3(THF)_x]$ it is necessary to separate it from the NaI by-product which is soluble in THF. $[U(BH_4)_3(THF)_x]$ was observed to have some solubility in both toluene and ether. Formation of $[U(BH_4)_3(sol)_x]$ by reaction in toluene or ether instead of THF, enabling the insoluble NaI to be removed by filtration, would have been convenient. However, no reaction occurred between UI_3 and $NaBH_4$ in toluene solvent. Similarly no reaction occurred in ether unless the dioxane adduct $UI_3(dioxane)_{1.5}$ was used as the U(III) starting material. In this latter case, a slow, out-of-phase reaction occurred with formation of a purple-red insoluble product over several hours. The product was evidently contaminated with NaI, somewhat defeating the object of using ether as the reaction solvent.

It was concluded that $[U(BH_4)_3(THF)_x]$ must be synthesised in THF and then separated from NaI and excess $NaBH_4$ by extraction. In order to minimise the volume of solvent required and reduce the risk of exposure of $[U(BH_4)_3(THF)_x]$ to air during a lengthy filtration procedure, the extraction was performed under continuous conditions using a Soxhlet apparatus fitted with a fine porosity glass frit (Figure 3.9). Initially toluene was employed as the extraction solvent in order to achieve the best separation of the product from NaI, necessitating temperatures of 160 °C in the reboil flask. After 16 hours white solids remained on the Soxhlet frit and the collection flask contained a red solution and a dark brown precipitate. The solution was decanted and the volatiles removed. ^1H and ^{11}B NMR analyses of the resulting solid residue confirmed the successful isolation of $[U(BH_4)_3(THF)_x]$ in 40 % yield (assuming x = 2, see below). However the dark precipitate from the reboil flask was found to

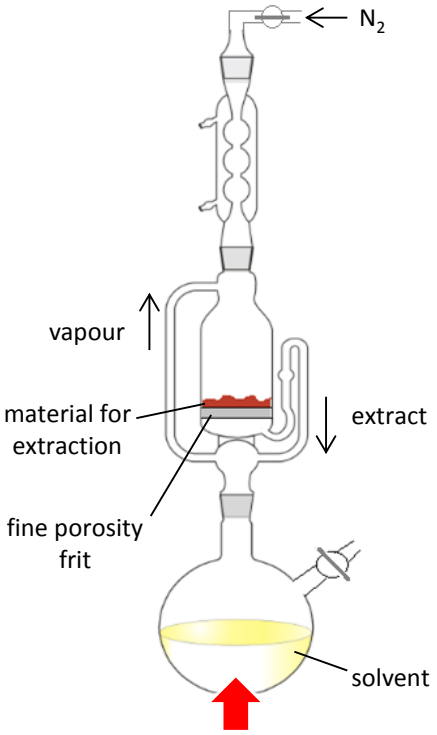

Figure 3.9 Experimental set-up for an air sensitive Soxhlet extraction.

contain a mixture of the desired product $[U(BH_4)_3(THF)_x]$ and a second species characterised by resonances at 65 ppm in the ^{1}H NMR spectrum and at 265 and 250 ppm in the ^{11}B NMR spectrum. This species is very dark brown in colour and has reduced solubility compared to $[U(BH_4)_3(THF)_x]$. We suggest that its formation is due to the thermal decomposition of extracted $[U(BH_4)_3(THF)_x]$ which is exposed to high temperatures in the reboil flask. It was concluded that toluene was not a suitable extraction solvent since the solution yield of uncontaminated product was mediocre and would be expected to decrease further for larger scale preparations. Therefore the Soxhlet extraction was repeated using diethyl ether as the solvent. $[U(BH_4)_3(THF)_x]$ has improved solubility in ether compared to toluene enabling the extraction to be completed in 6 hours at the reduced reboil temperature of 60 °C. The collection flask contained a red solution and a dark red precipitate. NMR analysis of both the solution and solid products revealed the sole presence of $[U(BH_4)_3(THF)_x]$ with no evidence of decomposition products.

$[U(BH_4)_3(THF)_2]$ (**14**) is isolated as a microcrystalline red solid in 90 % yield by removal of the volatiles from the ether-extract. The degree of THF solvation was determined by NMR competition experiments: DME was added to a C_6D_6 solution of **14** to liberate the co-ordinating THF molecules which were then integrated against $Si(SiMe_3)_4$ as an internal standard. The resulting formulation of $[U(BH_4)_3(THF)_2]$ is also supported by elemental microanalysis. The structure of the simple molecular *tris*-THF adduct $[U(BH_4)_3(THF)_3]$ has been reported [21] but we have not determined the molecular structure of **14**. On close inspection it was noted that the BH_4^- resonance in the ^{1}H NMR spectrum of **14** in d_8-THF is shifted to lower frequency, by 10 ppm, than the corresponding resonance of $[U(BH_4)_3(THF)_x]$ formed *in situ* in d_8-THF. The ^{11}B NMR spectrum is unchanged. It is likely that some of the co-ordinating THF dissociates from $[U(BH_4)_3(THF)_x]$ upon its exposure to high vacuum during experimental work-up to generate **14**. It is possible that the apparent low co-ordination number of the U(III) centres in **14** may be augmented in the solid state by oligomerisation. However the B-H stretching region of the solid state IR spectrum of **14** is relatively simple displaying a strong band at 2446 cm^{-1} attributed to B-H(terminal) stretching and two overlapping bands at 2205 and 2147 cm^{-1} assigned to B-(μ-H) stretches. The number and positioning of the bands is consistent with $\{(\mu\text{-H})_3BH\}$ binding modes for all three BH_4^- ligands.[62] Therefore the IR spectrum of **14** is indicative of a monomeric complex since the presence of bridging and terminal BH_4^- ligands in an oligomeric structure would likely result in a complex series of overlapping B-H stretching bands. When all bridging hydrides are taken into account, the U(III) centres in monomeric **14** are formally 11 co-ordinate.

3.3.2 Solid state structures of $[U(BH_4)_x(I)_y(sol)_z]$

Various recrystallisations of isolated **14** were carried out in attempts to obtain single crystals that might yield structural insights and further supporting evidence for the successful synthesis of a uranium *tris*-borohydride complex. Single crystals were obtained from the recrystallisation of **14** from ether at 0 °C and also from the slow diffusion of hexane into a benzene solution of **14** containing a few drops of DME. In both cases rapid, destructive desolvation of most of the crystals was observed under the microscope during crystal mounting but one crystal from each batch was successfully mounted and analysed by X-ray diffraction. The crystal isolated from ether was found to be an ionic U(III) mixed borohydride/iodide compound $[U(BH_4)_2(THF)_5][U_2(BH_4)_{4.90}(\mu\text{-}I)_2(I)_{0.10}(THF)_3]$ (**15**) which has an empirical formula of $[U(BH_4)_{2.30}(I)_{0.70}(THF)_{2.7}]$. The crystal analysed from the C_6D_6/DME/hexane mixture was the mixed borohydride/iodide DME adduct $[U(BH_4)_{2.59}(I)_{0.41}(DME)_2]$ (**16**). It is suspected that the incorporation of iodide into both these structures is due to imperfect experimental extraction resulting in the contamination of **14** with a small amount of NaI. Iodide/borohydride exchange may then occur during recrystallisation leading to the formation of various single crystals with different borohydride/iodide compositions. Since the elemental microanalysis results were satisfactory for **14** it must be concluded that **14** contains only trace amounts of NaI and thus **15** and **16** are not representative of the bulk composition of **14**. Rather, it is likely that the single crystals containing the highest levels of iodide were more stable, did not desolvate as rapidly as the pure borohydride crystals and gave the strongest X-ray diffraction patterns, leading to their preferential X-ray analysis over pure $[U(BH_4)_3(sol)_x]$ crystals, which may well also have been formed.

Complex **15** is an unusual example of a wholly U(III) ion pair, containing a monomeric U(III) cation and a dimeric U(III)/U(III) anion (Figure 3.10). The structure of the pentagonal bipyramidal cation $[U(BH_4)_2(THF)_5]^+$ has been reported previously by Ephritikhine and co-workers, prepared by the protonation of $U(BH_4)_3(THF)_3$ with the acidic ammonium salt $[HNEt_3][BPh_4]$ to form $[U(BH_4)_2(THF)_5][BPh_4]$.[63] They have also isolated an unusual mixed U(III)/U(IV)/U(IV) ion pair $[U(BH_4)_2(THF)_5][(BH_4)_3U(\mu\text{-}\eta^7,\eta^7\text{-}C_7H_7)U(BH_4)_3]$ (**3AJ**, Figure 3.11) from the reaction of $U(BH_4)_4$ with $K(C_7H_9)$.[64] Similarly to **15**, the ion pair **3AJ** also features a dimeric uranium anion. The metrics of the cation in **15** are similar to those observed in the previously published structures. The co-ordination environment of the two U(III) centres in the anionic portion of **15** is *pseudo*-octahedral. The U(III) centres form a dimer by means of the two bridging I^- ligands. To our knowledge, only

one other compound containing this $\{U^{III}(\mu\text{-}I)_2U^{III}\}$ motif has been structurally characterised: a dihydrobis(pyrazolyl)borate supported dimer featuring bridging and terminal I^- ligands (**3AK**, Figure 3.11). The U-(μ-I) distances (mean 3.23 Å) and U···U separation (4.973(2) Å) observed in **3AK** are similar to those found in **15** (mean U-(μ-I) = 3.25 Å, U2···U3 = 4.9379(9) Å). The U-I_{term} distance in **3AK** is 3.116(3) Å whereas the U2-I3 bond length in **15** was determined as 3.05(2) Å. However, the restraints necessarily imposed during the refinement of the part-occupied I3 resulted in a large standard uncertainty in the U-I bond length, giving a possible range of 2.99 – 3.11 Å. Likewise, positional refinement of the part-occupied borohydride B7 was challenging. However the resultant U2-B7 separation of 2.72(1) Å is similar to the other U-B separations in the anion (see Table 3.3). None of the borohydride protons could be located crystallographically but based on the U···B separations it is likely that all the borohydride ligands bind through three bridging hydrides in a $\{(\mu\text{-}H)_3BH\}$ fashion. Generally U···B separations of greater than 2.80 Å are observed when two or fewer hydrides bridge between boron and uranium.[65]

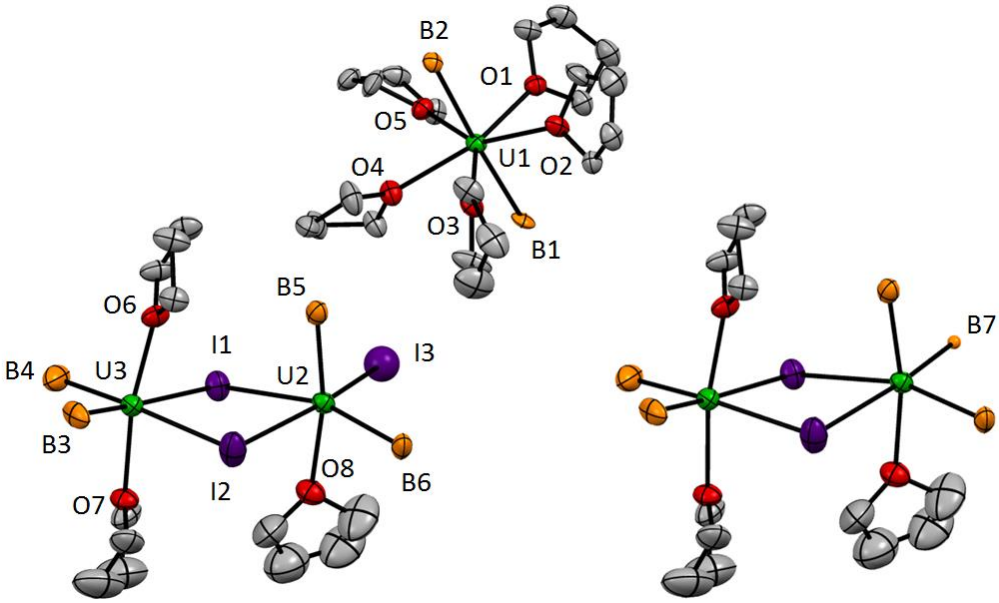

Figure 3.10 Solid state structure of **15**. Both the terminal iodide (left) and terminal borohydride (right) anionic components are shown. The ratio of I^-:BH_4^- occupancy is 0.1:0.9. B7 and I3 were refined isotropically. The cation is not duplicated. Thermal ellipsoids are drawn at 50 % probability. Lattice solvent and H atoms are omitted.

Table 3.3 Selected bond distances (Å) and angles (°) for **15**.

U1···B1	2.72(1)	U3-I1	3.265(1)
U1···B2	2.79(1)	U3-I2	3.163(2)
mean U1-O_{THF}	2.54	U2-O8	2.56(1)
U2···U3	4.9379(9)	U3-O6	2.44(1)
U2···B5	2.73(2)	U3-O7	2.521(9)
U2···B6	2.69(2)	U2-I1-U3	96.96(3)
U3···B3	2.69(2)	U2-I2-U3	100.92(4)
U3···B4	2.63(2)	I1-U2-I2	78.18(3)
U2···B7	2.72(1)	I1-U3-I2	80.24(3)
U2-I1	3.330(1)	B6-U2-B7	99.5(4)
U2-I2	3.240(1)	B3-U3-B4	99.3(6)
U2-I3	3.05(2)	B1-U1-B2	177.2(4)

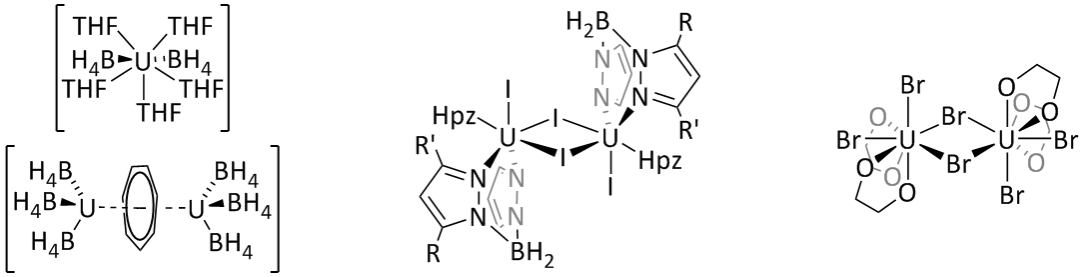

3AJ **3AK** **3AL**

Figure 3.11 Structures of a U(III)/U(IV) ion pair (**3AJ**),[64] an iodide bridged U(III)/U(III) scorpionate dimer (**3AK**)[52] and a U(III) DME complex (**3AL**, Me groups omitted).[66] R = Me, R′ = ^{t}Bu, Hpz = the neutral pyrazole, NH(CMe)(CH)(C^{t}Bu)N.

In contrast to **15**, **16** is a simple molecular complex with the co-ordination about U1 pentagonal bipyramidal (Figure 3.12). The equatorial sites are occupied by two DME molecules and a disordered borohydride/iodide ligand while two more borohydrides occupy the axial positions. The B1-U1-B1′ angle of 176.9(4) is essentially linear and the U1-B1 separation of 2.78(1) Å indicates that the binding mode of the axial borohydrides is {(μ-H)$_3$BH}. Refinement of the mixed borohydride/iodide position was more straightforward for **16**. Both I1 and B2 were successfully refined anisotropically and only the U1-B2 separation required restraining (to 2.80(2) Å, resulting in an observed U1-B2 separation of 2.82(2) Å); the observed U1-I1 distance of 3.097(4) Å is normal for a U^{III}-I bond. Due to the restraint employed, it is not possible to confidently assign the binding mode of the equatorial BH_4^- ligand but it is likely to be {(μ-H)$_2$BH$_2$} by analogy with the isostructural complex [U(BH$_4$)$_3$(DMPE)$_2$] (**3G**) discussed above.[22] An interesting structural comparison to **16** is provided by the complex [UBr$_3$(DME)$_2$] (**3AL**, Figure 3.11) which dimerises through bromide bridges in the solid state.[66] The U-O bonds of **16** (2.571(5), 2.609(7) Å) lie within

the reported range of U-O distances for the dimer (2.550(7) – 2.656(7) Å). The fact that **16** is monomeric in the solid state indicates that bridging is disfavoured for this system, either due to the greater steric bulk of I^-/BH_4^- *vs* Br^- or perhaps because the bridging mode is less favourable for the BH_4^- anion.

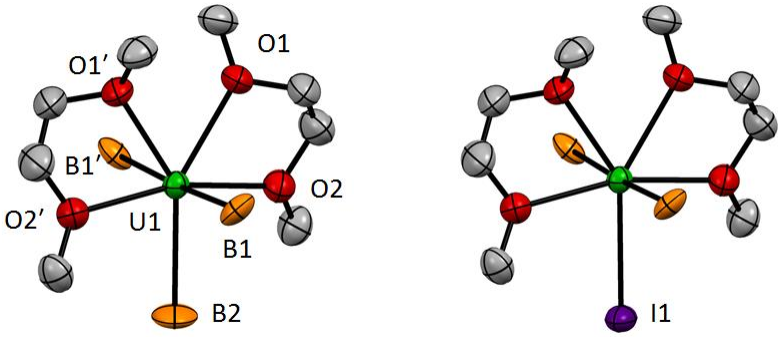

Figure 3.12 Solid state structure of **16**. Both the equatorial borohydride (left) and terminal iodide (right) containing components are shown. The ratio of I^-:BH_4^- occupancy is 0.41:0.59. Thermal ellipsoids are drawn at 50 % probability. Lattice solvent and H atoms are omitted.

Table 3.4 Selected bond distances (Å) and angles (°) for **16**.

U1···B1	2.78(1)	B1-U1-B1′	176.9(4)
U1-O1	2.571(5)	O1-U1-O2	63.5(2)
U1-O2	2.609(7)	B1-U1-B2	91.6(2)
U1-I1	3.097(4)	O1-U1-O1′	67.5(3)
U1···B2	2.82(2)	O2-U1-B2	82.9(1)

3.3.3 Reactions of $[U(BH_4)_3(THF)_2]$ with H_4L^A

Having developed a convenient, high yielding synthesis of **14** from UI_3 (albeit with a small degree of NaI contamination), salt elimination reactions of **14** with the different alkali metal salts of the anthracenyl macrocycle were investigated (Scheme 3.11). Reaction of two equivalents of **14** with *in situ* generated Li_4L^A, Na_4L^A, or K_4L^A in THF resulted in each case in the formation of a single product. The products of the Li and Na reactions have almost identical ^1H and ^{11}B NMR spectra. Their ^1H NMR spectra display paramagnetically contact-shifted resonances corresponding to a symmetric ligand environment in which the ethyl groups at the *meso* carbons have become desymmetrised. The ^{11}B NMR spectra show two broad, contact-shifted resonances in a 1:2 intensity ratio (Figure 3.13). These data are consistent with the formation of the salts $[M(THF)_4][\{U(BH_4)\}_2(\mu\text{-}BH_4)(L^A)(THF)_2]$ (**17**, M = Li, **18**, M = Na), which contain one bridging and two terminal BH_4^- ligands. The bridging BH_4^- ligand is sandwiched between two U(III) centres resulting in a higher ^{11}B chemical shift of 212 ppm compared to that of the terminal BH_4^- ligands at 207 ppm. A broad resonance is observed at –70.1 ppm with $W_{½}$ = 498 Hz in the ^1H NMR spectra which

sharpens to $W_{½}$ = 364 Hz upon ^{11}B decoupling. This is assigned to the protons of the terminal borohydride ligands. No resonances are observed for the bridging borohydride protons, even in the ^{1}H{^{11}B} NMR spectra.

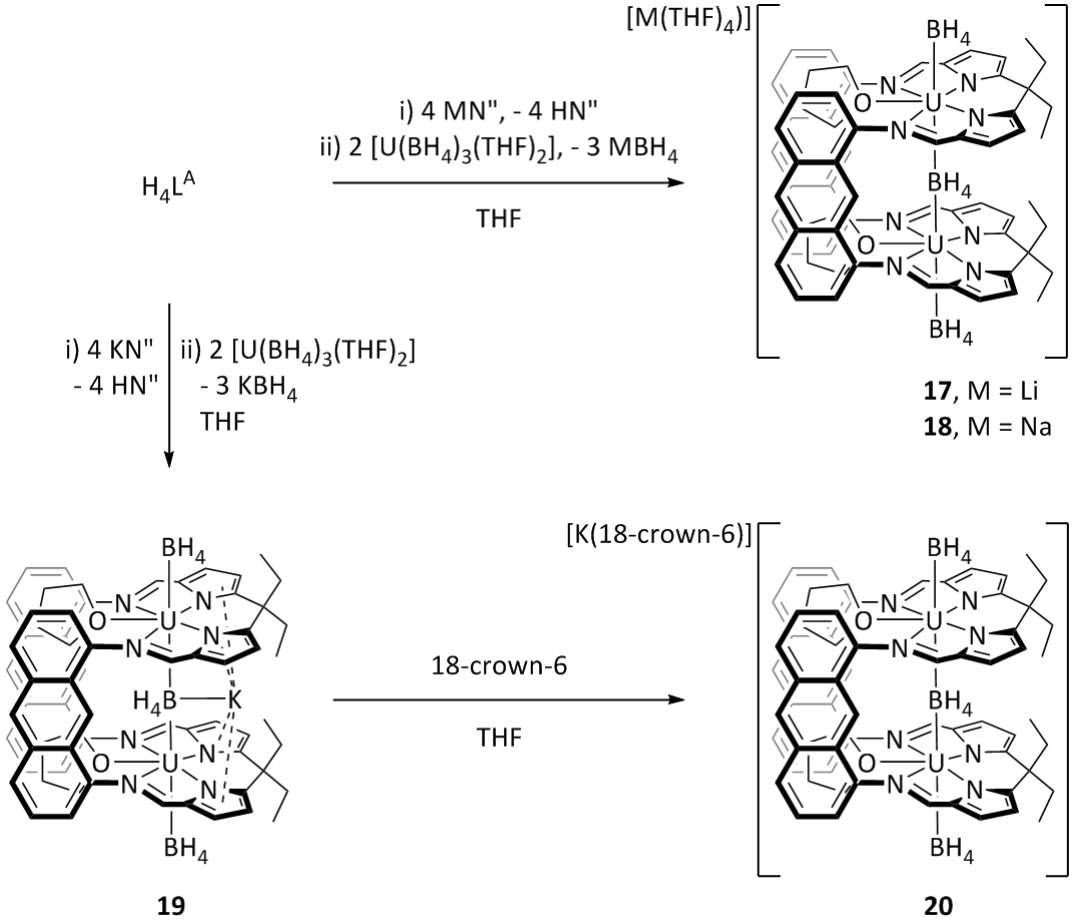

Scheme 3.11 Reactions of $[U(BH_4)_3(THF)_2]$ with the different alkali metal salts of H_4L^A.

The ^{1}H NMR spectrum of the product of the analogous potassium reaction (**19**) consists of a different set of paramagnetically contact-shifted resonances (Figure 3.13), again corresponding to a symmetric ligand environment with desymmetrised ethyl groups, though two ligand resonances are obscured by solvent signals. A broad resonance is observed at 31.8 ppm with $W_{½}$ = 441 Hz which sharpens to $W_{½}$ = 376 Hz upon ^{11}B decoupling. The ^{11}B NMR spectrum of **19** contains only a single broad resonance at 180 ppm. From this it might be concluded that a neutral complex is formed when the K salt of the ligand is employed, with no bridging BH_4^- moiety present. However addition of 18-crown-6 to **19** results in formation of a new species with very similar ^{1}H and ^{11}B NMR data to **17** and **18**, which rapidly precipitates from solution. This new species is assigned as $[K(18\text{-crown-}6)][\{U(BH_4)\}_2(\mu\text{-}BH_4)(L^A)(THF)_2]$ (**20**) the crown-ether solvated potassium analogue of **17** and **18**. Therefore **19** must also contain a K^+ ion and is formulated as $[\{U(BH_4)\}_2(\mu$-

$BH_4K)(L^A)(THF)_2]$ in which the large K^+ cation is bound within the cleft of the macrocycle between the four pyrrolide rings and in proximity to its bridging BH_4^- counterion. This binding mode has been crystallographically verified for related complexes (see 3.4.1). By coincidence the chemical shifts of the terminal and bridging boron atoms are identical in **19**. Complex **19** can be considered as a host-guest complex in which the macrocycle encapsulates one molecule of KBH_4, rather than as an ionic compound. The in-cleft binding mode is not favoured for the smaller Li^+ and Na^+ cations.

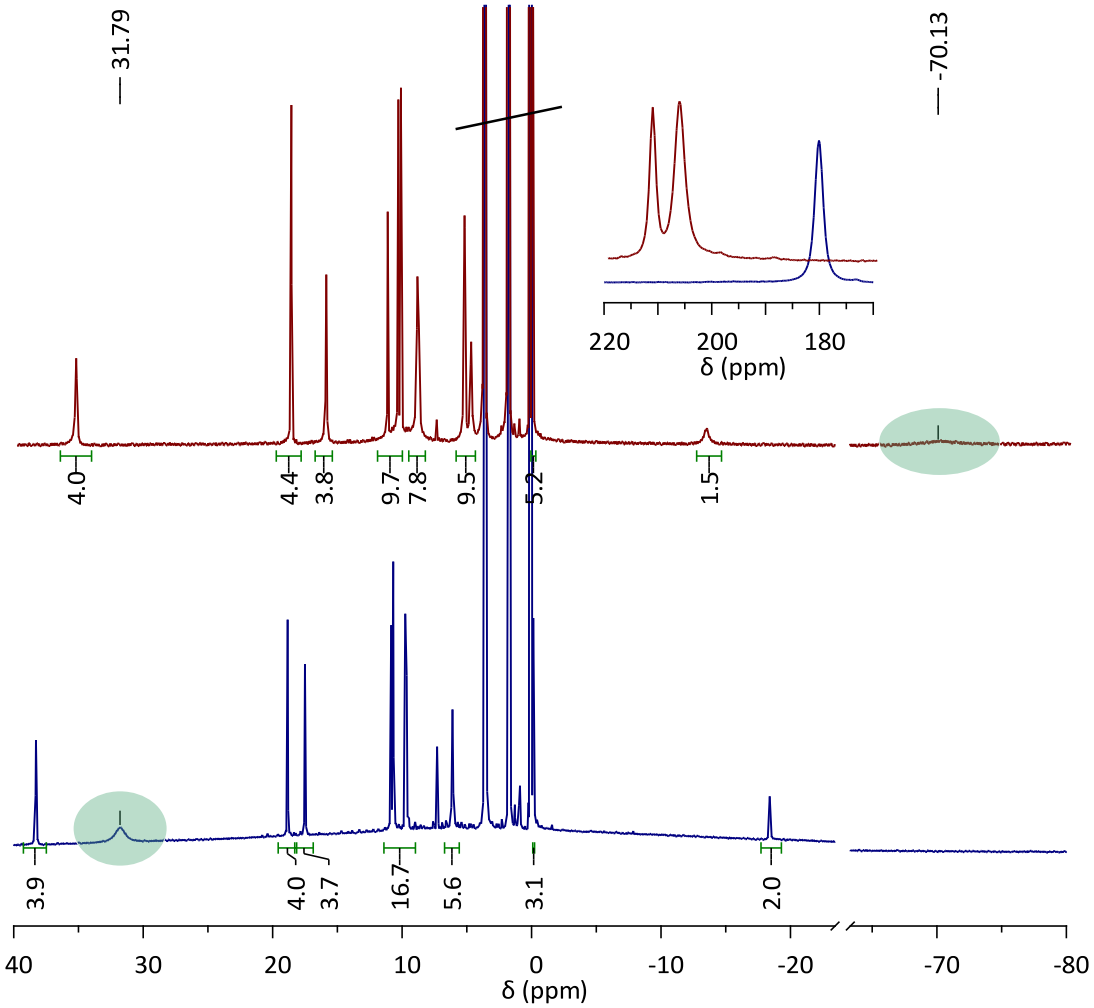

Figure 3.13 Comparison of the ^1H and ^{11}B (inset) NMR spectra of **18** (top, red) and **19** (bottom, blue). The terminal BH_4^- resonances are highlighted. *Protio* THF and HN" resonances are scored through.

The sodium salt **18** was found to be the most convenient of the complexes to synthesise on a preparative scale for further reactivity investigations. The $NaBH_4$ by-product eliminated during synthesis is insoluble in THF and therefore can be readily separated from soluble **18**. KBH_4 is also insoluble in THF but $LiBH_4$ is THF and ether soluble. **18** crystallises readily in bulk from THF at low temperature but crystalline **19** has not been

successfully obtained. The increased crystallinity of **18** may be attributed to its formal ionic nature compared to host-guest complex **19**. It is also of interest to note that formation of **18** is favoured over formation of **19**; the *in situ* trial reaction carried out between UI_3, $NaBH_4$ and K_4L^A, in which both Na^+ and K^+ cations were present in solution, resulted in exclusive formation of the sodium salt **18**. This indicates that the bonding enthalpy gained through the THF solvation of the small Na^+ cation outweighs the K^+-pyrrolide bonding enthalpy.

*3.3.3.1 Structure of $[Na(py)_4][\{U(BH_4)\}_2(\mu\text{-}BH_4)(L^A)(py)_2]$, **18$_{py}$***

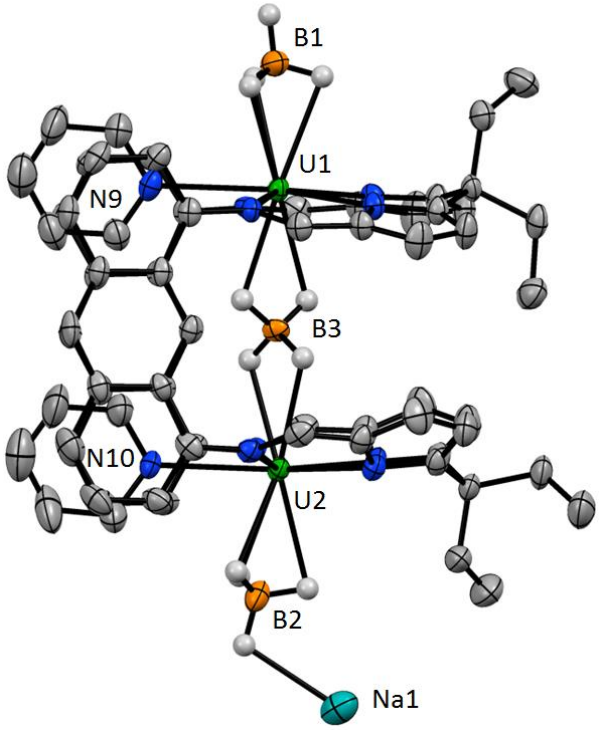

Figure 3.14 Solid state structure of **18$_{py}$**. Thermal ellipsoids are drawn at 50 % probability. Four molecules of pyridine solvent ligating Na1, lattice solvent and all H atoms except those of the BH_4 groups are omitted.

Table 3.5 Selected bond distances (Å) and angles (°) for **18$_{py}$**.

U1···U2	5.9243(3)	U1-N9	2.698(4)
mean U-N_{im}	2.62	U2-N10	2.709(4)
mean U-N_{pyr}	2.49	Na1···B2	2.932(9)
U1···B1	2.681(9)	U1-B3-U2	177.8(3)
U1···B3	2.977(7)	B1-U1-B3	175.5(2)
U2···B3	2.949(7)	B2-U2-B3	169.3(2)
U2···B2	2.723(8)	Na1-B2-U2	134.1(3)

18 may be isolated as a dark green crystalline solid in 30 % yield from the reaction of two equivalents of **14** with Na_4L^A (generated *in situ*) in THF. Recrystallisation of **18** from

a pyridine/hexane solution yielded single crystals of the pyridine adduct **18$_{py}$** that were suitable for X-ray diffraction analysis. The solid-state structure revealed that the anthracenyl macrocycle adopts the classic Pacman geometry with one U(III) cation occupying each pyrrole/imine N_4 donor pocket (Figure 3.14). The U(III) centres are pentagonal bipyramidal, with four of the equatorial donors provided by the imine and pyrrolide nitrogens of the macrocycle and the fifth site occupied by a pyridine molecule sandwiched between the aromatic hinges of the ligand. One terminal and one bridging BH_4^- occupy the axial sites. The {BH_4-U-(μ-BH_4)-U-BH_4} core is essentially linear (see Table 3.5) and results in a U···U separation of 5.9243(3) Å. The borohydride hydrogens were located from the difference Fourier map and their positions refined (see 4.6.14 for details). The terminal BH_4^- groups (B1 and B2) are bound to U1 and U2 at separations of 2.681(9) and 2.723(8) Å, respectively, in a {$(\mu\text{-H})_3$BH} fashion while the central bridging BH_4^- (B3) binds to each U(III) centre at distances of 2.977(7) and 2.949(7) Å through two bridging hydrides in a {$(\mu\text{-H})_2$B$(\mu\text{-H})_2$} fashion. In the solid state, the sodium cation is co-ordinated to the remaining H of one terminal BH_4^- group (B2) and four pyridine molecules. This Na···BH_4 co-ordination must be dynamic in solution since the ^{1}H NMR spectrum shows a symmetric ligand environment.

If NMR spectroscopy or X-ray or neutron diffraction are not amenable, IR spectroscopy is often employed to determine the binding mode of BH_4^- in metal complexes since the symmetries of the different bridging motifs give rise to characteristic groupings of bands.[62] This method is effective for complexes bearing a single BH_4^- ligand but IR spectra swiftly become complicated when two or more BH_4^- ligands are present, as such, the IR spectrum of **18** displays several overlapping bands in the region from 2500 to 2100 cm^{-1} consistent with multiple BH_4^- binding modes.

3.3.4 Reactions of [U(BH$_4$)$_3$(THF)$_2$] with H$_4$L^{Me}

Achieving the successful double metallation of the anthracenyl macrocycle H_4L^A using [$U(BH_4)_3(THF)_2$] encouraged us to re-visit the *ortho*-phenyl macrocycle H_4L^{Me}. Again, reactions of **14** with the different alkali metal salts of H_4L^{Me} were investigated. Reaction of two equivalents of **14** with Na_4L^{Me} or K_4L^{Me} in THF solution formed mixtures containing multiple paramagnetic products. However the reaction with Li_4L^{Me} resulted in the formation of [$Li(THF)_4$][{$U(BH_4)$}$_2$(μ-BH_4)(L^{Me})] (**21**) and a small quantity of bright orange precipitate (Scheme 3.12). The ^{1}H NMR spectrum of **21** displays seven paramagnetically contact-shifted resonances corresponding to a symmetric ligand environment with desymmetrised *meso* methyl groups and a broad resonance at 63 ppm ($W_{½}$ = 702 Hz) which

is assigned to the terminal BH_4^- ligands. In the ^{11}B NMR spectrum the bridging BH_4^- appears at 325 ppm while the terminal BH_4^- ligands have a chemical shift of 212 ppm.

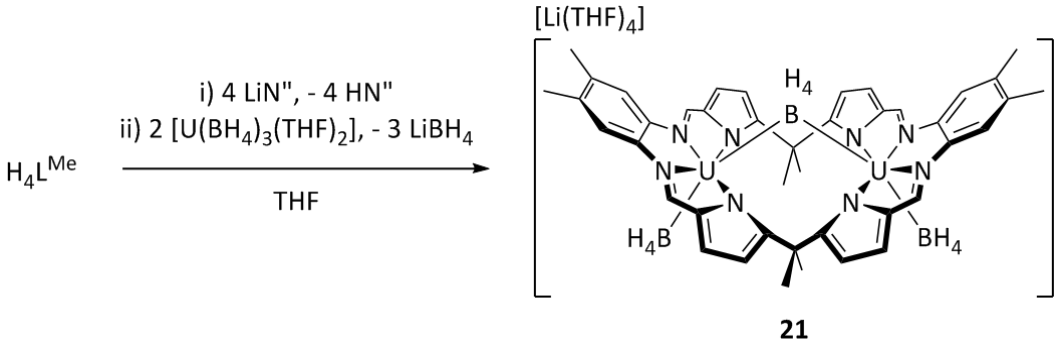

21

Scheme 3.12 Synthesis of **21**.

21 may be isolated as dark brown crystals in 24 % yield from the filtered reaction mixture stored at −30 °C. The somewhat mediocre isolated yield is attributed partly to the concomitant formation of the insoluble orange material but also to the fact that the THF solution of **21** can only be concentrated to a certain degree before an oily intractable mixture is formed, likely due to the presence of three equivalents of $LiBH_4$ in solution. The composition of the insoluble orange material is unknown; it could not be dissolved in d_5-pyridine for NMR spectroscopic analysis. On account of its poor solubility, it is suggested that the orange material may be polymeric. Its structure may be similar to that previously proposed for the oligomeric material of composition $[\{U(BH_4)\}_2(L^{Et})]$ obtained by reaction of $[\{U(I)\}_2(L^{Et})]$ with KBH_4.[50]

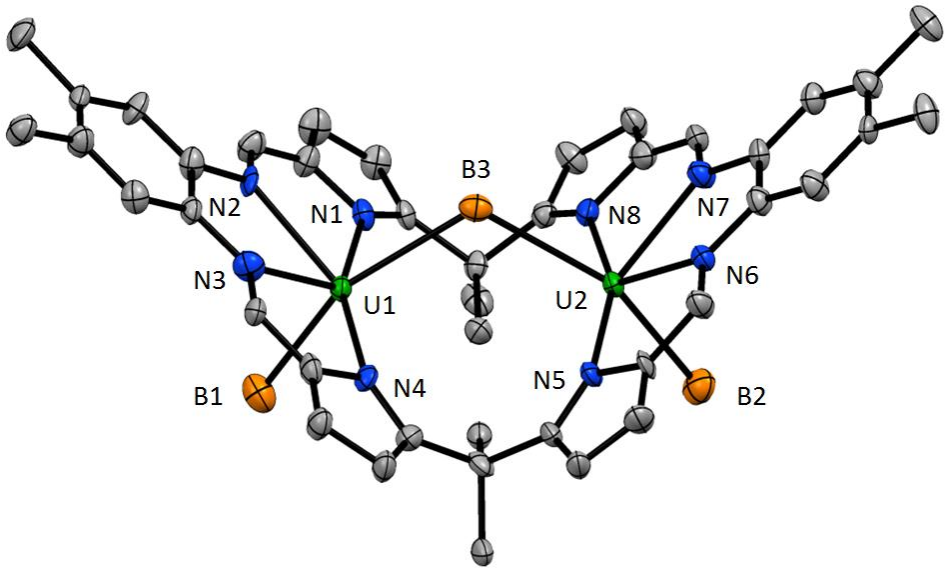

Figure 3.15 Solid state structure of the anionic portion of **21**. Thermal ellipsoids are drawn at 50 % probability. Lattice solvent and H atoms are omitted.

Table 3.6 Selected bond distances (Å) and angles (°) for **21**.

U1···U2	4.7884(3)	U2···B3	2.911(7)
mean U-N_{im}	2.50	U2···B2	2.640(9)
mean U-N_{pyr}	2.58	U1-B3-U2	110.5(3)
U1···B1	2.630(9)	B1-U1-B3	158.7(3)
U1···B3	2.915(7)	B2-U2-B3	158.6(3)

Single crystals of **21** suitable for X-ray diffraction analysis were grown by slow cooling a saturated THF solution from 70 °C to room temperature. The structure (Figure 3.15) reveals that the complex does not adopt the classic Pacman geometry where the *ortho*-phenyl rings of the macrocycle act as hinges, but instead the ligand flexes at the *meso* carbons, adopting a bowl-shaped geometry.[67] Each U(III) ion is pseudo-octahedral and bound in the equatorial plane to the two *ortho* imine nitrogens of one aryl ring of the macrocycle and to the two adjacent pyrrolide nitrogens, whilst two BH_4^- ligands, one terminal (B1/B2) and one bridging (B3), occupy the axial sites. The mean U-N(imine) distance of 2.50 Å is shorter than the mean U-N(pyrrolide) distance of 2.58 Å. This is the opposite of what would be expected on the grounds of electrostatic interaction and is also the reverse of what is generally observed in Pacman geometry complexes; in **18** the mean U-N(pyrrolide) bond length of 2.49 Å is shorter than the mean U-N(imine) bond length of 2.62 Å. Therefore it is concluded that the observed U-N distances are imposed by the bowl conformation of the ligand.

18 **21**

Figure 3.16 Diagram of the {U-(μ-BH_4)-U} cores of **18** and **21** showing the different hydride bridging modes.

The {BH_4-U-(μ-BH_4)-U-BH_4} core of **21** is significantly bent. The bridging angle U1-B3-U2 is 110.5(3) ° and the {BH_4-U-(μ-BH_4)} units also deviate from linearity with B-U-B angles of 158.7(3) ° and 158.6(3) °. The BH_4^- protons could not be located crystallographically but the U1···B1 and U2···B2 distances of 2.630(9) Å and 2.640(9) Å, respectively, are consistent with {(μ-H)$_3$BH} binding modes for the *exo* BH_4^- ligands, B1 and B2.[22] The *endo* BH_4^- protons bridge the two metal centres with longer U1/2···B3 separations of 2.915(7) Å and 2.911(7) Å. These distances are consistent with a {(μ-H)$_2$BH(μ-H)} interaction averaged over the two U(III) centres by rotation (Figure 3.16, right). By adopting the bowl conformation, the U1···B3···U2 interaction is optimized since the two U(III) cations can achieve greater separation (U1···U2 = 4.7884(3) Å) than is seen in

archetypal Pacman complexes of this ligand (M···M range: 3.1 – 4.2 Å).[68] The increased U1···U2 separation enables a more obtuse bridging angle at B3, approaching the optimum linear geometry observed in **18**. It has also been observed that larger metal cations favour adoption of the bowl conformation rather than the Pacman geometry (see 1.3.3).[69]

Isolated **21** cannot be re-dissolved in THF unless a suitable reagent is added (see 3.4.3). Dissolution of the complex in pyridine results in decomposition. This is in contrast to **18**, which simply forms the pyridine solvate $\mathbf{18_{py}}$ upon dissolution in pyridine by displacement of the THF ligands. However there is no accessible site for solvent to co-ordinate to the U(III) centres in **21** due to the bowl conformation of the ligand. The co-ordination numbers of the U(III) cations in **18** and **21** are 7 and 6 respectively. The lack of extra co-ordinated solvent molecules in **21** and the lengthened U-N(pyrrolide) interactions must destabilise the complex to such a degree that it is vulnerable to decomposition upon addition of pyridine.

Complexes **18** and **21** are highly unusual. Firstly, they are only the second and third structurally characterised examples of binuclear U(III)/U(III) complexes of a single ligand, the first being $[U_2I_4(L')]$ (**3AG**).[49] Furthermore **18** and **21** are rare examples of complex U(III) co-ordination compounds bearing ancillary BH_4^- ligands. Until this point, the only structurally characterised U(III) borohydride compounds were complexes of $U(BH_4)_3$ with various neutral donors such as $[U(BH_4)_3(THF)_3]$,[21] $[U(BH_4)_3(dmpe)_2]$[22] and $[U(BH_4)_3(C_6Me_6)]$.[17] The only exception as far as we are aware is the mixed valence U(III)/U(IV) organometallic salt $[Na(THF)_6][U(Cp^*)(BH_4)_3]_2$ which was formed by consecutive reaction of UCl_4 with excess NaH, 3 equivalents of $NaBH_4$ and $[Th(Cp^*)_2(PPh_2)_2]$, a somewhat convoluted reaction pathway.[70] Finally, while the solid state structures of $U^{IV}(BH_4)_4$ are oligomeric with bridging BH_4^- groups,[71,72] **18** and **21** are the first compounds to contain the $\{U^{III}\text{-}(\mu\text{-}BH_4)\text{-}U^{III}\}$ moiety. Indeed, the ability of BH_4^- to effectively bridge two U(III) centres in the intermetallic cleft appears to provide important stabilisation to these binuclear complexes and may explain their improved stability compared to the iodide complex **12**.

3.4 Reactivity of uranium(III) Pacman complexes

The isolation of compounds **18** and **21** presents a unique opportunity to explore both the reactivity of two U(III) cations bound in proximity within a macrocyclic framework and also the reactivity of BH_4^- ligands in terminal and bridging co-ordination sites at U(III). In particular, in order to investigate the co-operative activation potential of the U(III) centres it would be desirable to remove the bridging BH_4^- ligand to leave a vacant co-ordination site for substrate activation between the two U(III) centres.

3.4.1 Ligand substitution: synthesis of [{U(OAr)}$_2$(*endo*-BH$_4$K)(L^A)]

Various ligand substitution reactions of **18** or crude **19** with amide, alkoxide, aryloxide, cyclopentadienyl, alkyl and allyl alkali metal salts were investigated on a small scale in d_8-THF solution (see 4.3.11). The only reactions which appeared promising by ^{1}H NMR spectroscopy were those between **18** and two equivalents of the aryloxides MOAr where M = K, Na and Ar = 2,4,6-$C_6H_2(^tBu)_3$. The ^{1}H NMR spectra of both reaction mixtures were very similar and each displayed a new set of very broad, paramagnetically shifted resonances of low intensity, which nevertheless appeared to correspond to a single, symmetric Pacman ligand environment. A large quantity of dark green crystals formed over 4 h in the **18**/KOAr reaction mixture. Analysis of these by X-ray diffraction revealed their composition to be [{U(OAr)}$_2$(*endo*-BH$_4$K)(L^A)(THF)$_2$] (**22**) in which the two *exo* BH_4^- ligands have been exchanged for bulky aryloxides and the Na^+ cation of **18** has been exchanged for a K^+ cation which binds within the macrocyclic cleft. A few single crystals also formed in the **18**/NaOAr reaction mixture, but only after standing for two weeks. These were found to be the analogous Na^+ containing product [{U(OAr)}$_2$(*endo*-BH$_4$Na)(L^A)(THF)$_2$] (**23**) in which, in contrast to **18**, the Na^+ cation is also located within the macrocyclic cleft (Scheme 3.13). Interestingly, no reaction occurred between **18** and two equivalents of LiOAr and the reaction between two equivalents of KOAr and **21** in d_8-THF resulted in the formation of multiple paramagnetic products and was not investigated further.

On a preparative scale, reaction of **18** with KOAr in THF allows crystalline **22** to be isolated in 59 % yield. A preparative synthesis of **23** was not attempted due to its comparatively slow crystallisation in the NMR scale reaction. Isolated, crystalline **22** is insoluble in THF and pyridine but partially soluble in toluene and hot benzene. The ^{1}H NMR spectrum of **22** in C_6D_6 is sharper than that of the crude *in situ* formed product in d_8-THF and paramagentically shifted resonances corresponding to a symmetric macrocycle and two equivalent aryloxide ligands are present. One resonance that integrates to 18H is observed at

4.1 ppm for the two *para*-^{t}Bu groups and one of integral 36H at −0.1 ppm for the four *ortho*-^{t}Bu groups of the two aryloxides. The resonance corresponding to the four equivalent *meta* protons of the aryloxides cannot be distinguished from the macrocycle resonances of equal integral. A single broad resonance appears in the ^{11}B NMR spectrum at 188 ppm.

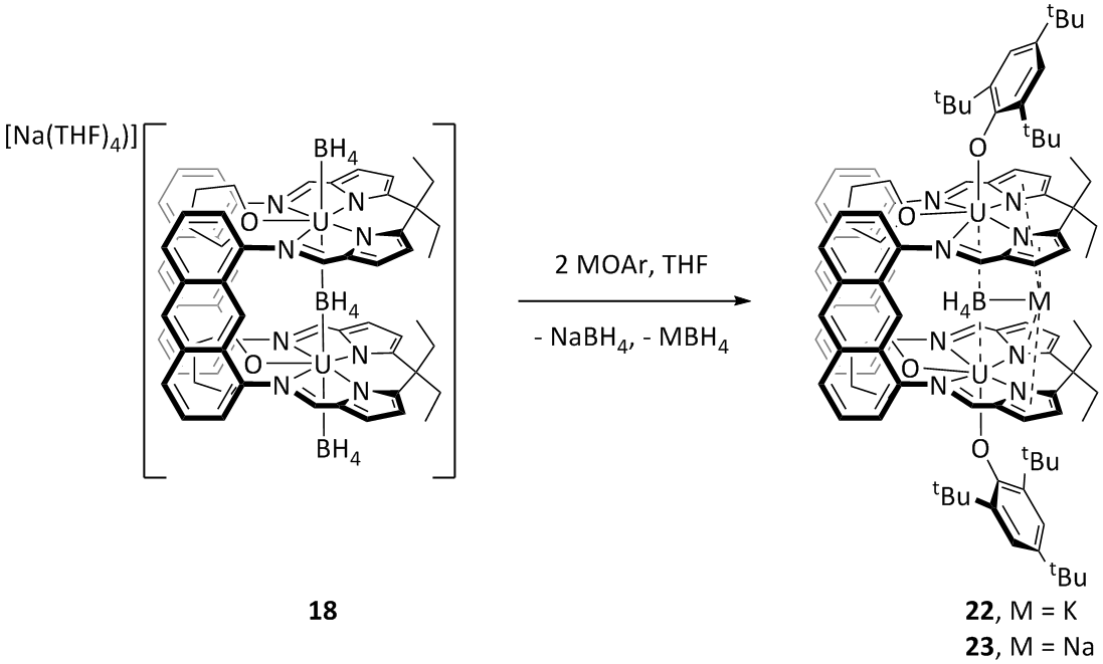

Scheme 3.13 Synthesis of the *exo* ligand exchange products **22** and **23.**

22 crystallises in the orthorhombic space group *Pnma*. The asymmetric unit consists of half the macrocycle; the other half is generated by reflection through the horizontal mirror plane which passes through B1 and K1, perpendicular to the planes of the anthracene hinges. **23** crystallises in the monoclinic space group *C2/c*. Again the asymmetric unit consists of half the macrocycle but this time the other half is generated by rotation about the C_2 axis which passes through B1 and the centre of the Na1/Na1′ positions (Figure 3.17).

The co-ordination environments of the U(III) ions in **22** and **23** are very similar (Table 3.7). In both structures, five equatorial donors are provided by the four nitrogens of the macrocycle and one molecule of THF solvent, which sits between the macrocycle hinges. The aryloxide ligand occupies the *exo* axial co-ordination site and a BH_4^- group (hydrogens not located) sits within the macrocyclic cleft between the two U(III) centres. The geometry of each U(III) centre can be described as either distorted pentagonal bipyramidal or pentagonal based pyramidal depending on whether the U1⋯B1 interaction is considered a true bonding interaction or not.

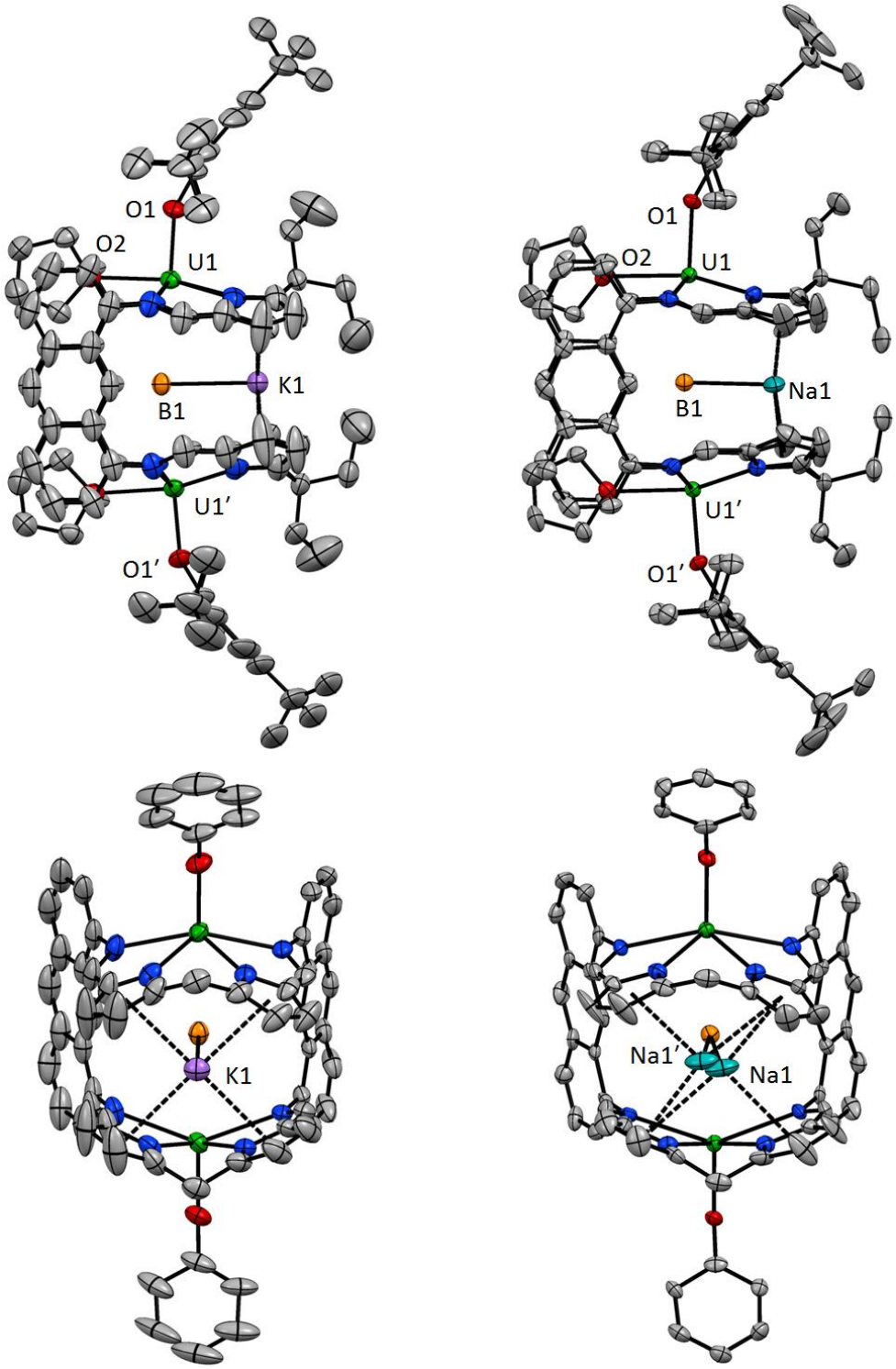

Figure 3.17 Solid state structures of **22** (left) and **23** (right), showing side view (top) and view into the jaws of the macrocycle (bottom). The major orientation of the ^{t}Bu groups in **22** is shown and the symmetry generated cation Na1′ is only shown in the bottom view of **23**. The *meso* ethyl groups, aryloxide substituents and THF molecules have been removed from the bottom structures for clarity. Thermal ellipsoids are drawn at 50 % probability. H atoms and lattice solvent are omitted.

Table 3.7 Comparison of selected distances (Å) and angles (°) in the structures of **22** and **23**.

		22	**23**
1.	U1⋯U1′	6.5881(3)	6.5265(7)
2.	mean U1-N_{im}	2.65	2.65
3.	mean U1-N_{pyr}	2.50	2.51
4.	U1-N_4 plane	+0.70	+0.69
5.	U1-O1	2.231(5)	2.245(6)
6.	U1⋯B1	3.312(1)	3.269(1)
7.	U1-O2	2.554(5)	2.592(6)
8.	B1⋯M1	3.036(11)	2.747(2)
9.	M1-[pyr]centroid	3.154(2), 3.153(2)	2.85(4), 3.04(2), 3.08(4), 3.61(2)
10.	U1-B1-U1′	168.2(4)	173.0(6)
11.	O1-U1-B1	178.3(2)	177.6(1)
12.	U1-O1-C_{ipso}	154.0(5)	153.3(6)

The aryloxide rings are perpendicular to the anthracenyl hinges of the macrocycle and the bend at the O atom (U1-O1-C_{ipso} = 154.0(5) ° (**22**), 153.3(6) ° (**23**)) orients the *ortho*-^{t}Bu groups away from the THF donor. The U(III) ions are considerably displaced out of the macrocycle N_4 donor planes, out of the intermetallic cleft, by 0.70 Å in **22** and 0.69 Å in **23**, and the sum of the four N-U-N angles in the two structures is 337.9(8) ° and 338.1(8) ° respectively. The separation of the bulky aryloxide ligand from the N_4 plane of the macrocycle is imposed by sterics. Therefore the displacement of the U(III) centres out of the N_4 plane is a compromise between optimised U-OAr and U-N bond lengths. The resulting mean U-N(imine) separations of 2.65 Å in both complexes and the mean U-N(pyrrolide) separations of 2.50 Å (**22**) and 2.51 Å (**23**) are lengthened compared to those observed in **18** (2.62 Å and 2.49 Å). The U1-O1 bond lengths in **22** and **23** are 2.231(5) Å and 2.245(6) Å respectively. These are longer than the U^{III}-OAr distances in [U{O(2,6-C_6H_3(^{i}Pr)$_2$}$_3$] [73] and [U{O(2,6-C_6H_3(^{t}Bu)$_2$}$_3$] [27] which range from 2.149(4) to 2.214(7) Å but similar to the mean U-OAr distance of 2.22 Å observed by Meyer and co-workers in the series of constrained aryloxide tacn complexes [U{tacn(OAr^R)$_3$}].[74,75]

The main difference between the structures of **22** and **23** is the binding mode of the K^+ and Na^+ cations within the cleft. The larger K^+ ion is sandwiched symmetrically between all four pyrrolide rings (Figure 3.17, bottom left) with K1-[pyr]centroid separations of 3.154(2) Å and 3.153(2) Å. By contrast the smaller Na^+ ion is disordered over two sites about the crystallographic C_2 axis, presumably because it cannot effectively bridge all four pyrrolides. This results in three short Na1-[pyr]centroid distances of 2.85(4), 3.04(2) and 3.08(4) Å and one long, non-bonding separation of 3.61(2) Å. K^+ is clearly a better size match for the Pacman macrocyclic cleft than Na^+. On the basis of the M1⋯B1 separations,

the M···BH_4 interactions are true bonds. Reported terminal K···BH_4 separations range from 2.947(3) [76] to 3.091(4) [77] Å with a mean value of 3.00 Å, while terminal Na···BH_4 separations range from 2.600(6) [78] to 2.841(2) [79] Å with a mean value of 2.68 Å. The K1···B1 (3.036(11) Å) and Na1···B1 (2.747(2) Å) separations in **22** and **23** lie within these ranges, close to the mean values. The elongated K1-B1 distance means that the BH_4^- group sits further back into the molecular cleft in **22** and the U1-B1-U1′ angle in **22** (168.2(4) °) is more acute than that in **23** (173.0(6) °).

The effect of the out-of-cleft distortion of the U(III) centres is a marked lengthening of both the U···U and the U···(*endo*-BH_4) separations. U1···U1′ is 6.5881(3) Å in **22** and 6.5265(7) Å in **23** compared to 5.9243(3) Å in **18**. U1-B1 is 3.312(1) Å in **22** and 3.269(1) in **23** compared to 2.977(7) Å and 2.949(7) Å in **18**. The U-B distances in **18** are the longest observed for any uranium borohydride complex, with the next longest being 2.927(7) Å in [U(BH_4)L′] (L′ = *trans*-calix[2]benzene[2]pyrrolide).[80] This raises the question of whether there is a bond between the U(III) ions and the *endo* BH_4^- group in **22** and **23** or whether the BH_4^- group is held within the cleft by association with its M^+ counterion. The observed ^{11}B NMR shift of the *endo* BH_4^- group in **22** is 188 ppm which is considerably contact shifted from that of free KBH_4 (−40 ppm) indicating that there is some electronic overlap between the U(III) centres and the BH_4^- group. It is likely that in-cleft cation binding in **22** and **23** is necessary to stabilise very weak, long range U-(BH_4)-U interactions.

3.4.2 Further reactivity of [{U(OAr)}$_2$(*endo*-BH_4K)(L^A)]

3.4.2.1 With 18-crown-6

It was hoped that the weakening of the U-(*endo*-BH_4)-U interaction observed in **22** could be exploited to remove the central BH_4^- group to leave two proximate U(III) centres ideally aligned for small molecule activation. 18-crown-6 has already been shown to effect the abstraction of the in-cleft bound K^+ cation from **19**. Therefore excess 18-crown-6 was added to a suspension of **22** in C_6D_6 to probe the fate of the *endo*-BH_4^- group following removal of the stabilising K^+ counterion.

The ^{11}B NMR spectrum of the resulting mixture did not contain any resonances, indicating that abstraction of the K^+ cation from **22** by 18-crown-6 causes the *endo* BH_4^- ligand to be released as insoluble [K(18-crown-6)][BH_4]. The ^1H NMR spectrum displayed contact-shifted resonances assignable to a new symmetric Pacman product (**24**). The resonances were considerably sharper than those in the spectrum of **22** due to the improved solubility of **24** in benzene. Five contact-shifted signals attributable to two aryloxide ligands

were observed in the ratio 18:18:18:2:2, four of which were significantly broader than the other resonances in the spectrum (Figure 3.18, highlighted resonances). This differs from the starting material **22**, which displayed only three aryloxide resonances in the ratio 36:18:4. The observed NMR data is consistent with a structure for **24** in which the *exo* aryloxide ligands have rotated about the U-O and O-C_{ipso} bonds so that the aryl rings are now coplanar with the anthracenyl hinges of the macrocycle (Scheme 3.14). In such a structure the two *ortho*-^{t}Bu groups (orange resonances) of each macrocycle are inequivalent since one is oriented between the macrocycle hinges while the other points towards the *meso* ethyl groups. The two *meta* protons (green resonances) of the aryloxides are similarly desymmetrised but the two pockets of the macrocycle remain equivalent, as do both *para*-^{t}Bu groups of the two aryloxides. The broadening of the *ortho*-^{t}Bu and *meta*-H resonances implies that they are in fluxional exchange on the NMR timescale by rotation of the rings about the O-C_{ipso} bonds. For the aryloxides to adopt this binding geometry, it is expected that the THF ligands which occupied the fifth equatorial co-ordination sites in the starting material **22** must have dissociated (see 3.4.2.2).

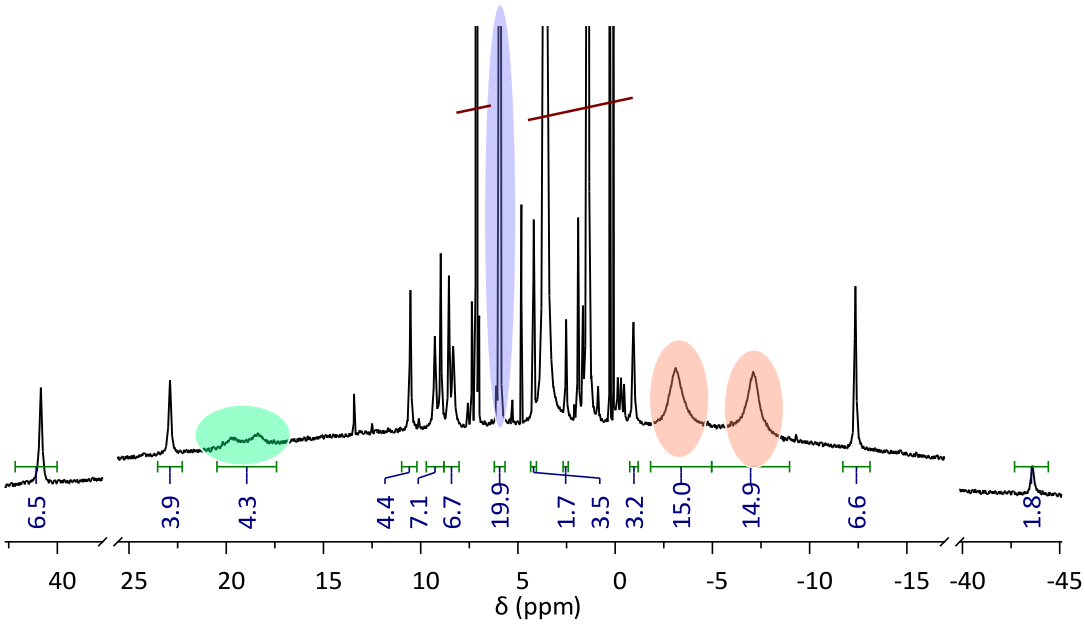

Figure 3.18 ^{1}H NMR spectrum of **24** formed by the reaction of **22** with excess 18-crown-6 in C_6D_6. The resonances of the aryloxide ligands are highlighted. Resonances assigned to residual *protio* solvent, THF, excess 18-crown-6 and trace HN" are scored through.

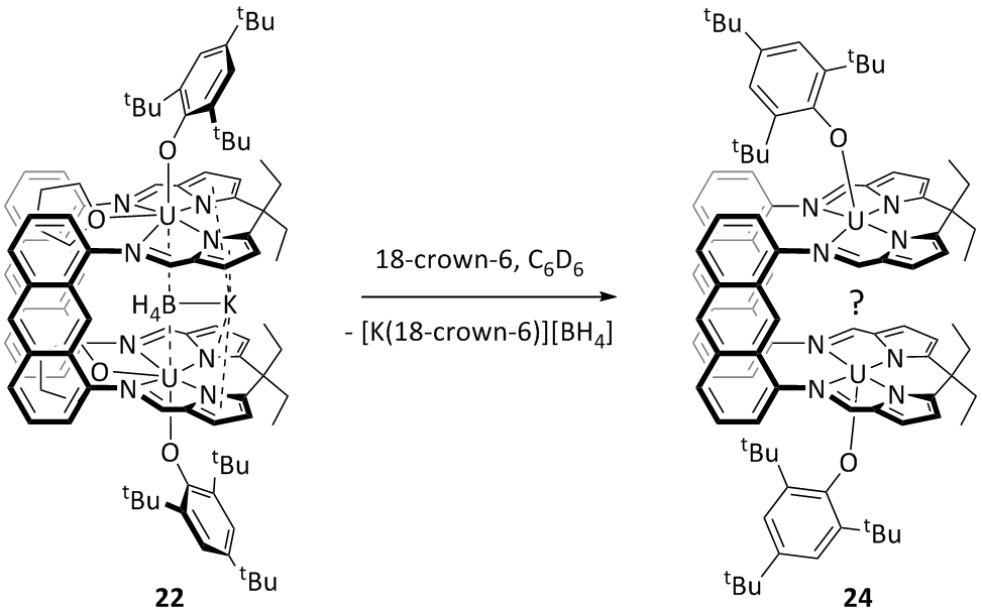

Scheme 3.14 Suggested reaction of **22** with 18-crown-6.

Single crystals of **24** were not obtained and neither was bulk material successfully isolated, preventing compositional or structural analysis of the complex. Therefore, it is not known whether any species is bound within the intermetallic cleft in place of KBH_4. As discussed in 3.1.2.1, co-operative N_2 binding by U(III) aryloxides has been demonstrated. Since the reaction between **22** and 18-crown-6 was carried out under a nitrogen atmosphere, it is possible that N_2 may be bound between the U(III) centres in **24**. To date, the only dinitrogen binding mode observed in binuclear uranium complexes is the side-on bridging mode. The side-on bridging mode necessitates a shorter M···M separation than the end-on bridging mode commonly observed in transition metal complexes. In the structurally characterised binuclear uranium dinitrogen complexes, U···U separations range from 4.572(4) Å in $[\{U(OSiMes_3)_3\}_2(\mu\text{-}\eta^2\text{:}\eta^2\text{-}N_2)]$ [81] to 4.7035(4) Å in $[\{U(NN'_3)\}_2(\mu\text{-}\eta^2\text{:}\eta^2\text{-}N_2)]$ (**3H**).[25] If the U···U separation observed in **22** (6.5881(3) Å) were maintained in **24** then the U(III) centres would be too distant to bind N_2 side-on between them. However, one attribute of the Pacman macrocycles is their flexibility, which leads to a wide range of bite angles and M···M distances in their complexes. The shortest U···U separation observed in a binuclear uranium complex of $(L^A)^{4-}$ is 4.1927(3) Å (see 3.5.1) while the shortest U···U separation measured in a binuclear uranium complex of $(L^A)^{4-}$ with *exo* aryloxide ligands is 5.1571(5) Å (see 3.4.2.2). Therefore side-on dinitrogen binding may be geometrically feasible in **24**. However it should be noted that all previously reported uranium dinitrogen complexes were prepared with the exclusion of co-ordinating solvents. **24** is synthesised in benzene but two equivalents of THF are present in **22** so it is also possible that THF may occupy the

intermetallic cleft. Unfortunately, attempts to carry out the reaction between **22** and 18-crown-6 in the absence of nitrogen to probe whether N_2 is bound in **24** were unsuccessful due to equipment malfunction.

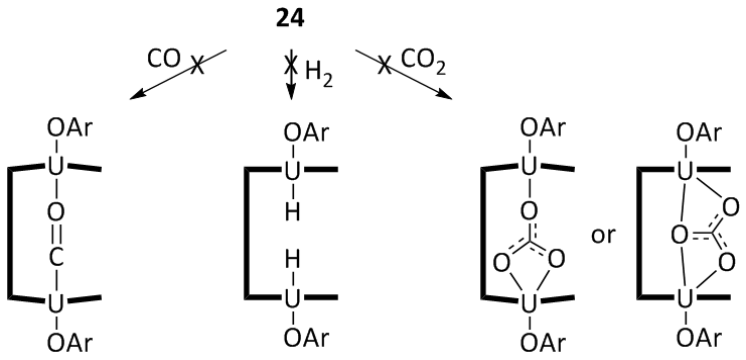

Scheme 3.15 *In situ* reactions attempted with **24** showing target products. Conditions: 1.0 bar gas pressure, C_6D_6 solvent.

Regardless of whether N_2, THF or no molecule occupies the intermetallic cleft in **24**, it is expected to be a reactive complex. Since **24** could not be isolated it was formed *in situ* in an NMR tube and its reactivities towards carbon monoxide, dihydrogen and carbon dioxide were investigated. Scheme 3.15 shows the target products that it was hoped might be formed in each of these reactions. The binuclear $(C_nO_n)^{2-}$ bridged U(IV)/U(IV) complexes formed by the reductive coupling of CO (see 3.1.2.2) contain U···U separations of 7.2214(2) Å [34] or longer which probably could not be supported by the Pacman framework. However the end-on CO-bridged binuclear U(III)/U(IV) complex reported by the Meyer group (**3Q**) features a U···U separation of 6.3868(4) Å.[33] This binding motif could likely be incorporated between the U(III) centres of the Pacman complex and might be expected to be favoured by the pre-organisation of the U(III) ions at an appropriate distance. Unfortunately **24** was unreactive towards CO.

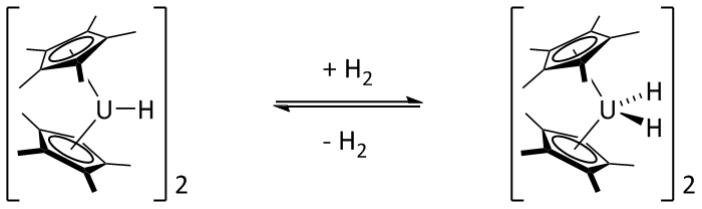

Scheme 3.16 Reversible addition of dihydrogen across a U(III)/U(III) dimer.[82]

Reversible oxidative addition of dihydrogen across two U(III) centres to form two U(IV) hydrides was demonstrated by the Marks group who reported that an equilibrium is established between the $[Cp^*_2U^{III}(\mu\text{-}H)]_2$ and $[Cp^*_2U^{IV}H(\mu\text{-}H)]_2$ dimers, its position depending on the applied H_2 pressure (Scheme 3.16).[82] Both equilibrium components have

been isolated and structurally characterised by Evans and co-workers.[83] Complex **24** does not exhibit similar chemistry and is unreactive towards H_2.

The Cloke,[41] Meyer,[42,43] and Mazzanti groups [44] have all reported the activation of CO_2 between two U(III) centres to form bridging carbonate complexes (see 3.1.2.3). Two distinct carbonate bridging modes have been observed in these complexes: μ-κ^1(O):κ^2(O′,O″) and μ-κ^2(O,O′):κ^2(O,O″), which result in approximate U···U separations of 6.28 Å and 5.26 Å, respectively. The flexible Pacman macrocycle could probably allow intermetallic carbonate incorporation in either bridging mode. Addition of CO_2 to a dark green benzene solution of **24** resulted in an immediate colour change to pale orange. The ^{1}H NMR spectrum of the mixture displayed several very low intensity, paramagnetically contact-shifted resonances which could not be assigned to a single product. This indicates that decomposition or multiple product formation occurred, rather than selective formation of a single, well-defined oxidised species.

3.4.2.2 With S_8: synthesis of [{U(OAr)}$_2$(μ-S_2)(L^A)]

The reactivity of **22** towards small molecules was also investigated. It was reasoned that since the KBH_4 unit is only weakly bound within the macrocyclic cleft in **22**, addition of a suitable substrate could result in KBH_4 displacement, negating the requirement for additional 18-crown-6. This indeed proved to be the case. Thus addition of excess S_8 to a suspension of **22** in C_6D_6 resulted in immediate formation of a pale orange solution and a pale yellow precipitate. The ^{1}H NMR spectrum of the mixture displayed contact-shifted resonances corresponding to a single symmetric Pacman environment and two equivalent aryloxide ligands. As was observed in the NMR spectrum of **24**, the aryloxide protons appear as 5 distinct resonances in an 18:18:18:2:2 ratio, implying that the aryloxide rings are coplanar with the macrocycle anthracene hinges. The two *ortho*-^{t}Bu signals at 29.51 and −31.72 ppm are slightly broadened compared to the *para*-^{t}Bu resonance at 15.09 ppm. However, the *meta* proton signals are not significantly broadened making it impossible to distinguish them from the macrocycle resonances of the same intensity. No resonances were observed in the ^{11}B NMR spectrum indicating that displacement of KBH_4 from the cleft and its precipitation from solution had occurred. Addition of hexane to the filtered reaction mixture resulted in the deposition of orange crystals of [{U(OAr)}$_2$(μ-η^2:η^2-S_2)(L^A)] (**25**) in 43 % yield (Scheme 3.17). Both uranium centres in complex **25** have been oxidised to U(IV) and the intermetallic cleft is occupied by a bridging persulphide ion, $(S_2)^{2-}$.

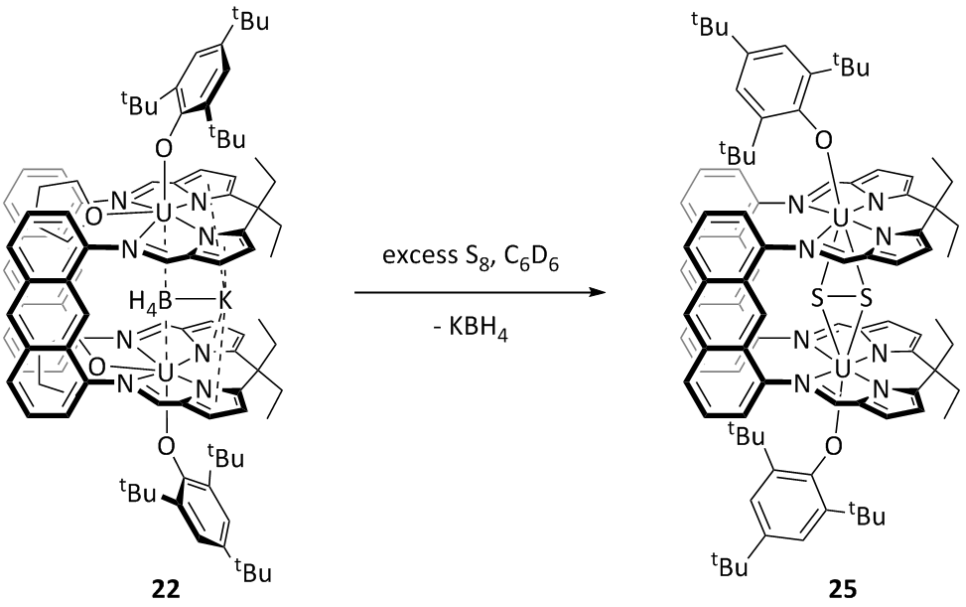

Scheme 3.17 Oxidation of **22** with S_8 to the U(IV)/U(IV) persulphide complex **25**.

Complex **25** crystallises in the monoclinic space group *C2/c*. The asymmetric unit consists of half the macrocycle and the other half is generated by rotation about the crystallographic C_2 axis. In the solid state the U(IV) ions in **25** are seven co-ordinate, binding to the four N donors of the macrocycle, the *exo* aryloxide ligand and both S atoms of the *endo* bridging persulphide ion (Figure 3.19). The solid state structure of **25** confirms that, in contrast to **22**, the aryloxide rings are indeed approximately coplanar with the anthracene hinges of the macrocycle with one *ortho*-^{t}Bu group on each ring sitting between the hinges. Also, the two THF molecules which were bound to the U centres in the equatorial sites in **22** have dissociated during formation of **25**. The U1-O1 bond length in **25** is 2.091(3) Å, which is reduced from 2.231(5) Å in **22** and is consistent with the oxidation of the U(III) centres to U(IV). The angle at the O atom of the aryloxides in **25** (U1-O1-C_{ipso} = 169.0(3) °) is less acute than that observed in **22** (154.0(5) °). The mean U1-N(pyrrolide) distance has contracted from 2.50 Å in **22** to 2.41 Å in **25**, though the difference in the mean U1-N(imine) distances is less marked (2.65 Å in **22** *vs* 2.63 Å in **25**).

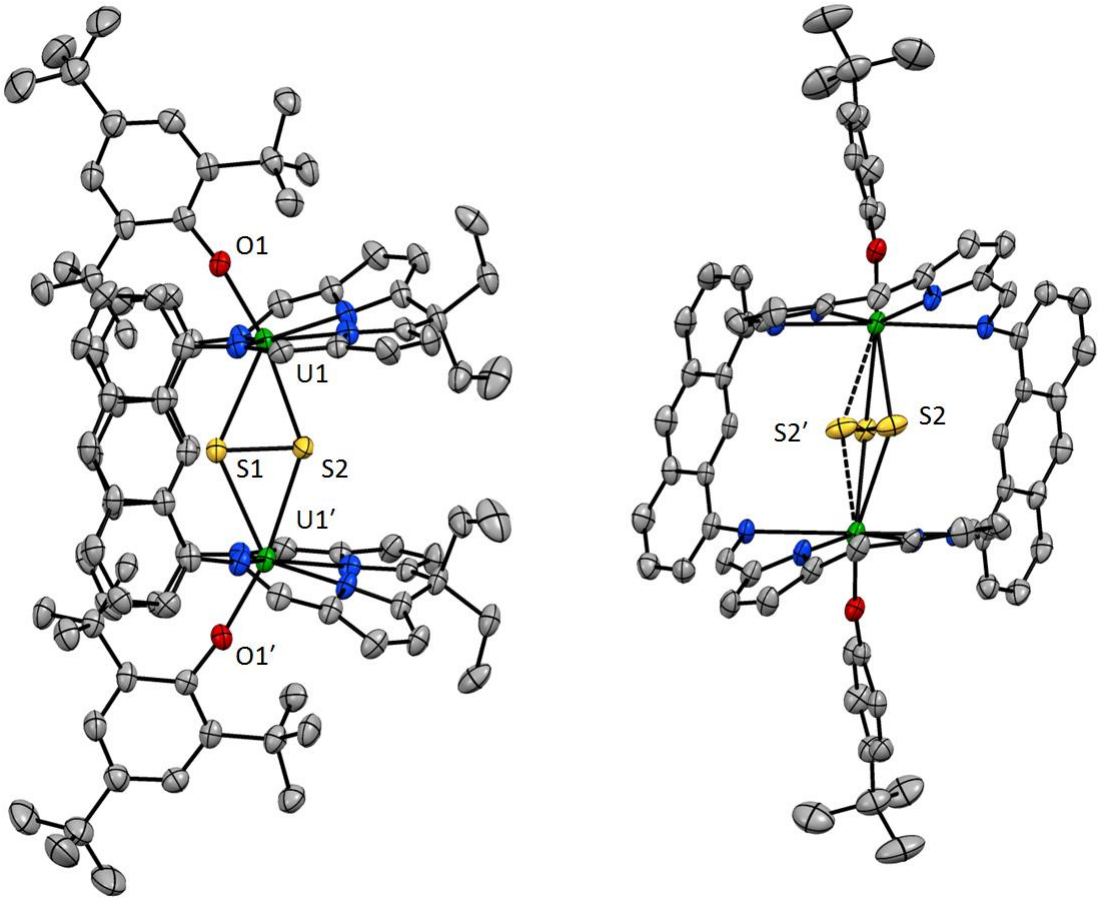

Figure 3.19 Solid state structure of **25** showing side view (left) and view into jaws of macrocycle (right). The alternative, symmetry generated S2 position, S2′ (dashed bonds), is only show in the right hand structure and the macrocycle *meso* ethyl groups and aryloxide *ortho* ^{t}Bu groups have been removed from this figure for clarity. Thermal ellipsoids are drawn at 50 % probability. H atoms and lattice solvent are omitted.

Table 3.8 Selected bond distances (Å) and angles (°) for **25**.

U1···U1′	5.1571(5)	O1-U1-S1	125.7(1)
mean U-N_{im}	2.63	O1-U1-S2	166.6(1)
mean U-N_{pyr}	2.41	U1-S1-U1′	131.98(7)
U1-N_4 plane	−0.07	U1-S2-U1′	135.0(1)
U1-O1	2.091(3)	S1-S2-U1	70.40(8)
U1-S1	2.8229(8)	S2-S1-U1	64.62(8)
U1-S2	2.707(3)	U1-(S_2)cent-U1′	165.4
S1-S2	2.118(3)	U1-O1-C_{ipso}	169.0(3)

The $(S_2)^{2-}$ unit is equidistant from the two U(IV) centres (as determined by the crystal symmetry) but the U1-S1 bond length of 2.8229(8) Å is longer than the U1-S2 length of 2.707(3). S2 was found to be disordered over two sites related by rotation about the C_2 axis and the occupancy of each site was fixed as 0.5. U1, U1′, S1 and S2 are not coplanar but instead the $\{U_2S_2\}$ unit forms a bent diamond with a U1-(S_2)centroid-U1′ angle of 165.4 °.

Bridging persulphide uranium complexes are rare. The only two examples have been reported in the last two years and both feature a persulphide ion bridging two U(IV) centres. Hayton and co-workers reported the structure of [{U(N″)$_3$}(μ-η^2:η^2-S$_2$)] (**3AA**) [45] whilst the Mazzanti group crystallised [{U((SiMe$_2$NPh)$_3$tacn)}$_2$(μ-η^2:η^2-S$_2$)] (**3AD**).[46] The S1-S2 bond length in **25** of 2.118(3) Å is slightly longer than those in the other published U(IV) persulphides (Table 3.9, entry 1.) and the mean U-S separation is slightly shorter (entry 2.). The diamond {U$_2$S$_2$} unit in **25** is the most bent, with the U-(S$_2$)centroid-U angle 175.8 ° in **3AA** while the {U$_2$S$_2$} unit is planar in **3AD** (entry 3.) Associated with this reduction in bend is an increase in the U···U separation from 5.1571(5) Å in **25** to 5.3638(7) Å in **3AD** (entry 4.). However the most significant difference between **25** and the other U(IV) persulphide complexes is that **25** is formed solely and selectively by reaction of excess S$_8$ with **22** whereas **3AA** is a by-product which cannot be rationally synthesised and **3AD** is one of a number of products formed by reduction of the U(V) persulphide [U((SiMe$_2$NPh)$_3$tacn)(η^2-S$_2$)] (**3AC**) with PPh$_3$. The Meyer group have reported the U(IV)/U(IV) bridged perselenide complex [{U(N(OAr)$_3$)}$_2$(μ-η^2:η^2-Se$_2$)] but were unable to prepare the sulphur analogue.[47] Therefore **25** is the only U(IV)/U(IV) persulphide complex which may be reliably and rationally prepared from the corresponding U(III)/U(III) starting material.

Table 3.9 Comparison of selected structural parameters of **25** with binuclear U(IV) persulphide complexes form the literature.

		25	**3AA**	**3AD**
1.	*S-S (Å)*	2.118(3)	2.105(2)	2.105(5)
2.	*mean U-S (Å)*	2.76	2.80	2.88
3.	*U-(S$_2$)centroid-U (°)*	165.4	175.8	180
4.	*U···U (Å)*	5.1571(5)	5.3037(4)	5.3638(7)

3.4.2.3 With CS$_2$

Selective formation of a single Pacman product was observed in the oxidation of **22** with S$_8$ while multiple products resulted from the oxidation of **24** with CO$_2$. Therefore the reaction of CS$_2$, another sulphur-containing small molecule, with **22** was investigated in the hope that a well-controlled reaction would occur which might shed light upon the interaction of **22** and/or **24** with CO$_2$. Addition of excess CS$_2$ to a suspension of **22** in d_8-toluene resulted in a slow colour change from dark green to orange-brown over the course of 10 min and formation of orange precipitate. The ^{1}H NMR spectrum of this mixture indicated that a single asymmetric Pacman species was formed in which the two pockets of the macrocycle are inequivalent. The two aryloxide ligands are also inequivalent appearing as nine signals: five of intensity 9H corresponding to five of the six ^{t}Bu groups (the resonance of the sixth

group is assumed to be concealed by the solvent resonances) and four of intensity 1H corresponding to each *meta* proton. Again, it is deduced that the aryloxide rings are coplanar with the macrocycle hinges. No resonances are observed in the ^{11}B NMR spectrum. On the basis of this spectroscopic evidence it is suggested that the species formed initially on combination of **22** with CS_2 is [{U(OAr)}$_2$(μ-CS_2)(L^A)] (**26**) in which the carbon disulphide reagent has been reduced to a bent $(CS_2)^{2-}$ unit that binds asymmetrically between the two U(IV) centres, thus rendering the top and bottom macrocycle pockets and the two *exo* aryloxides non-equivalent (Scheme 3.18).

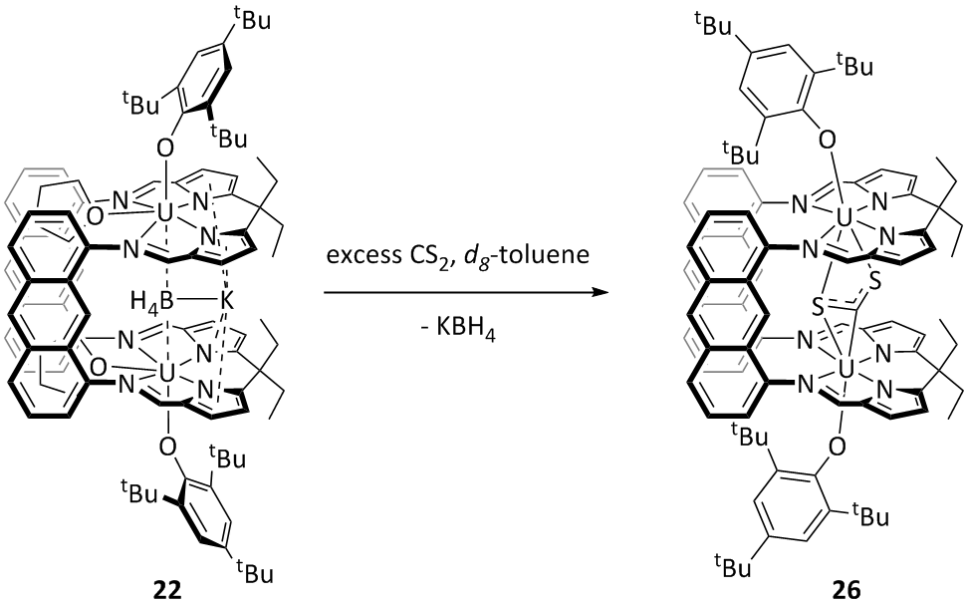

Scheme 3.18 Reaction of **22** with CS_2 to form the asymmetric, CS_2-bridged product **26**.

Carbon disulphide-bridged uranium complexes are rare but two examples have been characterised in the solid state. In 1986, Andersen and co-workers reported the structure of [{U(MeC_5H_4)$_3$}$_2$(μ-η^1(S):η^2(C,S)-CS_2)] (**3AM**) [84] while the Mazzanti group reported that of [{U(OSi(O^{t}Bu)$_3$)$_3$}$_2$(μ-η^2(C,S):η^2(S,S)-CS_2)] (**3AN**) in 2012 (Figure 3.20).[44] Both of these complexes feature reduced, bent $(CS_2)^{2-}$ ions bound asymmetrically between two U(IV) centres and were synthesised by reaction of the corresponding U(III) precursors with CS_2. The ^{1}H NMR spectra of **3AM** and **3AN** each display two distinct sets of signals for the cyclopentadienyl and siloxide ligands indicating that the asymmetric $(CS_2)^{2-}$ binding mode is preserved in solution and not averaged by fluxional processes. The different bridging geometries of the $(CS_2)^{2-}$ unit in **3AM** and **3AN** give rise to U···U separations of 6.396(1)Å and 5.4056(5)Å, respectively. On the basis of the U···U separation observed in **25** (5.1571(5) Å), the structure of which is very similar to that proposed for **26**, it is suggested that the

$(CS_2)^{2-}$ bridging mode in **26** is the same as that observed in **3AN**, namely {μ-η^2(C,S):η^2(S,S)-CS_2}.

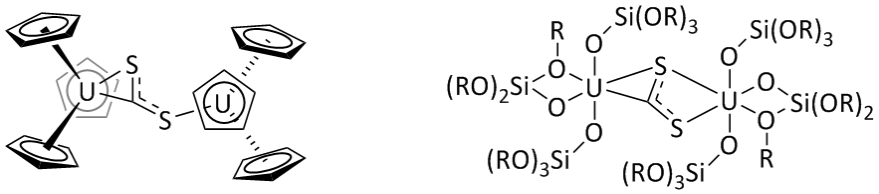

3AM **3AN**

Figure 3.20 Structurally characterised binuclear $(CS_2)^{2-}$ uranium complexes reported by the Andersen (left)[84] and Mazzanti (right)[44] groups. The Me substituents have been omitted from the C_5H_4Me rings in **3AM** for clarity. R = ^{t}Bu.

The toluene solution of **26** was filtered and hexane allowed to slowly vapour diffuse into the filtrate. Block-shaped orange crystals formed after five days. To our surprise X-ray diffraction analysis of the crystals revealed that they were not the asymmetric, $(CS_2)^{2-}$ bridged complex **26** but instead the symmetric, sulphide-bridged compound [{U(OAr)}$_2$(μ-S)(L^A)] (**27**). The co-ordination environment about the two U(IV) ions in **27** is distorted octahedral (Figure 3.21). The four N donors of the macrocycle occupy the equatorial plane and the *exo* aryloxide and *endo* bridging sulphide ligands occupy the axial sites. There is, however, a large deviation from idealised octahedral geometry; the angles between the *trans* axial ligands O1-U1-S1 and O2-U2-S2 are 143.2(2) ° and 140.1(2) °, respectively. The aryloxides are likely tilted back toward the hinges of the macrocycle to avoid unfavourable steric interactions between their *ortho*-^{t}Bu groups and the *exo meso* ethyl groups of the macrocycle. At 2.594(2) Å and 2.608(2) Å, the U-S bond lengths in **27** are reduced by *ca*. 0.16 Å compared to the mean U-S distance observed in the persulphide complex **25**. The geometry of the {U-(μ-S)-U} core in **27** is approaching linear (U1-S1-U2 is 172.0(1) °) and the U1···U2 separation is 5.1899(5) Å. Other mono-sulphide bridged complexes prepared to date include [{U(N″)$_3$}$_2$(μ-S)] (**3AA**),[45] [{U(OAr)$_3$}$_2$(μ-S)] (Ar = 2,6-C_6H_3(^{t}Bu)$_2$) [85] and [{U((^{Ad}ArO)$_3$N)(DME)}$_2$(μ-S)] (**3AE**).[48] In these compounds the U-S bond lengths range from 2.588(1) Å to 2.736(2) Å, the U···U separations vary from 5.176(3) Å to 5.4407(6) Å and the U-S-U angles range from 165.2(2) ° to 180 °. The structural parameters of the {U-(μ-S)-U} unit in **27** lie within these limits and so the confined environment of the Pacman macrocycle does not appear to cause unusual distortion.

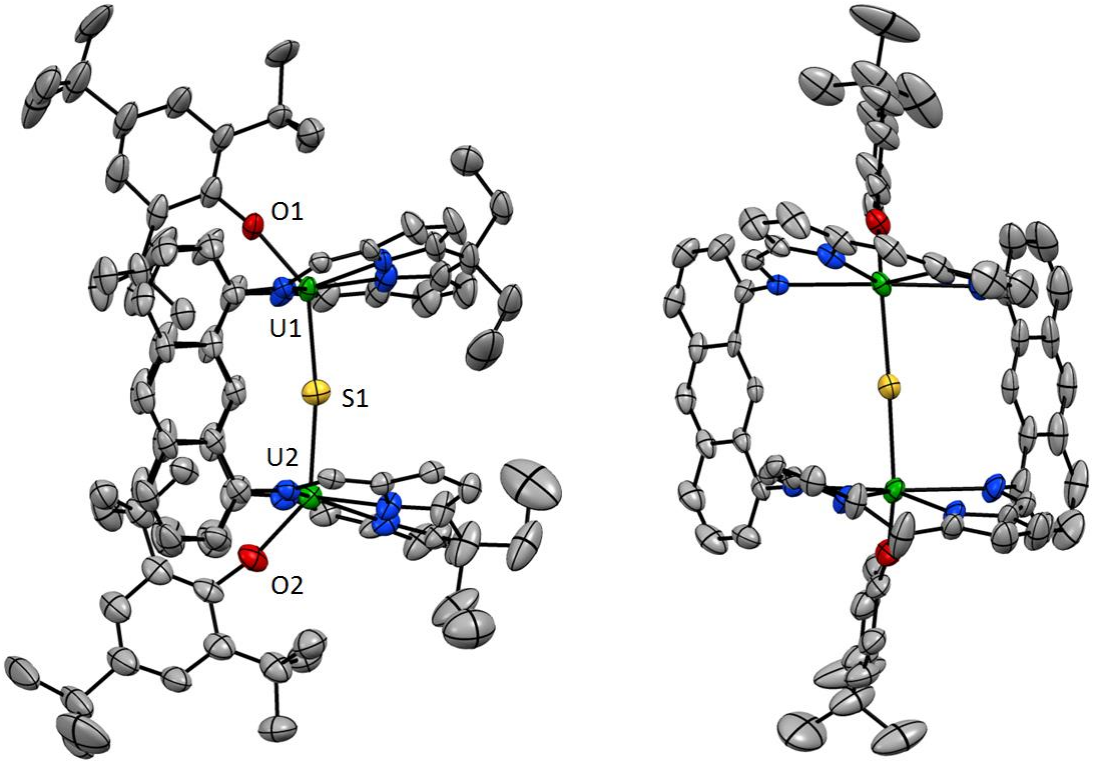

Figure 3.21 Solid state structure of **27** showing side view (left) and view into the jaws of the macrocycle (right). The *meso* ethyl groups and *ortho* aryloxide substituents have been removed from the right-hand structure. Thermal ellipsoids are drawn at 50 % probability. For clarity, H atoms and lattice solvent are omitted.

Table 3.10 Selected bond distances (Å) and angles (°) for **27**.

U1···U2	5.1899(5)	U2-S1	2.608(2)
mean U-N_{im}	2.59	U2-O2	2.099(6)
mean U-N_{pyr}	2.42	U1-S1-U2	172.0(1)
U1-N_4 plane	−0.10	O1-U1-S1	143.2(2)
U2-N_4 plane	−0.03	S1-U2-O2	140.1(2)
U1-O1	2.081(6)	U1-O1-C_{ipso}	170.4(5)
U1-S1	2.594(2)	U2-O2-C_{ipso}	167.8(6)

Complex **27** must logically have been formed by the slow reductive cleavage of the bound CS_2 molecule in **26** to form S^{2-} and release CS during recrystallisation (Scheme 3.20, step (ii)). To probe whether this transformation could be accelerated by heating, a solution of **26** in C_6D_6 was refluxed for 2.5 hours forming an orange solution and a brown precipitate. The subsequent ^{1}H NMR spectrum displayed a new major set of contact-shifted resonances assignable to a single, symmetric Pacman product and was therefore consistent with the transformation of **26** into **27**. A few other low intensity resonances were also observed which could not be assigned, indicating that other minor products were also formed. The ^{1}H NMR

spectrum of **27** exhibits just five aryloxide resonances in the ratio 18:18:18:2:2, as was seen for the similar symmetric persulphide complex **25**.

Transition metal complexes have been shown to effect the reductive cleavage of CS_2 to S^{2-} and CS,[86] and can also promote the disproportionation of CS_2 to $(CS_3)^{2-}$ and CS.[87] However cleavage of CS_2 by actinides remains rare and, to our knowledge, there are only two reported examples. The Th(II) synthon $[Th(Cp')_2(2,2\text{-bipy})]$ (**3AP**, Cp′ = $C_5H_3(^tBu)_2$) reacted with one equivalent of CS_2 to form the bis(sulphide)-bridged product $[\{Th(Cp')_2\}_2(\mu\text{-}S)_2]$ (**3AQ**), or with excess CS_2 to generate a bis(thiocarbonate)-bridged dimer **3AR** (Scheme 3.19, top).[88] The authors do not report whether addition of further equivalents of CS_2 to the isolated bis(sulphide) bridged complex **3AQ** generated the thiocarbonate complex **3AR**. The reaction of CS_2 with the U(III) aryloxide complex **3AS** formed the bridged U(IV)/U(IV) thiocarbonate complex **3AT**, which the authors suggest proceeds *via* formation of the sulphide bridged intermediate **3AE** (Scheme 3.19, bottom). A second product, a bridged U(IV)/U(IV) thio-oxalate complex, was also formed in the reaction.[89]

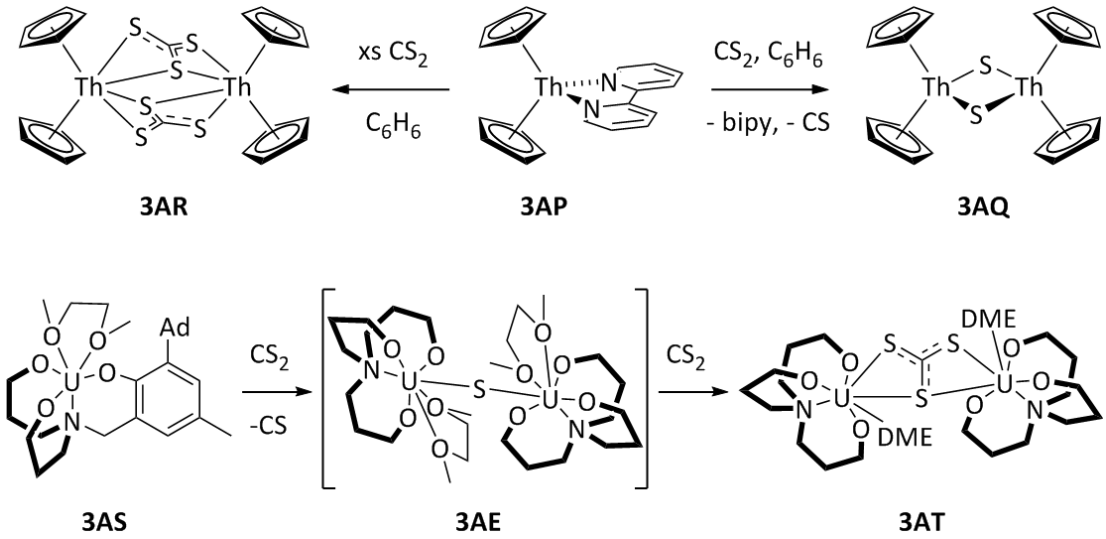

Scheme 3.19 Examples of CS_2 activation by actinide complexes reported by Zi and Walter (top)[88] and Meyer (bottom).[89] The ^tBu groups are omitted from the Cp rings in the top scheme and the tethered aryloxide ligand is shown in cartoon form in the bottom scheme.

Since excess CS_2 was employed in the reaction with **22**, it is interesting to note that the eventual product is the sulphide complex **27** and not a thiocarbonate complex. This may be controlled by sterics; the Pacman macrocycle may not be able to accomodate a thiocarbonate ion. The U···U separation in **3AT** is 6.2019(6) Å, and is considerably greater than that observed in the Pacman sulphide complex **27** (5.1899(5) Å). The KBH_4 incorporated Pacman complex **22** has a larger U···U separation of 6.5881(3) Å, but its

structure is considerably different to that of **27** since it features orthogonal aryloxide rings and an extra equatorial THF donor. Therefore it is unclear whether the U···U separation of **27** could expand sufficiently to incorporate a bridging thiocarbonate ion. Whether the CS_3^{2-} ion could fit between the jaws of the macrocycle must also be considered. The separation of the macrocycle pockets is, in large part, pre-determined by the anthracene hinges of the macrocycle and does not vary significantly with the position of the uranium ions. The S···S separation measured in **3AT** is 2.956(2) Å. Combining this with the Van der Waals radius of sulphur (1.80 Å)[90] yields an effective axial Van der Waals radius for the CS_3^{2-} ion of 6.56 Å at a separation of 2.32 Å from the U-U vector (Figure 3.22, left). Assuming that the bridging geometry of a CS_3^{2-} ion in a uranium Pacman complex would be the same as that in **3AT**, the sulphur atom which is directly bound to both U(IV) centres would have to point towards the aryl hinges of the macrocycle leaving the other two sulphurs oriented towards the mouth of the macrocycle to prevent their clashing with the aryloxide ^{t}Bu groups which sit between the anthracene hinges. The separation between the planes of the macrocycle pockets at a distance of 2.32 Å from the U(IV) centres in the direction of the *meso* carbons, was measured as 6.27 Å in structure **27** (Figure 3.22, right). Therefore binding of CS_3^{2-} in the intermetallic cleft would cause overlap between the sulphur atoms and the carbon and nitrogen atoms of the macrocycle pockets. In conclusion, the Pacman macrocycle could not accommodate a CS_3^{2-} ion in the cleft without considerable distortion so the reaction of the sulphide bridged complex **27** with another equivalent of CS_2 is disfavoured.

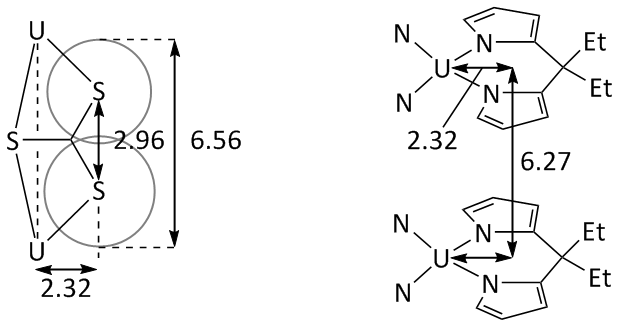

3AT **27**

Figure 3.22 Structural metrics of the {U-(μ-CS_3)-U} core in **3AT** [89] and the macrocyclic cleft in **27**. Only the relevant fragments of the macrocycle pockets are shown. All distances are in Å.

The cleavage of CO_2 by two U(III) ions to form O^{2-} and CO has been demonstrated (see 3.1.2.3),[33,39] there are several examples of carbonate formation from CO_2 in low oxidation state uranium systems,[41,42,44] and $[U(C_5H_4Me)_2(THF)]$ has been shown to abstract S^{2-} from OCS to form $[\{U(C_5H_4Me)_2\}_2(\mu\text{-}S)]$ and CO.[91] In all of these reactions CO, a stable gaseous molecule containing the very strong C≡O bond, is eliminated. By contrast, CS is an

unstable and short-lived species which undergoes spontaneous polymerisation.[92] Indeed the brown precipitate observed during formation of **27** is likely $(CS)_n$. The reduced stability of CS compared to CO explains the relative scarcity of sulphide and thiocarbonate complexes derived from CS_2 compared to oxide and carbonate complexes derived from CO_2.

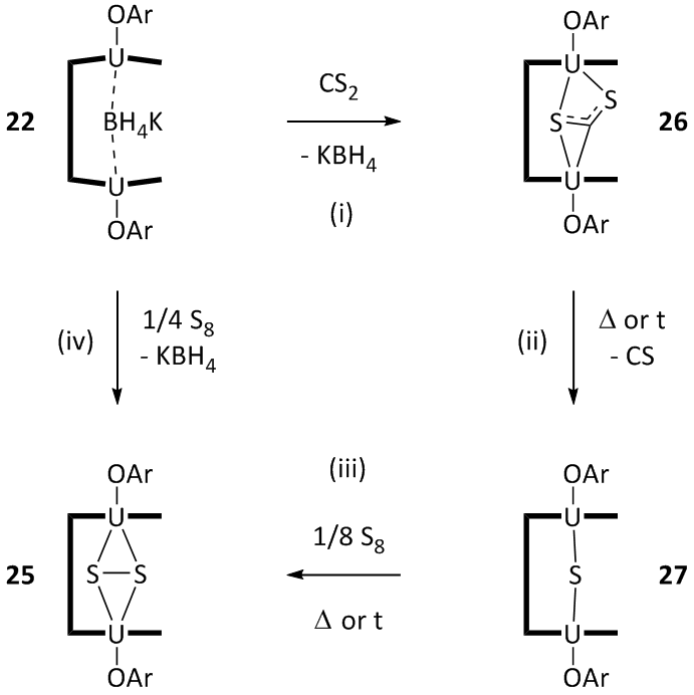

Scheme 3.20 Synthesis and interconversion of the different sulphur-containing uranium Pacman complexes. In all cases the solvent is C_6D_6. The ligand is shown in cartoon form. The equatorial THF ligands are omitted from **22**.

As discussed in 3.1.2.4, Meyer and co-workers reported the reaction of the sulphide bridged U(IV)/U(IV) complex **3AE** with elemental sulphur to generate complex **3AF**, which contains two bridging $(S_2)^{n-}$ units.[47] We were therefore curious to investigate the reactivity of **27** towards S_8. Accordingly, excess S_8 was added to *in situ* generated **27** in C_6D_6 and the reaction monitored by ^{1}H NMR spectroscopy. The mixture did not undergo an obvious colour change and the ^{1}H NMR spectrum acquired two hours after sulphur addition displayed only resonances corresponding to **27**. However, a second spectrum of the mixture acquired after 7 days revealed the presence of the sulphide complex **27** and the persulphide complex **25** in a 2:1 ratio. The mixture was then refluxed for 6 h after which the persulphide complex **25** was observed exclusively (Scheme 3.20, step (iii)). Therefore we have demonstrated that similarly to **3AF**, the sulphide complex **27** reacts with elemental sulphur, though in this case only one further sulphur equivalent is taken up to yield the persulphide complex **25**. In contrast to the formation of **25** from **22** and S_8, which is complete within

minutes, the reaction of **27** with S_8 is slow and must be driven to completion by heating. This is unlikely to be a steric effect since in both reactions the S_8 molecule must be inserted into the macrocyclic cleft and cleaved. Instead, it is suggested that oxidation of the U(III) centres in **22** to U(IV) in **25** and the reduction of elemental sulphur with concurrent formation of four U-S bonds provides a good enthalpic driving force for the reaction. In contrast, the oxidation state of the uranium centres does not change in the transformation of **27** to **25**; rather a comproportionation reaction takes place between the sulphide ion and elemental sulphur to generate persulphide and two new U-S bonds. The new U-$(S_2)^{2-}$ bonds in **25** are longer and weaker than the U-(S^{2-}) bonds in **27** so there is likely not a large enthalpic gain in the reaction.

3.4.2.4 With O_2

Having explored the reactivity of the KBH_4 incorporated U(III)/U(III) Pacman complex **22** with S_8, CO_2, and CS_2, it was logical to also investigate its reaction with O_2. It was hoped that in the absence of moisture, the U-OAr bonds in **22** would be preserved upon addition of O_2 and that the resulting product would contain an *endo* oxo or peroxo group, i.e an oxygen analogue of complex **27** or **25**. When an atmosphere of O_2 (1.0 bar) was introduced to an NMR tube containing a dark green suspension of **22** in C_6D_6 the solution immediately turned dark red. The ^{1}H NMR spectrum of the mixture contained many peaks in both the paramagnetic and diamagnetic regions indicating that multiple products had been formed. Due to the large number of resonances present, it was not possible to assign any set of resonances to a single product. However when the tube was left to stand for 4 days, dark red single crystals formed which were analysed by X-ray diffraction and found to be the bis-uranyl(VI) Pacman complex $[\{UO_2\}_2(L^A)(THF)_2]$ (**28**) (Scheme 3.21). The analogous pyridine solvate $[\{UO_2\}_2(L^A)(py)_2]$ (**1V**) has previously been synthesised and fully characterised from the reaction of H_4L^A with two equivalents of $[UO_2(N'')_2(py)_2]$ in pyridine.[93] U(VI) is the most stable oxidation state of uranium in aerobic conditions and within U(VI) compounds the uranyl motif is ubiquitous. It is therefore not surprising that a certain amount of the bis(uranyl) complex was formed from **22** in the presence of excess O_2. The fate of the aryloxide ligands is unknown; they may be incorporated into other reaction products or trace water in the O_2 gas may have caused hydrolysis.

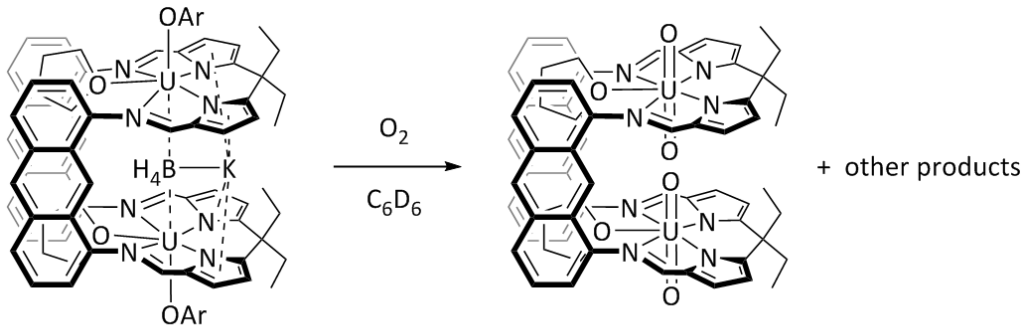

22 **28**

Scheme 3.21 Oxidation of **22** with O_2 to form the bis(uranyl) complex **28** and other unidentified products.

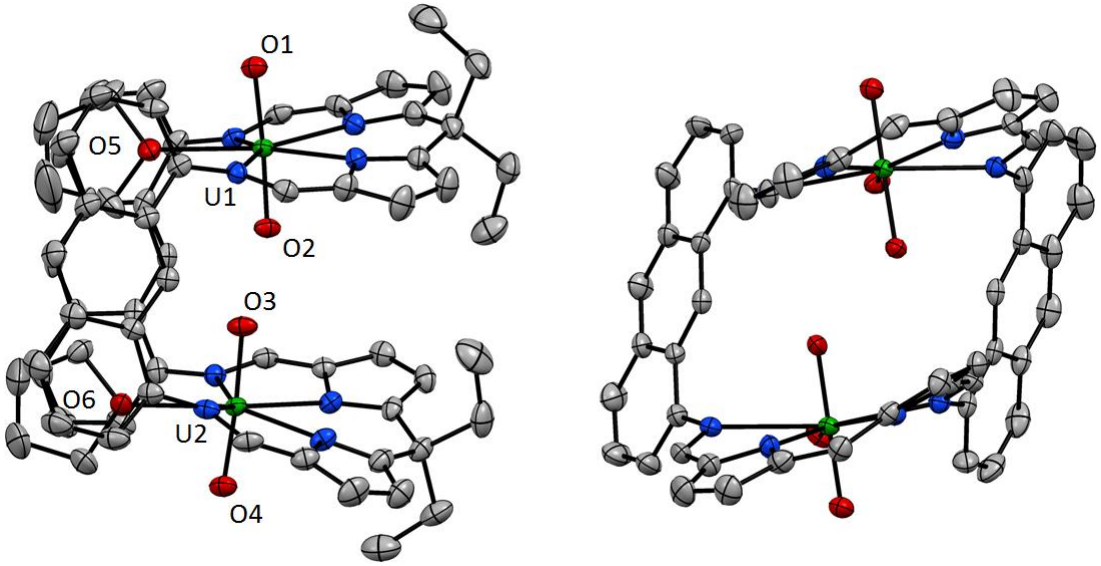

Figure 3.23 Solid state structure of **28** showing side view (left) and view into the jaws of the macrocycle (right). For clarity, the *meso* ethyl groups and the THF carbons have been removed from the right hand structure. Thermal ellipsoids are drawn at 50 % probability. H atoms and lattice solvent are omitted.

Table 3.11 Selected bond distances (Å) and angles (°) for **28**.

U1···U2	5.6727(5)	U2-O3	1.762(3)
mean U-N_{im}	2.56	U2-O4	1.774(3)
mean U-N_{pyr}	2.43	U1-O5	2.457(3)
U1-N_4 plane	+0.09	U2-O6	2.470(3)
U2-N_4 plane	+0.18	O2···O3	2.707(5)
U1-O1	1.772(3)	O1-U1-O2	176.4(2)
U1-O2	1.754(3)	O3-U2-O4	175.6(2)

The solid state structure of **28** (Figure 3.23) is very similar to that of the pyridine solvate. The U(VI) cations display pentagonal bipyramidal geometries in which the four N donors of the macrocycle and a THF molecule occupy the equatorial plane with the two

mutually *trans* oxo ligands in the axial sites. The mean U-N(imine) and U-N(pyrrolide) distances are not significantly reduced from those found in the U(IV) Pacman complexes **25** and **27**, which is attributed to the geometry of the macrocycle, but the U-O(THF) distances (2.457(3), 2.470(3) Å) are shortened compared to those in the U(III) complexes **22** and **23** (2.554(5), 2.592(6) Å), supporting the oxidation of the uranium centres. The linear $\{UO_2\}$ units (O1-U1-O2 = 176.4(2) °, O3-U2-O4 = 175.6(2) °) feature short U-O bond lengths ranging from 1.754(3) Å to 1.774(3) Å which are consistent with the +6 oxidation state of uranium. The absence of a bridging group between the two U(VI) centres allows the macrocycle pockets to slip past each other (twist angle 19 °); this twisting is essential to maximise the separation of the two *endo* oxo groups, O2 and O3. Even so, the O2···O3 separation of 2.707(5) Å in **28** is short, and is identical within error to that reported for the pyridine solvate (2.709(6) Å).

3.4.3 Protonolysis reactions

In the ligand substitution reaction of the borohydride complex **18** with KOAr to form the *exo* aryloxide complex **22**, the *exo* BH_4^- ligands behaved as *pseudo* halides, undergoing salt elimination. However, unlike the halides, BH_4^- is also basic in nature. For example, Ephritikhine and co-workers have demonstrated the protonation of $[U(BH_4)_3(THF)_3]$ with the acidic ammonium salt $[HNEt_3][BPh_4]$ to form the unusual cationic U(III) compound $[U(BH_4)_2(THF)_5][BPh_4]$.[63] Therefore we investigated the reactivity of **18** towards a mild acid, expecting that neutral or cationic derivatives of the Pacman anion in **18** would exhibit enhanced reactivity.

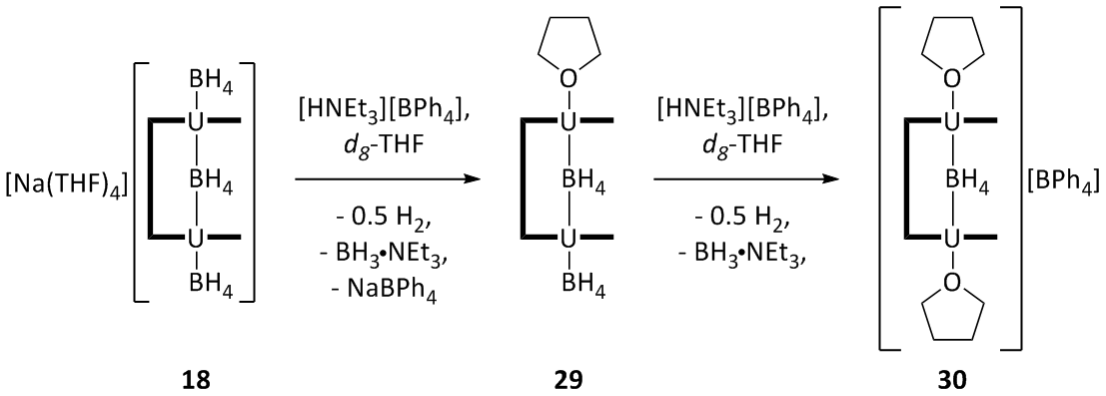

18 **29** **30**

Scheme 3.22 Protonolysis of the anionic uranium borohydride complex **18** with successive equivalents of $[HNEt_3][BPh_4]$. The ligand is shown in cartoon form and the equatorially bound THF molecules are omitted from each complex.

One equivalent of $[HNEt_3][BPh_4]$ was added to a dark green solution of **18** in d_8-THF. No obvious colour change occurred but effervescence was observed. The ^{1}H NMR

spectrum of the mixture displayed twenty-one contact shifted resonances corresponding to a single Pacman product with magnetically inequivalent pockets (one ligand resonance is assumed to be obscured by solvent signals). A single broad borohydride proton resonance was observed at −76.8 ppm. The spectral data are consistent with the protonolysis of one BH_4^- ligand. The presence of a low intensity, sharp signal at 4.59 ppm in the ^{1}H NMR spectrum confirmed that dihydrogen was formed in the reaction. The other by-products of protonolysis, $H_3B{\bullet}NEt_3$ and $NaBPh_4$ were most clearly evidenced in the ^{11}B NMR spectrum, appearing as a quartet at −13.0 ppm and a singlet at −6.64 ppm, respectively. A stoichiometric quantity of NEt_3 is formed in the reaction whereas THF is present in large excess as the solvent. Therefore it is interesting to note that the amine-borane adduct, $H_3B{\bullet}NEt_3$, is observed exclusively (the $H_3B{\bullet}$THF adduct would be readily distinguished by its ^{11}B chemical shift of −1.1 ppm). The ^{11}B NMR spectrum also contains two broad signals of equal intensity shifted to high frequency at 234 and 178 ppm. The asymmetry of the Pacman macrocycle and the presence of two contact shifted resonances in the ^{11}B NMR spectrum indicate that one of the *exo* BH_4^- ligands has been removed. The product is therefore assigned as the neutral complex $[\{U(BH_4)\}\{U(THF)\}(\mu\text{-}BH_4)(L^A)(THF)_2]$ (**29**, Scheme 3.22, centre). It is assumed that a THF molecule will occupy the *exo* axial site vacated by the BH_4^- ligand.

Addition of a second equivalent of $[HNEt_3][BPh_4]$ to the NMR tube containing **29** resulted in further effervescence. The ^{1}H NMR spectrum of the resultant mixture displayed half the number of resonances indicating that the two macrocycle pockets are equivalent. The ^{11}B NMR spectrum contained just one signal at very high frequency (334 ppm). These data suggest that the remaining *exo* BH_4^- group has been removed to form the symmetric, cationic, U(III)/U(III) borohydride-bridged complex $[\{U(THF)\}_2(\mu\text{-}BH_4)(L^A)(THF)_2][BPh_4]$ (**30**, Scheme 3.22, right). No further reaction occurred upon addition of excess $[HNEt_3][BPh_4]$, indicating that the remaining $(\mu\text{-}BH_4)$ group is not susceptible to protonolysis. This is not entirely surprising since the electrostatic repulsion induced by the formation of two cationic U(III) centres confined within one Pacman ligand is expected to be prohibitive.

Single crystals of **29** or **30** could not obtained from THF/hexane solution. Instead, precipitation of pale solids occurred, possibly indicating decomposition. Synthesis of **30** in DME was investigated in the hope that the neutral bidentate ligand would stabilise the cationic complex by binding to the U(III) centres in both the inter-hinge equatorial site and the *exo* axial site. The ^{11}B NMR spectrum displayed one contact shifted resonance at 246

ppm which suggests successful formation of [{U(DME)}$_2$(μ-BH$_4$)(L^A)] but single crystals were not obtained. In a similar strategy, 2,2-bipyridyl was added to a solution of **30** in d_8-THF but in this case immediate decomposition occurred with no product resonances visible in the ^{1}H NMR spectrum.

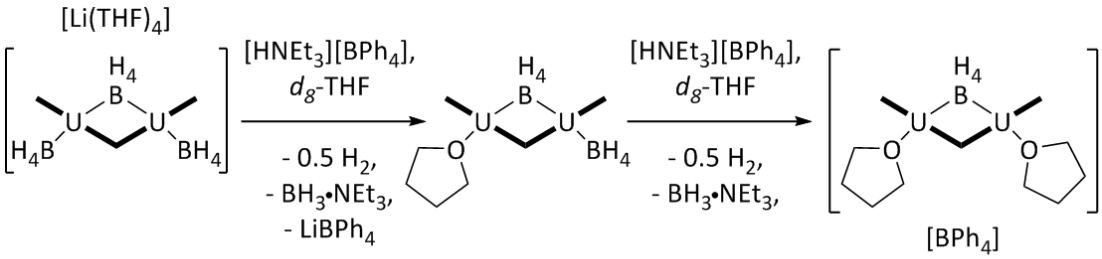

21 **31** **32**

Scheme 3.23 Protonolysis of the anionic uranium borohydride complex **21** with successive equivalents of [HNEt$_3$][BPh$_4$]. The ligand is shown in cartoon form.

Ligand substitution reactions of the U(III)/U(III) complex of the *ortho*-phenyl macrocycle, **21**, had proved unsuccessful but this was not the case with protonolysis reactions. Addition of one equivalent or excess [HNEt$_3$][BPh$_4$] to a dark green suspension of **21** in d_8-THF resulted in immediate dissolution of the solids, with effervescence, to form a dark green solution. The reactivity of **21** was analogous to that of **18**. Thus the product of the reaction with one equivalent of [HNEt$_3$][BPh$_4$] is assigned as the neutral complex [{U(BH$_4$)}{U(THF)}(μ-BH$_4$)(L^{Me})] (**31**, Scheme 3.23, centre). The remaining *exo* BH$_4^-$ ligand appears at 205 ppm in the ^{11}B NMR spectrum and the bridging BH$_4^-$ group at 370 ppm. The ^{1}H NMR spectrum of this binuclear uranium borohydride complex is unique in that resonances are observed for both the terminal and bridging BH$_4^-$ protons, at 85.3 ppm and 61.1 ppm respectively, assigned on the basis of selective ^{11}B decoupling experiments.

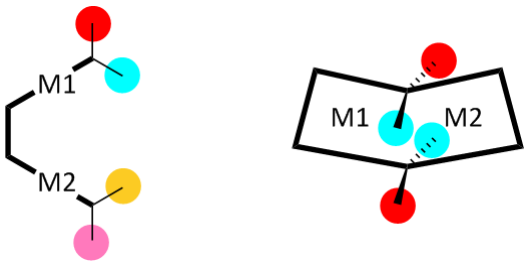

Figure 3.24 Cartoon illustrating the different *meso* methyl environments in asymmetric Pacman (left) and bowl (right) complexes.

^{1}H NMR spectroscopy also confirms that the bowl co-ordination geometry of the macrocycle in **21** is retained upon protonolysis to form **31**. For symmetric complexes, the bowl and Pacman geometries are indistinguishable by NMR spectroscopy but if the two metal binding pockets are inequivalent, the two geometries give rise to different splitting

patterns of the *meso* methyl groups. In the Pacman geometry all four *meso* methyl groups become inequivalent if the two binding pockets are different and so give rise to four signals of relative integral 3H, yielding a total of fourteen ligand resonances. However, in the bowl geometry the two *endo* and two *exo* Me groups retain their equivalence even when the metal pockets are inequivalent (Figure 3.24) and therefore give rise to two signals of integral 6H and a total of twelve ligand resonances, as is observed in the ^{1}H NMR spectrum of **31**.

The product of the reaction of **21** with excess [HNEt$_3$][BPh$_4$] is assigned as the symmetric cationic U(III)/U(III) compound [{U(THF)}$_2$(μ-BH$_4$)(L^{Me})][BPh$_4$] (**32**, Scheme 3.23, right), which is assumed to retain the bowl geometry. Resonances corresponding to the (μ-BH$_4$) group are observed at 80.7 and 432 ppm in the ^{1}H and ^{11}B NMR spectra, respectively. Single crystals of **31** and **32** have not been obtained. These series of protonolysis reactions illustrate the considerable power of heteronuclear NMR spectroscopy for structure determination in paramagnetic systems, where the amount of information that can be extracted from ^{1}H NMR spectra is reduced. In particular, the ^{11}B NMR spectra of compounds **18**, **29** and **30**, and **21**, **31** and **32**, besides yielding information on the number of borohydride ligand environments, display a strong correlation with the charge of the uranium complex. As the charge changes from 1−, to neutral, to 1+, there is a concurrent shift to higher frequency of the (μ-BH$_4$) resonance in both series of compounds (Figure 3.25).

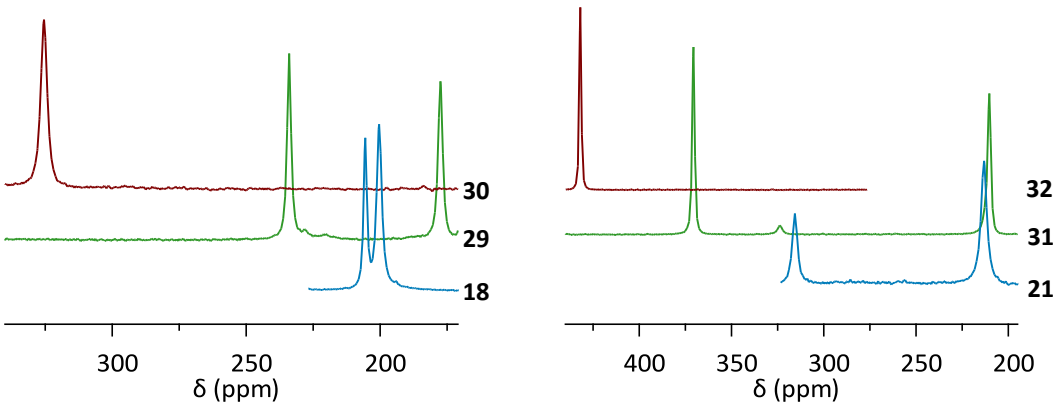

Figure 3.25 ^{11}B NMR spectra (d_8-THF) of the anionic (blue), neutral (green) and cationic (red) uranium borohydride Pacman complexes of (L^{A})$^{4-}$ (left) and (L^{Me})$^{4-}$ (right).

Due to time constraints, preparative syntheses of compounds **29** - **32** were not developed but some reactivity studies were carried out with the cationic complexes **30** and **32** formed *in situ* in d_8-THF. It was discovered that **30** does not react with H$_2$ but a slow reaction occurs between **30** or **32** and CO. In both cases many low intensity paramagnetic resonances were observed in the ^{1}H NMR spectra of the reaction mixtures indicating that

multiple product formation and/or decomposition had occurred. The anionic complex **18** was unreactive towards CO, so although the cationic complex **30** does not react with CO in a selective manner, there can be no doubt that it displays enhanced reactivity.

3.5 Metallation reactions using UCl_4

As an alternative to UI_3 and $[U(BH_4)_3(THF)_2]$, UCl_4 was also investigated as a low oxidation state precursor for the formation of binuclear uranium Pacman compounds. Although U(III)/U(III) Pacman compounds are expected to be most reactive towards inert small molecule targets, it was reasoned that a U(IV)/U(IV) Pacman complex might be more stable and easier to synthesise and may then provide an alternative route into U(III)/U(III) Pacman chemistry *via* reduction.

3.5.1 Synthesis of $[Li(THF)_4][\{UCl\}_2(\mu\text{-}Cl)_3(L^A)]$

Deprotonation of the anthracenyl macrocycle H_4L^A with four equivalents of LiN″ in THF solution followed by addition of two equivalents of UCl_4 resulted in the precipitation of $[Li(THF)_4][\{UCl\}_2(\mu\text{-}Cl)_3(L^A)]$ (**33**) as a microcrystalline orange solid in up to 39 % yield (Scheme 3.24). Complex **33** is an "-ate" salt with one equivalent of LiCl incorporated. Attempts to prepare the K^+ analogue were unsuccessful, resulting in mixtures of paramagnetic products. The salt **33** is insoluble in THF but is soluble in pyridine. The ^1H NMR spectrum of **33** in d_5-pyridine displays contact-shifted resonances assignable to a symmetric Pacman ligand environment with desymmetrised *meso* ethyl groups. One signal is observed in the ^7Li NMR spectrum at 3.5 ppm arising from the solvated counterion $[Li(py)_4]^+$. This is not much shifted from the value expected for LiCl indicating that in solution there is little association between the cation and the paramagnetic Pacman anion.

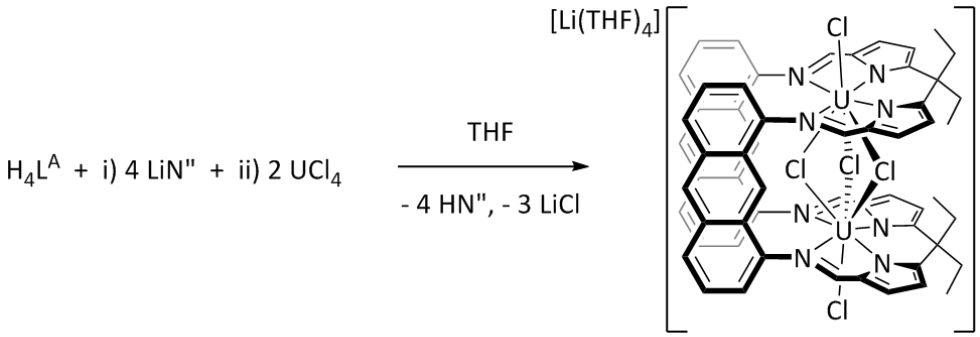

Scheme 3.24 Metallation of H_4L^A with UCl_4 to form the U(IV)/U(IV) Pacman complex **33**.

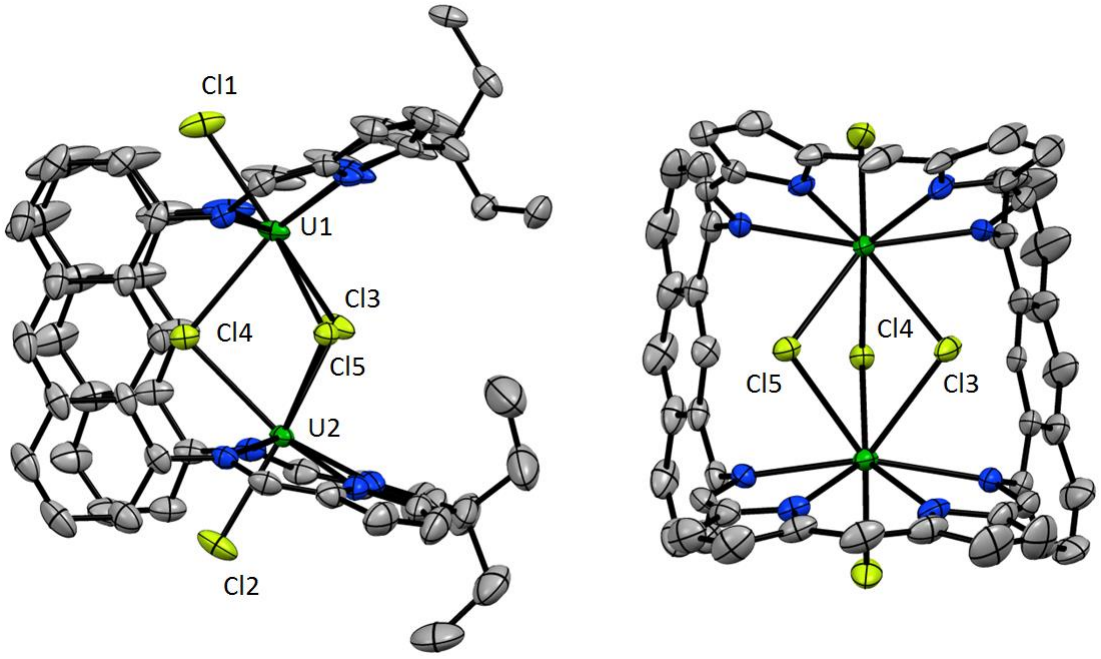

Figure 3.26 Solid state structure of the anionic portion of **33$_{py}$** showing side view (left) and view into the jaws of the macrocycle (right). For clarity, the *meso* ethyl groups have been removed from the right hand structure, and H atoms and lattice solvent are omitted.

Table 3.12 Selected bond distances (Å) and angles (°) for **33$_{py}$**.

U1···U2	4.1927(3)	U1-Cl1	2.595(1)
mean U-N_{im}	2.61	U2-Cl2	2.610(2)
mean U-N_{pyr}	2.38	mean U-(μ-Cl)	2.86
U1-$N_{4\ plane}$	−0.57	mean U1-(μ-Cl)-U2	94.9
U2-$N_{4\ plane}$	−0.65		

Single crystals of the pyridine solvate **33$_{py}$** were grown by slow diffusion of toluene into a pyridine solution of **33**. In the solid state **33$_{py}$** is a discrete ion pair though one of the ligating pyridine rings of the $[Li(py)_4]^+$ cation sits between the anthracene hinges of the Pacman macrocycle and engages in π-stacking with a mean C(py)-C(hinge) separation of 3.74 Å to one hinge and 4.06 Å to the other. In the anion, the U(IV) centres occupy *pseudo* equivalent eight co-ordinate sites, binding to the four N donors of the macrocycle, one *exo* axial chloride (Cl1/Cl2) and three *endo* bridging chlorides (Cl3, Cl4, Cl5) (Figure 3.26). There are no additional pyridine ligands in the equatorial sites between the macrocycle hinges. The terminal U-Cl distances (U1-Cl1 = 2.595(1) Å, U2-Cl2 = 2.610(2) Å) are significantly shorter than the bridging U-Cl distances (mean U-(μ-Cl) = 2.86 Å). This is in keeping with the trend observed in the handful of other U(IV) complexes containing the $\{U_2(\mu\text{-}Cl)_3\}$ core that have been structurally characterised. The mean terminal and bridging U-Cl distances reported for **3AU** (Figure 3.27, left) are 2.64 Å and 2.83 Å, respectively.[94]

Complex **3AV** (Figure 3.27, centre) contains only bridging chlorides but these occupy three distinct environments with associated distinct U-Cl bond lengths: (1) {U(μ-Cl)Li}, U-Cl = 2.68 Å, (2) {U_2(μ-Cl)}, U-Cl = 2.82 Å and (3) {U_2(μ^3-Cl)Li}, U-Cl = 2.84 Å.[95]

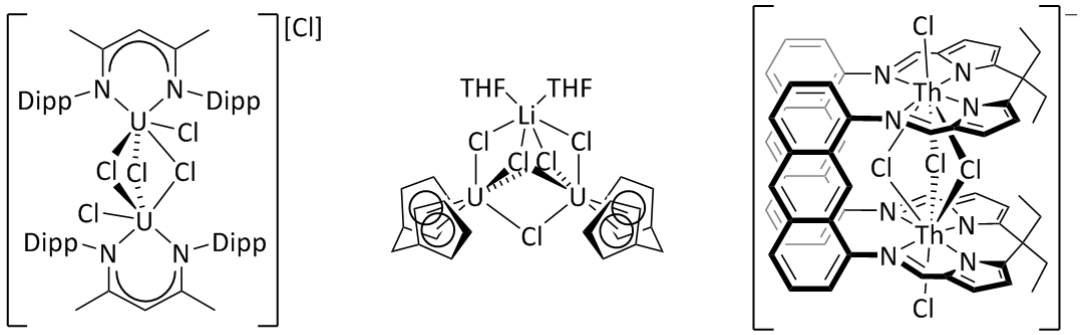

Figure 3.27 Examples of An(IV) complexes containing {$An_2(\mu\text{-}Cl)_3$} cores.[94-96] The $[Li(THF)_4]^+$ cation is omitted from **3AW**.

The {$U_2(\mu\text{-}Cl)_3$} core in $\mathbf{33_{py}}$ is pentagonal bipyramidal with the three chloride ions located at the equatorial vertices and the two U(IV) ions at the axial apexes. Cl4 is oriented between the anthracene hinges on the macrocycle while Cl3 and Cl5 are angled sideways and forwards, out of the macrocyclic cleft. The presence of the three *endo* bridging chlorides and their acute bridging angles (mean U1-(μ-Cl)-U2 = 94.9 °) results in a U1···U2 separation of 4.1927(3) Å, which is the shortest observed in any of the uranium complexes of $(L^A)^{4-}$. The U(IV) ions are therefore considerably displaced out of the N_4 planes of the macrocycle, into the cleft, by an average of −0.61 Å. Dr Rebecca White synthesised the Th(IV) analogue of **33**, $[Li(THF)_4][\{ThCl\}_2(\mu\text{-}Cl)_3(L^A)]$ (**3AW**, Figure 3.27, right) by reaction of two equivalents of $ThCl_4$ with *in situ* generated Li_4L^A.[96] The solid state structure of **3AW** is very similar to that of $\mathbf{33_{py}}$. However, all the Th-Cl bonds in **3AW** are slightly lengthened compared to the U-Cl bonds in $\mathbf{33_{py}}$ (mean terminal Th-Cl = 2.68 Å, mean Th(μ-Cl) = 2.89 Å). This is consistent with the larger radius of Th(IV) compared to U(IV). As a result of the elongated Th-Cl bonds, the Th···Th separation in **3AW** is also lengthened to 4.252(5) Å and the magnitude of the out-of-plane displacement of the Th(IV) ions is reduced to −0.59 Å.

3.5.2 Reactivity of $[Li(THF)_4][\{UCl\}_2(\mu\text{-}Cl)_3(L^A)]$

Having synthesised a novel binuclear U(IV)/U(IV) Pacman complex we were keen to explore its reactivity, the reduction of complex **33** and the formation of a uranium alkyl derivative being areas of particular interest. However we were hampered by the negligible solubility of the complex in aromatic or ethereal solvents. Nevertheless, reduction of a

suspension of **33** in THF with soluble potassium naphthalenide was attempted. The ^{1}H NMR spectrum of the resultant mixture did not contain any paramagnetic resonances but it was impossible to say whether this was due to decomposition of **33** caused by the reducing agent or whether the complex had never gone into solution. Compound **33** will only dissolve in pyridine. This is an unsuitable solvent for potassium reductions or reactions with alkali-metal alkylating agents since these reagents react with pyridine. Therefore initial efforts were concentrated on synthesising a more soluble derivative of **33** for use in further reactivity studies.

3.5.2.1 Ligand substitution: structure of [{U(O^{t}Bu)(Cl)}{U(O^{t}Bu)(py)}(μ-Cl)(L^{A})]

Various ligand substitution reactions of **33** with amide, alkoxide, aryloxide, cyclopentadienyl, and acetylacetonate alkali metal salts were investigated on a small scale in d_5-pyridine solution (see 4.3.26). The only reaction that appeared promising was that of **33** with two equivalents of KO^{t}Bu. In this case the ^{1}H NMR spectrum of the mixture displayed twenty-two contact-shifted resonances assigned to an asymmetric Pacman ligand and two resonances of relative integral 9H at 85.95 ppm and 69.74 ppm, indicating that the product contained two non-equivalent (O^{t}Bu)$^{-}$ ligands. The product did indeed have improved solubility compared to **33**; after removal of the d_5-pyridine solvent from the NMR sample, the solid residues were re-dissolved in benzene. Yellow single crystals of [{U(O^{t}Bu)(Cl)}{U(O^{t}Bu)(py)}(μ-Cl)(L^{A})] (**34**) were obtained by vapour diffusion of hexane into the benzene solution (Scheme 3.25).

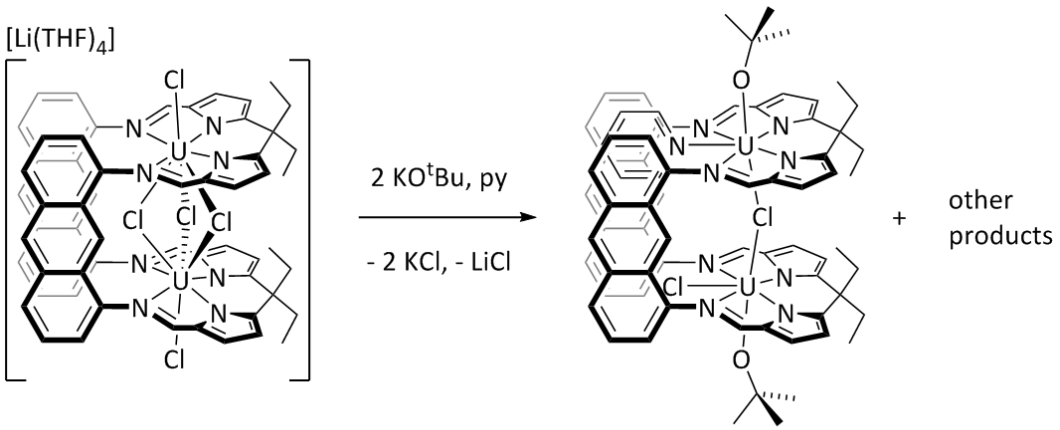

33 **34**

Scheme 3.25 Ligand substitution reaction of ionic **33** to form neutral alkoxide complex **34**.

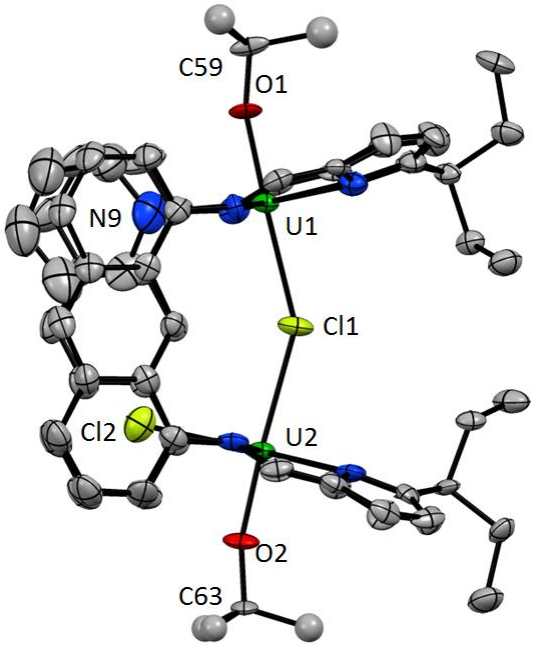

Figure 3.28 Solid state structure of **34** showing the major orientation of the *tert* butyl groups. Thermal ellipsoids are drawn at 50 % probability and lattice solvent and H atoms are omitted.

Table 3.13 Selected bond distances (Å) and angles (°) for **34**.

U1···U2	5.4155(8)	U2-Cl1	2.826(5)
mean U-N_{im}	2.56	U1-N9	2.52(1)
mean U-N_{pyr}	2.42	U2-Cl2	2.700(6)
U1-N_4 plane	−0.02	U1-Cl1-U2	150.8(2)
U2-N_4 plane	+0.03	O1-U1-Cl1	177.7(4)
U1-O1	2.049(11)	O2-U2-Cl1	176.7(4)
U2-O2	2.012(12)	C59-O1-U1	164(1)
U1-Cl1	2.771(5)	C63-O2-U2	165(1)

The solid state structure of **34** reveals that the two U(IV) ions occupy inequivalent *pseudo* pentagonal bipyramidal binding sites and is therefore consistent with the observed solution structure. U1 binds to the four N donors of the macrocycle and one molecule of pyridine in the equatorial plane, one *exo* axial alkoxide ligand and the *endo* bridging chloride, Cl1. U2 is ligated by the macrocycle nitrogens, one terminal chloride (Cl2) in the equatorial plane between the anthracene hinges of the macrocycle, one *exo* axial alkoxide and the *endo* bridging chloride, Cl1. The U1-O1 and U2-O2 bond lengths of 2.049(11) Å and 2.012(12) Å, respectively, are similar to those observed in other neutral U(IV) *tert*-butoxide complexes [97,98] and are slightly reduced compared to the U^{IV}-OAr distances in complexes **25** and **27**, where the shortest U-OAr distance is 2.081(6) Å. This is consistent with the increased Lewis basicity of the alkoxide compared to the aryloxide, and its reduced steric

bulk. The axial ligands are linearly disposed with O1-U1-Cl1 and O2-U2-Cl1 angles of 177.7(4) ° and 176.7(4) °, respectively. The bridging chloride ligand, Cl1, is bound unsymmetrically between the U(IV) centres; the U1-Cl1 bond (2.770(4) Å) is shorter than the U2-Cl1 bond (2.826(4) Å). However, both U-(μ-Cl) bonds in **34** are shorter than any of the U-(μ-Cl) interactions in **33** (mean 2.86 Å). This change is to be expected upon reduction of the number of bridging chlorides, as is the more obtuse U1-Cl1-U2 bridging angle of 150.8(2) ° in **34** compared to an average of 94.9 ° in **33**. These structural changes allow the U(IV) ions to relax back into the planes of the macrocycle N_4 donor pockets and result in an increased U···U separation of 5.4155(8) Å. Interestingly the terminal U2-Cl2 bond length of 2.700(6) Å is considerably elongated compared to those in complex **33** (mean 2.60 Å).

Binuclear uranium complexes featuring a single bridging chloride ligand are quite rare, the $\{U_2(\mu\text{-Cl})_2\}$ and $\{U_2(\mu\text{-Cl})(\mu\text{-OR})\}$ motifs being far more common. Two neutral $\{U^{IV}{}_2(\mu\text{-Cl})\}$-containing complexes, **3AX** and **3AY**, have been structurally characterised (Figure 3.29). Complexes **3AX** and **3AY** are similar to complex **34** in that the two U(IV) centres are inequivalent in each structure and this in reflected in asymmetric bridging U-Cl distances (Table 3.14, entry 2.). A comparison of the structural metrics of the $\{U_2(\mu\text{-Cl})\}$ units in **34**, **3AX** and **3AY** (Table 3.14) reveals that all three are very similar and thus the Pacman macrocycle can readily incorporate a single bridging chloride between two U(IV) ions without imposing any structural distortion.

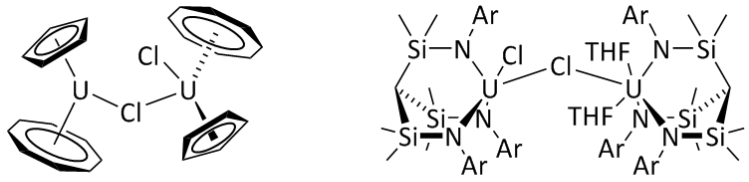

3AX **3AY**

Figure 3.29 Mono(chloride-bridged) uranium complexes reported by the Evans (left)[99] and Liddle (right)[100] groups. Ar = 4-C_6H_4(^{t}Bu).

Table 3.14 Comparison of selected structural parameters of **34**, **3AX** and **3AY**.

		34	**3AX**	**3AY**
1.	*U···U (Å)*	5.4155(8)	5.4412(7)	5.5011(6)
2.	*U-(μ-Cl) (Å)*	2.770(4), 2.826(4)	2.728(3), 2.921(3)	2.812(2), 2.881(2)
3.	*U-Cl-U (°)*	150.8(2)	148.1(1)	150.17(7)

Complex **34** is formed from **33** by substitution of both *exo* chloride ligands for alkoxides, cleavage of two of the three chloride bridges and spontaneous loss of the equivalent of incorporated LiCl (Scheme 3.25). Compound **34** is a neutral complex with two solubilising *tert*-butyl groups. Therefore its improved solubility compared to ionic **33** is not

difficult to rationalise. However it is not clear why loss of the incorporated equivalent of LiCl in **33** is favoured during the formation of **34**. A possible explanation is that *exo* axial co-ordination of two *tert*-butoxide ligands is not compatible with maintenance of the $\{U_2(\mu\text{-}Cl)_3\}$ core because the in-to-cleft displacement of the U(IV) ions imposed by three bridging chlorides would result in a steric clash between the bulky alkoxide ^{t}Bu groups and the ligand framework. Therefore we suggest that *exo* alkoxide co-ordination cleaves two of the chloride bridges and that one of these chlorides then dissociates in order to recombine with its Li^+ counterion. This dissociation is likely due to competitive displacement by the strongly Lewis basic pyridine solvent. In light of this, it is interesting to note that this reaction does not proceed in THF solvent to yield the THF solvate $\mathbf{34_{THF}}$ but instead forms a poorly defined mixture of products.

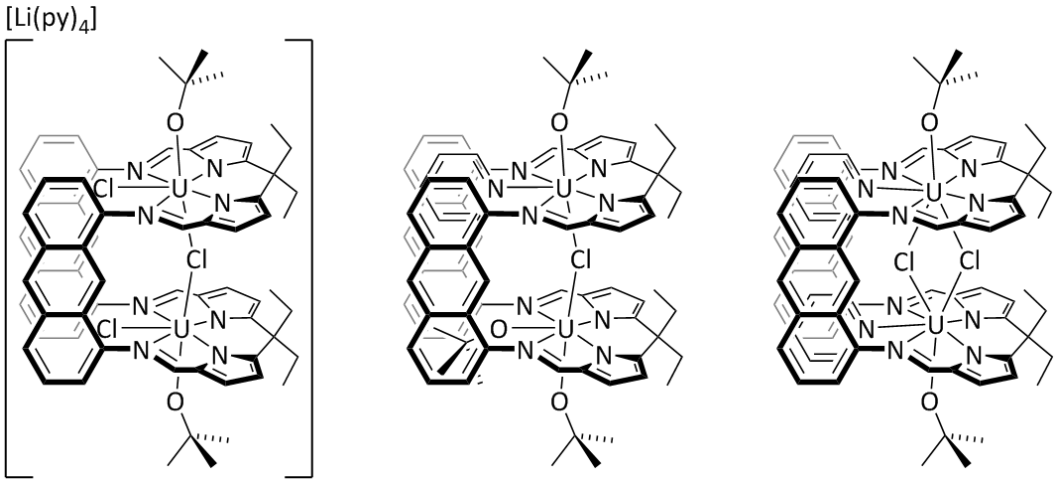

Figure 3.30 Suggested structures of minor products formed by reaction of **33** with KO^{t}Bu.

Attempts were made to synthesise **34** on a preparative scale. Compound **33** was combined with two equivalents of KO^{t}Bu in pyridine and stirred for one hour before the volatiles were removed and the resulting yellow-brown solids extracted with toluene. Storage of the concentrated extract at −30 °C resulted in precipitation of yellow solids. NMR analysis of the solids revealed that the major component was indeed **34** but at least two other minor products were also present. None of these minor products have been identified but three suggested structures are shown in Figure 3.30. The observation of a very low intensity resonance in the ^{7}Li NMR spectrum of the mixture at 4 ppm may suggest that one of the minor products is an "-ate" salt (left). If a slight excess of KO^{t}Bu had been employed then over-substitution of the chloride groups may have occurred to form products with more than two alkoxide ligands (centre). It is also possible that *exo* alkoxides might be compatible with a symmetric $\{U_2(\mu\text{-}Cl)_2\}$ motif (right). Unfortunately, attempts to obtain analytically pure **34**

by recrystallisation were unsuccessful and thus further study of the reactivity of **34** was not undertaken.

3.5.2.2 Cation exchange

Another strategy investigated to improve the solubility of the salt **33** was exchange of the small and highly polarising Li^+ cation for a larger, more soluble counterion. To this end, one equivalent of bis(triphenylphosphine)iminium chloride was added to a solution of **33** in d_5-pyridine (Scheme 3.26, left). Multiple, very low intensity resonances were observed in the paramagnetic region of the resultant ^{1}H NMR spectrum, indicating that decomposition had occurred. Excess tetrabutylammonium bromide was mixed with **33** in THF and then the solvent was removed and the solid residue re-suspended in C_6D_6. Signals only slightly shifted from those of **33** in d_5-pyridine were observed in the ^{1}H NMR spectrum of the C_6D_6 sample, along with large resonances arising from the $[NBu_4]^+$ cation. Since **33** is completely insoluble in benzene, this indicates that at least partial cation exchange of Li^+ for $[NBu_4]^+$ has occurred (Scheme 3.26, right). Therefore with judicious choice of reagent it appears possible to better solubilise complex **33**. Due to time constraints this investigation was not pursued further, but it would be interesting to explore whether addition of Bu_4NBr could be used to catalyse reactions of **33** in solvents in which the Li^+ salt is poorly soluble.

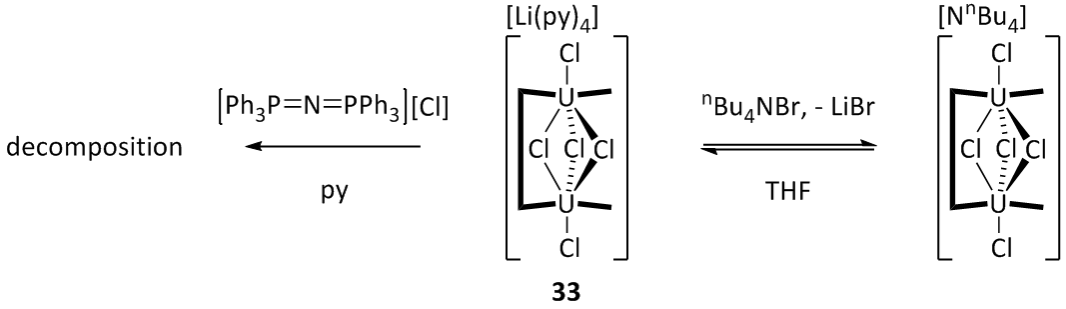

Scheme 3.26 Reactions of **33** with different cation exchange agents.

3.6 Conclusions

The first investigation into the reactivity of low oxidation state uranium precursors with the anthracene-hinged Pacman macrocycle, H_4L^A, has been carried out. The halide precursors UI_3 and UCl_4 both react with the deprotonated macrocycle to form binuclear uranium Pacman complexes. The Pacman product (**12**) of the reaction of UI_3 with K_4L^A was unstable and could not be isolated in the solid state. The product of the reaction of UCl_4 with Li_4L^A was the "-ate" salt $[Li(THF)_4][\{UCl\}_2(\mu\text{-}Cl)_3(L^A)]$ (**33**) which has been isolated and structurally characterised. The increased stability of **33** compared to **12** is not unexpected;

the +4 oxidation state of uranium is far less reducing than the +3 state and U-Cl bonds are considerably stronger than U-I bonds. The unique steric requirements of the Pacman macrocycle must also be considered. Given the other results described in this chapter, it is likely that complex **12** is an "-ate" salt, probably of general formula $[K(sol)_x][\{U(I)\}_2(\mu\text{-}I)(L^A)(sol)_y]$, necessitating *endo* binding of an iodide ion within the macrocyclic cleft. Previous work has shown that $[Zn_2(L^A)]$ selectively binds chloride over iodide in the *endo* site and calculations have confirmed that an iodide-incorporated complex would have greatly reduced thermodynamic stability.[101] Therefore, the *endo* iodide in **12** would be a poor size match for the macrocyclic cleft and would destabilise the complex. Unfortunately complexes **12** and **33** were of limited further synthetic usefulness.

A new, convenient, high-yielding synthesis of the alternative U(III) precursor $[U(BH_4)_3(THF)_2]$ (**14**) has been developed, and its synthetic versatility has been demonstrated. It is hoped that **14** will prove a valuable addition to the limited stock of existing U(III) precursors and will be of benefit to the uranium research community. Although **14** has not been structurally characterised the structures of two iodide substituted complexes $[U(BH_4)_2(THF)_5][U_2(BH_4)_{4.90}(\mu\text{-}I)_2(I)_{0.10}(THF)_3]$ (**15**) and $[U(BH_4)_{2.59}(I)_{0.41}(DME)_2]$ (**16**) were obtained. Complex **15** was isolated from ether solution and serves to illustrate the complexity of uranium aggregation in weakly co-ordinating solvents. By contrast, addition of the strongly co-ordinating chelator DME resulted in isolation of the simple molecular complex **16**.

Two distinct types of U(III)/U(III) Pacman "-ate" complex were identified from the reactions of **14** with M_4L^A (M= Li, Na, K): the salts $[M(THF)_4][\{U(BH_4)\}_2(\mu\text{-}BH_4)(L^A)(THF)_2]$ (M = Li, **17**, Na, **18**) and the host-guest complex $[\{U(BH_4)\}_2(\mu\text{-}BH_4K)(L^A)(THF)_2]$ (**19**), in which the K^+ counterion sits between the four pyrrolide rings of the macrocycle due to an adventitious size match between cavity and cation. Compound **14** also facilitated the isolation and structural characterisation of the bowl-shaped "-ate" complex $[Li(THF)_4][\{U(BH_4)\}_2(\mu\text{-}BH_4)(L^{Me})]$ (**21**) from the lithium salt of the *ortho*-phenyl macrocycle, H_4L^{Me}. Complex **21** is a discreet ionic complex in contrast to the previously reported poorly-defined oligomeric materials of composition $[\{U(BH_4)\}_2(L^{Et})]_n$.[50] Complexes **18** and **21** represent the second and third structurally characterised examples of binuclear U(III)/U(III) complexes of a single ligand.[49] They are also the first compounds to feature the $\{U^{III}\text{-}(\mu\text{-}BH_4)\text{-}U^{III}\}$ motif and therefore provide structural insight that may well be valuable in the future design of uranium complexes incorporating borohydride ligands.

The isolation of complexes **18** and **21** has allowed the first study into the reactivity of binuclear U(III)/U(III) Pacman complexes. The distinct *exo* and *endo* borohydride environments in **18** and **21** resulted in differing reactivity, which was exploited in selective transformations. The *exo* BH_4^- ligands were susceptible to protonolysis whereas the *endo* BH_4^- ligands were not. Reaction of **18** with the bulky aryloxides MOAr (M = K, Na) resulted in exclusive substitution of the *exo* BH_4^- ligands and formation of the host guest complexes $[\{U(OAr)\}_2(\textit{endo}\text{-}BH_4M)(L^A)(THF)_2]$ (M = K, **22**, Na, **23**). It is clear from a comparison of the solid state structures of **22** and **23** that the K^+ cation is an optimum size match for the macrocyclic cleft while the Na^+ cation is too small and cannot bind symmetrically to all four pyrrolide rings of the macrocycle.

Complex **22** may be regarded as a synthon for a U(III)/U(III) Pacman complex with a vacant intermetallic site because the *endo* BH_4^- ligand is weakly bound, as evidenced by the abstraction of KBH_4 upon addition of 18-crown-6. As such, the reactivity of **22** towards the small molecules O_2, S_8, CO_2 and CS_2 was investigated. The reactions with the oxygen-containing reagents were rapid and unselective. However, the reactions with S_8 and CS_2 resulted in the formation of $[\{U(OAr)\}_2(\mu\text{-}S_2)(L^A)]$ (**25**) and $[\{U(OAr)\}_2(\mu\text{-}S)(L^A)]$ (**27**), respectively. The selectivity of these two transformations is unique; oxidation of U(III) by sulphur usually forms a bridging sulphide and previously only CS_2-complexation or thiocarbonate and thio-oxalate formation has been observed upon reaction of CS_2 with U(III) complexes.[44,84,89] The unusual reactivity of **22** is attributed to the uniquely restrictive steric environment imposed by the Pacman macrocycle. It is concluded that the *endo* persulphide ion may be comfortably incorporated in **25** but further equivalents of sulphur cannot be taken up. Similarly the sulphide ion bridges the U(IV) centres effectively in **27** but in-cleft formation of the bulky thiocarbonate ion is disfavoured. Complex **27** can be converted into complex **25** by the addition of S_8, which is consistent with the reported reactivity of related U(III) systems.[47] The selectivity of the S_8 and CS_2 reactions compared to the O_2 and CO_2 reactions is likely due to the reduced affinity of uranium for sulphur *vs* oxygen and the lower strength of the U-S bond compared to the U-O bond. Upon introduction of a sulphur based oxidant, the strong U-N(macrocycle) and U-O(aryloxide) bonds are maintained thereby directing the substrate to the intermetallic cleft where good steric control is exerted on the reactivity. However, the addition of excess O-based oxidants may compromise the integrity of the uranium Pacman complex and result in demetallation or decomposition.

As was observed with the chromium Pacman complexes of the *ortho*-phenyl macrocycle, the uranium Pacman complexes of the anthracenyl macrocycle also display impressive flexibility. U···U separations ranging from 4.1927(3) Å to 6.5881(3) Å have been measured and many different *endo* ligands and bridging modes have been observed. One theme which has emerged in this work is the effect of varying the alkali metal cation on reaction outcome. Thus metallation was only achieved using UI_3 in combination with the potassium salt of the ligand, K_4L^A, while UCl_4 only reacted successfully with the lithium salt, Li_4L^A. $[U(BH_4)_3(THF)_2]$ underwent successful metallation with all three alkali metal salts of the anthracene ligand, though the products were different for Li and Na compared to K, but only reacted with the lithium salt of the *ortho*-phenyl macrocycle, Li_4L^{Me}. The speed of crystallisation of the aryloxide complexes **22** and **23** was determined by the goodness of fit of the K^+ or Na^+ cation within the macrocyclic cleft; **22** crystallised in hours while **23** required weeks and the Li^+ analogue could not be prepared. While it may be difficult to predict the effect of changing the alkali metal counterion, the work described in this chapter reinforces the importance, and subtlety, of cation selection in uranium chemistry.

3.7 References

(1) N. N. Greenwood, A. Earnshaw *Chemistry of the Elements*; 2nd ed.; Butterworth-Heinemann, 1997.

(2) M. R. MacDonald, M. E. Fieser, J. E. Bates, J. W. Ziller, F. Furche, W. J. Evans, *J. Am. Chem. Soc.,* **2013**, *135,* 13310.

(3) H. S. La Pierre, A. Scheurer, F. W. Heinemann, W. Hieringer, K. Meyer, *Angew. Chem.,* **2014**, *126*, 7286.

(4) N. Kaltsoyannis, P. Scott *The f elements*; Oxford University Press, 1999.

(5) J. C. Renshaw, L. J. C. Butchins, F. R. Livens, I. May, J. M. Charnock, J. R. Lloyd, *Environ. Sci. Technol.,* **2005**, *39*, 5657.

(6) P. L. Arnold, J. B. Love, D. Patel, *Coord. Chem. Rev.,* **2009**, *253*, 1973.

(7) D. C. Moody, J. D. Odom, *J. Inorg. Nucl. Chem.,* **1979**, *41*, 533.

(8) W. G. Van der Sluys, C. J. Burns, A. P. Sattelberger, *Organometallics,* **1989**, *8,* 855.

(9) *Synthesis of Lanthanide and Actinide Compounds*; G. Meyer, L. R. Morss, Eds.; Springer Netherlands, 1991.

(10) D. Brown, J. Edwards, *J. Chem. Soc., Dalton Trans.,* **1972**, 1757.

(11) D. L. Clark, A. P. Sattelberger, S. G. Bott, R. N. Vrtis, *Inorg. Chem.,* **1989**, *28*, 1771.

(12) L. R. Avens, S. G. Bott, D. L. Clark, A. P. Sattelberger, J. G. Watkin, B. D. Zwick, *Inorg. Chem.,* **1994**, *33*, 2248.

(13) C. D. Carmichael, N. A. Jones, P. L. Arnold, *Inorg. Chem.*, **2008**, *47*, 8577.

(14) M. J. Monreal, R. K. Thomson, T. Cantat, N. E. Travia, B. L. Scott, J. L. Kiplinger, *Organometallics*, **2011**, *30*, 2031.

(15) M. Ephritikhine, *Dalton Trans.*, **2006**, 2501.

(16) K. W. Bagnall, D. Brown, P. J. Jones, J. G. H. Du Preez, *J. Chem. Soc.*, **1965**, 350.

(17) D. Baudry, E. Bulot, P. Charpin, M. Ephritikhine, M. Lance, M. Nierlich, J. Vigner, *J. Organomet. Chem.*, **1989**, *371*, 155.

(18) S. R. Daly, G. S. Girolami, *Inorg. Chem.*, **2010**, *49*, 5157.

(19) H. I. Schlesinger, H. C. Brown, *J. Am. Chem. Soc.*, **1953**, *75*, 219.

(20) V. V. Volkov, K. G. Myakishev, *Radiokhimiya*, **1980**, 745.

(21) D. Männig, H. Nöth, *Z. Anorg. Allg. Chem.*, **1986**, *543*, 66.

(22) H. J. Wasserman, D. C. Moody, R. R. Ryan, *J. Chem. Soc., Chem. Commun.*, **1984**, 532.

(23) B. M. Gardner, S. T. Liddle, *Eur. J. Inorg. Chem.*, **2013**, *2013*, 3753.

(24) A. R. Fox, S. C. Bart, K. Meyer, C. C. Cummins, *Nature*, **2008**, *455*, 341.

(25) P. Roussel, P. Scott, *J. Am. Chem. Soc.*, **1998**, *120*, 1070.

(26) F. G. N. Cloke, P. B. Hitchcock, *J. Am. Chem. Soc.*, **2002**, *124*, 9352.

(27) S. M. Mansell, N. Kaltsoyannis, P. L. Arnold, *J. Am. Chem. Soc.*, **2011**, *133*, 9036.

(28) A. L. Odom, P. L. Arnold, C. C. Cummins, *J. Am. Chem. Soc.*, **1998**, *120*, 5836.

(29) I. Korobkov, S. Gambarotta, G. P. A. Yap, *Angew. Chem., Int. Ed. Engl.*, **2002**, *41*, 3433.

(30) C. Elschenbroich *Organometallics*; 3rd ed.; WILEY-VCH, 2006.

(31) J. Parry, E. Carmona, S. Coles, M. Hursthouse, *J. Am. Chem. Soc.*, **1995**, *117*, 2649.

(32) W. J. Evans, S. A. Kozimor, G. W. Nyce, J. W. Ziller, *J. Am. Chem. Soc.*, **2003**, *125*, 13831.

(33) I. Castro-Rodriguez, K. Meyer, *J. Am. Chem. Soc.*, **2005**, *127*, 11242.

(34) O. T. Summerscales, F. G. N. Cloke, P. B. Hitchcock, J. C. Green, N. Hazari, *Science*, **2006**, *311*, 829.

(35) A. S. Frey, F. G. N. Cloke, P. B. Hitchcock, I. J. Day, J. C. Green, G. Aitken, *J. Am. Chem. Soc.*, **2008**, *130*, 13816.

(36) B. M. Gardner, J. C. Stewart, A. L. Davis, J. McMaster, W. Lewis, A. J. Blake, S. T. Liddle, *PNAS*, **2012**, *109*, 9265.

(37) O. T. Summerscales, F. G. N. Cloke, P. B. Hitchcock, J. C. Green, N. Hazari, *J. Am. Chem. Soc.*, **2006**, *128*, 9602.

(38) N. Tsoureas, O. T. Summerscales, F. G. N. Cloke, S. M. Roe, *Organometallics*, **2012**, *32*, 1353.

(39) J.-C. Berthet, J.-F. Le Maréchal, M. Nierlich, M. Lance, J. Vigner, M. Ephritikhine, *J. Organomet. Chem.*, **1991**, *408*, 335.

(40) I. Castro-Rodriguez, H. Nakai, L. N. Zakharov, A. L. Rheingold, K. Meyer, *Science*, **2004**, *305*, 1757.

(41) O. T. Summerscales, A. S. P. Frey, F. G. N. Cloke, P. B. Hitchcock, *Chem. Commun.*, **2008**, 200.

(42) O. P. Lam, S. C. Bart, H. Kameo, F. W. Heinemann, K. Meyer, *Chem. Commun.*, **2010**, *46*, 3137.

(43) A.-C. Schmidt, A. V. Nizovtsev, A. Scheurer, F. W. Heinemann, K. Meyer, *Chem. Commun.*, **2012**, *48*, 8634.

(44) V. Mougel, C. Camp, J. Pécaut, C. Copéret, L. Maron, C. E. Kefalidis, M. Mazzanti, *Angew. Chem., Int. Ed. Engl.*, **2012**, *51*, 12280.

(45) J. L. Brown, G. Wu, T. W. Hayton, *Organometallics*, **2012**, *32*, 1193.

(46) C. Camp, M. A. Antunes, G. Garcia, I. Ciofini, I. C. Santos, J. Pecaut, M. Almeida, J. Marcalo, M. Mazzanti, *Chem. Sci.*, **2014**, *5*, 841.

(47) S. M. Franke, F. W. Heinemann, K. Meyer, *Chem. Sci.*, **2014**, *5*, 942.

(48) O. P. Lam, F. W. Heinemann, K. Meyer, *Chem. Sci.*, **2011**, *2*, 1538.

(49) P. L. Arnold, J. H. Farnaby, R. C. White, N. Kaltsoyannis, M. G. Gardiner, J. B. Love, *Chem. Sci.*, **2014**, *5*, 756.

(50) P. L. Arnold, N. A. Potter, N. Magnani, C. Apostolidis, J.-C. Griveau, E. Colineau, A. Morgenstern, R. Caciuffo, J. B. Love, *Inorg. Chem.*, **2010**, *49*, 5341.

(51) A. M. J. Devoille PhD Thesis, University of Edinburgh, 2011.

(52) L. Maria, Â. Domingos, I. Santos, *Inorg. Chem.*, **2003**, *42*, 3323.

(53) B. M. Gardner, W. Lewis, A. J. Blake, S. T. Liddle, *Inorg. Chem.*, **2011**, *50*, 9631.

(54) D. P. Mills, F. Moro, J. McMaster, J. van Slageren, W. Lewis, A. J. Blake, S. T. Liddle, *Nat. Chem.*, **2011**, *3*, 454.

(55) F. H. Allen, *Acta Crystallogr., Sect. B: Struct. Sci.*, **2002**, *58*, 380.

(56) L. Natrajan, M. Mazzanti, J.-P. Bezombes, J. Pécaut, *Inorg. Chem.*, **2005**, *44*, 6115.

(57) L. Karmazin, M. Mazzanti, J. Pécaut, *Inorg. Chem.*, **2003**, *42*, 5900.

(58) M.-R. Spirlet, J. Rebizant, C. Apostolidis, E. Dornberger, B. Kanellakopulos, B. Powietzka, *Polyhedron*, **1996**, *15*, 1503.

(59) S. Fortier, J. L. Brown, N. Kaltsoyannis, G. Wu, T. W. Hayton, *Inorg. Chem.*, **2012**, *51*, 1625.

(60) A. J. Lewis, P. J. Carroll, E. J. Schelter, *J. Am. Chem. Soc.*, **2013**, *135*, 13185.

(61) D. L. Clark, S. D. Conradson, R. J. Donohoe, D. W. Keogh, D. E. Morris, P. D. Palmer, R. D. Rogers, C. D. Tait, *Inorg. Chem.*, **1999**, *38*, 1456.

(62) T. J. Marks, J. R. Kolb, *Chem. Rev.*, **1977**, *77*, 263.

(63) T. Arliguie, L. Belkhiri, S.-E. Bouaoud, P. Thuéry, C. Villiers, A. Boucekkine, M. Ephritikhine, *Inorg. Chem.*, **2008**, *48*, 221.

(64) T. Arliguie, M. Lance, M. Nierlich, J. Vigner, M. Ephritikhine, *J. Chem. Soc., Chem. Commun.*, **1994**, 847.

(65) N. Edelstein, *Inorg. Chem.*, **1981**, *20*, 297.

(66) D. D. Schnaars, G. Wu, T. W. Hayton, *Dalton Trans.*, **2008**, 6121.

(67) E. Tomat, L. Cuesta, V. M. Lynch, J. L. Sessler, *Inorg. Chem.*, **2007**, *46*, 6224.

(68) G. Givaja, M. Volpe, J. W. Leeland, M. A. Edwards, T. K. Young, S. B. Darby, S. D. Reid, A. J. Blake, C. Wilson, J. Wolowska, E. J. L. McInnes, M. Schröder, J. B. Love, *Chem. Eur. J.*, **2007**, *13*, 3707.

(69) J. W. Leeland PhD Thesis, University of Edinburgh, 2011.

(70) R. R. Ryan, K. V. Salazar, N. N. Sauer, J. M. Ritchey, *Inorg. Chim. Acta*, **1989**, *162*, 221.

(71) E. R. Bernstein, W. C. Hamilton, T. A. Keiderling, S. J. La Placa, S. J. Lippard, J. J. Mayerle, *Inorg. Chem.*, **1972**, *11*, 3009.

(72) P. Charpin, M. Nierlich, D. Vigner, M. Lance, D. Baudry, *Acta Crystallogr., Sect. C: Cryst. Struct. Commun.*, **1987**, *43*, 1465.

(73) W. G. Van der Sluys, C. J. Burns, J. C. Huffman, A. P. Sattelberger, *J. Am. Chem. Soc.*, **1988**, *110*, 5924.

(74) I. Castro-Rodriguez, H. Nakai, P. Gantzel, L. N. Zakharov, A. L. Rheingold, K. Meyer, *J. Am. Chem. Soc.*, **2003**, *125*, 15734.

(75) H. Nakai, X. Hu, L. N. Zakharov, A. L. Rheingold, K. Meyer, *Inorg. Chem.*, **2004**, *43*, 855.

(76) C. Villiers, P. Thuery, M. Ephritikhine, *Acta Crystallogr., Sect. C: Cryst. Struct. Commun.*, **2006**, *62*, m275.

(77) F. Jaroschik, F. Nief, X.-F. Le Goff, L. Ricard, *Organometallics*, **2007**, *26*, 1123.

(78) P. Sirsch, N. L. N. Clark, L. a. Onuţ, R. P. L. Burchell, A. Decken, G. S. McGrady, A. Daoud-Aladine, M. J. Gutmann, *Inorg. Chem.*, **2010**, *49*, 11395.

(79) S. Trzaska, F. Olbrich, Private Communication.

(80) P. L. Arnold, C. J. Stevens, J. H. Farnaby, M. G. Gardiner, G. S. Nichol, J. B. Love, *J. Am. Chem. Soc.*, **2014**, *136*, 10218.

(81) S. M. Mansell, J. H. Farnaby, A. I. Germeroth, P. L. Arnold, *Organometallics*, **2013**, *32*, 4214.

(82) P. J. Fagan, J. M. Manriquez, E. A. Maatta, A. M. Seyam, T. J. Marks, *J. Am. Chem. Soc.*, **1981**, *103*, 6650.

(83) W. J. Evans, K. A. Miller, S. A. Kozimor, J. W. Ziller, A. G. DiPasquale, A. L. Rheingold, *Organometallics*, **2007**, *26*, 3568.

(84) J. G. Brennan, R. A. Andersen, A. Zalkin, *Inorg. Chem.*, **1986**, *25*, 1756.

(85) L. R. Avens, D. M. Barnhart, C. J. Burns, S. D. McKee, W. H. Smith, *Inorg. Chem.*, **1994**, *33*, 4245.

(86) A. R. Manning, L. O'Dwyer, P. A. McArdle, D. Cunningham, *J. Chem. Soc., Chem. Commun.*, **1992**, 897.

(87) B. Li, X. Tan, S. Xu, H. Song, B. Wang, *J. Organomet. Chem.*, **2008**, *693*, 667.

(88) W. Ren, H. Song, G. Zi, M. D. Walter, *Dalton Trans.*, **2012**, *41*, 5965.

(89) O. P. Lam, L. Castro, B. Kosog, F. W. Heinemann, L. Maron, K. Meyer, *Inorg. Chem.*, **2011**, *51*, 781.

(90) A. Bondi, *J. Phys. Chem.*, **1964**, *68*, 441.

(91) J. G. Brennan, R. A. Andersen, A. Zalkin, *Inorg. Chem.*, **1986**, *25*, 1761.

(92) E. K. Moltzen, K. J. Klabunde, A. Senning, *Chem. Rev.*, **1988**, *88*, 391.

(93) P. L. Arnold, G. M. Jones, Q.-J. Pan, G. Schreckenbach, J. B. Love, *Dalton Trans.*, **2012**, *41*, 6595.

(94) M. J. Monreal, R. J. Wright, D. E. Morris, B. L. Scott, J. T. Golden, P. P. Power, J. L. Kiplinger, *Organometallics*, **2013**, *32*, 1423.

(95) C. A. Secaur, V. W. Day, R. D. Ernst, W. J. Kennelly, T. J. Marks, *J. Am. Chem. Soc.*, **1976**, *98*, 3713.

(96) R. C. White PhD Thesis, University of Edinburgh, 2014.

(97) R. Thomson, C. Graves, B. Scott, J. Kiplinger, *J. Chem. Crystallogr.*, **2011**, *41*, 1241.

(98) R. K. Thomson, C. R. Graves, B. L. Scott, J. L. Kiplinger, *Inorg. Chim. Acta*, **2011**, *369*, 270.

(99) W. J. Evans, S. A. Kozimor, J. W. Ziller, *Polyhedron*, **2006**, *25*, 484.

(100) D. Patel, W. Lewis, A. J. Blake, S. T. Liddle, *Dalton Trans.*, **2010**, *39*, 6638.

(101) A. M. J. Devoille, P. Richardson, N. L. Bill, J. L. Sessler, J. B. Love, *Inorg. Chem.*, **2011**, *50*, 3116.

Chapter Four

Experimental Procedures

4.1 General methods and instrumentation

Unless otherwise stated all reactions were carried out under an atmosphere of dry N_2 using standard Schlenk and glovebox techniques. Solvents were dried by passage through a column of activated sieves (hexane), passage through a column of activated alumina (diethyl ether, THF, toluene), being refluxed over potassium and distilled (pyridine, benzene, 1,4-dioxane, DME) or being stirred over CaH_2 and distilled (fluorobenzene). All solvents were stored over freshly activated 4 Å molecular sieves and degassed prior to use. Deuterated solvents (C_6D_6, *d*$_8$-toluene, *d*$_8$-THF, *d*$_5$-pyridine) were refluxed over potassium or stirred over CaH_2 (CD_2Cl_2), then distilled, freeze-pump-thaw degassed three times and stored in a glovebox.

^{1}H NMR spectra were recorded on either Bruker AVA 400, AVA 500 or PRO 500 spectrometers at operating frequencies of 399.90 and 500.23 MHz and referenced internally to residual *protio* solvent resonances. Where the solvent is listed below as (THF/C_6D_6) the sample was dissolved in THF and a couple of drops of C_6D_6 were added to enable the spectrometer to lock the sample. A ^{1}H NMR spectrum was then acquired without suppression of the THF resonances since it was found that this could also result in suppression of sample signals. ^{7}Li, ^{11}B and ^{19}F NMR spectra were recorded on a Bruker PRO 500 spectrometer at operating frequencies of 194.71, 160.49 and 470.39 MHz respectively and were referenced to the external standards 1 M LiCl in D_2O, BF_3•OEt_2 and CCl_3F, respectively. ^{31}P{^{1}H} NMR spectra were recorded on a Bruker AVA 400 spectrometer at an operating frequency of 161.92 MHz and referenced to the external standard 85 % phosphoric acid.

IR spectra were acquired on a Jasco 410 FT-IR spectrophotometer as nujol mulls between KBr or BaF_2 plates (w = weak, m = medium, s = strong intensity). Variable temperature magnetic measurements (SQUID) and EPR spectroscopy were carried out by Dr Floriana Tuna and Prof. Eric McInnes at the National EPR service at Manchester University. Elemental analyses were performed by Mr Stephen Boyer at London Metropolitan University.

H_4L^{Me},[1] H_4L^{A},[2] $[Cr(N'')_2(THF)_2]$,[3] UI_3,[4] $UI_3(dioxane)_{1.5}$,[5] $UCl_4(THF)_x$,[6] xylyl isocyanide,[7] and $[Na(THF)_2][B\{(OC_6H_2(^tBu)_2)_2\}_2]$[8] were synthesised by published methods. $[NEt_3H][BPh_4]$ was synthesized by reaction of NEt_3.HCl with $NaBPh_4$ in water and recrystallised from methanol. NaN″ and KN″ were synthesised by reaction of NaH or KH with $HN(SiMe_3)_2$ in toluene followed by toluene recrystallisation. NaH and KH were purchased as dispersions in mineral oil and washed with hexane before use. LiN″ was

purchased from Alfa Aesar and recrystallised from hexane before use. *Tert*-butyl isocyanide was purchased from Sigma Aldrich, dried over activated 4 Å molecular sieves, distilled and degassed prior to use. Naphthalene, 2,4,6-tri-*tert*-butylphenol, 1,2-dimethylimidazole, $Si(SiMe_3)_4$, tri-*tert*-butylbenzene, KO^tBu and NaO^tBu were sublimed before use. $NaBH_4$ and K(acac) were dried at 100 °C for 16 h. K(OTtbp) was donated by Rebecca White who synthesised it by reaction of HOTtbp with K metal in THF. Anhydrous $CrCl_2$, $OPPh_3$, I_2, EtMgBr (1.0 M in THF), $ZnEt_2$ (1.0 M in hexanes), 18-crown-6, adamantyl azide, DMAP, KCp*, $[CPh_3][B(Ar^F)_4]$ and $MgMe_2$ were purchased and used without further purification.

4.2 Synthetic procedures for Chapter Two: Chromium Pacman Complexes

Note on reporting of NMR data: Due to their paramagnetism, the ^{1}H NMR spectra of Cr(II) and Cr(III) complexes display only extremely contact-shifted and broadened resonances. Spectral data are recorded only to allow the differentiation of the various Cr(II) and Cr(III) complexes and are not exhaustively analysed. Width at half-height, $W_{½}$, values are given for those resonances for which they can be accurately determined; otherwise the resonances are simply described as "very broad" (v br). It is often not possible to reliably integrate the resonances and no attempt is made to assign specific environments since for no single complex are the required number of ligand proton environments observed.

4.2.1 Synthesis of $[Cr_2(L^{Me})]$, 1

Method A: A solution of $[Cr(N'')_2(THF)_2]$ (390 mg, 0.754 mmol) in toluene (10 mL) was added to a solution of H_4L^{Me} (250 mg, 0.378 mmol) in toluene (10 mL). The resulting brown solution was stirred for 2 h and then stored at -30 °C overnight to afford the product as dark brown microcrystals which were isolated by filtration, washed with hexane (2 x 3 mL) and dried under vacuum. The filtrate was concentrated to afford a second crop. Combined yield: 206 mg, 72 %.

Method B: A solution of KN'' (2.52 g, 12.63 mmol) in THF (30 mL) was added to a stirred solution H_4L^{Me} (2.09 g, 3.16 mmol) in THF (50 ml). The mixture was stirred for 16 h and then transferred onto a suspension of $CrCl_2$ (0.78 g, 6.35 mmol) in THF (40 mL). The dark red mixture was stirred for a further 24 h before being filtered. The volatiles were removed from the filtrate and the resulting brown solid dried overnight under reduced pressure. The solid was extracted with hot toluene (150 mL). The filtrate was concentrated to quarter volume and stored at −30 °C to afford the product as dark brown crystals which were

isolated by filtration, washed with hexane (2 x 15 mL) and dried under vacuum. Yield: 1.73 g, 72 %.

^{1}H NMR (d_5-pyridine): δ 16.9 (br, $W_{½}$ 1084 Hz, 4H), 14.0 (br, $W_{½}$ 838 Hz, 4H), 6.7 (br, $W_{½}$ 142 Hz, 12H), −29.2 (br, $W_{½}$ 400 Hz, 4H), −97.7 (br, $W_{½}$ 868 Hz, 4H) ppm. **^{1}H NMR (THF/C_6D_6):** δ 21.1 (br, $W_{½}$ 649, 4H), 14.9 (br, $W_{½}$ 444 Hz, 6H), 5.81 (br $W_{½,}$ 130 Hz, 12H), −44.1 (br, $W_{½}$ 438 Hz, 4H), −58.9 (br, $W_{½}$ 745 Hz, 4H) ppm. **^{1}H NMR (C_6D_6):** δ 18.0 (br, $W_{½}$ 978 Hz, 6H), 4.2 (br, $W_{½}$ 185 Hz, 24H), −22.7 (br, $W_{½}$ 643 Hz, 4H), −35.3 (br, $W_{½}$ 949 Hz, 4H) ppm. **Evans' method magnetic moment (THF/C_6D_6, 298 K):** 6.34 μ_B. **Elemental Analysis:** Found: C, 66.10: H, 5.17; N, 14.68 %, $C_{42}H_{40}Cr_2N_8$ requires: C, 66.30; H, 5.30; N, 14.73 %. Single crystals suitable for X-ray diffraction analysis were obtained from a saturated benzene solution.

Author's note: Method B is preferred due to the low literature yield of $Cr(N'')_2(THF)_2$ and its extreme air and moisture sensitivity.

4.2.2 Synthesis of $[Cr_2(L^A)]$, 2

A purple solution of $[Cr(N'')_2(THF)_2]$ (270 mg, 0.522 mmol) in THF (5 mL) containing a small quantity of decomposed solids was filtered onto a solution of H_4L^A (165 mg, 0.192 mmol) in THF (5 mL) and the resulting red suspension stirred overnight. The supernatant was decanted and the remaining solid washed with toluene (3 mL) and dried under reduced pressure to afford the product as a red powder. Yield: 110 mg, 60 %.

^{1}H NMR (C_6D_6): δ 26 (v br), 14 (v br), 11 (v br), 9 (v br), 6 (v br), 3.64 (br, $W_{½}$ 115 Hz, THF), 1.66 (br, $W_{½}$ 23 Hz, THF), −50 (v br), −56 (v br) ppm. **Elemental Analysis:** Found: C, 72.29: H, 5.19; N, 11.46 %, $C_{58}H_{48}Cr_2N_8$ requires: C, 72.49; H, 5.03; N, 11.66 %. Single crystals suitable for X-ray diffraction analysis were obtained from an NMR scale reaction in THF.

Author's note: Although $[Cr_2(L^A)]$ precipitates from THF solution, once dry, it may be re-dissolved to form a dilute solution in C_6D_6.

4.2.3 Synthesis of $[Cr_2(OPPh_3)_2(L^{Me})]$, 3

Toluene (10 mL) was added to a dry mix of $[Cr_2(L^{Me})]$ (140 mg, 0.18 mmol) and triphenylphosphine oxide (105 mg, 0.38 mmol). The mixture was stirred for 2 h, during which time a dark red microcrystalline solid formed, and then stored at −30 °C overnight. The red crystals were isolated, washed with hexane (3 x 3 mL) and dried under vacuum. Yield: 153 mg, 63 %.

^{1}H NMR (C_6D_6): δ 17.6 (br, $W_{½}$ 870 Hz), 7.7 (br, $W_{½}$ 218 Hz), 6.9 (br, $W_{½}$ 34 Hz), 4.6 (br, $W_{½}$ 154 Hz), −26 (br, $W_{½}$ 978 Hz), −42 (v br) ppm. **^{1}H NMR (THF/C_6D_6):** δ 17.9 – 16.9 (2

overlapping, br, [$Cr_2(L^{Me})$]), 7.46 (br, $W_{½}$ 31 Hz, Ph-H, free $OPPh_3$), 7.13 (s, Ph-H, free $OPPh_3$), 6.1 (br, $W_{½}$ 116 Hz, Ph-H, free $OPPh_3$), −41.2 (br, $W_{½}$ 440 Hz, [$Cr_2(L^{Me})$]), −64 (br, $W_{½}$ 624 Hz, [$Cr_2(L^{Me})$]) ppm. **$^{31}P\{^1H\}$ NMR (C_6D_6):** no resonances observed. **$^{31}P\{^1H\}$ NMR (d_8-THF):** no resonances observed. **$^{31}P\{^1H\}$ NMR (d_8-THF), 203 K:** δ 24 (br, $W_{½}$ 4245 Hz, free $OPPh_3$) ppm. **Elemental Analysis:** Found: C, 70.81; H, 5.45; N, 8.40 %, $C_{78}H_{70}Cr_2N_8O_2P_2$ requires: C, 71.11; H, 5.36; N, 8.51 %. Single crystals suitable for X-ray diffraction analysis were obtained from an NMR scale reaction in toluene.

4.2.4 Synthesis of [Cr_2(μ-CNXyl)(L^{Me})], 4

A solution of xylyl isocyanide (35 mg, 0.27 mmol) in benzene (5 mL) was added to a dark brown suspension of [$Cr_2(L^{Me})$] (200 mg, 0.26 mmol) in benzene (5 mL). The resultant dark green mixture was stirred and briefly refluxed to ensure complete dissolution of [$Cr_2(L^{Me})$]. On standing overnight dark red crystals formed which were isolated, washed with hexane (2 x 3 mL) and dried under vacuum. Yield: 170 mg, 73 %.

^1H NMR (C_6D_6 or THF/C_6D_6): no resonances observed. **^1H NMR (d_5-pyridine):** resonances corresponding to [$Cr_2(L^{Me})$] observed, δ 1.8 (br, free CNXyl) ppm. **IR (nujol mull, KBr):** ν (C≡N) 1990, 1970 cm^{-1}. **Elemental Analysis:** Found: C, 68.45; H, 5.42; N, 13.96 %, $C_{51}H_{49}Cr_2N_9$ requires: C, 68.67; H, 5.54; N, 14.13 %. Single crystals suitable for X-ray diffraction analysis were obtained from an NMR scale reaction carried out in fluorobenzene.

4.2.5 Synthesis of [Cr_2(μ-CN^{t}Bu)(L^{Me})], 5

A solution of *tert*-butyl isocyanide in benzene (5 mL, 1.1 M) was added by syringe to a suspension of [$Cr_2(L^{Me})$] (270 mg, 0.35 mmol) in benzene (15 mL) in a Teflon-tapped ampoule and the mixture refluxed for 48 h. The resultant deep red solution was filtered and the filtrate dried under vacuum forming a sticky red solid. This was washed with hexane (2 x 5 mL) and dried under reduced pressure to afford the product as a red powder. Yield: 250 mg, 83 %.

^1H NMR (C_6D_6): δ 20 (br, $W_{½}$ 3607 Hz), 2.3 (br), −50 (br, $W_{½}$ 4600 Hz) ppm. **IR (nujol mull, KBr):** ν(C≡N) 2150 cm^{-1}. **Evans' method magnetic moment (C_6D_6, 298 K):** 4.75 μ_B. **Elemental Analysis:** Found: C, 66.78; H, 5.81; N, 14.86 %, $C_{47}H_{49}Cr_2N_9$ requires: C, 66.89; H, 5.85; N, 14.94 %. Single crystals suitable for X-ray diffraction analysis were obtained from an NMR scale reaction in a THF/C_6D_6 mixture.

4.2.6 Reactions of $[Cr_2(L^{Me})]$, 1, with Lewis bases

4.2.6.1 PPh_3

$[Cr_2(L^{Me})]$ (9 mg, 0.012 mmol) and PPh_3 (7 mg, 0.027 mmol) were combined in C_6D_6 (0.5 mL) in a Teflon-tapped NMR tube, forming a brown suspension. **^{1}H NMR (C_6D_6):** δ 7.39 (br, 10H, Ph-H), 7.16 (br, 5H, *para*-Ph-H), 7.04 (br, 10H, Ph-H) ppm. **^{31}P{^{1}H} NMR (C_6D_6):** δ 4.3 (br, $W_{½}$ 1617 Hz, $\underline{P}Ph_3$) ppm.

A few drops of THF were added to dissolve the suspension forming a red-brown solution. **^{1}H NMR (THF/C_6D_6):** δ 20.1 (br, $[Cr_2(L^{Me})]$), 15.5 (br, $[Cr_2(L^{Me})]$), 7.23-7.10 (m, PPh_3), 5.9 (br, $[Cr_2(L^{Me})]$), 3.54 (br, THF), 1.57 (br, THF), −43.8 (br, $[Cr_2(L^{Me})]$), −59.4 (br, $[Cr_2(L^{Me})]$) ppm. **^{31}P{^{1}H} NMR (THF/C_6D_6):** δ 2.8 (br, $W_{½}$ 537 Hz, $\underline{P}Ph_3$) ppm.

4.2.6.2 PMe_3

Excess PMe_3 (0.1 mL, 1.0 M in toluene)was added to a suspension of $[Cr_2(L^{Me})]$ (11 mg, 0.014 mmol) in C_6D_6 (0.5 mL) in a Teflon-tapped NMR tube forming a red-brown suspension. **^{1}H NMR (C_6D_6):** δ 7.13-7.02 (m, $\underline{Ph}$Me), 2.11 (s, Ph$\underline{Me}$), 1.83 (br, $W_{½}$ 60 Hz, PMe_3) ppm. **^{31}P{^{1}H} NMR (C_6D_6):** no resonances observed.

A few drops of THF were added to dissolve the suspension forming a red-brown solution. **^{1}H NMR (THF/C_6D_6):** δ 19.9 (br, $[Cr_2(L^{Me})]$), 14.3 (br, $[Cr_2(L^{Me})]$), 7.09-7.00 (m, $\underline{Ph}$Me), 5.8 (br, $[Cr_2(L^{Me})]$), 3.58 (br, THF), 2.12 (s, Ph$\underline{Me}$), 1.57 (br, THF), −40.4 (br, $[Cr_2(L^{Me})]$), −62.2 (br, $[Cr_2(L^{Me})]$) ppm. **^{31}P{^{1}H} NMR (THF/C_6D_6):** no resonances observed.

4.2.6.3 1,2-dimethylimidazole

Excess 1,2-dimethylimidazole (9 mg, 0.094 mmol) was added to a solution of $[Cr_2(L^{Me})]$ (11 mg, 0.014 mmol) in THF/C_6D_6 (0.5 mL). A brown precipitate formed immediately. The reaction was repeated in d_5- pyridine. **^{1}H NMR (d_5-pyridine):** δ 16.7 (br, $[Cr_2(L^{Me})]$), 14.0 (br, $[Cr_2(L^{Me})]$), 8.76 (br, $W_{½}$ 53 Hz, py), 7.22 (m, imidazole-H and py), 6.62 (br, $W_{½}$ 147 Hz, py), 3.40 (br, $W_{½}$ 24 Hz, N-Me), 2.80 (br, $W_{½}$ 69 Hz, C-Me), −28.8 (br, $[Cr_2(L^{Me})]$), −98.5 (br, $[Cr_2(L^{Me})]$) ppm.

4.2.6.4 Adamantyl azide

Adamantyl azide (7 mg, 0.039 mmol) was added to a solution of $[Cr_2(L^{Me})]$ (14 mg, 0.018 mmol in THF/C_6D_6 (0.5 mL) in a Teflon-tapped NMR tube. The red-brown solution turned dark brown. **^{1}H NMR (THF/C_6D_6):** only solvent resonances observed, adamantyl proton region obscured by THF solvent. The sample was layered with hexane in the NMR tube but single crystals were not obtained.

4.2.7 Reactions of $[Cr_2(L^{Me})]$, 1, with gases

4.2.7.1 CO_2

$[Cr_2(L^{Me})]$ (13 mg, 0.017 mmol) was dissolved in THF (0.5 mL) in a Teflon-tapped NMR tube and one drop of C_6D_6 was added as a reference. The mixture was freeze-pump-thaw degassed three times and then an atmosphere of CO_2 (1.0 bar) was introduced and the tube shaken vigorously. No colour change was observed. ^{1}H NMR spectra were acquired immediately, after 4 h and after heating the mixture at 70 °C for 4 h. In all cases only resonances corresponding to $[Cr_2(L^{Me})]$ were observed.

4.2.7.2 CO

$[Cr_2(L^{Me})]$ (12 mg, 0.016 mmol) was dissolved in THF (0.5 mL) in a Teflon-tapped NMR tube and one drop of C_6D_6 was added as a reference. The mixture was freeze-pump-thaw degassed three times and then an atmosphere of CO (1.0 bar) was introduced and the tube shaken vigorously. No colour change was observed. The ^{1}H NMR spectra acquired immediately and after 24 h showed only resonances corresponding to $[Cr_2(L^{Me})]$.

4.2.7.3 O_2

$[Cr_2(L^{Me})]$ (12 mg, 0.016 mmol) was dissolved in d_5-pyridine (0.5 mL) in a Teflon-tapped NMR tube. The mixture was freeze-pump-thaw degassed three times and then an atmosphere of O_2 (1.0 bar) was introduced and the tube shaken vigorously. No obvious colour change was noted and no precipitate formed. Only solvent resonances were observed in the ^{1}H NMR spectrum.

4.2.7.4 H_2

$[Cr_2(L^{Me})]$ (103 mg, 0.135 mmol) was dissolved in THF (7 mL) in a Teflon-tapped ampoule. The red-brown solution was freeze-pump-thaw degassed three times and then an atmosphere of H_2 (1.0 bar) was introduced and the ampoule shaken vigorously. The solution was stirred for 1 week. No colour change was observed.

4.2.8 Reactions of $[Cr_2(L^{Me})]$, 1, with reducing agents

4.2.8.1 KC_8

$[Cr_2(L^{Me})]$ (11 mg, 0.014 mmol) was dissolved in THF (0.5 mL) in a Teflon-tapped NMR tube and one drop of C_6D_6 was added as a reference. KC_8 (4 mg, 0.030 mmol) was added and the mixture changed from dark red to dark brown. The ^{1}H NMR spectrum showed only solvent resonances, no resonances corresponding to a chromium compound were observed.

4.2.8.2 K metal

$[Cr_2(L^{Me})]$ (18 mg, 0.024 mmol) was dissolved in THF (0.5 mL) in a Teflon-tapped NMR tube, with a drop of C_6D_6 added. Excess K metal (13 mg, 0.332 mmol) was added and the mixture was heated at 80 °C for 16 h in order to melt the potassium. After this time copious black precipitate formed in the NMR tube, precluding NMR analysis.

4.2.8.3 K metal/ naphthalene

K metal (15 mg, 0.384 mmol), naphthalene (55 mg, 0.429 mmol) and 18-crown-6 (105 mg, 0.398 mmol) were dissolved in THF (15 mL) and transferred onto a stirred solution of $[Cr_2(L^{Me})]$ (140 mg, 0.184 mmol) in THF (15 mL). Pale brown precipitate formed within 15 min. This was allowed to settle and the supernatant decanted and layered with hexane (15 mL). A brown solid formed which was isolated, washed with hexane (5 mL) and dried under reduced pressure to yield 96 mg of brown powder. The identity of the product(s) is unknown; various recrystallisation attempts were unsuccessful. **^{1}H NMR (d_5-pyridine):** only solvent resonances observed.

4.2.9 Synthesis of $[Cr_2(\mu\text{-}I)(I)(THF)(L^{Me})]$, 6

THF (15 mL) was added to a dry mix of $[Cr_2(L^{Me})]$ (490 mg, 0.644 mmol) and iodine crystals (165 mg, 0.650 mmol) in a Schlenk tube and the mixture was stirred for 16 h, during which time the solution changed colour from brown to deep red. The solution was filtered and the volatiles removed from the filtrate under reduced pressure to leave a sticky red solid, which was washed with hexane (2 x 10mL) and dried to afford the product as a microcrystalline red powder. Yield: 585 mg, 84 %.

^{1}H NMR (THF/C_6D_6): δ 24 (v br), 17 (v br), 14 (v br), 5.9, 4.3, 3.6 (overlapped, br), 1.4 (br, THF), −55 (v br), −58 (v br), −67 (v br) ppm. **Evans' method magnetic moment (THF/C_6D_6, 298 K):** 5.43 μ_B. **Elemental Analysis:** Found: C, 50.94; H, 4.35; N, 10.27 %, $C_{46}H_{48}Cr_2I_2N_8O$ requires: C, 50.84; H, 4.45; N, 10.31 %. Single crystals suitable for X-ray diffraction analysis were obtained by vapour diffusion of hexane into a THF solution of $[Cr_2(\mu\text{-}I)(I)(THF)(L^{Me})]$.

4.2.10 Synthesis of $[Cr_2(\mu\text{-}I)(py)_2(L^{Me})][I]$, 7

Pyridine (15 mL) was added to a Schlenk containing $[Cr_2(L^{Me})]$ (265 mg, 0.348 mmol) and iodine crystals (90 mg, 0.355 mmol) and the mixture was stirred for 1 h forming a purple-red solution containing a bronze suspension. The solid was allowed to settle and then isolated, washed with hexane (5 mL) and dried under reduced pressure. Yield: 205 mg, 50 %.

No ^{1}H NMR data were obtained for the product due to its poor solubility. **Elemental Analysis:** Found: C, 53.14; H, 4.25; N, 11.87 %, $C_{55}H_{50}Cr_2I_2N_{10}$ requires: C, 53.25; H, 4.30; N, 11.94 %. Single crystals suitable for X-ray diffraction analysis, though of poor quality, were obtained by slow diffusion of a pyridine solution of [$Cr_2(L^{Me})$] into a pyridine solution of iodine at ambient temperature over 48 h.

4.2.11 Synthesis of [Cr_2(μ-I)(py)$_2$(L^{Me})][B{($OC_6H_2(^tBu)_2)_2$}$_2$], 8

Pyridine (15 mL) was added to a Schlenk containing [$Cr_2(L^{Me})$] (128 mg, 0.168 mmol) and iodine crystals (43 mg, 0.169 mmol) and the mixture was stirred for 2 h forming a purple-red solution containing a bronze suspension. A solution of [$Na(THF)_2$][B{($OC_6H_2(^tBu)_2)_2$}$_2$] (192 mg, 0.168 mmol) in pyridine (5 mL) was added to the mixture. No change was observed until the mixture was briefly refluxed causing the bronze precipitate to dissolve and forming a red solution. After 16 h the solvent was removed under reduced pressure leaving a sticky red oil which was washed with hexane to remove residual pyridine and dried. The resulting powder was extracted with boiling toluene (10 mL) to exclude the NaI by-product. The extract was stored at −30 °C for 16 h to afford the product as a red solid, which was isolated, washed with hexane (5mL) and dried. The filtrate was concentrated to afford a second crop. Combined yield: 128 mg, 40 %.

^{1}H NMR (C_6D_6/THF): no resonances observed. **Elemental Analysis:** Found: C, 69.27; H, 6.93; N, 7.41 %, $C_{108}H_{130}BCr_2IN_{10}O_4$ requires: C, 69.22; H, 6.99; N, 7.47 %. Single crystals suitable for X-ray diffraction analysis were not obtained.

4.2.12 Reactions of [Cr_2(μ-I)(I)(THF)(L^{Me})], 6, with metal alkyls

4.2.12.1 $ZnEt_2$ in toluene

$ZnEt_2$ in hexane (0.6 mL, 1.0 M) was added dropwise to a red suspension of [Cr_2(μ-I)(I)(THF)(L^{Me})] (170 mg, 0.156 mmol) in toluene (10 mL),. The resulting green mixture was stirred for 2.5 h then concentrated to 3 mL. Hexane (3 mL) was added, the mixture was filtered and the filtrate stored at −30 °C. A small number of large, green crystals formed over 72 h. Single crystal X-ray diffraction analysis revealed that the composition of these crystals was [{Cr(Et)}$_2$(μ-IZnEt)(L^{Me})] (**9**). Bulk material was not isolated.

4.2.12.2 $ZnEt_2$ in pyridine

$ZnEt_2$ in hexane (0.2 mL, 1.0 M) was added dropwise to a solution of [Cr_2(μ-I)(I)(THF)(L^{Me})] (130 mg, 0.120 mmol) in pyridine (5 mL). The mixture was stirred for 16 h and then the solvent was removed under reduced pressure. The resultant red-brown solids were extracted with toluene (10 mL), the extract was concentrated to 2 mL and hexane (5

mL) was added. The mixture was filtered and the filtrate stored at −30 °C overnight. Clusters of green needles formed. The crystals were isolated and recrystallized from a THF/hexane mix at −30 °C to afford single crystals suitable for X-ray diffraction analysis. The composition of these crystals was found to be [{Cr(Et)}$_2$(*endo*-py)(L^{Me})] (**10**). Yield: 30 mg, 28 %. **Elemental Analysis:** Found: C, 68.19; H, 6.26; N, 13.97 %, $C_{51}H_{55}Cr_2N_9$ requires: C, 68.21; H, 6.17; N, 14.04 %. Attempts to carry out this reaction on a larger scale in order to isolate sufficient material for reactivity studies were unsuccessful; the reaction was found to be unrepeatable and no crystalline material was obtained again.

4.2.12.3 $MgMe_2$

THF (10 mL) was added to a dry mix of [Cr_2(μ-I)(I)(THF)(L^{Me})] (110 mg, 0.101 mmol) and $MgMe_2$ (3 mg, 0.055 mmol) forming a red solution containing white solids. This mixture was stirred vigorously for 2 d, filtered and the solvent removed under reduced pressure. The resulting sticky red solid was washed with hexane (5 mL) and dried. The ^{1}H NMR spectrum of the isolated material revealed that it was the starting material and that no reaction had taken place.

4.2.13 Synthesis of [{Cr(Et)}$_2$(*endo*-THF)(L^{Me})], 11

A solution of EtMgBr in THF (1.30 mL, 1.0 M)was added to a red solution of [Cr_2(*μ*-I)(I)(THF)(L^{Me})] (690 mg, 0.634 mmol) in THF (15 mL). The resulting brown mixture was stirred for 45 min, during which time a pale precipitate formed, and then concentrated to one-third volume. Hexane (10 mL) was added and the mixture was stirred for 30 min, filtered and stored at −30 °C to afford the product as green-brown crystals. Yield: 215 mg, 38 %.

^{1}H NMR (C_6D_6): δ 21 (v br), 9.9 (br, $W_{½}$ 517Hz), 6.5 (br, $W_{½}$ 140 Hz) 5.3 (br, $W_{½}$ 190 Hz), 3.8 (v br), 2.55 (v br), -42 (v br) ppm. **^{1}H NMR (CD_2Cl_2):** δ 23.1 (v br), 15.1 (v br), 11.3 (v br), 7.1, 6.3 (br, overlapped), 5.4 (br, $W_{½}$ 177 Hz), 3.91 (br, $W_{½}$ 105 Hz, THF), 3.2 (v br) 1.95 (br, $W_{½}$ 37 Hz, THF), −36.6 (v br), −44.4 (v br) ppm. **Elemental Analysis:** Found: C, 67.31; H, 6.43; N, 12.55 %, $C_{50}H_{58}Cr_2N_8O$ requires: C, 67.40; H, 6.56; N, 12.58 %. The crystals obtained from the reaction mixture were suitable for single crystal X-ray diffraction analysis.

4.2.14 Reactions of [{Cr(Et)}$_2$(*endo*-THF)(L^{Me})], 11

4.2.14.1 CO

[{Cr(Et)}$_2$(*endo*-THF)(L^{Me})] (7 mg, 0.008 mmol) was dissolved in C_6D_6 (0.5 mL) to form a green-brown solution. The solution was freeze-pump-thaw degassed three times and then an

atmosphere of CO (1.0 bar) was introduced. No obvious colour change occurred. The ^{1}H NMR spectrum acquired after 6 h showed only starting material resonances.

4.2.14.2 H_2

[{Cr(Et)}$_2$(*endo*-THF)(L^{Me})] (13 mg, 0.014 mmol) was dissolved in C_6D_6 (0.5 mL) to form a green-brown solution. The solution was freeze-pump-thaw degassed three times and then an atmosphere of H_2 (1.0 bar) was introduced. No obvious colour change occurred. ^{1}H NMR spectra acquired after over 48 h showed only starting material resonances.

4.2.14.3 CH_2CH_2

[{Cr(Et)}$_2$(*endo*-THF)(L^{Me})] (13 mg, 0.014 mmol) was dissolved in C_6D_6 (0.5 mL) to form a green-brown solution. The solution was freeze-pump-thaw degassed three times and then an atmosphere of ethylene (1.0 bar) was introduced. No obvious colour change occurred. ^{1}H NMR spectra acquired after over 48 h showed only starting material resonances and dissolved ethylene. The solution gradually turned red over 2 weeks. **^{1}H NMR (CD_2Cl_2, 14 d):** δ 15.5 (v br), 7.7 (v br), 6.4 (v br), 5.41 (s, CH_2CH_2) 4.7, 4.2 (br, overlapped), 3.3 (v br), 1.8 (br, $W_{½}$ 40 Hz) ppm.

4.2.14.4 $[CPh_3][B(Ar^F)_4]$

[{Cr(Et)}$_2$(*endo*-THF)(L^{Me})] (12 mg, 0.013 mmol) and [CPh_3][B(Ar^F)$_4$] (12 mg, 0.013 mmol) were dissolved in CD_2Cl_2 (0.5 mL) forming a red-brown solution.

^{1}H NMR (CD_2Cl_2): δ 17.8, 16.1, 13.7 (overlapping, v br), 8.10 (br, $W_{½}$ 193 Hz), 7.30 (m, 8H, *meta* ArH, $HCPh_3$), 7.23 (m, 4H, *para* ArH, $HCPh_3$), 7.15 (d, $^{3}J_{HH}$ 5.20 Hz, 8H, *ortho* ArH, $HCPh_3$), 5.56 (s, 1h, $HCPh_3$), 5.41 (s, 1H, CH_2CH_2), 4.29 (br, $W_{½}$ 105 Hz), 2.64 (m, 1H), 2.30 (br, $W_{½}$ 226 Hz), 1.29 (m, 0.6H, hexane CH_2), 1.23 (m, 0.1 H), 0.90 (m, 0.5H, hexane CH_3), 0.87 (s, 0.4H, CH_3CH_3), 0.76 (m, 0.2H), −30.6 (v br), −40.6 (v br), −49.7 (v br) ppm. **^{11}B NMR (CD_2Cl_2):** δ −16.6 (s, [B(Ar^F)$_4$]$^-$) ppm. **^{19}F NMR (CD_2Cl_2):** δ −133.1 (s), −163.4 (s), −167.3 (s) ppm.

The sample was freeze-pump-thaw degassed three times and then an atmosphere of ethylene (1.0 bar) was introduced. The mixture turned red overnight.

^{1}H NMR (CD_2Cl_2, 16h): δ 35.5 (v br), 17.8, 16.10 (overlapping, br), 7.30 (m, 8H, *meta* ArH, $HCPh_3$), 7.23 (m, 4H, *para* ArH, $HCPh_3$), 7.15 (d, $^{3}J_{HH}$ 5.20 Hz, 8H, *ortho* ArH, $HCPh_3$), 5.56 (s, 1H, $HCPh_3$), 5.41 (s, 23H, CH_2CH_2), 5.1 (v br), 4.0 (v br), 2.64 (m, 0.2H), 1.99 (v br), 1.29 (m, 0.6H, hexane CH_2), 1.23 (m, 0.1H), 0.90 (m 0.5H, hexane CH_3), 0.87 (s, 2.4H, CH_3CH_3), 0.76 (m, 0.2H), −30.6 (v br), −53.7 (v br), −69.5 (v br) ppm.

The ^{19}F NMR spectrum was unchanged.

4.3 Synthetic procedures for Chapter Three: Uranium Pacman Complexes

Note on reporting of NMR data: Though U(III) and U(IV) by their paramagnetism induce broadening and contact-shifting of NMR resonances, this is to a far lesser extent than observed for the Cr(II) and Cr(III) complexes. Signals remain reasonably sharp and can be reliably integrated, though H-H coupling is not usually resolved. In most cases separate resonances are expected for every different ligand proton environment. Therefore the number and relative integrations of the resonances reveal the symmetry of the macrocyclic environment. Limited information can be deduced from the value of the chemical shift of each resonance so it is usually impossible to assign different ligand environments which have the same relative integration.

4.3.1 NMR scale reactions of UI_3 with K_4L^A

H_4L^A (9 mg, 0.010 mmol) and KN″ (9 mg, 0.045mmol) were combined in d_5-pyridine (0.5 mL) in a Teflon-tapped NMR tube. The mixture was allowed to stand for 10 min forming an orange suspension. Solid $UI_3(dioxane)_{1.5}$ (16 mg, 0.021 mmol) was added and the mixture turned dark green. **^{1}H NMR (d_5-pyridine):** δ 38.34 (s, 4H), 20.67 (s, 4H), 19.44 (s, 4H), 18.73 (s, 4H), 11.72 (s, 4H), 10.28 (s, 2H, ArH), 10.11 (s, 4H), 10.01 (s, 4H), 5.51 (s, 6H, *meso* Me), 3.63 (s, 37H, dioxane), 1.45 (s, 4H), 0.17 (s, 106H, $HN(SiMe_3)_2$), −2.09 (s, 6H, *meso* Me), −24.26 (s, 2H, ArH).

The reaction was repeated in THF/C_6D_6 and a very simillar product was observed to form by ^{1}H NMR spectroscopy. When the solvent was removed under reduced pressure, the solid remaining turned yellow-brown and could not be redissolved for NMR analysis, indicating that decomposition had occurred.

The reaction was repeated in THF. Hexane was slowly diffused into the sample in an attempt to crystallise the product. After 3 d a pale brown precipitate formed which could not be re-dissolved for NMR analysis.

4.3.2 Attempted scaled-up reactions of UI_3 with K_4L^A

Method A: A solution of KN″ (200 mg, 1.00 mmol) in pyridine (5mL) was added to a solution of H_4L^A (215 mg, 0.25 mmol) in pyridine (5 mL) and the mixture was stirred for 4 h before being transferred onto a suspension of $UI_3(THF)_4$ (453 mg, 0.50 mmol) in pyridine (10 mL). The dark green mixture was stirred for 16 h and then the solvent was removed under reduced pressure. The resulting sticky dark green solid was washed with hexane (3 x

10 mL) to remove residual pyridine and the green powder formed was dried. It was then extracted with hot toluene (20 mL) to separate the product from the KI by-product. Slow, continuous formation of pale yellow-green precipitate was observed in the extract. Considering that the product may be unstable in the absence of co-ordinating solvent, the toluene was removed under reduced pressure and the solids extracted with THF (10 mL). The extract was stored at −30 °C for 2 weeks, upon which a pale green precipitate formed which was isolated and dried. **^{1}H NMR (d_5-pyridine):** resonances corresponding to THF were observed in addition to many low intensity paramagnetic resonances that could not be assigned to a single product. None of the resonances corresponding to "$[(UI)_2(L^A)]$" were seen.

Method B: THF (20 mL) was added to a dry mix of H_4L^A (220 mg, 0.26 mmol) and KN″ (210 mg, 1.05 mmol) and the orange suspension stirred for 3 h before being transferred onto a suspension of $UI_3(dioxane)_{1.5}$ (339 mg, 0.51 mmol) in THF (5 mL). The dark green mixture was stirred (1 h), allowed to settle (1 h) and filtered. Pyridine (10 mL) was added to the filtrate in order to stabilise the product and the volatiles were removed under reduced pressure. The resulting sticky solid was dried for 16 h to yield a brown powder (353 mg). **^{1}H NMR (d_5-pyridine):** the resonances corresponding to "$[(UI)_2(L^A)]$" were observed but another set of resonances of roughly equal intensity to those of "$[(UI)_2(L^A)]$" were also present at δ 47.09 (s, 6H), 31.56 (s, 5H), 20.99 (s, 3H), 15.97 (s, 4H), 13.61 (s, 8H), 6.41 (s, 4H), 3.87 (s, 4H), −3.29 (s, 4H), −5.46 (s, 3H), −12.52 (s, 5H), −13.59 (s, 4H), −15.35 (s, 4H), −19.44 (s, 4H), −27.27 (s, 3H), −54.91 (s, 2H) ppm.

4.3.3 Attempted *in situ* reactions of "$[(UI)_2(L^A)]$", 12

The following reactions were carried out in either d_5-pyridine or in a THF/C_6D_6 mixture. When d_5-pyridine was used, a fresh sample of "$[(UI)_2(L^A)]$" was prepared as described in 4.3.1 above. Otherwise 0.5 mL portions of a 0.019 M stock solution of "$[(UI)_2(L^A)]$" in THF/C_6D_6 were used, which was prepared as follows: H_4L^A (150 mg, 0.17 mmol) and KN″ (140 mg, 0.70 mmol) were combined in THF (8.5 mL) and C_6D_6 (0.9 mL) and stirred for 15 min. $UI_3(dioxane)_{1.5}$ (230 mg, 0.35 mmol) was added and the mixture stirred for a further 15 min before being centrifuged at 4500 rpm for 10 min leaving a green solution and a compact brown precipitate. The solution was decanted and stored in the glovebox.

4.3.3.1 DMAP

DMAP (2 mg, 0.016 mmol) was added to a stock solution of "$[(UI)_2(L^A)]$" in THF/C_6D_6 (0.5 mL, 0.010 mmol) in a Teflon-tapped NMR tube. Green precipitate formed within 5 min. **^{1}H NMR (THF/C_6D_6):** no paramagnetic resonances were observed. The solvent was removed

under reduced pressure and the sample re-dissolved in d_5-pyridine. **^{1}H NMR (d_5-pyridine):** several low intensity paramagnetic resonances were observed which could not be assigned to one product.

4.3.3.2 KO^{t}Bu

KO^{t}Bu (2.5 mg, 0.022 mmol) was added to "[$(UI)_2(L^A)$]" (0.010 mmol) in d_5-pyridine (0.5 mL) in a Teflon-tapped NMR tube. **^{1}H NMR (d_5-pyridine):** several low intensity resonances were observed over the range δ 90 to −55 ppm which could not be assigned to one product.

4.3.3.3 LiCl

Excess LiCl (5 mg, 0.118 mmol) was added to a stock solution of "[$(UI)_2(L^A)$]" in THF/C_6D_6 (0.5 mL, 0.010 mmol) in a Teflon-tapped NMR tube. A large amount of microcrystalline green precipitate formed within 5 min. The volatiles were removed under reduced pressure and the solid re-dissolved in d_5-pyridine. **^{1}H NMR (d_5-pyridine):** several resonances were observed in the diamagnetic aromatic region as well as several low intensity paramagnetic resonances over the range δ 70 to −30 ppm.

4.3.3.4 NaBH$_4$

Excess $NaBH_4$ (5 mg, 0.132 mmol) was added to a stock solution of "[$(UI)_2(L^A)$]" in THF/C_6D_6 (0.5 mL, 0.010 mmol) in a Teflon-tapped NMR tube. No obvious colour change was noted. **^{1}H NMR (THF/C_6D_6):** δ 36.29 (s, 4H), 18.87 (s, 4H), 18.72 (s, 1H), 18.50 (s, 3H), 11.49 (d, $^3J_{HH}$ 7.79 Hz, 4H, pyrrole H), 11.25 (s, 4H), 10.85 (s, 2H), 10.61 (s, 1H), 10.05 (d, $^3J_{HH}$ 7.79 Hz, 4H, pyrrole H), 9.79 (s, 1H), 6.24 (s, 4H), 0.64 (s, 6H), −23.03 (s, 2H) ppm.

4.3.3.5 Sulphur

Excess S_8 (4 mg, 0.125 mmol) was added to a stock solution of "[$(UI)_2(L^A)$]" in THF/C_6D_6 (0.5 mL, 0.010 mmol) in a Teflon-tapped NMR tube. The solution immediately turned red-brown and a brown precipitate formed. The solvent was removed under reduced pressure and the solid re-dissolved in d_5-pyridine. **^{1}H NMR (d_5-pyridine):** many resonances were observed in the range δ 70 to −30 ppm, consistent with the formation of multiple paramagnetic products.

4.3.3.6 CO

A solution of "[$(UI)_2(L^A)$]" (0.010 mmol) in d_5-pyridine (0.5 mL) in a Teflon-tapped NMR tube was freeze-pump-thaw degassed three times and then an atmosphere of CO (1.0 bar) was introduced. **^{1}H NMR (d_5-pyridine, 15 min):** showed mainly "[$(UI)_2(L^A)$]" but several

new low intensity paramagnetic resonances were observed. A second spectrum acquired after 7 h was identical to the first. This indicates that some decomposition of the starting material occurred, probably due to ppm quantities of H_2O in the CO gas.

4.3.3.7 KC_8

KC_8 (3 mg, 0.022 mmol) was added to a solution of "$[(UI)_2(L^A)]$" (0.010 mmol) in d_5-pyridine (0.5 mL) in a Teflon-tapped NMR tube. **^{1}H NMR (d_5-pyridine, 15 min):** showed only "$[(UI)_2(L^A)]$". A second spectrum acquired after 3 d showed "$[(UI)_2(L^A)]$" and at least two new paramagnetic products of roughly equal intensity. A third spectrum acquired after 3 weeks was identical to the second.

4.3.4 Reactions between $UI_3(solvent)_x$ and $NaBH_4$

The trial reactions carried out and their results are summarised in Table 4.1. In all cases $UI_3(solvent)_x$ was combined with 3.3 equivalents of $NaBH_4$ in the stated solvent. For entries (1) – (4) (Table 4.1) the reaction mixture was stirred for 24 h after which no change had occurred and the mixture was discarded. $UI_3(dioxane)_{1.5}$ is only sparingly soluble in Et_2O so reaction mixture (5) was stirred for 16 h, during which the suspended solid gradually changed colour from blue to purple-red. When the solvent was added to a dry mix of the reagents in entry (6) there was an immediate colour change from deep blue to brown-red and complete dissolution of the solids. ^{1}H NMR spectra of the crude products of reactions (5) and (6) were recorded in d_8-THF.

Table 4.1 Summary of observed reactivity of $NaBH_4$ with different UI_3 starting materials.

	Starting material	Solvent	Likely product	Product solubility		δ $B\underline{H}_4$ (ppm)
				Soluble in	Insoluble in	
(1)	UI_3	toluene	no reaction	-	-	-
(2)	$UI_3(THF)_4$	toluene	no reaction	-	-	-
(3)	UI_3	Et_2O	no reaction	-	-	-
(4)	$UI_3(THF)_4$	Et_2O	no reaction	-	-	-
(5)	$UI_3(dioxane)_{1.5}$	Et_2O	$[U(BH_4)_3(dioxane)_x]$	THF	Et_2O	75
(6)	UI_3	THF	$[U(BH_4)_3(THF)_x]$	toluene Et_2O, THF	-	85

4.3.5 Synthesis of $[U(BH_4)_3(THF)_2]$, 14

THF (30 mL) was added to a dry mix of UI_3 (2.86 g, 4.62 mmol) and $NaBH_4$ (520 mg, 13.7 mmol) in a Schlenk tube. The resultant red mixture was stirred at ambient temperature for 1 h. The THF solvent was removed under vacuum and the solid residue dried overnight. The

crude reaction mixture was soxhlet-extracted into Et_2O (150 mL) at 65 °C for 6 h. The volatiles were removed under vacuum and the solid residue dried overnight to yield $[U(BH_4)_3(THF)_2]$ as a microcrystalline red solid. Yield: 1.75 g, 90 %.

^{1}H NMR (d_8-THF): δ 85 (br, $W_{½}$ 2152 Hz, BH_4) ppm. **^{11}B NMR (d_8-THF):** δ 232 (br, $W_{½}$ 2252 Hz, U-$\underline{B}H_4$) ppm. **^{1}H NMR (d_8-toluene):** δ 125 (12H, br, $W_{½}$ 499 Hz, BH_4), 5.17 (br, 14H, THF), 3.34 (br, 14H, THF) ppm. The degree of solvation was confirmed by NMR displacement reactions using DME (see 4.5.2 below) in C_6D_6, **^{1}H NMR (C_6D_6, 2 drops DME):** δ 98 (br, $W_{½}$ 2312 Hz, 12H, BH_4), 3.50 (m, 12H, THF), 3.26 (s, 200H, DME CH_2), 3.06 (s, 300H, DME CH_3), 1.46 (m, 12H, THF) ppm. **^{11}B NMR (C_6D_6, 2 drops DME):** δ 230 (br, $W_{½}$ 2258 Hz, U-$\underline{B}H_4$) ppm. **IR (nujol mull, BaF_2):** ν 2446 (s, $\nu_{B\text{-}Ht}$), 2205 and 2147 (s, $\nu_{B\text{-}Hb}$), 1162 (s, bridge deformation) cm^{-1}. **Elemental Analysis:** Found: C, 22.33; H, 6.51%, $C_8H_{28}B_3O_2U$ requires: C, 22.52; H, 6.61%.

4.3.6 Synthesis of $[Na(THF)_4][\{U(BH_4)\}_2(\mu\text{-}BH_4)(L^A)(THF)_2]$, 18

THF (30 mL) was added to a dry mix of H_4L^A (763 mg, 0.89 mmol) and NaN″ (650 mg, 3.54 mmol) in a Schlenk tube and the resulting orange suspension was stirred for 20 min before being transferred onto a stirred suspension of $[U(BH_4)_3(THF)_2]$ (760 mg, 1.78 mmol) in THF (15 mL). The brown-green mixture was stirred overnight and then the solvent was removed under reduced pressure leaving khaki solids which were extracted with THF (10 mL).The extract was stored at −30°C for 1 week to afford the product as dark green needles. Yield: 480 mg, 30%.

^{1}H NMR (d_8-THF): δ 35.14 (s, 4H), 18.52 (s, 4H), 15.83 (s, 4H), 11.08(s, 2H, Ar-H), 10.27 (d, $^3J_{HH}$ 8.3 Hz, 4H, pyrrole H), 10.05 (d, $^3J_{HH}$ 8.3 Hz, 4H, pyrrole H), 8.79 and 8.71 (overlapping, 8H), 5.15 (s, 6H, $CH_2C\underline{H}_3$), 4.64 (s, 4H), −0.14 (s, 6H, $CH_2C\underline{H}_3$), −13.60 (s, 2H, Ar-H), −70.1 (br, $W_{½}$ 498 Hz, terminal BH_4) ppm. **^{1}H{^{11}B} NMR (d_8-THF):** resonance at δ −70.1 ppm sharpens to $W_{½}$ 364 Hz. **^{11}B NMR (d_8-THF):** δ 212 (s, 1B, μ-BH_4), 207 (s, 2B, terminal BH_4) ppm. **IR (nujol mull, BaF_2):** ν(B-H) 2435 (w), 2313 (w), 2200 (w), 2144 (w) cm^{-1}. **Elemental Analysis:** Found: C, 53.59; H, 6.07; N, 6.17 %, $C_{82}H_{108}B_3N_8NaO_6U_2$ requires: C, 53.72; H, 5.94; N, 6.11 %.

4.3.7 Synthesis of crude $[Li(THF)_4][\{U(BH_4)\}_2(\mu\text{-}BH_4)(L^A)(THF)_2]$, 17

THF (15 mL) was added to a dry mix of UI_3 (458 mg, 0.74 mmol) and $LiBH_4$ (50 mg, 2.30 mmol) forming a dark red solution and a red microcrystalline solid. The mixture was stirred for 30 mins before being transferred onto an orange solution of Li_4L^A in THF (15 mL), formed *in situ* from H_4L^A (318 mg, 0.37 mmol) and LiN″ (250 mg, 1.49 mmol). The resultant green-brown solution was stirred for 16 h before the volatiles were removed under

reduced pressure to yield an oily dark green residue. This was extracted with toluene (10 mL) and the extract was stored at −30 °C for 1 week to afford 293 mg of dark green microcrystals contaminated with $LiBH_4$.

^{1}H NMR (THF/C_6D_6): δ 35.51 (s, 4H), 18.80 (s, 4H), 15.88 (s, 4H), 10.88 (s, 2H, Ar-H), 10.03 (s, 4H), 9.89 (s, 4H), 8.99 (s, 4H), 8.72 (s, 4H), 5.12 (s, 6H, *meso* $CH_2C\underline{H}_3$), 4.49 (s, 4H), 0.15 (1:1:1:1 q, $^1J_{BH}$ 80 Hz, 60H, $LiBH_4$), −0.09 (s, 6H, *meso* $CH_2C\underline{H}_3$), −12.70 (s, 2H, Ar-H), −69.4 (br, $W_{½}$ 527 Hz, terminal BH_4).

4.3.8 Synthesis of crude [{U(BH$_4$)}$_2$(μ-BH$_4$K)(L^A)(THF)$_2$], 19

THF (15 mL) was added to a dry mix of H_4L^A (390 mg, 0.45 mmol) and KN″ (362 mg, 1.81 mmol) forming an orange suspension, which was stirred for 15 min. It was then transferred onto a suspension of $[U(BH_4)_3(THF)_2]$ (390 mg, 0.91 mmol) in THF (10 mL) forming a green-brown mixture which was stirred for 2 h and then left to settle for 16 h. The mixture was filtered and the volatiles removed from the filtrate under reduced pressure yielding brown-green solids (642 mg) containing KN″ and HN″ in addition to **19**.

^{1}H NMR (d_8-THF): δ 38.28 (s, 4H), 31.8 (br, $W_{½}$ 441 Hz, terminal BH_4), 18.84 (s, 4H), 17.50 (s, 4H), 10.85 (d, $^3J_{HH}$ 8.70 Hz, 4H, pyrrole H), 10.69 (s, 4H), 9.77 (d, $^3J_{HH}$ 8.70 Hz, 4H, pyrrole H),9.65 (s, 4H), 6.11 (s, 6H, *meso* $CH_2C\underline{H}_3$), 0.13 (s, 12H, KN″), 0.05 (s, 24H, HN″), −0.13 (s, 6H, *meso* $CH_2C\underline{H}_3$), −18.40 (s, 2H, Ar-H) ppm. Two macrocycle resonances cannot be located. **^{1}H{^{11}B} NMR (d_8-THF):** resonance at δ 31.8 ppm sharpens to $W_{½}$ 376 Hz. **^{11}B NMR (d_8-THF):** δ 180 (s, terminal and bridging BH_4 overlapped) ppm.

4.3.9 Reaction of crude [{U(BH$_4$)}$_2$(μ-BH$_4$K)(L^A)(THF)$_2$], 19, with 18-crown-6

Crude $[\{U(BH_4)\}_2(\mu\text{-}BH_4K)(L^A)(THF)_2]$ (14 mg, 0.009 mmol) and excess 18-crown-6 (5 mg, 0.019 mmol) were combined in d_8-THF in a Teflon-tapped NMR tube. Green microcrystalline solid began to precipitate from the mixture immediately. As a result the ^{1}H NMR spectrum obtained was broad and of low intensity so some resonances could not be integrated reliably. **^{1}H NMR (d_8-THF):** δ 34.76 (s, 4H), 18.44 (s, 4H), 15.46 (s, 4H), 10.96 (s, 2H, Ar-H), 10.17 (s, 4H), 9.96 (s, 4H), 8.68(s, 4H), 8.42 (2, 4H), 4.88 (s, overlapped), 3.48 (s, overlapped, 18-crown-6), −0.23 (s, overlapped), −12.48 (s, 2H, Ar-H), −66.1 (br, 8H, terminal BH_4) ppm. **^{11}B NMR (d_8-THF):** δ 255 (br, 0.5B, unknown impurity), 211 (br, $W_{½}$ 208 Hz, 1B, μ-BH_4), 207 (br, $W_{½}$ 296 Hz, 2B, terminal BH_4) ppm.

4.3.10 Synthesis of [Li(THF)$_4$][{U(BH$_4$)}$_2$(μ-BH$_4$)(L^{Me})], 21

THF (20 mL)was added to a dry mix of H_4L^{Me} (410 mg, 0.62 mmol) and LiN″(415 mg, 2.48 mmol). The resulting brown solution was stirred for 10 min before being transferred onto a

stirred suspension of $[U(BH_4)_3(THF)_2]$ (530 mg, 1.24 mmol) in THF (20 mL). The dark red-brown mixture was stirred overnight during which time a small quantity of orange precipitate formed. The mixture was filtered, and the filtrate concentrated to 15 mL and stored at −30°C to afford the product as dark brown crystals. Yield: 220 mg, 24%.

^{1}H NMR (d_8-THF): δ 63.07 (br, $W_{½}$ 702 Hz, terminal BH_4), 50.66 (s, 4H), 33.88 (s, 4H), 30.50 (s, 4H), 8.25 (s, 6H, *meso* Me), −2.45 (s, 6H *meso* Me) −2.53 (s, 12H, aryl Me), −66.86 (s, 4H) ppm. **^{11}B NMR (d_8-THF):** δ 325 (s, 1B, bridging BH_4), 212 (s, 2B, terminal BH_4) ppm. **^{7}Li NMR (d_8-THF):** δ −1.1 (s, $[Li(THF)_4]$) ppm. **IR (nujol mull, BaF_2):** ν(B-H) 2414(w), 2333(w), 2193(w), 2124(w) cm^{-1}. **Elemental Analysis:** Found: C, 47.11; H, 5.55; N, 7.78 %, $C_{58}H_{84}B_3LiN_8O_4U_2$ requires: C, 47.30; H, 5.75; N, 7.61 %.

Author's Note: Isolated crystalline $[Li(THF)_4][\{U(BH_4)\}_2(\mu\text{-}BH_4)(L^{Me})]$ cannot be redissolved in THF so the resonances reported above are taken from a small scale reaction in a Teflon-tapped NMR tube to form the product *in situ*. Dissolving $[Li(THF)_4][\{U(BH_4)\}_2(\mu\text{-}BH_4)(L^{Me})]$ in pyridine results in decomposition.

4.3.11 Attempted ligand substitution reactions of $[Na(THF)_4][\{U(BH_4)\}_2(\mu\text{-}BH_4)(L^A)(THF)_2]$, 18, and $[\{U(BH_4)\}_2(\mu\text{-}BH_4K)(L^A)(THF)_2]$, 19

4.3.11.1 NaOAr (Ar = 2,4,6-$C_6H_2(^tBu)_3$)

Solid $[Na(THF)_4][\{U(BH_4)\}_2(\mu\text{-}BH_4)(L^A)(THF)_2]$ (13 mg, 0.007 mmol) and NaOAr (4 mg, 0.014 mmol) were combined in d_8-THF (0.5 mL) in a Teflon-tapped NMR tube forming a dark green solution. **^{1}H NMR (d_8-THF):** δ 45.9 (br, 4H), 38.5 (br, 4H), 24.0 (br, 4H), 23.0 (br, 2H), 20.1 (br, 10H), 18.2 (br, 2H), 16.9 (br, 2H), 15.5 (br, 4H), 8.58 (br, 4H), 6.89 (s, 14.5H, NaOAr Ar-H), 6.1 (br, 14H), 1.40 (s, 130H, NaOAr *o*-^{t}Bu), 1.22 (s, 65H, NaOAr *p*-^{t}Bu), −0.44 (1:1:1:1 q, $^1J_{BH}$ 81 Hz, 20H, $NaBH_4$), −5.9 (br, 4H), −7.3 (br, 12H), −13.9 (br, 6H), −24.7 (br, 4H) ppm. All paramagnetic resonances were very broad and of very low intensity. Dark green crystals formed in the NMR tube over 3 weeks. X-ray diffraction analysis revealed their composition to be $[\{U(OAr)\}_2(endo\text{-}BH_4Na)(L^A)(THF)_2]$ (**23**).

4.3.11.2 KN″

Solid $[Na(THF)_4][\{U(BH_4)\}_2(\mu\text{-}BH_4)(L^A)(THF)_2]$ (14 mg, 0.007 mmol) and KN″ (4 mg, 0.020 mmol) were combined in d_8-THF (0.5 mL) in a Teflon-tapped NMR tube forming a dark brown solution containing a pale brown precipitate. The ^{1}H NMR spectrum acquired after 2 h showed a mixture of paramagnetic and diamagnetic compounds. After 16 h a different set of low intensity paramagnetic resonances were observed which could not be

assigned to a single product. No resonance corresponding to $NaBH_4$ or KBH_4 could be identified.

4.3.11.3 NaO^{t}Bu

Excess Na^{t}OBu (4 mg, 0.042 mmol) was combined with crude [{U(BH$_4$)}$_2$(μ-BH$_4$K)(L^A)(THF)$_2$] (14 mg, 0.09 mmol) in d_8-THF (0.5 mL) in a Teflon-tapped NMR tube. The mixture turned brown. **^{1}H NMR (d_8-THF):** δ 13.33 (s, 1H), 7.20 (s, 1H), 2.55 (s, 1H), 1.32 (s, 12H), 1.08 (s, 280H, excess NaO^{t}Bu), −0.41 (1:1:1:1 q, $^1J_{BH}$ 85 Hz, 44H, $NaBH_4$), −8.67 (s, 2H) ppm. These resonances cannot be assigned to a Pacman complex. Other very low intensity resonances were observed over the range δ 98 to −33 ppm so it is likely that decomposition has occurred.

*4.3.11.4 KCp**

Crude [{U(BH$_4$)}$_2$(μ-BH$_4$K)(L^A)(THF)$_2$] (15 mg, 0.010 mmol) and KCp* (5 mg, 0.029 mmol) were combined in d_8-THF (0.5 mL) in a Teflon-tapped NMR tube. The mixture turned pale orange and an orange precipitate formed over 1 h. The ^{1}H NMR spectrum showed multiple low intensity paramagnetic resonances that could not be assigned to one product.

4.3.11.5 Benzyl potassium

Crude [{U(BH$_4$)}$_2$(μ-BH$_4$K)(L^A)(THF)$_2$] (14 mg, 0.009 mmol) and benzyl potassium (2.3 mg, 0.018 mmol) were combined in d_8-THF (0.5 mL) in a Teflon-tapped NMR tube. The ^{1}H NMR spectrum showed multiple low intensity paramagnetic resonances that could not be assigned to one product, along with toluene (δ 7.24 (m, 2H, *meta*-H), 7.18 (d, $^3J_{HH}$ 7.3 Hz, 2H, *ortho*-H), 7.13 (t, $^3J_{HH}$ 7.4 Hz, 1H, *para*-H), 2.36 (s, 3H, Me) ppm), and KN″ (δ 0.17 (s, 8H) ppm).

4.3.11.6 Methylallyl lithium

Crude [{U(BH$_4$)}$_2$(μ-BH$_4$K)(L^A)(THF)$_2$] (15 mg, 0.010 mmol) and methylallyl lithium (2 mg, 0.032 mmol) were combined in d_8-THF (0.5 mL) in a Teflon-tapped NMR tube. The ^{1}H NMR spectrum showed multiple, very low intensity paramagnetic resonances that could not be assigned to one product. $LiBH_4$ was observed at δ −0.51 (1:1:1:1 q, $^1J_{BH}$ 80 Hz) ppm.

4.3.12 Attempted gas reactions of [Na(THF)$_4$][{U(BH$_4$)}$_2$(μ-BH$_4$)(L^A)(THF)$_2$], 18

In each case [Na(THF)$_4$][{U(BH$_4$)}$_2$(μ-BH$_4$)(L^A)(THF)$_2$] (12 mg, 0.007 mmol) was dissolved d_8-THF (0.5 mL) and the solution was freeze-pump-thaw degassed three times

before an atmosphere of the appropriate gas (1.0 bar) was introduced. The results are tabulated below.

Gas	*Result*
CO	No reaction.
H_2	No reaction.
CO_2	Solution changed colour from dark green to pale orange and a yellow precipitate formed over 6 h. No paramagnetic resonances were observed in the ^{1}H NMR spectrum.

4.3.13 Attempted reaction of [Li(THF)$_4$][{U(BH$_4$)}$_2$(μ-BH$_4$)(L^{Me})], 21, with KOAr

[Li(THF)$_4$][{U(BH$_4$)}$_2$(μ-BH$_4$)(L^{Me})] (12 mg, 0.008 mmol) and KOAr (6 mg, 0.020 mmol Ar = 2,4,6-C$_6$H$_2$(^{t}Bu)$_3$) were combined in d_8-THF (0.5 mL) in a Teflon-tapped NMR tube to form a dark brown solution. The subsequent ^{1}H NMR spectrum showed multiple paramagnetic products with resonances appearing over the range δ 42 to −81 ppm.

4.3.14 Synthesis of [{U(OAr)}$_2$(*endo*-BH$_4$K)(L^A)(THF)$_2$], 22

THF (15 mL) was added to a dry mix of [Na(THF)$_4$][{U(BH$_4$)}$_2$(μ-BH$_4$)(L^A)(THF)$_2$] (385 mg, 0.210 mmol) and KOAr (127 mg, 0.423 mmol, Ar = 2,4,6-C$_6$H$_2$(^{t}Bu)$_3$) and the mixture was stirred for 16 h. Dark green crystals formed that were isolated by filtration and dried under reduced pressure. Yield: 253 mg, 59 %. Single crystals suitable for X-ray diffraction were grown from an NMR scale reaction in d_8-THF.

^{1}H NMR (C$_6$D$_6$): δ 27.0 (br, 4H), 24.9 (br, 4H), 17.7 (br, 4H), 14.6 (br, 2H, ArH), 13.9 (br, 4H), 12.4 (br, 4H), 10.5 (br, 4H), 8.6 (br, 2H ArH), 7.7 (br, 6H, *meso* CH$_2$C<u>H</u>$_3$ + 4H), 6.0 (br, 4H), 4.1 (br, 18H, *para* ^{t}Bu), 3.60 (br, 24H, THF), 1.42 (br, 24H, THF), −0.1 (br, 36 H, *ortho* ^{t}Bu), −10.0 (br, 4H), −12.8 (br, 6H, *meso* CH$_2$C<u>H</u>$_3$) ppm. **^{11}B NMR (C$_6$D$_6$):** δ 188 (br, $W_{½}$ 1161 Hz, (μ-BH$_4$K)) ppm. **Elemental Analysis** Found: C, 59.46; H, 5.91; N, 5.36 %, C$_{102}$H$_{126}$B$_1$K$_1$N$_8$O$_4$U$_2$ requires: C, 59.64; H, 6.18; N, 5.46 %.

4.3.15 Reaction of [{U(OAr)}$_2$(*endo*-BH$_4$K)(L^A)(THF)$_2$], 22, with 18-crown-6

Solid 18-crown-6 (4 mg, 0.015 mmol) was added to a dark green suspension of [{U(OAr)}$_2$(μ-BH$_4$K)(L^A)(THF)$_2$] (20 mg, 0.010 mmol) in C$_6$D$_6$ (0.5 mL). A green solution containing a pale green precipitate formed.

^{1}H NMR (C$_6$D$_6$): δ 40.85 (s, 6H, *meso* CH$_2$C<u>H</u>$_3$) 22.91 (s, 4H), 19.7 (br, $W_{½}$ 400 Hz, 2H, OAr *meta*-H), 18.4 (br, $W_{½}$ 366 Hz, 2H, OAr *meta*-H), 10.53 (s, 4H), 9.27 (s, 4H), 8.97 (s, 4H), 8.55 (s, 4H), 8.34 (s, 4H), 5.93 (s, 18H, *para*-^{t}Bu), 4.18 (s, 4H), 3.69 (s, 220H, 18-crown-6 + THF), 2.52 (s, 2H, ArH), 1.42 (br, 20H, THF), −0.22 (1:1:1:1 q, $^1J_{BH}$ 82 Hz, 2H,

MBH_4), −0.94 (s, 4H), −3.1 (br, $W_{½}$ 379 Hz, 18H, *ortho*-^{t}Bu), −7.1 (br, $W_{½}$ 359 Hz, 18H, *ortho*-^{t}Bu), −12.36 (s, 6H, *meso* $CH_2C\underline{H}_3$), −43.61 (s, 2H, ArH) ppm. **^{11}B NMR (C_6D_6):** no resonances visible over the range 340 – 60 ppm.

4.3.16 Attempted gas reactions of [{U(OAr)}$_2$(L^A)], 24

In each case "[{U(OAr)}$_2$(L^A)]" was formed *in situ* in a Teflon-tapped NMR tube by reaction of [{U(OAr)}$_2$(μ-BH_4K)(L^A)(THF)$_2$] with excess 18-crown-6 in C_6D_6. The solution was then freeze-pump-thaw degassed three times before an atmosphere of the appropriate gas (1.0 bar) was introduced. The results are tabulated below.

Gas	*Result*
CO	No reaction.
H_2	No reaction.
CO_2	Solution turned light orange, very low intensity resonances were observed that could not be assigned to a single product.

4.3.17 Synthesis of [{U(OAr)}$_2$(μ-S_2)(L^A)], 25

C_6D_6 (0.5 mL) was added to a dry mix of [{U(OAr)}$_2$(*endo*-BH_4K)(L^A)(THF)$_2$] (10 mg, 0.005 mmol) and S_8 (0.6 mg, 0.002 mmol) in a vial in the glovebox forming a pale orange solution. The mixture was left to stand for 2 h before being filtered. Hexane (1.5 mL) was added and the mixture left to stand. Dark orange crystals and yellow powder formed after 1 week. The yellow powder was re-suspended, the supernatant decanted and the crystals dried under vacuum. Yield: 4 mg, 43 %. Single crystals were grown by vapour diffusion of hexane into a benzene solution at ambient temperature.

^{1}H NMR (C_6D_6): δ 65.54 (s, 4H), 48.45 (s, 2H), 36.97 (s, 2H), 35.67 (2, 6H, *meso* $CH_2C\underline{H}_3$), 29.51 (s, 18H, *ortho*-^{t}Bu), 15.09 (s, 18H, *para*-^{t}Bu), 13.94 (s, 4H), 4.30 (s, 4H), −4.04 (s, 4H), −6.96 (s, 4H), −10.95 (s, 4H), −11.55 (s, 4H), −12.13 (s, 2H), −13.19 (s, 4H), −31.15 (s, 4H), −31.72 (s, 18H, *ortho*-^{t}Bu), −56.12 (s, 2H) ppm. **^{11}B NMR (C_6D_6):** no resonances visible over the range 250 – −50 ppm. **Elemental Analysis** Found: C, 59.02; H, 5.63; N, 5.76 %, $C_{94}H_{106}N_8O_2S_2U_2$ requires: C, 58.80; H, 5.56; N, 5.84 %.

4.3.18 Reactions of [{U(OAr)}$_2$(*endo*-BH_4K)(L^A)(THF)$_2$], 22, with CS_2

4.3.18.1 Room temperature

Three drops of CS_2 were added to a green suspension of [{U(OAr)}$_2$(*endo*-BH_4K)(L^A)(THF)$_2$] (10 mg, 0.005 mmol) in d_8-toluene (0.5 mL) in a Teflon-tapped NMR tube. The solution turned orange-brown over 10 min.

^{1}H NMR (d_8-toluene, 1 h): δ 77.54 (s, 2H), 45.38 (s, 1H, OAr *meta*-H), 42.67 (s, 1H, OAr *meta*-H), 41.87 (s, 2H), 40.05 (s, 1H, OAr *meta*-H), 36.51 (s, 9H, ^{t}Bu), 31.31 (s, 1H, OAr *meta*-H), 26.94 (s, 3H, *meso* $CH_2C\underline{H}_3$), 20.82 (s, 3H, *meso* $CH_2C\underline{H}_3$), 17.18 (s, 9H, ^{t}Bu), 15.01 (s, 9H, ^{t}Bu), 13.40 (s, 9H, ^{t}Bu), 12.67 (s, 2H), 5.35 (s, 2H), 5.27 (s, 2H), 3.59 (br, 30H, THF), 3.06 (s, 2H), 2.78 (s, 2H), 1.45 (br, 30H, THF), −5.05 (s, 2H), −5.94 (s, 2H), −7.28 (s, 2H), −7.95 (s, 2H), −8.15 (s, 2H), −9.90 (s, 3H, *meso* $CH_2C\underline{H}_3$), −10.36 (s, 2H), −10.63 (s, 3H, *meso* $CH_2C\underline{H}_3$), −15.45 (s, 2H), −18.75 (s, 2H), −27.13 (s, 2H), −27.51 (s, 2H), −35.20 (s, 9H, ^{t}Bu), −36.25 (s, 2H) ppm. One of the aryloxide ^{t}Bu resonances is missing; it may be concealed by a THF resonance. **^{11}B NMR (d_8-toluene):** no resonances observed between 240 and −60 ppm.

The mixture was filtered and hexane was vapour diffused into the filtrate. Orange crystals formed after 5 d. X-ray diffraction analysis revealed their composition to be $[U(OAr)\}_2(\mu\text{-}S)(L^A)]$ (**27**).

4.3.18.2 High temperature

The reaction was repeated in C_6D_6 and the reaction mixture was heated at 80 °C for 2.5 h forming an orange solution containing brown precipitate.

^{1}H NMR (C_6D_6): δ 72.40 (br, 4H), 39.49 (br, $W_{½}$ 140 Hz, 18H, *ortho*-^{t}Bu), 18.66 (s, 4H), 16.91 (s, 4H), 15.78 (br, 2H, OAr *meta*-H), 15.20 (s, 2H, Ar-H), 13.59 (s, 18H, *para*-^{t}Bu), 9.02 (s, 4H), 6.15 (br, 6H, *meso* $CH_2C\underline{H}_3$), 5.24 (s, 4H), 2.38 (s, 2H, Ar-H), −6.31 (s, 4H), −7.60 (s, 4H), −11.39 (s, 4H), −15.42 (br, 2H, OAr *meta*-H), −18.03 (s, 6H, *meso* $CH_2C\underline{H}_3$), −55.00 (br, $W_{½}$ 278 Hz, 18H, *ortho*-^{t}Bu) ppm. This symmetric product is assigned as $[\{U(OAr)\}_2(\mu\text{-}S)(L^A)]$ (**27**). A few lower intensity resonances were also observed.

Excess S_8 (3 mg, 0.012 mmol) was added to the filtered sample. The ^{1}H NMR spectrum was unaltered after 2 h but after 7 d resonances corresponding to both $[\{U(OAr)\}_2(\mu\text{-}S)(L^A)]$ and $[\{U(OAr)\}_2(\mu\text{-}S_2)(L^A)]$ were observed in a 2:1 ratio. The sample was heated at 80 °C for 3h. The subsequent ^{1}H NMR spectrum showed that the ratio of $[\{U(OAr)\}_2(\mu\text{-}S)(L^A)]$:$[\{U(OAr)\}_2(\mu\text{-}S_2)(L^A)]$ present had shifted to 1:7. After another 3 h heating at 80 °C only resonances corresponding to $[\{U(OAr)\}_2(\mu\text{-}S_2)(L^A)]$ were observed along with some unassigned low intensity resonances.

4.3.19 Reaction of $[\{U(OAr)\}_2(endo\text{-}BH_4K)(L^A)(THF)_2]$, 22, with O_2

$[\{U(OAr)\}_2(endo\text{-}BH_4K)(L^A)(THF)_2]$ (12 mg, 0.006 mmol) was suspended in C_6D_6 (0.5 mL) in a Teflon-tapped NMR tube. The mixture was freeze-pump-thaw degassed three times and an atmosphere of dry O_2 was introduced. An immediate colour change from dark green to dark red occurred. The ^{1}H NMR spectrum displayed resonances corresponding to a mixture

of paramagnetic and diamagnetic compounds. Dark red crystals formed over 4 d which were analysed by X-ray diffraction and found to be [{UO_2}$_2$(THF)$_2$(L^A)] (**28**).

4.3.20 Protonolysis reactions of [Na(THF)$_4$][{U(BH$_4$)}$_2$(μ-BH$_4$)(L^A)(THF)$_2$], 18

4.3.20.1 One equivalent of [HNEt$_3$][BPh$_4$]

[Na(THF)$_4$][{U(BH$_4$)}$_2$(μ-BH$_4$)(L^A)(THF)$_2$] (14 mg, 0.008 mmol) and [HNEt$_3$][BPh$_4$] (4 mg, 0.010 mmol) were combined in d_8-THF (0.5 mL) in a Teflon-tapped NMR tube, forming a green solution.

^{1}H NMR (d_8-THF): δ 36.00 (s, 2H), 33.01 (s, 2H), 19.54 (s, 2H), 18.67 (s, 2H), 16.77 (s, 2H), 15.20 (s, 2H), 12.39 (s, 2H), 11.77 (s, 2H), 11.29 (s, 3H), 10.95 (s, 3H), 10.29 (s, 2H), 8.52 (s, 2H), 7.71 (s, 2H), 7.20 (m, 21H, [BPh$_4$]$^-$ *ortho* H), 6.99 (s, 2H), 6.80 (t, $^3J_{HH}$ 7.37 Hz, 21H, [BPh$_4$]$^-$ *meta* H), 6.68 (t, $^3J_{HH}$ 7.17 Hz, 10.5H, [BPh$_4$]$^-$ *para* H), 6.30 (s 2H), 5.12 (s, 3H), 4.59 (s, 0.3H, H_2), 2.75 (q, $^3J_{HH}$ 7.32 Hz, 14H, H_3B•N(C<u>H</u>$_2$CH$_3$)$_3$) 2.49 (q, $^3J_{HH}$ 7.32 Hz, 2H, [HN(C<u>H</u>$_2$CH$_3$)$_3$]), 1.55 (s, 2H), 1.35 (s, 2H), 1.16 (t, $^3J_{HH}$ 7.34 Hz, 22H, H_3B•N(CH$_2$C<u>H</u>$_3$)$_3$), 1.02 (t, $^3J_{HH}$ 7.13 Hz, 3H, [HN(CH$_2$C<u>H</u>$_3$)$_3$]), −0.08 (s, 2H), −1.13 (s, 3H), −18.70 (s, 2H), −76.8 (br, $W_{½}$ 591 Hz, 4H, BH_4) ppm. One ligand resonance was not found. **^{11}B NMR (d_8-THF):** δ 234 (br, $W_{½}$ 275 Hz, 1B, μ-BH_4), 178 (br, $W_{½}$ 317 Hz, 1B, terminal BH_4), −6.6 (s, 0.3B, [BPh$_4$]$^-$), −13.0 (q, $^1J_{BH}$ 97 Hz, 2B, H_3B•NEt_3) ppm.

4.3.20.2 Excess [HNEt$_3$][BPh$_4$]

[Na(THF)$_4$][{U(BH$_4$)}$_2$(μ-BH$_4$)(L^A)(THF)$_2$] (14 mg, 0.008 mmol) and [HNEt$_3$][BPh$_4$] (10 mg, 0.024 mmol) were combined in d_8-THF (0.5 mL) in a Teflon-tapped NMR tube, forming a green solution.

^{1}H NMR (d_8-THF): δ 32.44 (s, 4H), 17.95 (s, 4H), 16.82 (s, 4H), 16.13 (s, 4H), 13.97 (s, 2H, Ar-H), 12.46 (s, 4H), 11.05(s, 4H), 9.18 (br, 6H, *meso*-CH$_2$C<u>H</u>$_3$ + 4H), 1.54 (s, overlapped with THF signals), −0.86 (s, 6H, *meso* CH$_2$C<u>H</u>$_3$), −24.36 (s, 2H, Ar-H) ppm. **^{11}B NMR (d_8-THF):** δ 334 (br, 1B, μ-BH_4) ppm.

4.3.20.3 Excess [HNEt$_3$][BPh$_4$] in DME

[Na(THF)$_4$][{U(BH$_4$)}$_2$(μ-BH$_4$)(L^A)(THF)$_2$] (15 mg, 0.008 mmol) and [HNEt$_3$][BPh$_4$] (8 mg, 0.019 mmol) were combined in DME (0.5 mL) in a Teflon tapped NMR tube. Effervescence was observed. A drop of C_6D_6 was added. **^{1}H NMR (DME/C_6D_6):** spectrum was swamped by DME signals. **^{11}B NMR (DME/C_6D_6):** 246 (s) ppm.

4.3.20.4 Excess [HNEt$_3$][BPh$_4$] with 2,2-bipyridyl

[Na(THF)$_4$][{U(BH$_4$)}$_2$(μ-BH$_4$)(L^A)(THF)$_2$] (12 mg, 0.006 mmol), [HNEt$_3$][BPh$_4$] (6 mg, 0.014 mmol) and 2,2-bipyridyl (3 mg, 0.019 mmol) were combined in d_8-THF in a Teflon-tapped NMR tube, forming a green solution. No resonances were observed in the paramagnetic region of the ^{1}H NMR spectrum.

4.3.21 Protonolysis reactions of [Li(THF)$_4$][{U(BH$_4$)}$_2$(μ-BH$_4$)(L^{Me})], 21

4.3.21.1 One equivalent of [HNEt$_3$][BPh$_4$]

[Li(THF)$_4$][{U(BH$_4$)}$_2$(μ-BH$_4$)(L^{Me})] (12 mg, 0.008 mmol) and [HNEt$_3$][BPh$_4$] (3.5 mg, 0.008 mmol) were combined in d_8-THF (0.5 mL) in a Teflon-tapped NMR tube forming a dark brown solution with some brown precipitate. NMR spectra were obtained and then the solvent was removed under reduced pressure and C_6D_6 added to investigate the solubility of the product in non-coordinating solvent. ^{1}H NMR spectra were acquired with selective decoupling of each ^{11}B resonance in turn in order to assign the BH$_4$ protons to the terminal and bridging BH$_4$ environments.

^{1}H NMR (d_8-THF): δ 85.3 (br, $W_{½}$ 325 Hz, terminal BH$_4$), 61.1 (br, $W_{½}$ 363 Hz, μ-BH$_4$), 51.65 (s, 2H), 37.58 (s, 2H), 31.16 (s, 2H), 26.39 (s, 2H), 20.52 (s, 2H), 20.00 (s, 2H), 7.25 (m, 8H, LiBPh$_4$ *ortho* H), 6.84 (t, $^3J_{HH}$ 7.38 Hz, 8H, LiBPh$_4$ *meta* H), 6.70 (t, $^3J_{HH}$ 7.12 Hz, 4H, LiBPh$_4$ *para* H), 5.78 (s, 6H), 2.75 (q, $^3J_{HH}$ 7.23 Hz, 6H, H$_3$B•N(C<u>H</u>$_2$CH$_3$)$_3$) 2.27 (s, 2H), 1.16 (t, $^3J_{HH}$ 7.23 Hz, 9H, H$_3$B•N(CH$_2$C<u>H</u>$_3$)$_3$) 0.15 (s, 6H), −0.07 (s, 2H), −1.16 (s, 6H), −48.48 (s, 6H) ppm. **^{11}B NMR (d_8-THF):** δ 371 (s, 1B, μ-BH$_4$), 210 (s, 1B, terminal BH$_4$), −6.6 (s, LiBPh$_4$), −12.9 (q, $^1J_{BH}$ 98 Hz, H$_3$B•NEt$_3$) ppm. **^{1}H NMR (C_6D_6):** δ 87.3 (br, $W_{½}$ 338 Hz, terminal BH$_4$), 64.6 (br, $W_{½}$ 396 Hz, μ-BH$_4$), 51.64 (s, 2H), 37.58 (s, 2H), 37.33 (s, 2H), 26.80 (s, 2H), 20.49 (s, 2H), 19.89 (s, 2H), 7.67 (br, 6H, LiBPh$_4$ *ortho* H), 6.91 (br, 6H, BPh$_4$ *meta* H), 6.81 (br, 3H, BPh$_4$ *para* H), 5.83 (s, 6H), 4.57 (s, 0.01H, H$_2$), 2.47 (s, 2H), 2.26 (br, 8H, H$_3$B•N(C<u>H</u>$_2$CH$_3$)$_3$) 0.76 (br, 12H, H$_3$B•N(CH$_2$C<u>H</u>$_3$)$_3$) 0.19 (s, 6H), 0.13 (s, 2H), −1.21 (s, 6H), −46.16 (s, 6H) ppm. **^{11}B NMR (C_6D_6):** δ 370 (s, 1B, μ-BH$_4$), 205 (s, 1B, terminal BH$_4$), −6.6 (s, LiBPh$_4$), −12.9 (q, $^1J_{BH}$ 98 Hz, H$_3$B•NEt$_3$) ppm. **^{1}H{^{11}B @ 205 ppm} NMR (C_6D_6):** resonance at δ 87.3 ppm sharpens to $W_{½}$ 263 Hz, resonance at δ 64.6 ppm does not sharpen ($W_{½}$ 391 Hz). **^{1}H{^{11}B @ 370 ppm} NMR (C_6D_6):** resonance at δ 64.6 ppm sharpens to $W_{½}$ 309 Hz, resonance at δ 87.3 ppm does not sharpen ($W_{½}$ 346 Hz).

4.3.21.2 Excess [HNEt$_3$][BPh$_4$]

[Li(THF)$_4$][{U(BH$_4$)}$_2$(μ-BH$_4$)(L^{Me})] (10 mg, 0.007 mmol) and [HNEt$_3$][BPh$_4$] (9 mg, 0.021 mmol) were combined in d_8-THF (0.5 mL) in a Teflon-tapped NMR tube forming a dark brown solution.

^{1}H NMR (d_8-THF): δ 80.7(br, $W_{½}$ 402 Hz, μ-BH$_4$), 38.31 (s, 4H), 25.88 (s, 4H), 21.94 (s, 4H), 7.10 (m, 28H, [BPh$_4$]$^-$ *ortho* H), 6.71 (t, $^3J_{HH}$ 7.28 Hz, 28H, [BPh$_4$]$^-$ *meta* H), 6.59 (t, $^3J_{HH}$ 7.17 Hz, 14H, [BPh$_4$]$^-$ *para* H), 4.58 (s, 0.1H, H$_2$), 3.17 (s, 6H, *meso* Me), 3.09 (s, 4H), 2.75 (q, $^3J_{HH}$ 7.20 Hz, 12H, H$_3$B•N(C<u>H</u>$_2$CH$_3$)$_3$) 2.65 (q, $^3J_{HH}$ 7.35 Hz, 9H, [HN(C<u>H</u>$_2$CH$_3$)$_3$]$^+$), 1.17 (t, $^3J_{HH}$ 7.20 Hz, 18H, H$_3$B•N(CH$_2$C<u>H</u>$_3$)$_3$), 0.98 (t, $^3J_{HH}$ 7.35 Hz, 12H, [HN(CH$_2$C<u>H</u>$_3$)$_3$]$^+$), 0.27 (s, 12H), −48.48 (s, 6H, *meso* Me) ppm. **^{11}B NMR (d_8-THF):** δ 432 (s, μ-BH$_4$), −6.8 (s, [BPh$_4$]), −13.0 (q, $^1J_{BH}$ 98 Hz, H$_3$B•NEt$_3$) ppm.

4.3.22 Reactions of [U$_2$(μ-BH$_4$)(L^A)][BPh$_4$], 30, with gases

"[U$_2$(μ-BH$_4$)(L^A)][BPh$_4$]" (**30**) was formed *in situ* in a Teflon-tapped NMR tube by reaction of [Na(THF)$_4$][{U(BH$_4$)}$_2$(μ-BH$_4$)(L^A)(THF)$_2$] with excess [HNEt$_3$][BPh$_4$] in d_8-THF (0.5 mL). The solution was then freeze-pump-thaw degassed three times before an atmosphere of the appropriate gas (1.0 bar) was introduced. The results are tabulated below.

Gas	*Result*
H$_2$	No reaction.
CO	Slow reaction occurred. After 24 h several very low intensity resonances were observed in the ^{1}H NMR spectrum, indicating multiple product formation.

4.3.23 Reaction of [U$_2$(μ-BH$_4$)(L^{Me})][BPh$_4$], 32, with CO

[Li(THF)$_4$][{U(BH$_4$)}$_2$(μ-BH$_4$)(L^{Me})] (15 mg, 0.010 mmol) and [HNEt$_3$][BPh$_4$] (9 mg, 0.021 mmol) were combined in d_8-THF (0.5 mL) in a Teflon-tapped NMR tube. The green solution was freeze-pump-thaw degassed three times and then an atmosphere of CO (1.0 bar) was introduced. **^{1}H NMR (d_8-THF, 1 h):** many resonances were observed over the range 60 - −30 ppm corresponding to formation of multiple species. **^{1}H NMR (d_8-THF, 7 d):** only very low intensity paramagnetic and diamagnetic resonances remain.

4.3.24 Synthesis of [Li(THF)$_4$][{U(Cl)}$_2$(μ-Cl)$_3$(L^A)], 33

A mixture of H$_4$L^A (586 mg, 0.681 mmol) and LiN″ (456 mg, 2.725 mmol) in THF (20 mL) was stirred for 4 h and then added to a stirred solution of UCl$_4$(THF)$_{0.75}$ (591 mg, 1.362 mmol) in THF (10 mL). Orange precipitate began to form in the resulting orange solution within 30 min. The mixture was stirred gently for 3 d, after which the precipitate was

isolated, washed with THF (2 x 5 mL) and dried to give an orange powder. Yield: 488 mg, 39 %.

^{1}H NMR (d_5-pyridine): δ 42.80 (br, 4H), 15.93 (s, 6H, $CH_2C\underline{H}_3$), 14.79 (s, 4H), 9.71 (s, 4H), 9.04 (s, 4H), 5.64 (s, 4H), 5.23 (s, 4H), 4.30 (s, 2H, Ar-H), 3.63 (m, 26H, THF), 1.59 (m, 26H, THF), 0.92 (s, 4H), 0.23 (s, 6H, $CH_2C\underline{H}_3$) −0.72 (s, 4H), −49.82 (s, 2H, Ar-H) ppm. **^{7}Li NMR (d_5-pyridine):** δ 3.5 (s, $[Li(py)_4]^+$) **Elemental Analysis:** Found: C, 48.97: H, 4.60; N, 6.18 %, $C_{74}H_{80}Cl_5LiN_8O_4U_2$ requires: C, 49.22; H, 4.47; N, 6.21 %. Single crystals suitable for X-ray diffraction analysis were obtained by slow diffusion of toluene into a pyridine solution of $[Li(py)_4][\{U(Cl)\}_2(\mu\text{-}Cl)_3(L^A)]$.

4.3.25 Attempted reduction of $[Li(THF)_4][\{U(Cl)\}_2(\mu\text{-}Cl)_3(L^A)]$, 33

K metal (3 mg, 0.077 mmol) and naphthalene (20 mg, 0.156 mmol) were dissolved in THF (0.5 mL) forming a green solution which turned purple-brown when transferred onto $[Li(THF)_4][\{U(Cl)\}_2(\mu\text{-}Cl)_3(L^A)]$ (15 mg, 0.008 mmol) in a Teflon-tapped NMR tube. A drop of C_6D_6 was added. **^{1}H NMR (THF/C_6D_6):** no resonances observed in the paramagnetic region.

4.3.26 Attempted ligand substitution reactions of $[Li(THF)_4][\{U(Cl)\}_2(\mu\text{-}Cl)_3(L^A)]$, 33

4.3.26.1 KO^{t}Bu

$[Li(THF)_4][\{U(Cl)\}_2(\mu\text{-}Cl)_3(L^A)]$ (15 mg, 0.008 mmol) and KO^{t}Bu (2 mg, 0.018 mmol) were combined in d_5-pyridine (0.5 mL) in a Teflon-tapped NMR tube, forming a yellow solution. **^{1}H NMR (d_5-pyridine):** δ 85.95 (s, 9H, O^{t}Bu), 77.00 (s, 2H), 69.74 (s, 9H, O^{t}Bu), 9.69 (s, 2H), 6.37 (s, 2H), 5.66 (s, 3H, *meso* $CH_2C\underline{H}_3$), 5.22 (s, 2H), 4.97 (s, 3H, *meso* $CH_2C\underline{H}_3$), 4.06 (s, 2H), 1.44 (s, 3H, *meso* $CH_2C\underline{H}_3$), 1.20 (s, 2H), 0.46 (br, 2H), −0.68 (s, 2H), −5.09 (s, 2H), −5.21 (s, 2H), −5.55 (s, 2H), −6.50 (s, 3H, *meso* $CH_2C\underline{H}_3$), −7.73 (s, 2H), −8.66 (s, 2H), −9.72 (s, 2H), −14.28 (s, 2H), −17.37 (s, 2H), −17.44 (s, 2H), −33.17 (s, 2H) ppm. The resonances recorded correspond to the major asymmetric product and other low intensity resonances were also observed.

The solvent was removed under reduced pressure and the resultant solids extracted into C_6D_6 (0.5 mL). Vapour diffusion of hexane into this solution led to the formation of yellow single crystals which were found to have composition $[\{U(O^tBu)(Cl)\}\{U(O^tBu)(py)\}(\mu\text{-}Cl)(L^A)]$ (**34**) by X-ray diffraction analysis.

4.3.26.2 KN″

$[Li(THF)_4][\{U(Cl)\}_2(\mu\text{-}Cl)_3(L^A)]$ (14 mg, 0.008 mmol), and KN″ (4 mg, 0.020 mmol) were combined in d_5-pyridine (0.5 mL) in a Teflon-tapped NMR tube. The ^{1}H NMR spectrum

acquired after 1 h showed a mixture of paramagnetic products with resonances appearing between δ 56 and −30 ppm. The sample was heated at 80 °C for 2 h during which the colour of the solution changed from orange to dark brown. The subsequent ^{1}H NMR spectrum showed a few very low intensity paramagnetically shifted resonances which could not be assigned to one product and indicated that thermal decomposition had occurred.

4.3.26.3 LiN″

$[Li(THF)_4][\{U(Cl)\}_2(\mu\text{-}Cl)_3(L^A)]$ (13 mg, 0.007 mmol), and LiN″ (3 mg, 0.018 mmol) were combined in d_5-pyridine (0.5 mL) in a Teflon-tapped NMR tube. The ^{1}H NMR spectrum acquired after 1 h showed starting material and LiN″. The sample was heated at 80 °C for 2 h. The subsequent ^{1}H NMR spectrum still only showed starting material resonances but these had decreased in intensity relative to the solvent signals by 50 %.

4.3.26.4 $LiNEt_2$

$LiNEt_2$ (2 mg, 0.025 mmol) was added to a solution of $[Li(THF)_4][\{U(Cl)\}_2(\mu\text{-}Cl)_3(L^A)]$ (18 mg, 0.010 mmol) in d_5-pyridine (0.5 mL) in a Teflon-tapped NMR tube. The solution changed colour from orange to yellow-brown and a yellow precipitate was formed. No paramagnetic resonances were observed in the ^{1}H NMR spectrum.

4.3.26.5 K(OTtbp)

$[Li(THF)_4][\{U(Cl)\}_2(\mu\text{-}Cl)_3(L^A)]$ (15 mg, 0.008 mmol), and K(OTtbp) (6 mg, 0.020 mmol) were combined in d_5-pyridine (0.5 mL) in a Teflon-tapped NMR tube. The ^{1}H NMR spectrum acquired after 1 h showed a mixture of paramagnetic products with resonances appearing between δ 53 and −35 ppm. The sample was heated at 80 °C for 4 h in an attempt to convert this mixture to one thermodynamic product. The subsequent ^{1}H NMR spectrum showed very low intensity, very broad, paramagnetically shifted resonances which could not be assigned to one product and indicated that thermal decomposition had occurred.

4.3.26.6 K(acac)

$[Li(THF)_4][\{U(Cl)\}_2(\mu\text{-}Cl)_3(L^A)]$ (15 mg, 0.008 mmol), and K(acac) (4 mg, 0.029 mmol) were combined in d_5-pyridine (0.5 mL) in a Teflon-tapped NMR tube. No obvious colour change occurred. The ^{1}H NMR spectrum showed a mixture of several paramagnetic and diamagnetic products with resonances appearing over the range δ 105 to −45 ppm.

4.3.26.7 NaCp

$[Li(THF)_4][\{U(Cl)\}_2(\mu\text{-}Cl)_3(L^A)]$ (22 mg, 0.012 mmol), and NaCp (2 mg, 0.023 mmol) were combined in d_5-pyridine (0.5 mL) in a Teflon-tapped NMR tube. A large amount of orange

precipitate formed immediately. **^{1}H NMR (d_5-pyridine):** multiple paramagnetic peaks of different intensity observed, consistent with the formation of 2 - 3 different products.

4.3.26.8 NaN_3

$[Li(THF)_4][\{U(Cl)\}_2(\mu\text{-}Cl)_3(L^A)]$ (14 mg, 0.008 mmol), and NaN_3 (3 mg, 0.046 mmol) were combined in d_5-pyridine (0.5 mL) in a Teflon-tapped NMR tube. No paramagnetic resonances were observed in the ^{1}H NMR spectrum.

4.3.26.9 $MgMe_2$

$[Li(THF)_4][\{U(Cl)\}_2(\mu\text{-}Cl)_3(L^A)]$ (15 mg, 0.008 mmol), and excess $MgMe_2$ (4 mg, 0.074 mmol) were combined in d_5-pyridine (0.5 mL) in a Teflon-tapped NMR tube. The ^{1}H NMR spectrum acquired after 1 h showed several very low intensity paramagnetically shifted resonances from δ 51 to −31 ppm. After 72 h, all paramagnetic resonances had disappeared, indicating decomposition.

4.3.26.10 KH

$[Li(THF)_4][\{U(Cl)\}_2(\mu\text{-}Cl)_3(L^A)]$ (14 mg, 0.008 mmol), and KH (3 mg, 0.075 mmol) were combined in d_5-pyridine (0.5 mL) in a Teflon-tapped NMR tube. No paramagnetic resonances were observed in the ^{1}H NMR spectrum.

4.3.27 Attempted synthesis of $[\{U(O^tBu)(Cl)\}\{U(O^tBu)(py)\}(\mu\text{-}Cl)(L^A)]$, 34

A solution of KO^tBu (71 mg, 0.633 mmol) in THF (5 mL) was added to an orange solution of $[Li(THF)_4][\{U(Cl)\}_2(\mu\text{-}Cl)_3(L^A)]$ (570 mg, 0.313 mmol) in pyridine (25 mL). The mixture was stirred for 1 h during which its colour changed to yellow-brown. The solvent was removed under reduced pressure leaving a sticky brown residue which was extracted with toluene (25 mL). The extract was concentrated to 3 mL and stored at −30 °C for 48 h. The yellow solid that formed was isolated (140 mg) but found to contain a mixture of products. **^{1}H NMR (d_5-pyridine):** the major product formed was the target compound $[\{U(O^tBu)(Cl)\}\{U(O^tBu)(py)\}(\mu\text{-}Cl)(L^A)]$ but resonances corresponding to roughly two other minor products were also observed. **^{7}Li NMR (d_5-pyridine):** δ 4.0 (v br, v low intensity) ppm.

4.3.28 Attempted cation substitution reactions of $[Li(THF)_4][\{U(Cl)\}_2(\mu\text{-}Cl)_3(L^A)]$, 33

4.3.28.1 $[Ph_3PNPPh_3][Cl]$ (PPNCl)

$[Li(THF)_4][\{U(Cl)\}_2(\mu\text{-}Cl)_3(L^A)]$ (15 mg, 0.008 mmol), and PPNCl (5 mg, 0.009 mmol) were combined in d_5-pyridine (0.5 mL) in a Teflon-tapped NMR tube. **^{1}H NMR (d_5-**

pyridine): several very low intensity paramagnetic resonances were observed between δ 24 and −30 ppm, which could not be assigned to one product.

4.3.28.2 [$^{n}Bu_4N$][Br]

Excess [$^{n}Bu_4N$][Br] (7 mg, 0.022 mmol) was dissolved in THF (0.5 mL) and added to solid [Li(THF)$_4$][{U(Cl)}$_2$(μ-Cl)$_3$(L^{A})] (10 mg, 0.005 mmol) in a Teflon-tapped NMR tube. An orange solution formed. The solvent was removed under reduced pressure and C_6D_6 (0.5 mL) was added to the residue. **^{1}H NMR (C_6D_6):** δ 45.23 (s, 3H) 16.98 (s, 5H), 16.42 (s, 4H), 9.92 (s, 3H), 8.22 (s, 4H), 5.33 (s, 4H), 3.59 (m, 120H, [$^{n}Bu_4N$]), 2.21 (m, 310H, [$^{n}Bu_4N$]), 0.30 (s, 3H), −0.40 (s, 6H), −0.86 (s, 4H), −1.73 (s, 4H), −54.74 (s, 2H) ppm.

4.4 Evans' method determination of magnetic moments

Measurement of the solution phase magnetic moments of complexes was carried out in triplicate at 298 K on a Bruker 400 MHz spectrometer. The magnetic moments of [Cr$_2$(L^{Me})] and [Cr$_2$(μ-I)(I)(THF)(L^{Me})] were measured in a THF/C_6D_6 mixture and that of [Cr$_2$(μ-CN^{t}Bu)(L)] in C_6D_6. Solutions of concentration 0.01 - 0.02 mM were prepared and placed into NMR tubes along with capillary tubes containing the respective solvent or solvent mixture as a reference. In all cases the frequency difference between the reference and contact shifted C_6D_6 residual *protio* resonances was measured. The magnetic moment was then calculated by the Evans' method using the equations below.[9] A solvent correction was not applied. The results are tabulated in Table 4.2.

$$\chi_m = \frac{3\Delta\nu M_r}{4\pi c\nu} - \chi_D\,, \qquad \mu_{eff} = \sqrt{8\,\chi_m T}$$

χ_m	molar susceptibility (cm^{3}mol^{-1})	ν	spectrometer frequency (Hz)
$\Delta\nu$	change in frequency (Hz)	χ_D	diamagnetic correction (cm^{3}mol^{-1})
M_r	molar mass (gmol^{-1})	μ_{eff}	magnetic moment (μ_B)
c	concentration (gcm^{-3})	T	temperature (K)

Table 4.2. Determination of solution phase magnetic moments of chromium complexes.

Complex	*c (g cm^{-3})*	*Δν (Hz)*	*χ_D (cm^3 mol^{-1})*	*μ_{eff} (μ_B)*
[$Cr_2(L^{Me})$] **1**	0.027	984	−0.0004088	6.31
	0.026	960		6.38
	0.025	908		6.34
[$Cr_2(\mu$-$CN^tBu)(L^{Me})$] **5**	0.030	536	−0.0004705	4.72
	0.024	456		4.90
	0.021	356		4.64
[$Cr_2(\mu$-I)(I)(THF)(L^{Me})] **6**	0.030	552	−0.0005618	5.44
	0.027	476		5.38
	0.031	576		5.46

4.5 NMR quenching experiments

4.5.1 Determination of x in $[Cr_2(CNXyl)_x(L^{Me})]$

$[Cr_2(CNXyl)_x(L^{Me})]$ was hydrolysed by the addition of d_4-methanol forming an insoluble orange chromium-containing precipitate and liberating CNXyl into solution. The quantity of free CNXyl was calculated from the ^{1}H NMR spectrum by integration against a 1,3,5-tri-*tert*-butylbenzene (benz*) internal standard. To ensure that all available CNXyl had been liberated into solution, two drops of conc. HCl were added to the samples, dissolving the precipitate. The new ^{1}H NMR spectra acquired showed the same ratio of CNXyl : benz*. The experiment was carried out in duplicate with the results tabulated below.

	Mass $[Cr_2(CNXyl)_x(L^{Me})]$ (mg)	Mass benz* (mg)	Theoretical integration CNXyl : benz*		Experimental integration CNXyl : benz*
			x = 1	x = 2	
1.	21.0	4.8	**1 : 3.72**	1 : 2.14	1 : 3.54
2.	18.7	4.7	**1 : 4.09**	1 : 2.35	1 : 3.61

4.5.2 Determination of x in $[U(BH_4)_3(THF)_x]$

Excess DME was added to a suspension of $[U(BH_4)_3(THF)_x]$ in C_6D_6, forming a pale red solution and liberating the coordinated THF which was then integrated against an internal standard, $Si(SiMe_3)_4$. Integration against the broad BH_4 resonance was found to be unreliable. The competitive displacement experiment was carried out in duplicate with the results tabulated below.

	Mass $[U(BH_4)_3(THF)_x]$ (mg)	Mass $Si(SiMe_3)_4$ (mg)	Integration THF : $Si(SiMe_3)_4$			
			Theoretical			Experi-mental
			x = 1	**x = 2**	x = 3	
1.	5.2	3.0	1 : 5.74	**1 : 3.45**	1 : 2.69	1 : 3.49
2.	6.2	3.9	1 : 6.26	**1 : 3.77**	1 : 2.94	1 : 3.69

4.6 X-ray crystallography

Single crystal X-ray diffraction data were recorded on either an Excalibur Eos diffractometer at 170(2) K using Mo *K*α radiation (λ = 0.71073 Å) or on a Supernova dual source Atlas diffractometer, utilising the Cu *K*α source (λ = 1.54184 Å) at 120(2) K. All of the structures were solved using either SIR-92 or SHELXS-97 direct methods and least-square refined using SHELXL97 in the WinGX suite of programs.[10] Unless otherwise stated, all non-H atoms were refined anisotropically and all H atoms were placed in calculated positions and refined using a riding model. All BH_4 protons were omitted from the crystallographic models unless they could be located in the residual electron density map. A summary of the crystal data, data collection and structure refinement for each X-ray structure is presented in Table 4.3.

Where structures were found to contain disordered solvent molecules that could not be successfully modelled, the SQUEEZE [11] routine of PLATON was used to remove the associated residual electron density. The use of SQUEEZE and any restraints applied to the main molecular residue during refinement are detailed below, along with selected structural parameters for each structure. Where it was necessary to restrain the bond distances of THF solvent molecules in order for them to be chemically sensible, the 1,2 and 1,3 distances were fixed to the values shown in Figure 4.1.

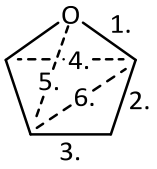

1. 1.46(2) 4. 2.29(4)
2. 1.52(2) 5. 2.34(4)
3. 1.53(2) 6. 2.41(4)

Figure 4.1 Metrics used to restrain THF molecules. All distances are in Å.

High pressure X-ray diffraction data were collected for **1** by Dr Alessandro Prescimone at the Diamond Light Source utilising synchrotron radiation (λ = 0.48590 Å) at 300 K. A single crystal of **1** was inserted into a diamond-anvil cell containing a hydrostatic medium and a ruby chip.[12,13] The pressure in the cell was determined from the ruby

luminescence.[14] Dr Alessandro Prescimone carried out the structure solution and refinement for all high pressure data sets.

4.6.1 Structure of $[Cr_2(L^{Me})]$, 1

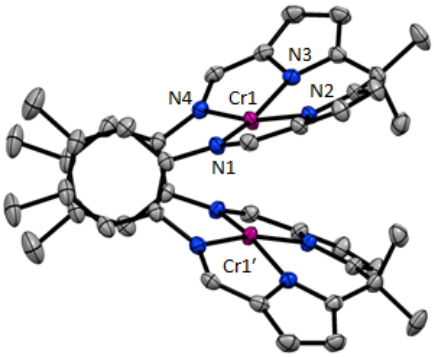

Selected bond distances (Å) and angles (°)			
Cr1···Cr1′	3.1221(1)	N4-Cr1-N1	114.02(6)
Cr1-N1	2.114(2)	N1-Cr1-N2	80.06(6)
Cr1-N2	1.970(2)	N2-Cr1-N3	85.52(6)
Cr1-N3	1.976(2)	N3-Cr1-N4	78.64(6)
Cr1-N4	2.078(2)	bite angle	48
Cr1-$N_{4\ plane}$	−0.19	twist angle	34

Figure 4.2 Structure of **1**. Thermal ellipsoids are drawn at 50 % probability. H atoms and lattice solvent are omitted.

Single crystals were obtained by cooling a saturated benzene solution of $[Cr_2(L^{Me})]$ from 80 °C to room temperature.

4.6.2 Structure of $[Cr_2(L^{A})(THF)_2]$, 2_{THF}

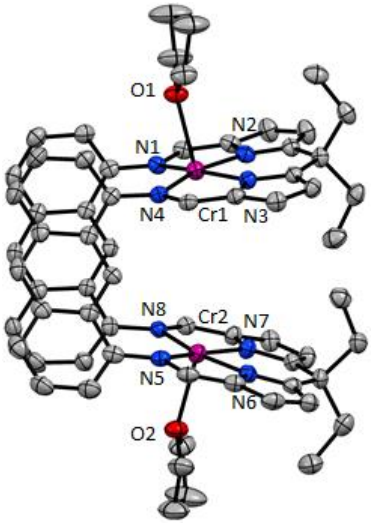

Selected bond distances (Å) and angles (°)			
Cr1···Cr2	5.6353(1)	Cr1-O1	2.349(3)
Cr1-N1	2.136(4)	Cr2-O2	2.356(3)
Cr1-N2	2.004(4)	N4-Cr1-N1	116.8(1)
Cr1-N3	1.973(4)	N1-Cr1-N2	78.9(1)
Cr1-N4	2.157(4)	N2-Cr1-N3	83.4(2)
Cr2-N5	2.149(4)	N3-Cr1-N4	80.1(1)
Cr2-N6	1.988(4)	N8-Cr2-N5	116.4(1)
Cr2-N7	1.987(4)	N5-Cr2-N6	79.8(2)
Cr2-N8	2.142(4)	N6-Cr2-N7	83.5(2)
Cr1-$N_{4\ plane}$	+0.12	N7-Cr2-N8	80.1(1)
Cr2-$N_{4\ plane}$	+0.07	twist angle	36

Figure 4.3 Structure of $\mathbf{2_{THF}}$. There are two molecules in the asymmetric unit, only one is shown. Thermal ellipsoids are drawn at 50 % probability. H atoms and lattice solvent are omitted.

Single crystals were obtained from the NMR scale reaction of $[Cr(N'')_2(THF)_2]$ with H_4L^A in THF. Hereafter the imine and pyrrole nitrogen atoms will not be labelled explicitly for each structure. The same atom labelling scheme has been used in all cases such that N1,

N4, N5 and N8 refer to the imine nitrogens whilst N2, N3, N6 and N7 are the pyrrole nitrogens. M1 is bound to N1-N4 whilst M2 is bound to N5-N8.

4.6.3 Structure of $[Cr_2(OPPh_3)_2(L^{Me})]$, 3

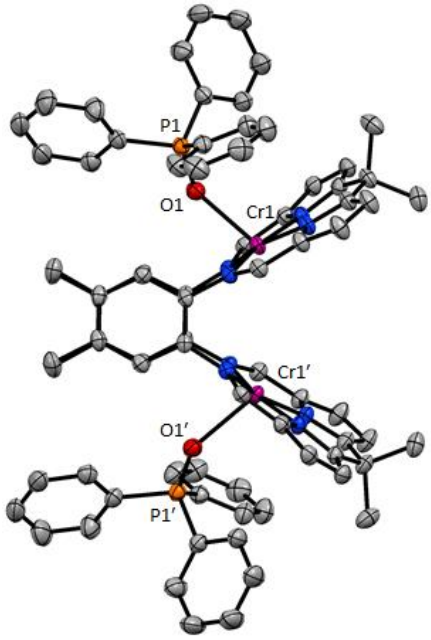

Selected bond distances (Å) and angles (°)			
Cr1···Cr1′	4.3210(5)	Cr1-O1	2.327(2)
Cr1-N1	2.107(2)	O1-P1	1.497(2)
Cr1-N2	1.995(2)	Cr1-O1-P1	137.6(1)
Cr1-N3	1.983(2)	bite angle	67
Cr1-N4	2.145(2)	twist angle	24
Cr1-$N_{4\ plane}$	+0.16		

Figure 4.4 Structure of **3**. Thermal ellipsoids are drawn at 50 % probability. H atoms are omitted.

Single crystals were obtained from the NMR scale reaction of $[Cr_2(L^{Me})]$ with $OPPh_3$ in toluene. The crystal analysed was found to be merohedrally twinned. The twin law [0 1 0, 1 0 0, 0 0 -1] was applied to the data and the contribution from the two twin components refined as 0.106:0.894.

4.6.4 Structure of [Cr_2(μ-CNXyl)(L^{Me})], 4

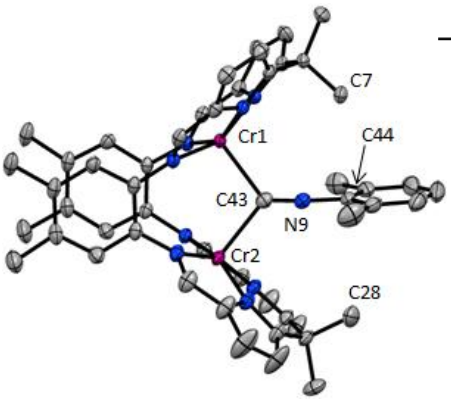

Selected bond distances (Å) and angles (°)			
Cr1···Cr2	3.5877(5)	Cr1-C43	2.259(2)
Cr1-N1	2.104(2)	Cr2-C43	2.261(2)
Cr1-N2	1.996(2)	C43-N9	1.169(3)
Cr1-N3	2.004(1)	C7···C44	3.351(3)
Cr1-N4	2.122(2)	C28···C44	3.580(3)
Cr2-N5	2.098(2)	Cr1-C43-Cr2	105.08(9)
Cr2-N6	1.985(2)	Cr1-C43-N9	127.9(2)
Cr2-N7	1.980(2)	Cr2-C43-N9	126.7(2)
Cr2-N8	2.105(2)	C43-N9-C44	175.9(2)
Cr1-$N_{4\ plane}$	−0.44	bite angle	53
Cr2-$N_{4\ plane}$	−0.34	twist angle	2

Figure 4.5 Structure of **4**. Thermal ellipsoids are drawn at 50 % probability. H atoms and lattice solvent are omitted.

Single crystals were obtained from the NMR scale reaction of [$Cr_2(L^{Me})$] with CNXyl in fluorobenzene.

4.6.5 Structure of [Cr_2(μ-CN^tBu)(L^{Me})], 5

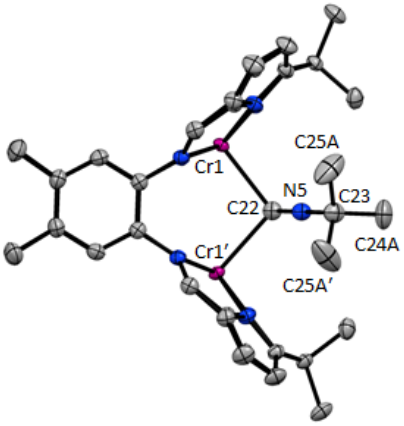

Selected bond distances (Å) and angles (°)			
Cr1···Cr1′	3.7101(3)	C22-N5	1.151(3)
Cr1-N1	2.139(1)	Cr1-C22-Cr1′	96.35(7)
Cr1-N2	2.010(1)	Cr1-C22-N5	128.50(2)
Cr1-N3	2.009(1)	C22-N5-C23	172.8(2)
Cr1-N4	2.153(1)	bite angle	56
Cr1-$N_{4\ plane}$	−0.37	twist angle	10
Cr1-C22	2.490(2)		

Figure 4.6 Structure of **5** with major orientation of the isocyanide *tert*-Bu group shown. Thermal ellipsoids are drawn at 50 % probability. H atoms and lattice solvent are omitted.

Single crystals were obtained from the NMR scale reaction of [$Cr_2(L^{Me})$] with CN^tBu in THF/C_6D_6. The *tert* butyl group of [Cr_2(μ-CN^tBu)(L)] was found to be rotationally disordered over two sites in the ratio 0.716(7):0.284(7). All disordered C atoms were refined anisotropically with distance restraints applied to the 1,2 and 1,3 C-C distances of the ^{t}Bu group of 1.51(2) Å and 2.53(4) Å respectively. In order not to violate the crystallographic symmetry, the hydrogen atoms attached to the disordered carbon atoms C24A and C24B were located in the electron density difference map. The positions of these hydrogens were

refined with a distance restraint of 0.98(1) Å applied to the C-H bond lengths and H24A and H24D were constrained to lie upon the crystallographic mirror plane.

4.6.6 Structure of $[Cr_2(\mu\text{-}I)(I)(L^{Me})(THF)]$, 6

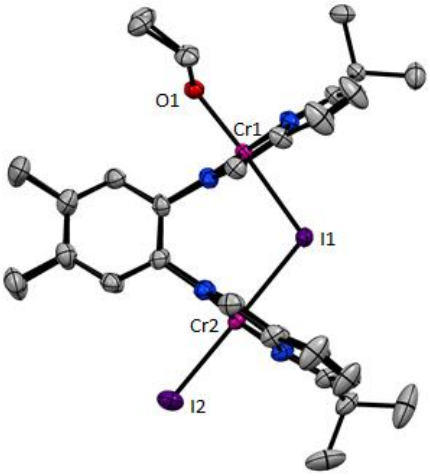

Selected bond distances (Å) and angles (°)			
Cr1···Cr2	4.3811(9)	Cr2-$N_{4\ plane}$	+0.11
Cr1-N1	2.083(3)	Cr1-O1	2.076(3)
Cr1-N2	1.950(3)	Cr1-I1	2.7131(7)
Cr1-N3	1.962(4)	Cr2-I1	2.7883(7)
Cr1-N4	2.086(3)	Cr2-I2	2.7018(8)
Cr2-N5	2.079(4)	Cr1-I1-Cr2	105.56(2)
Cr2-N6	1.959(4)	O1-Cr1-I1	179.96(9)
Cr2-N7	1.957(4)	I1-Cr2-I2	179.05(3)
Cr2-N8	2.097(3)	bite angle	67
Cr1-$N_{4\ plane}$	+0.03	twist angle	5

Figure 4.7 Structure of **6**. Thermal ellipsoids are drawn at 50 % probability. H atoms and lattice solvent are omitted.

Single crystals were grown by vapour diffusion of hexane into a THF solution of $[Cr_2(\mu\text{-}I)(I)(L^{Me})(THF)]$ at room temperature.

4.6.7 Structure of $[Cr_2(\mu\text{-}I)(L^{Me})(py)_2][I]$, 7

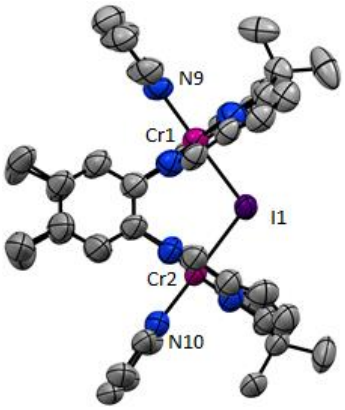

Selected bond distances (Å) and angles (°)			
Cr1···Cr2	4.417(4)	Cr2-$N_{4\ plane}$	+0.09
Cr1-N1	2.09(1)	Cr1-I1	2.756(3)
Cr1-N2	1.95(1)	Cr2-I1	2.754(2)
Cr1-N3	1.98(1)	Cr1-N9	2.10(2)
Cr1-N4	2.07(1)	Cr2-N10	2.08(1)
Cr2-N5	2.06(1)	Cr1-I1-Cr2	106.59(7)
Cr2-N6	1.97(1)	N9-Cr1-I1	179.0(4)
Cr2-N7	1.92(2)	I1-Cr2-N10	179.3(5)
Cr2-N8	2.03(1)	bite angle	69
Cr1-$N_{4\ plane}$	+0.08	twist angle	3

Figure 4.8 Structure of the cationic portion of **7**. Thermal ellipsoids are drawn at 50 % probability. H atoms are omitted.

Single crystals were obtained by layering a pyridine solution of $[Cr_2(L^{Me})]$ on top of a pyridine solution of iodine. The crystal data resolution of $[Cr_2(\mu\text{-}I)(L^{Me})(py)_2][I]$ was poor which led to problems with refinement of the structure. The carbon atoms of each aryl ring of the macrocycle and their substituents were constrained to line upon common planes with a

standard deviation of 0.01 Å from planarity. The C_{ring}-C_{Me} distances between the *ipso* aryl carbons and the aryl Me substituents were restrained to 1.51(2) Å (C17-C21, C38-C41) and 1.510(5) Å (C16-C20, C37-C42). The SIMU (su 0.04 Å^2) and DELU (su 0.01 Å^2) commands were applied to all atoms in the structure to normalise the magnitude and direction of the atomic displacement parameters of neighbouring atoms. The data were treated with SQUEEZE to remove residual electron density equating to 4.4 molecules of pyridine per formula unit from the unit cell.

4.6.8 Structure of [{Cr(Et)}$_2$(μ-IZnEt)(L^{Me})], 9

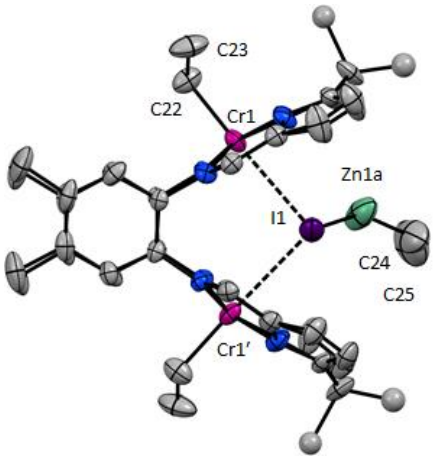

Selected bond distances (Å) and angles (°)			
Cr1···Cr1′	4.621(1)	Zn1a-C24	2.04(1)
Cr1-N1	2.069(5)	I1-Zn1b	2.701(6)
Cr1-N2	1.958(5)	Zn1b-C24	1.92(2)
Cr1-N3	1.976(5)	C22-Cr1-I1	177.2(2)
Cr1-N4	2.107(4)	Cr1-I1-Cr1′	95.34(3)
Cr1-$N_{4\ plane}$	+0.22	Cr1-C22-C23	118.6(5)
Cr1-C22	2.063(7)	I1-Zn1a-C24	151.6(8)
Cr1-I1	3.126(1)	I1-Zn1b-C24	143.4(8)
C22-C23	1.51(1)	bite angle	71
I1-Zn1a	2.497(3)	twist angle	8

Figure 4.9 Structure of **9**. The major Zn and *meso*-Me positions are shown. Thermal ellipsoids are drawn at 50 % probability. H atoms are omitted.

Single crystals were obtained from a toluene/hexane mixture stored at −30 °C for 48 hours. The *meso* Me groups were found to be disordered over two positions related by tilting of the *meso* carbon into and out of the cleft. The contributions of the two orientations were refined to 0.53(3):0.47(3). The disordered carbons were refined isotropically. The Zn atom is disordered both over two sites and about a C_2 crystallographic rotation axis which passes through I1 and the centroid of the macrocycle aryl rings. The occupancies of the Zn sites was set to 0.5 to allow for the disorder about the rotational axis and then the contributions of the two different sites refined as 0.63(1):0.37(1). The Zn atoms were refined anisotropically with distance restraints of 2.75(2) Å and 2.00(2) Å applied to the Zn-I and Zn-C_{Et} distances respectively. The large thermal ellipsoids of C24 and C25 indicate some unresolved disorder; this could not be satisfactorily modelled so the SIMU (su 0.04 Å^2) and DELU (su 0.01 Å^2) commands were applied to C24 and C25 to normalise the magnitude and direction of their atomic displacement parameters. The data were treated with SQUEEZE to remove residual electron density equating to 1 molecule of hexane or toluene per unit cell.

4.6.9 Structure of [{Cr(Et)}$_2$(*endo*-py)(L^{Me})], 10

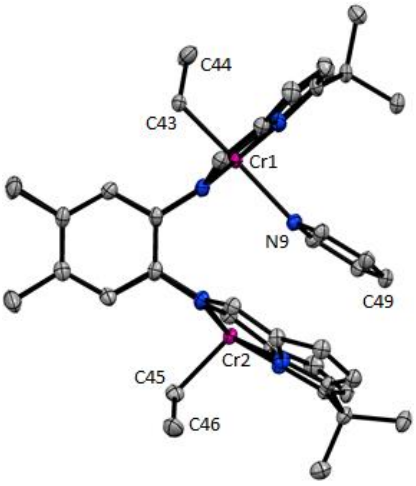

Selected bond distances (Å) and angles (°)			
Cr1···Cr2	4.550(1)	Cr1-N9	2.196(3)
Cr1-N1	2.136(3)	Cr2-C45	2.051(4)
Cr1-N2	1.984(3)	Cr2···N9	3.379(3)
Cr1-N3	1.987(3)	C43-C44	1.512(5)
Cr1-N4	2.123(3)	C45-C46	1.513(5)
Cr2-N5	2.082(3)	C43-Cr1-N9	177.5(1)
Cr2-N6	1.978(3)	Cr1-C43-C44	116.6(2)
Cr2-N7	1.975(3)	Cr2-C45-C46	115.7(2)
Cr2-N8	2.091(3)	Cr1-N9-C49	164.8(1)
Cr1-N$_{4\ plane}$	−0.02	bite angle	71
Cr2-N$_{4\ plane}$	+0.27	twist angle	7
Cr1-C43	2.087(3)		

Figure 4.10 Structure of **10**. Thermal ellipsoids are drawn at 50 % probability. H atoms and lattice solvent are omitted.

Single crystals were obtained by recrystallisation of [{Cr(Et)}$_2$(*endo*-py)(L^{Me})] from a THF/hexane mixture at −30 °C.

4.6.10 Structure of [{Cr(Et)}$_2$(*endo*-THF)(L^{Me})], 11

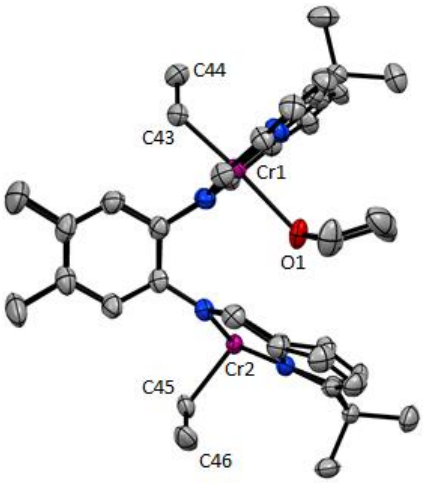

Selected bond distances (Å) and angles (°)			
Cr1···Cr2	4.6020(9)	Cr1-C43	2.087(4)
Cr1-N1	2.107(3)	Cr1-O1	2.359(3)
Cr1-N2	1.967(3)	Cr2-C45	2.064(4)
Cr1-N3	1.971(3)	Cr2···O1	3.345(3)
Cr1-N4	2.111(3)	C43-C44	1.520(6)
Cr2-N5	2.080(3)	C45-C46	1.509(6)
Cr2-N6	1.964(3)	C43-Cr1-O1	175.6(1)
Cr2-N7	1.975(3)	Cr1-C43-C44	118.0(3)
Cr2-N8	2.091(3)	Cr2-C45-C46	115.7(3)
Cr1-N$_{4\ plane}$	−0.03	bite angle	71
Cr2-N$_{4\ plane}$	+0.30	twist angle	5

Figure 4.11 Structure of **11**. The major orientation of the bridging THF molecule is shown. Thermal ellipsoids are drawn at 50 % probability. H atoms and lattice solvent are omitted.

Single crystals were obtained from a THF/hexane mixture stored at −30 °C for 48 hours. The carbon atoms at the 2 and 3 positions of the in-cleft THF molecule were found to be disordered over two sites in a 0.73(2):0.27(2) ratio. The disordered components were

refined anisotropically. Appropriate C-C and C-O distance restraints were applied to two molecules of THF lattice solvent.

4.6.11 Structure of [{UI(py)}{U(OH)(py)}(μ-O)(L^A)], 13

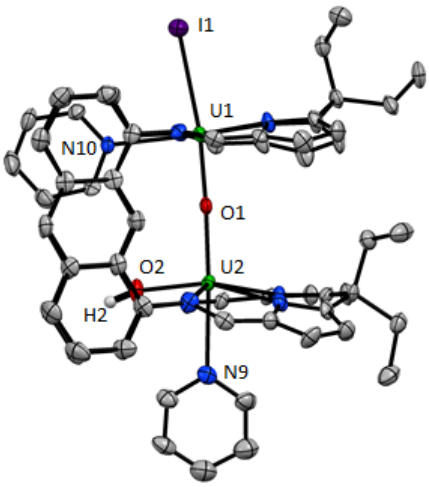

Selected bond distances (Å) and angles (°)			
U1···U2	4.2472(5)	U2-$N_{4\ plane}$	−0.54
U1-N1	2.550(7)	U1-I1	3.1032(8)
U1-N2	2.417(9)	U1-N10	2.655(8)
U1-N3	2.439(6)	U1-O1	2.047(7)
U1-N4	2.557(8)	U2-O1	2.201(7)
U2-N5	2.588(9)	U2-O2	2.065(8)
U2-N6	2.523(7)	U2-N9	2.629(7)
U2-N7	2.511(9)	U1-O1-U2	177.0(4)
U2-N8	2.569(7)	I1-U1-O1	171.5(2)
U1-$N_{4\ plane}$	−0.13	O1-U2-N9	176.4(2)

Figure 4.12 Structure of **13**. Thermal ellipsoids are drawn at 50 % probability. All H atoms except H2 and lattice solvent are omitted.

Single crystals grew as a result of serendipitous oxidation of a pyridine/hexane solution of **12** stored in the glovebox. The OH proton of [{UI(py)}{U(OH)(py)}(μ-O)(L^A)] was located in the residual electron density map and its position refined with a distance restraint of 0.82(2) Å applied to the O-H bond length. The SIMU (su 0.04 $Å^2$) and DELU (su 0.01 $Å^2$) commands were applied to all atoms in the structure to normalise the magnitude and direction of the atomic displacement parameters of neighbouring atoms. The data were treated with SQUEEZE to remove residual electron density equating to half a molecule of hexane per unit cell.

4.6.12 Structure of $[U(BH_4)_2(THF)_5][U_2(BH_4)_{4.89}I_{2.11}(THF)_3]$, 15

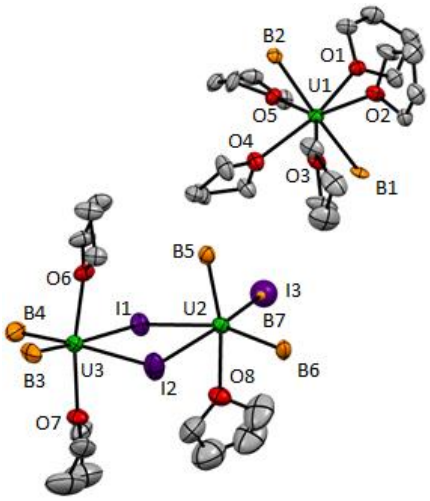

Selected bond distances (Å) and angles (°)			
U1···B1	2.72(1)	U2···B5	2.73(2)
U1···B2	2.79(1)	U2···B6	2.69(2)
U1-O1	2.563(7)	U2···B7	2.72(1)
U1-O2	2.531(9)	U2-I1	3.330(1)
U1-O3	2.561(9)	U2-I2	3.240(1)
U1-O4	2.53(1)	U2-I3	3.05(2)
U1-O5	2.511(9)	U2-O8	2.56(1)
U2···U3	4.9379(9)	U2-I1-U3	96.96(3)
U3···B3	2.69(2)	U2-I2-U3	100.92(4)
U3···B4	2.63(2)	I1-U2-I2	78.18(3)
U3-I1	3.265(1)	I1-U3-I2	80.24(3)
U3-I2	3.163(2)	B6-U2-B7	99.5(4)
U3-O6	2.44(1)	B3-U3-B4	99.3(6)
U3-O7	2.521(9)	B1-U1-B2	177.2(4)

Figure 4.13 Structure of **15** showing both components at the disordered BH_4/I site and only the major orientation of disordered THF ligands. Thermal ellipsoids are drawn at 50 % probability. H atoms are omitted.

Single crystals were grown by recrystallisation of **14** from Et_2O at 4 °C. One terminal equatorial ligand site of the anion was found to be part occupied by BH_4^- and part by I^- in a 0.897(7):0.103(7) ratio. B7 and I3 were refined isotropically with the U-B and U-I distances fixed to 2.70(2) Å and 3.20(2) Å respectively. The THF ligand (O8, C29-C32) was found to be exist in two conformations related by rotation about the U2-O8 bond. Their relative occupancy was refined as 0.35(3):0.65(3) and all atoms were modelled anisotropically. C11, the carbon at the 2 position of THF ligand (O3, C9-C12) was also found to be disordered over two sites in a 0.54(6):0.46(6) ratio.

4.6.13 Structure of $[U(BH_4)_{2.59}I_{0.41}(DME)_2]$, 16

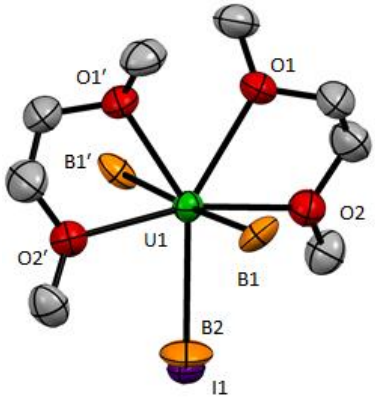

Selected bond distances (Å) and angles (°)			
U1···B1	2.78(1)	B1-U1-B1′	176.9(4)
U1-O1	2.571(5)	O1-U1-O2	63.5(2)
U1-O2	2.609(7)	B1-U1-B2	91.6(2)
U1-I1	3.097(4)	O1-U1-O1′	67.5(3)
U1···B2	2.82(2)	O2-U1-B2	82.9(1)

Figure 4.14 Structure of **16** showing both components at the disordered BH_4/I site. Thermal ellipsoids are drawn at 50 % probability. H atoms are omitted.

Single crystals were grown by slow diffusion of hexane into a DME/benzene solution of **14**. One terminal equatorial ligand site of the molecule was found to be part occupied by BH_4^- and part by I^- in a 0.586(6):0.414(6) ratio. B2 and I1 were refined anisotropically with the U···B distance fixed to 2.80(2) Å.

4.6.14 Structure of $[Na(py)_4][\{U(BH_4)\}_2(\mu\text{-}BH_4)(L^A)(py)_2]$, 18_{py}

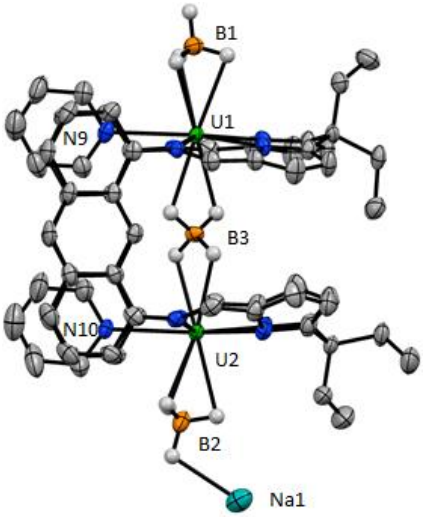

Selected bond distances (Å) and angles (°)			
U1···U2	5.9243(3)	U1···B1	2.681(9)
U1-N1	2.639(5)	U1···B3	2.977(7)
U1-N2	2.476(4)	U2···B3	2.949(7)
U1-N3	2.480(4)	U2···B2	2.723(8)
U1-N4	2.592(5)	U1-N9	2.698(4)
U2-N5	2.618(5)	U2-N10	2.709(4)
U2-N6	2.499(4)	Na1···B2	2.932(9)
U2-N7	2.496(4)	U1-B3-U2	177.8(3)
U2-N8	2.631(5)	B1-U1-B3	175.5(2)
U1-$N_{4\ plane}$	+0.37	B2-U2-B3	169.3(2)
U2-$N_{4\ plane}$	+0.34	Na1-B2-U2	134.1(3)

Figure 4.15 Structure of $\mathbf{18_{py}}$. Thermal ellipsoids are drawn at 50 % probability. Four molecules of pyridine solvent ligating Na1, lattice solvent and all H atoms except those of the BH_4 groups are omitted.

Single crystals were grown from a pyridine/hexane solution of **18** at room temperature. The H atoms of the three BH_4 groups were located in the residual electron density map and their positions refined. The following constraints were imposed on the BH_4

groups: (a) all B-H distances were constrained to be equal within a standard uncertainty of 0.02 Å (b) H···H distances within the same BH_4 group were constrained to be equal within a standard uncertainty of 0.04 Å (c) the atomic displacement parameters of all H atoms were constrained to be equal (d) for the bridging BH_4 group only, all H-U distances were constrained to be equal within a standard uncertainty of 0.02 Å. Two molecules of pyridine lattice solvent located at the corners of the unit cell were necessarily refined for reasons of crystal symmetry with two ring positions half-N and half-C occupied. The N and C components were constrained to occupy the same position and possess the same atomic displacement parameters. The SIMU (su 0.04 $Å^2$) and DELU (su 0.01 $Å^2$) commands were applied to the atoms of two pyridine rings (one ligating Na1, the other bound to U2 in the fifth equatorial site) to normalise the magnitude and direction of the atomic displacement parameters of neighbouring atoms.

4.6.15 Structure of $[Li(THF)_4][\{U(BH_4)\}_2(\mu\text{-}BH_4)(L^{Me})]$, 21

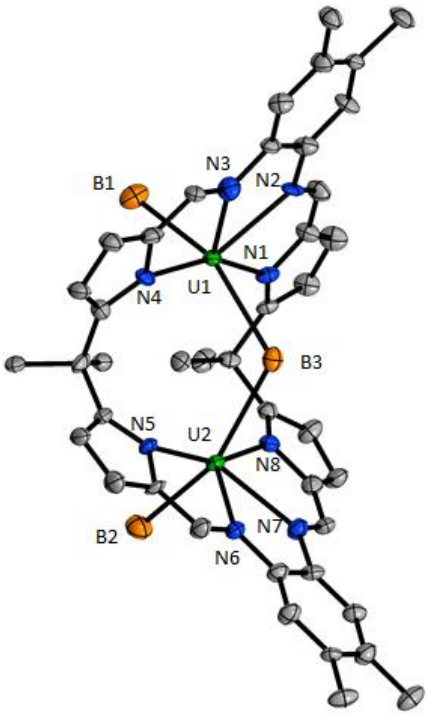

Selected bond distances (Å) and angles (°)			
U1···U2	4.7884(3)	U1-$N_{4\ plane}$	+0.12
U1-N1	2.590(9)	U2-$N_{4\ plane}$	+0.12
U1-N2	2.491(7)	U1···B1	2.630(9)
U1-N3	2.51(1)	U1···B3	2.915(7)
U1-N4	2.585(9)	U2···B3	2.911(7)
U2-N5	2.575(9)	U2···B2	2.640(9)
U2-N6	2.512(8)	U1-B3-U2	110.5(3)
U2-N7	2.487(9)	B1-U1-B3	158.7(3)
U2-N8	2.585(9)	B2-U2-B3	158.6(3)

Figure 4.16 Structure of the anionic portion of **21**. Thermal ellipsoids are drawn at 50 % probability. H atoms and lattice solvent are omitted.

Single crystals were obtained by recrystallisation of **21** from refluxing THF. The $[Li(THF)_4]^+$ cation of **21** was found to be considerably disordered. Unfortunately, this disorder could not be satisfactorily modelled and instead appropriate restraints were applied to the 1,2 and 1,3 distances of the THF rings and all Li-O distances were fixed to 1.94(2) Å.

Due to this unresolved disorder of the ligating THF molecules, H atoms on neighbouring THF molecules approached too close to one another. The BUMP command was used to increase the separation of the carbon atoms whose H atoms were approaching too close to each other.

4.6.16 Structure of [{U(OAr)}$_2$(*endo*-BH$_4$K)(L^A)(THF)$_2$], 22

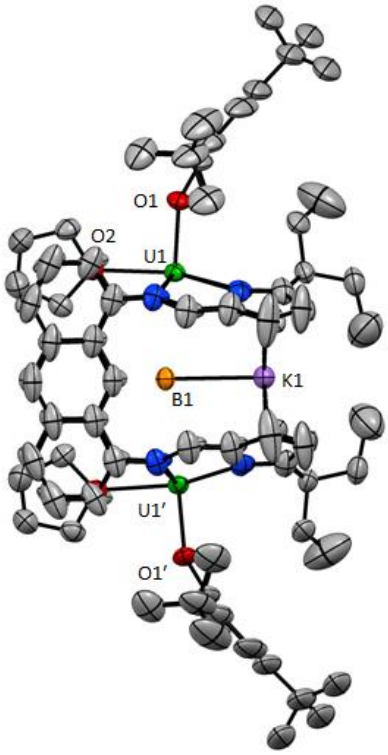

Selected bond distances (Å) and angles (°)			
U1···U1′	6.5881(3)	U1-O2	2.554(5)
U1-N1	2.654(6)	K1-B1	3.036(11)
U1-N2	2.513(6)	K1-Pyr$_{cent}$	3.154(2),
U1-N3	2.494(6)		3.153(2)
U1-N4	2.654(6)	U1-B1-U1′	168.2(4)
U1-N$_{4\ plane}$	+0.70	O1-U1-B1	178.3(2)
U1···B1	3.3116(11)	U1-B1-K1	84.1(2)
U1-O1	2.231(5)	U1-O1-C$_{ipso}$	154.0(5)

Figure 4.17 Structure of **22** showing the major orientation of the ^{t}Bu groups. Thermal ellipsoids are drawn at 50 % probability. H atoms and lattice solvent are omitted.

Single crystals were obtained from the NMR scale reaction of **18** with K(OAr) in d_8-THF, left to stand for 24 hours. The *para* tert-butyl group of the aryloxide ligand was found to be rotationally disordered over two sites in the ratio 0.42(2):0.58(2). All atoms were successfully refined anisotropically with distance restraints of 1.53(2) Å applied to the 1,2 C-CH_3 distances, 2.44(4) Å to the 1,3 CH_3···CH_3 distances and 2.50(4) Å to the 1,3 *ipso*-C···CH_3 distances. The atomic displacement parameters of the three carbon atoms in each orientation were constrained to be equal.

4.6.17 Structure of [{U(OAr)}$_2$(*endo*-BH$_4$Na)(L^A)(THF)$_2$], 23

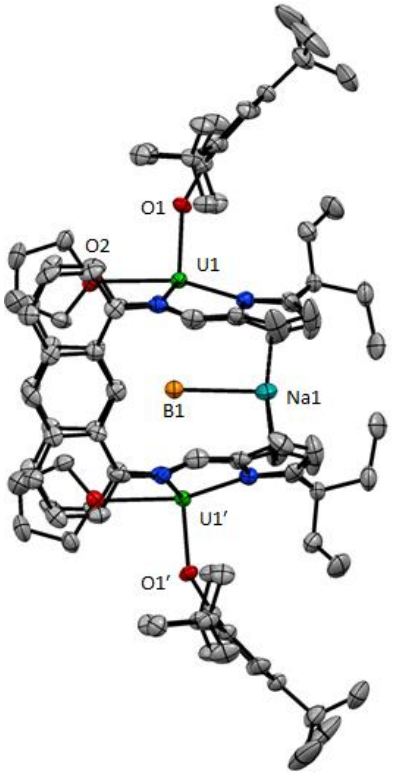

Selected bond distances (Å) and angles (°)			
U1···U1′	6.5265(7)	Na1-B1	2.747(2)
U1-N1	2.636(7)	Na1-Pyr$_{cent}$	2.85(4)
U1-N2	2.506(7)		3.04(2)
U1-N3	2.506(7)		3.08(4)
U1-N4	2.654(5)		3.61(2)
U1-N$_{4\ plane}$	+0.69	U1-B1-U1′	173.0(6)
U1-O2	2.592(6)	O1-U1-B1	177.6(1)
U1···B1	3.269(1)	U1-B1-Na1	89.1(8)
U1-O1	2.245(6)	U1-O1-C$_{ipso}$	153.3(6)

Figure 4.18 Structure of **23** showing major orientation of *meso* Et groups and only one Na position. Thermal ellipsoids are drawn at 50 % probability. H atoms and lattice solvent are omitted.

Single crystals were obtained from the NMR scale reaction of **18** with Na(OAr) in d_8-THF, left to stand for 10 days. The CH_3 groups of the *meso* ethyl groups were found to be disordered over two sites in the ratio 0.51(1):0.49(1). All disordered atoms were refined anisotropically. In the initial solution Na1 lay on the crystallographic C_2 rotational axis. However, its thermal ellipsoid was severely elongated so the position of Na1 was perturbed creating two half-occupied Na sites related by rotation about the C_2 axis. The data were treated with SQUEEZE to remove residual electron density equating to 3 molecules of THF per unit cell.

4.6.18 Structure of [{U(OAr)}$_2$(μ-S$_2$)(L^A)], 25

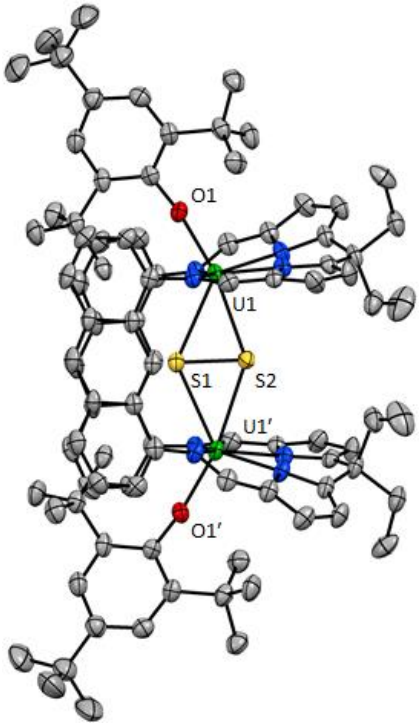

Selected bond distances (Å) and angles (°)			
U1···U1′	5.1571(5)	S1-S2	2.118(3)
U1-N1	2.534(6)	O1-U1-S1	125.7(1)
U1-N2	2.433(5)	O1-U1-S2	166.6(1)
U1-N3	2.391(5)	U1-S1-U1′	131.98(7)
U1-N4	2.728(6)	U1-S2-U1′	135.0(1)
U1-N$_{4\ plane}$	−0.07	S1-S2-U1	70.40(8)
U1-O1	2.091(3)	S2-S1-U1	64.62(8)
U1-S1	2.8229(8)	U1-S$_{2\ cent}$-U1′	165.4
U1-S2	2.707(3)	U1-O1-C$_{ipso}$	169.0(3)

Figure 4.19 Structure of **25** omitting the second, symmetry generated S2 position. Thermal ellipsoids are drawn at 50 % probability. H atoms and lattice solvent are omitted.

Single crystals were grown by vapour diffusion of hexane into a benzene solution of [{U(OAr)}$_2$(μ-S$_2$)(L^A)] at room temperature. S2 was found to be disordered over two sites about the crystallographic C_2 rotational axis so the occupancy of each site was set to 0.5. The C-C bonds of a molecule of benzene lattice solvent were fixed to a distance of 1.38(1) Å and all six carbon atoms were constrained to lie upon a single plane. The SIMU (su 0.04 Å^2) and DELU (su 0.01 Å^2) commands were applied to the benzene carbon atoms. The data were treated with SQUEEZE to remove residual electron density equating to 2.5 molecules of hexane per unit cell.

4.6.19 Structure of [{U(OAr)}$_2$(μ-S)(L^A)], 27

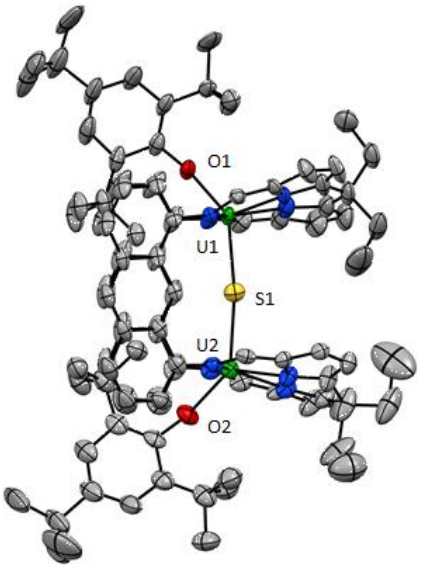

Selected bond distances (Å) and angles (°)			
U1···U2	5.1899(5)	U2-$N_{4\ plane}$	−0.03
U1-N1	2.627(7)	U1-O1	2.081(6)
U1-N2	2.415(7)	U1-S1	2.594(2)
U1-N3	2.418(6)	U2-S1	2.608(2)
U1-N4	2.561(8)	U2-O2	2.099(6)
U2-N5	2.621(7)	U1-S1-U2	172.0(1)
U2-N6	2.427(7)	O1-U1-S1	143.2(2)
U2-N7	2.409(7)	S1-U2-O2	140.1(2)
U2-N8	2.555(7)	U1-O1-C_{ipso}	170.4(5)
U1-$N_{4\ plane}$	−0.10	U2-O2-C_{ipso}	167.8(6)

Figure 4.20 Structure of **27**. Thermal ellipsoids are drawn at 50 % probability. H atoms and lattice solvent are omitted.

Single crystals were grown by vapour diffusion of hexane into a mixture of [{U(OAr)}$_2$(*endo*-BH_4K)(L^A)(THF)$_2$] and CS_2 in toluene at room temperature. One meso carbon atom of the macrocycle and the two ethyl groups bound to it appeared to be disordered. However, this disorder could not be modelled successfully so instead distance restraints were applied to the 1,2 C-C distances of 1.56(1) Å (C_{meso}-CH_2) and 1.52(1) Å (CH_2-CH_3). The magnitude and direction of the atomic displacement parameters of these five C atoms were normalised using the SIMU (su 0.04 Å^2) and DELU (su 0.01 Å^2) commands. The six ring carbon atoms of the molecule of toluene lattice solvent were refined as a perfect hexagon and the methyl carbon was constrained to lie in the plane of the ring with distance restraints placed on the 1,3 CH_3-C_{ortho} distances of 2.55(2) Å. The SIMU (su 0.04 Å^2) and DELU (su 0.01 Å^2) commands were applied to all the toluene carbon atoms.

4.6.20 Structure of $[\{UO_2\}_2(L^A)(THF)_2]$, 28

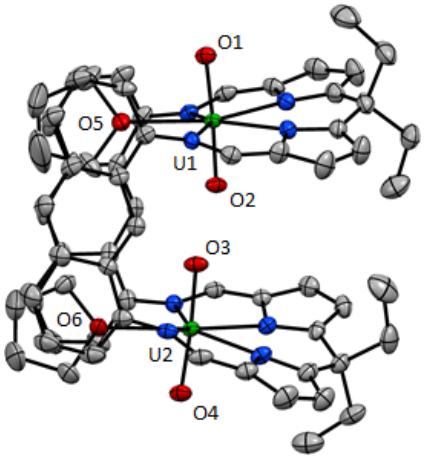

Selected bond distances (Å) and angles (°)			
U1···U2	5.6727(5)	U2-$N_{4\ plane}$	+0.18
U1-N1	2.559(4)	U1-O1	1.772(3)
U1-N2	2.432(4)	U1-O2	1.754(3)
U1-N3	2.436(4)	U2-O3	1.762(3)
U1-N4	2.566(4)	U2-O4	1.774(3)
U2-N5	2.532(4)	U1-O5	2.457(3)
U2-N6	2.420(4)	U2-O6	2.470(3)
U2-N7	2.442(4)	O2···O3	2.707(5)
U2-N8	2.595(4)	O1-U1-O2	176.4(2)
U1-$N_{4\ plane}$	+0.09	O3-U2-O4	175.6(2)

Figure 4.21 Structure of **28**. Thermal ellipsoids are drawn at 50 % probability. H atoms and lattice solvent are omitted.

Single crystals formed in both a THF solution of $[Na(THF)_4][\{U(BH_4)\}_2(\mu\text{-}BH_4)(L^A)(THF)_2]$ under O_2 and in a C_6D_6 solution of $[\{U(OAr)\}_2(endo\text{-}BH_4K)(L^A)(THF)_2]$ under O_2. The data quality for the crystal isolated from THF was superior and is presented here. The unit cell parameters (*a*, *b*, *c* (Å), α, β, γ (°), *V* (Å^3)) of the crystal from C_6D_6 were 14.0407(5), 14.6897(5), 19.0950(6), 89.884(3), 86.652(3), 81.574(3), 3889.1(2). The structure of the pyridine adduct $[\{UO_2\}_2(L^A)(py)_2]$ has been reported.[15]

During structure refinement appropriate 1,2 and 1,3 distance restraints were applied to two molecules of THF lattice solvent. The SIMU (su 0.04 Å^2) and DELU (su 0.01 Å^2) commands were applied to the atoms of all the THF molecules to normalise the magnitude and direction of the atomic displacement parameters of neighbouring atoms. The data were treated with SQUEEZE to remove residual electron density equating to 0.5 molecules of THF per unit cell.

4.6.21 Structure of $[Li(py)_4][\{U(Cl)\}_2(\mu\text{-}Cl)_3(L^A)]$, 33

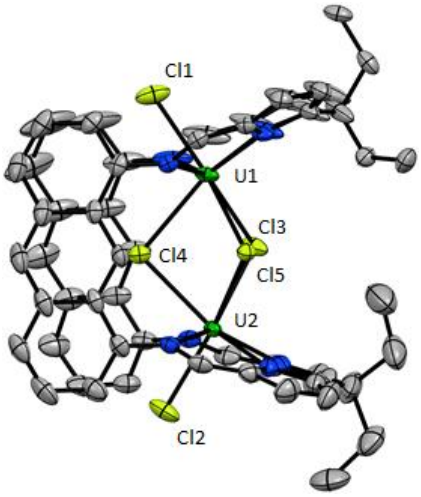

Selected bond distances (Å) and angles (°)			
U1···U2	4.1927(3)	U1-Cl4	2.833(1)
U1-N1	2.582(3)	U1-Cl5	2.872(1)
U1-N2	2.383(4)	U2-Cl3	2.871(1)
U1-N3	2.383(4)	U2-Cl4	2.840(1)
U1-N4	2.643(3)	U2-Cl5	2.849(1)
U2-N5	2.611(3)	U1-Cl3-U2	95.04(3)
U2-N6	2.387(4)	U1-Cl4-U2	95.32(3)
U2-N7	2.377(4)	U1-Cl5-U2	94.23(4)
U2-N8	2.597(3)	Cl1-U1-Cl3	147.56(4)
$U1\text{-}N_{4\ plane}$	−0.57	Cl1-U1-Cl4	104.73(4)
$U2\text{-}N_{4\ plane}$	−0.65	Cl1-U1-Cl5	144.65(4)
U1-Cl1	2.595(1)	Cl2-U2-Cl3	145.89(4)
U2-Cl2	2.610(2)	Cl2-U2-Cl4	105.90(4)
U1-Cl3	2.868(1)	Cl2-U2-Cl5	145.73(4)

Figure 4.22 Structure of the anionic portion of **33** showing major orientation of *meso* Et groups. Thermal ellipsoids are drawn at 50 % probability. H atoms and lattice solvent are omitted.

Single crystals were grown by layering toluene on top of a pyridine solution of $[Li(py)_4][\{U(Cl)\}_2(\mu\text{-}Cl)_3(L^A)]$ in an NMR tube. Two of the *meso* Et groups were found to be disordered over two sites each. The contributions of the two conformers were refined as 0.58(4):0.42(4) and 0.52(1):0.48(1). One pyridine molecule co-ordinated to the Li cation was found to exist in two orientations related by rotation about the Li-N bond in the ratio 0.51(1):0.49(1). Two molecules of pyridine lattice solvent located at inversion centres were necessarily refined for reasons of crystal symmetry with two ring positions half-N and half-C occupied. The N and C components were constrained to occupy the same position and possess the same atomic displacement parameters. The SIMU (su 0.04 $Å^2$) and DELU (su 0.01 $Å^2$) commands were applied to the atoms of the pyridine rings bound to the Li cation to normalise the magnitude and direction of the atomic displacement parameters of neighbouring atoms.

4.6.22 Structure of [{U(O^{t}Bu)Cl}{U(O^{t}Bu)py}(μ-Cl)(L^A)], 34

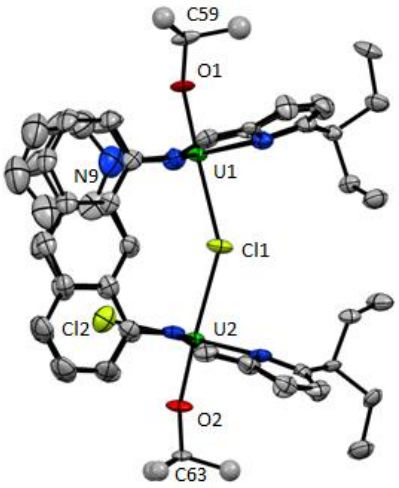

Selected bond distances (Å) and angles (°)			
U1···U2	5.4155(8)	U1-O1	2.049(11)
U1-N1	2.55(2)	U2-O2	2.012(12)
U1-N2	2.39(2)	U1-Cl1	2.771(5)
U1-N3	2.43(2)	U2-Cl1	2.826(5)
U1-N4	2.55(2)	U1-N9	2.52(1)
U2-N5	2.56(1)	U2-Cl2	2.700(6)
U2-N6	2.44(1)	U1-Cl1-U2	150.8(2)
U2-N7	2.43(2)	O1-U1-Cl1	177.7(4)
U2-N8	2.59(1)	O2-U2-Cl1	176.7(4)
U1-$N_{4\ plane}$	−0.02	C59-O1-U1	164(1)
U2-$N_{4\ plane}$	+0.03	C63-O2-U2	165(1)

Figure 4.23 Structure of **34** showing major orientation of ^{t}Bu groups. Thermal ellipsoids are drawn at 50 % probability. H atoms and lattice solvent are omitted.

Single crystals were grown by vapour diffusion of hexane into a benzene solution of [{U(O^{t}Bu)Cl}{U(O^{t}Bu)py}(μ-Cl)(L^A)] at room temperature. The ^{t}Bu groups of the alkoxides were found to be rotationally disordered over two sites in the ratio 0.45(3):0.55(3). The SIMU (su 0.04 Å^2) and DELU (su 0.01 Å^2) commands were applied to *ca.* half the atoms of the macrocycle to normalise the magnitude and direction of the atomic displacement parameters of neighbouring atoms. The data were treated with SQUEEZE to remove residual electron density equating to 5.4 molecules of hexane per unit cell.

Table 4.3: Summary of crystal data, data collection and structure refinement.

Compound	**1**	**2_{THF}**	**3**	**4**
Chemical formula	$C_{42}H_{40}Cr_2N_8 \cdot (C_6H_6)$	$C_{66}H_{64}Cr_2N_8O_2 \cdot C_8H_{16}O_2$	$C_{78}H_{70}Cr_2N_8O_2P_2$	$C_{51}H_{49}Cr_2N_9 \cdot C_6H_5F$
M_r	838.93	1249.46	1317.36	988.09
Crystal system, space group	Monoclinic, *C*2/*c*	Monoclinic, $P2_1/C$	Tetragonal, $I4_1/A$	Triclinic, $P\bar{1}$
Temperature (K)	170	120	120	170
***a*, *b*, *c* (Å)**	21.1687 (4) 13.6236 (2) 15.7156 (3)	16.3764 (3) 31.3196 (5) 25.4554 (5)	17.3884 (2) 17.3884 (2) 43.7105 (8)	8.8576 (2) 11.7478 (3) 24.1946 (5)
α, β, γ (°)	90 114.066 (2) 90	90 104.808 (2) 90	90 90 90	92.446 (2) 99.316 (2) 96.709 (2)
***V* (Å^3)**	4138.32 (13)	12622.5 (4)	13216.2 (3)	2462.53 (10)
Z	4	8	8	2
Radiation type	Mo *K*α	Cu *K*α	Cu *K*α	Mo *K*α
μ (mm^{-1})	0.57	3.29	3.60	0.49
Crystal size (mm)	0.34×0.20×0.11	0.25×0.07×0.03	0.16×0.08×0.04	0.57×0.19×0.10
Diffractometer	Xcalibur, Eos	SuperNova	SuperNova	Xcalibur, Eos
Absorption correction	Multi-scan	Gaussian	Gaussian	Multi-scan
T_{min}, T_{max}	0.974, 1.000	0.665, 1.070	0.700, 0.869	0.836, 1.000
No. of measured, independent and observed {$I > 2\sigma(I)$} reflections	29441, 4751, 3952	189180, 22526, 15529	53067, 6667, 6256	56973, 11283, 9000
R_{int}	0.036	0.095	0.041	0.037
$(\sin\theta/\lambda)_{max}$ (Å^{-1})	0.649	0.597	0.623	0.649
$R[F^2 > 2\sigma(F^2)]$, $wR(F^2)$, S	0.036, 0.112, 0.69	0.075, 0.226, 1.03	0.038, 0.111, 1.06	0.043, 0.111, 1.02
No. of parameters	266	1593	418	620
No. of restraints	0	40	0	0
H-atom treatment	riding	riding	riding	riding
$\Delta\rangle_{max}$, $\Delta\rangle_{min}$ (e Å^{-3})	0.34, -0.33	0.95, −1.04	0.94, -0.42	0.51, -0.51
CCDC Number	958989	-	958992	958990

Compound	**5**	**6**	**7**	**9**
Chemical formula	$C_{47}H_{49}Cr_2N_9 \cdot 2(C_6H_6)$	$C_{46}H_{48}Cr_2I_2N_8O \cdot C_6H_6$	$[C_{52}H_{50}Cr_2IN_{10}][I]$	$C_{48}H_{55}Cr_2IN_8Zn$
M_r	1000.16	1164.83	1172.82	1040.27
Crystal system, space group	Monoclinic, $P2_1/m$	Monoclinic, $P2_1/n$	Hexagonal, $P3_121$	Orthorhombic, $Pbcn$
Temperature (K)	170	170	120	170
***a*, *b*, *c* (Å)**	9.6071 (2) 19.8185 (5) 13.4726 (3)	13.0276 (3) 15.5305 (4) 24.4412 (6)	18.671 (5) 18.671 (5) 35.936 (5)	13.2716 (4) 26.3101 (8) 14.8764 (4)
α, β, γ (°)	90 90.911 (2) 90	90 93.101 (2) 90	90 90 120	90 90 90
***V* (Å^3)**	2564.84 (10)	4937.8 (2)	10849 (4)	5194.5 (3)
Z	2	4	6	4
Radiation type	Mo *K*α	Mo *K*α	Cu *K*α	Mo *K*α
μ (mm^{-1})	0.47	1.74	9.43	1.50
Crystal size (mm)	0.84×0.16×0.14	0.53×0.19×0.03	0.31×0.08×0.08	0.73×0.52×0.23
Diffractometer	Xcalibur, Eos	Xcalibur, Eos	SuperNova	Xcalibur, Eos
Absorption correction	Multi-scan	Multi-scan	Gaussian	Multi-scan
T_{min}, T_{max}	0.804, 1.000	0.783, 1.000	0.179, 0.624	0.735, 1.000
No. of measured, independent and observed {$I > 2\sigma(I)$} reflections	36945, 6053, 5065	47034, 11320, 8585	56758, 14791, 10423	5953, 5953, 5119
R_{int}	0.032	0.050	0.043	0.028
$(\sin\theta/\lambda)_{max}$ (Å^{-1})	0.649	0.649	0.630	0.649
$R[F^2 > 2\sigma(F^2)]$, $wR(F^2)$, S	0.034, 0.087, 1.01	0.047, 0.125, 1.04	0.089, 0.290, 1.13	0.083, 0.255, 1.08
No. of parameters	357	582	575	302
No. of restraints	10	48	649	7
H-atom treatment	riding and independent	riding	riding	riding
$\Delta\rangle_{max}$, $\Delta\rangle_{min}$ (e Å^{-3})	0.33, -0.38	1.14, −1.05	1.48, −1.03	3.11, −1.81
CCDC Number	958991	-	-	-

Compound	**10**	**11**	**13**	**15**
Chemical formula	$C_{51}H_{55}Cr_2N_9 \cdot C_4H_8O$	$C_{50}H_{58}Cr_2N_8O \cdot 2(C_4H_8O)$	$C_{68}H_{59}IN_{10}O_2U_2 \cdot 3(C_5H_5N)$	$[C_{20}H_{40}B_2O_5U][C_{12}H_{24}B_{4.90}I_{2.10}O_3U_2]$
M_r	970.14	1035.25	1888.51	1620.39
Crystal system, space group	Orthorhombic, *Pbca*	Orthorhombic, *Pbca*	Triclinic, $P\bar{1}$	Monoclinic, $P2_1/c$
Temperature (K)	120	170	170	120
***a*, *b*, *c* (Å)**	17.785 (5) 17.040 (5) 32.446 (5)	21.777 (7) 13.6434 (12) 36.836 (3)	11.0751 (2), 15.0152 (3), 24.1321 (5)	12.408 (5), 12.605 (5), 34.820 (5)
α, β, γ (°)	90 90 90	90 90 90	87.395 (2), 84.766 (2), 69.187 (2)	90 90.440 (5) 90
***V* (Å^3)**	9833 (4)	10944 (4)	3735.17 (13)	5446 (3)
Z	8	8	2	4
Radiation type	Cu *K*α	Mo *K*α	Mo *K*α	Cu *K*α
μ (mm^{-1})	4.02	0.45	4.80	34.01
Crystal size (mm)	0.33×0.10×0.09	0.67×0.29×0.20	0.24×0.11×0.01	0.29×0.24×0.20
Diffractometer	SuperNova	Xcalibur, Eos	Xcalibur, Eos	SuperNova
Absorption correction	Gaussian	Analytical	Multi-scan	Multi-scan
T_{min}, T_{max}	0.884, 0.953	0.969, 0.991	0.784, 1.000	0.430, 1.000
No. of measured, independent and observed {$I > 2\sigma(I)$} reflections	40676, 10014, 8449	67719, 11106, 9128	9100, 9100, 7133	131284, 11371, 11140
R_{int}	0.085	0.042	0.102	0.124
$(\sin\theta/\lambda)_{max}$ (Å^{-1})	0.629	0.624	0.526	0.630
$R[F^2 > 2\sigma(F^2)]$, $wR(F^2)$, S	0.061, 0.155, 1.05	0.070, 0.182, 1.12	0.045, 0.105, 0.91	0.073, 0.194, 1.12
No. of parameters	608	663	918	507
No. of restraints	0	91	962	96
H-atom treatment	riding	riding	riding and independent	riding
$\Delta\rangle_{max}$, $\Delta\rangle_{min}$ (e Å^{-3})	0.74, −0.68	0.82, −0.53	1.80, -0.72	5.22, −5.43
CCDC Number	-	-	999594	-

Compound	**16**	**18$_{py}$**	**21**	**22**
Chemical formula	$C_8H_{20}B_{2.59}I_{0.41}O_4U$	$C_{88}H_{90}B_3N_{14}NaU_2\cdot 3(C_5H_5N)$	$C_{42}H_{40}B_3N_8U_2\cdot C_{16}H_{32}LiO_4\cdot 3(C_4H_8O)$	$C_{102}H_{122}BKN_8O_4U_2\cdot C_4H_8O$
M_r	498.76	2112.52	1676.98	2122.15
Crystal system, space group	Tetragonal, $I4_1a$	Triclinic, $P\bar{1}$	Monoclinic, $P2_1$	Orthorhombic, *Pnma*
Temperature (K)	120	170	120	120
***a*, *b*, *c* (Å)**	12.125 (5), 12.125 (5), 23.793 (5)	11.6073 (2), 16.4500 (3), 26.2923 (6)	14.2234 (1), 17.8038 (2), 14.2288 (1)	29.6933 (4), 29.9161 (4), 10.8656 (1)
α, β, γ (°)	90 90 90	103.397 (2), 101.111 (2), 99.360 (2)	90 90.588 (1) 90	90 90 90
***V* (Å^3)**	3498 (3)	4677.74 (16)	3602.98 (5)	9652.0 (2)
Z	8	2	2	4
Radiation type	Cu *K*α	Mo *K*α	Cu *K*α	Cu *K*α
μ (mm^{-1})	31.59	3.52	12.99	10.19
Crystal size (mm)	0.20×0.12×0.02	0.64×0.20×0.02	0.13×0.12×0.08	0.14×0.10×0.03
Diffractometer	SuperNova	Xcalibur, Eos	SuperNova	SuperNova
Absorption correction	Multi-scan	Multi-scan	Multi-scan	Gaussian
T_{min}, T_{max}	0.119, 1.000	0.526, 1.000	0.703, 1.000	0.789, 0.952
No. of measured, independent and observed {$I > 2\sigma(I)$} reflections	28860, 1847, 1553	68401, 19119, 13698	119820, 15028, 14418	159878, 10302, 8057
R_{int}	0.111	0.055	0.046	0.067
$(\sin\theta/\lambda)_{max}$ (Å^{-1})	0.634	0.625	0.631	0.632
$R[F^2 > 2\sigma(F^2)]$, $wR(F^2)$, S	0.040, 0.121, 1.12	0.043, 0.092, 1.06	0.039, 0.102, 1.06	0.047, 0.131, 1.06
No. of parameters	82	1172	824	575
No. of restraints	8	180	324	130
H-atom treatment	riding	riding and independent	riding	riding
$\Delta\rangle_{max}$, $\Delta\rangle_{min}$ (e Å^{-3})	0.99, −2.54	2.34, -0.83	2.28, -1.19	2.44, −2.11
CCDC Number	-	999593	999592	-

Compound	**23**	**25**	**27**
Chemical formula	$C_{102}H_{122}BN_8Na O_4U_2 \cdot 2(C_4H_8O)$	$C_{94}H_{106}N_8O_2S_2 U_2 \cdot C_6H_6$	$C_{94}H_{97}N_8O_2SU_2 \cdot C_7H_8$
M_r	2178.14	1998.15	1971.05
Crystal system, space group	Monoclinic, *C*2/*c*	Monoclinic, *C*2/*c*	Triclinic, $P\bar{1}$
Temperature (K)	170	170	170
***a*, *b*, *c* (Å)**	15.5798 (8), 33.7862 (17), 20.7334 (12)	17.3745 (5), 34.2240 (8), 17.0130 (5)	15.9605 (3), 16.6905 (3), 18.0699 (4)
α, β, γ (°)	90 105.543 (6) 90	90 112.037 (3) 90	67.132 (2), 86.551 (2), 82.450 (2)
V **(Å^3)**	10514.6 (10)	9377.3 (5)	4396.61 (15)
Z	4	4	2
Radiation type	Mo *K*α	Mo *K*α	Mo *K*α
μ (mm^{-1})	3.14	3.55	3.76
Crystal size (mm)	0.25×0.11×0.04	0.47×0.06×0.03	0.41×0.23×0.07
Diffractometer	Xcalibur, Eos	Xcalibur, Eos	Xcalibur, Eos
Absorption correction	Analytical	Multi-scan	Analytical
T_{min}, T_{max}	0.867, 0.976	0.570, 1.000	0.035, 0.356
No. of measured, independent and observed {I > 2σ(I)} reflections	49850, 7555, 5446	57840, 9563, 7001	108077, 17944, 14244
R_{int}	0.119	0.069	0.058
(sin θ/λ)$_{max}$ (Å^{-1})	0.556	0.625	0.625
$R[F^2 > 2\sigma(F^2)]$, $wR(F^2)$, S	0.059, 0.108, 1.08	0.039, 0.102, 0.80	0.058, 0.141, 1.05
No. of parameters	602	519	1015
No. of restraints	104	24	98
H-atom treatment	riding	riding	riding
Δ⟩$_{max}$, Δ⟩$_{min}$ (e Å^{-3})	0.83, −1.44	2.59, −1.04	7.56, −4.45
CCDC Number	-	-	-

Compound	**28**	**33**	**34**
Chemical formula	$C_{66}H_{64}N_8O_6U_2 \cdot 4(C_4H_8O)$	$C_{58}H_{48}Cl_5N_8U_2 \cdot C_{20}H_{20}LiN_4 \cdot 3(C_5H_5N)$	$C_{71}H_{71}Cl_2N_9O_2U_2 \cdot C_6H_6$
M_r	1829.72	2070.99	1707.44
Crystal system, space group	Triclinic, $P\bar{1}$	Triclinic, $P\bar{1}$	Monoclinic, $P2_1/c$
Temperature (K)	170	170	170
***a*, *b*, *c* (Å)**	14.2852 (2), 16.2683 (3), 17.1398 (3)	13.2794 (2), 18.0654 (3), 18.7167 (4)	14.1202 (3), 33.8208 (12), 16.6571 (4)
α, β, γ (°)	96.866 (2), 102.010 (1), 91.407 (1)	79.854 (2), 86.369 (2), 72.946 (2)	90 91.328 (2) 90
***V* (Å^3)**	3863.08 (11)	4225.21 (13)	7952.6 (4)
Z	2	2	4
Radiation type	Mo *K*α	Mo *K*α	Mo *K*α
μ (mm^{-1})	4.25	4.04	4.18
Crystal size (mm)	0.35x0.17x0.05	0.36×0.30×0.07	0.28×0.22×0.03
Diffractometer	Xcalibur, Eos	Xcalibur, Eos	Xcalibur, Eos
Absorption correction	Multi-scan	Multi-scan	Multi-scan
T_{min}, T_{max}	0.675, 1.000	0.734, 1.000	0.523, 1.000
No. of measured, independent and observed {$I > 2\sigma(I)$} reflections	63978, 15789, 12604	79205, 17287, 14003	13540, 13540, 9695
R_{int}	0.042	0.043	0.074
(sin θ/λ)$_{max}$ (Å^{-1})	0.625	0.625	0.588
$R[F^2 > 2\sigma(F^2)]$, $wR(F^2)$, S	0.035, 0.089, 0.93	0.035, 0.079, 0.99	0.100, 0.226, 1.16
No. of parameters	919	1096	817
No. of restraints	215	279	427
H-atom treatment	riding	riding	riding
Δ⟩$_{max}$, Δ⟩$_{min}$ (e Å^{-3})	1.87, −0.70	1.15, −1.13	4.48, −9.55
CCDC Number	-	-	-

4.7 References

(1) G. Givaja, A. J. Blake, C. Wilson, M. Schröder, J. B. Love, *Chem. Commun.*, **2003**, 2508.

(2) E. Askarizadeh, A. M. J. Devoille, D. M. Boghaei, A. M. Z. Slawin, J. B. Love, *Inorg. Chem.*, **2009**, *48*, 7491.

(3) B. Horvath, J. Strutz, E. G. Horvath, *Z. Anorg. Allg. Chem.*, **1979**, *457*, 38.

(4) C. D. Carmichael, N. A. Jones, P. L. Arnold, *Inorg. Chem.*, **2008**, *47*, 8577.

(5) M. J. Monreal, R. K. Thomson, T. Cantat, N. E. Travia, B. L. Scott, J. L. Kiplinger, *Organometallics*, **2011**, *30*, 2031.

(6) G. B. Deacon, T. D. Tuong, *Polyhedron*, **1988**, *7*, 249.

(7) A. S. K. Hashmi, C. Lothschütz, C. Böhling, T. Hengst, C. Hubbert, F. Rominger, *Adv. Synth. Catal.*, **2010**, *352*, 3001.

(8) M. Wrede, V. Ganza, G. Kannenberg, F. Rominger, B. F. Straub, *Inorg. Chim. Acta*, **2011**, *369*, 71.

(9) D. F. Evans, *J. Chem. Soc.*, **1959**, 2003.

(10) L. J. Farrugia, *J. Appl. Crystallogr.*, **1999**, *32*, 837.

(11) P. van der Sluis, A. L. Spek, *Acta Crystallogr., Sect. A: Found. Crystallogr.*, **1990**, *46*, 194.

(12) L. Merrill, W. A. Bassett, *Rev. Sci. Instrum.*, **1974**, *45*, 290.

(13) S. A. Moggach, D. R. Allan, S. Parsons, J. E. Warren, *J. Appl. Crystallogr.*, **2008**, *41*, 249.

(14) R. A. Forman, G. J. Piermarini, J. D. Barnett, S. Block, *Science*, **1972**, *176*, 284.

(15) P. L. Arnold, G. M. Jones, Q.-J. Pan, G. Schreckenbach, J. B. Love, *Dalton Trans.*, **2012**, *41*, 6595.

Appendix I

Publications based on the work presented in this thesis

Isocyanide and Phosphine Oxide Coordination in Binuclear Chromium Pacman Complexes

Charlotte J. Stevens , Gary S. Nichol , Polly L. Arnold , and Jason B. Love *

Organometallics, 2013, *32* (23), pp 6879–6882

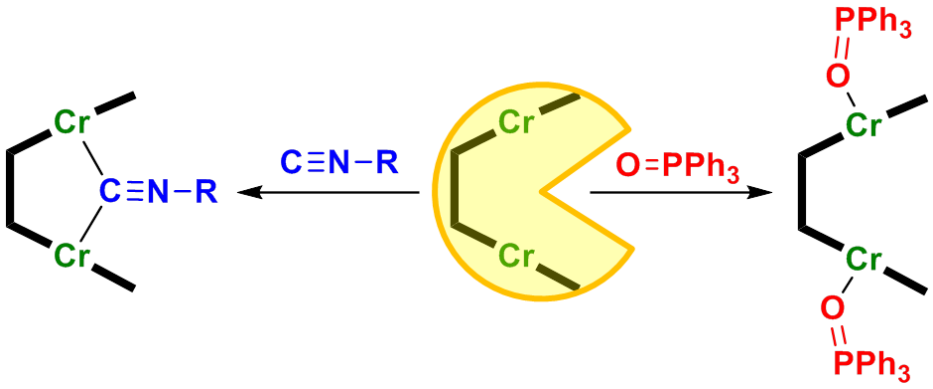

New Chemistry from an Old Reagent: Mono- and Dinuclear Macrocyclic Uranium(III) Complexes from $[U(BH_4)_3(THF)_2]$

Polly L. Arnold,* Charlotte J. Stevens, Joy H. Farnaby, Micheal G. Gardiner, Gary S. Nichol, Jason B. Love *

J. Am. Chem. Soc., 2014, *136* (29), pp 10218–10221